

Microalgal Adhesion to Model Substrates:  
A Quantitative *in vivo* Study on the  
Biological Mechanisms and Surface Forces

Christian Titus Kreis  
Göttingen, 2017





# Microalgal Adhesion to Model Substrates: A Quantitative *in vivo* Study on the Biological Mechanisms and Surface Forces

## Dissertation

to acquire the doctoral degree in mathematics and natural science  
“Doctor rerum naturalium”  
at the Georg-August-Universität Göttingen

in the doctoral degree program

Physics of Biological and Complex Systems  
of the Göttingen Graduate School of Neurosciences, Biophysics, and  
Molecular Biosciences (GGNB)  
of the Georg-August University School of Sciences (GAUSS)

submitted by

**Christian Titus Kreis**  
from Trier, Germany  
Göttingen, 2017

## **Thesis Committee**

**Dr. Oliver Bäumchen,**

Dynamics of Complex Fluids, Max Planck Institute for Dynamics and Self-Organization, Göttingen

**Prof. Dr. Christoph Schmidt,**

Third Institute of Physics – Biophysics, Georg-August University, Göttingen

**Prof. Dr. Marcus Müller,**

Institute for Theoretical Physics, Georg-August University, Göttingen

## **Members of the Examination Board**

**Referee: Dr. Oliver Bäumchen,**

Dynamics of Complex Fluids, Max Planck Institute for Dynamics and Self-Organization, Göttingen

**Co-Referee: Prof. Dr. Stefan Klumpp,**

Institute for Nonlinear Dynamics, Georg-August University, Göttingen

## **Further members of the Examination Board**

**Prof. Dr. Christoph Schmidt,**

Third Institute of Physics – Biophysics, Georg-August University, Göttingen

**Prof. Dr. Marcus Müller,**

Institute for Theoretical Physics, Georg-August University, Göttingen

**Dr. Karen Alim,**

Max Planck Institute for Dynamics and Self-Organization, Göttingen

**Prof. Dr. Jörg Enderlein,**

Third Institute of Physics – Biophysics, Georg-August University, Göttingen

Date of oral examination: 16.11.2017





# Abstract

Microalgae are the most important primary producers of biomass on Earth. They inherit enormous technological potential to harness photosynthesis for the sustainable production of biofuels, proteins, and food components. In aqueous environments, microalgal surface colonization and biofouling cause severe implications on anthropogenic structures. Despite the fundamental interest in understanding microalgal adhesion, the biological mechanisms that trigger microalgal adhesion to surfaces and the surface forces that govern their adhesion remain unknown. In this work, the flagella-mediated adhesion to surfaces of soil-dwelling, green microalgae is studied quantitatively on a single-cell level. Micropipette-based force spectroscopy experiments are performed to quantify microalgal adhesion to model substrates in various experimental configurations and environmental conditions. *In vivo* force measurements show that the adhesion of microalgae to surfaces can be reversibly switched on and off within seconds by tailoring the light conditions. The light-switchable adhesion appears to be based on a relocalization of the adhesion-mediating protein. An active adhesion process, termed auto-adhesion, enables the alga to establish adhesive contact to surfaces once a small part of one flagellum adhered to the surface. Experiments with other species of the family Chlamydomonadaceae suggest that the light-switchable flagellar adhesiveness might be a generic trait of soil-dwelling microalgae. Force spectroscopy experiments on model substrates with tailored intermolecular interactions with the *Chlamydomonas* flagella demonstrate that *Chlamydomonas* inherits an universal adhesion mechanisms that allows the algae to adhere to virtually all types of substrates. In conjunction with light-directed motility, the ability to adhere to any surfaces that provide optimal light exposure might have evolved as an adaptation of photosynthetic organisms to heterogeneous light conditions in their natural habitats. The findings of this work will raise the interest of an interdisciplinary audience, from biologists working on behavior and evolution of microalgae to biophysicists to bioengineers, and might stimulate further work on the molecular biology and functionality of eukaryotic flagella.



# Contents

<b>1. Introduction</b>	<b>1</b>
<b>2. State of the Art</b>	<b>5</b>
2.1. Ecological and Technological Relevance of Microalgae . . . . .	5
2.2. Microbial Adhesion and Biofilm Formation . . . . .	7
2.3. The Model Organism <i>Chlamydomonas reinhardtii</i> . . . . .	9
2.3.1. The <i>Chlamydomonas</i> Cell Body and its Flagella . . . . .	9
2.3.2. Structures and Proteins in the Flagellar Membrane of <i>Chlamydomonas</i> .	12
2.3.3. Cell Behavior and Motility . . . . .	15
2.3.4. Dynamic Properties of the Flagellar Membrane . . . . .	18
2.4. Micropipettes as Tools in Biological Research . . . . .	21
2.4.1. Micropipettes as Object Support and Injection Needles . . . . .	21
2.4.2. Micropipettes as Force Sensors . . . . .	23
2.5. Intermolecular Interactions and Surface Forces . . . . .	24
2.5.1. Electrostatic Interactions . . . . .	24
2.5.2. Van der Waals-Interactions . . . . .	26
2.5.3. Steric Repulsion . . . . .	27
2.5.4. Hydrogen Bonds and Hydrophobic Interactions . . . . .	28
<b>3. Materials and Methods</b>	<b>29</b>
3.1. Micropipette Force Spectroscopy . . . . .	29
3.1.1. A Micropipette Cantilever as Force Sensor . . . . .	31
3.1.2. Experimental Setup . . . . .	35
3.2. Microalgae Strains . . . . .	40
3.2.1. <i>Chlamydomonas reinhardtii</i> . . . . .	41
3.2.2. Other Microalgae Strains . . . . .	42
3.3. Substrates . . . . .	42
3.3.1. Overview of the Model Substrates . . . . .	43
3.3.2. Substrate Characterization . . . . .	44
3.4. Force Spectroscopy Experiments . . . . .	46
3.4.1. Preparation of the Experiment . . . . .	46
3.4.2. Force-Distance Experiments . . . . .	49
3.4.3. Standard Parameters in Force-Distance Experiments . . . . .	50
3.4.4. Light Conditions . . . . .	51

3.4.5.	Experimental Protocols . . . . .	52
3.4.6.	Auto-Adhesion Experiments . . . . .	54
3.5.	Surface Colonization Experiments of Cell Populations . . . . .	54
3.6.	Statistical Analysis of the Experimental Data . . . . .	55
3.6.1.	Visualizations of Datasets . . . . .	55
3.6.2.	Logarithmic-Normal Distribution . . . . .	57
3.6.3.	Statistical Significance Testing: the Kolmogorov-Smirnoff Test . . . . .	57
<b>4.</b>	<b>Conceptual Aspects of Microalgal Single-Cell Force Spectroscopy Experiments</b>	<b>61</b>
4.1.	Adhesion Experiments with Micropipette Force Spectroscopy . . . . .	63
4.2.	Flagellar Dynamics During Flagella-Mediated Cell Adhesion . . . . .	65
4.2.1.	Flagella Adhesion versus Cell Body Adhesion . . . . .	65
4.2.2.	Flagellar Dynamics During Flagella-Substrate Contact . . . . .	65
4.2.3.	Flagellar Dynamics After Cell Detachment . . . . .	67
4.3.	Consistency Checks in Force Spectroscopy Studies . . . . .	69
4.3.1.	Temporal Evolution of the Adhesion Force . . . . .	69
4.3.2.	Cell-Substrate Contact Time . . . . .	71
4.3.3.	Substrate Velocity – Force Ramp Rate . . . . .	72
4.3.4.	Force Trigger – Force at Contact . . . . .	73
4.4.	Summary . . . . .	74
<b>5.</b>	<b>Quantitative Characterization of <i>Chlamydomonas</i> Adhesion Forces</b>	<b>75</b>
5.1.	Adhesion Force Statistics on Silicon Model Substrates . . . . .	77
5.1.1.	Statistical Distribution of Mean Adhesion Forces . . . . .	77
5.1.2.	Adhesion Forces – Revised Statistics . . . . .	80
5.1.3.	Discussion and Summary: Adhesion Forces . . . . .	81
5.2.	Adhesion and Characteristics of the <i>Chlamydomonas</i> Flagellar Membrane . . . . .	83
5.2.1.	Contact Area in Adhesion Experiments . . . . .	83
5.2.2.	Signatures of Force-Distance Curves . . . . .	86
5.2.3.	Discussion: Signatures of the Detachment Process . . . . .	91
5.3.	Summary and Discussion . . . . .	92
<b>6.</b>	<b>Light-Switchable Adhesion of Microalgae</b>	<b>95</b>
6.1.	Force Spectroscopy in Different Illumination Conditions . . . . .	97
6.1.1.	Light-Switchable Adhesion: A General Description of the Effect . . . . .	97
6.1.2.	Color Discrimination . . . . .	98
6.1.3.	Photoreceptor Sensitivity and Light Intensity Dependence . . . . .	100
6.1.4.	Temporal Evolution of the Adhesion Force After Turning the Light on . . . . .	102
6.1.5.	Concluding Remarks . . . . .	103
6.2.	Surface Colonization Experiments . . . . .	104



6.3.	Auto-Adhesion: An Active Process to Establish Adhesive Contact to Surfaces .	105
6.3.1.	Experimental Design and Description of the Auto-Adhesion Process . .	105
6.3.2.	Characterizing Timescales in the Auto-Adhesion Process . . . . .	109
6.3.3.	Auto-Adhesion and Gliding Motility . . . . .	113
6.3.4.	Concluding Remarks . . . . .	113
6.4.	Unraveling the Molecular Mechanism of Light-Switchable Adhesion . . . . .	115
6.5.	Preliminary and Ongoing Work . . . . .	118
6.5.1.	Active Regulation of Flagellar Adhesiveness . . . . .	118
6.5.2.	Photoreceptor Deletion-Mutants . . . . .	119
6.6.	Discussion, Conclusions, and Outlook . . . . .	122
<b>7.</b>	<b>Surface Forces Governing Microalgal Adhesion</b>	<b>125</b>
7.1.	Force Spectroscopy on Model Substrates with Tailored Properties . . . . .	127
7.1.1.	Hydrophobic Interactions: Surface Energy and Surface Hydrophobicity .	127
7.1.2.	Van der Waals Interactions . . . . .	131
7.1.3.	Electrostatic Interactions . . . . .	133
7.2.	Force Spectroscopy on Additional Substrates . . . . .	135
7.3.	Discussion, Conclusions, and Outlook . . . . .	136
7.4.	Summary . . . . .	140
<b>8.</b>	<b>Light-Switchable Adhesion: A Generic Trait of Soil-Dwelling Microalgae?</b>	<b>141</b>
8.1.	<i>Chlamydomonas reinhardtii</i> Gametes . . . . .	143
8.2.	<i>Chlamydomonas noctigama</i> . . . . .	143
8.3.	<i>Oogamochlamys gigantea</i> . . . . .	144
8.4.	Summary and Outlook . . . . .	147
<b>9.</b>	<b>Summary and Outlook</b>	<b>149</b>
<b>A.</b>	<b>Additional Material and Figures</b>	<b>155</b>
A.1.	Auto-Correlation Analysis . . . . .	155
A.2.	Statistical Analysis of Data Sets . . . . .	157
A.3.	Additional Material and Figures . . . . .	159
<b>B.</b>	<b>Further Work: Microalgae in Confined Geometries</b>	<b>171</b>
B.1.	Mechanical Properties of <i>Volvox</i> Colonies: Deformation and Relaxation . . . .	171
B.2.	Spectral Analysis of Micropipette Fluctuations: <i>Chlamydomonas</i> Propulsion . .	174
B.3.	Drying Droplets of Microalgal Suspensions . . . . .	176
	<b>Bibliography</b>	<b>178</b>
<b>C.</b>	<b>The Story of my PhD Research and the Discovery of Light-Switchable Adhesion</b>	<b>199</b>



# 1. Introduction

Microbial life is the oldest and most abundant form of life on Earth [Oro et al., 1990; Martin et al., 2008]. Microorganisms have evolved into diverse shapes and conquered all habitats on Earth that allow growth and survival [Rothschild and Mancinelli, 2001; Rampelotto, 2013]. As the primary producers of organic carbon compounds in each ecosystem, microorganisms convert inorganic compounds and energy (mostly sunlight) into biomass, which supports the existence of higher-level forms of life. In open water bodies, like oceans or lakes, microorganisms are mostly found in a planktonic state, whereas they tend to form complex communities at surfaces, such as biofilms. Biofilms are colonies of microbes embedded in a self-produced extracellular matrix that protects the individual organism, serves as reservoir of nutrients, allows for cell-to-cell communication, and enables horizontal gene transfer, among other functions [Jefferson, 2004; Flemming and Wingender, 2010; Flemming et al., 2016]. Biofilms can be found in association with abiotic materials, such as rocks, soil, or aquatic sediments, as well as biotic materials, such as trees, dropped leaves, dead animals and plants, but also in and on living animals, in wounds and their intestines.

Microbes may be disseminated over large distances by water currents, rain drops, wind, insects, etc. In addition, they often inherit a directed motility, such as phototaxis or chemotaxis, which allows them to locate areas that provide optimal growth conditions in their habitats. At a new location, the microbes may attach to a surface, proliferate, and secrete biopolymers that form the extracellular matrix, which is necessary for biofilm maturation [O’Toole et al., 2000; Watnick and Kolter, 2000; Flemming and Wingender, 2010]. The steps from initial surface attachment to the formation of a mature biofilm have been widely studied in bacteria, mostly due to their implications in the health sector [Donlan, 2001; Hall-Stoodley et al., 2004]. However, bacteria are not the only form of microbial life that is of particular interest to human lives. Other microbes of profound ecological and technological relevance are microalgae.

Microalgae are phototrophic eukaryotes that live in aqueous environments. They are the main primary producers on Earth, as they are capable of converting inorganic compounds into biomass with the energy provided by photosynthesis [Porter, 1977; Field et al., 1998; Finlay and Esteban, 1998; Bidle and Falkowski, 2004; Arrigo, 2005]. Furthermore, algae play a major role in various industrial applications, such as water treatment and purification systems. Algae farms harness photosyntheses for a sustainable production of biofuels, food components like  $\beta$ -carotene, and proteins for drugs [Siaut et al., 2011; Singh and Sharma, 2012; Chacón-Lee and González-Mariño, 2010; Guedes et al., 2011; Hamed, 2016; Wells et al., 2017]. Microalgal

biofouling causes severe implications in these systems and affects any surface in wet environments, for example pipes and cables, ship hulls, aquaculture systems, and other anthropogenic structures [Chambers et al., 2006; Callow and Callow, 2011; Landoulsi et al., 2011]. Controlling microalgal biofilms in these settings requires a comprehensive understanding of the mechanisms that trigger surface colonization and biofilm formation and the underlying physical forces that mediate adhesion. In this context, force spectroscopy studies provide a valuable characterization of the initial adhesion process. However, there are no quantitative single-cell adhesion studies with living, flagellated microalgae. In general, microalgal studies remain limited as conventional atomic force microscopes, the most commonly used device in force spectroscopy studies, and optical tweezers cannot access the necessary size and/or force ranges, as of today. In addition, these techniques lack a control of the cellular orientation required for studying flagellated microalgae.

The overarching goal of this work is to study the adhesion strategies of microalgae to surfaces. Therefore, micropipette-based, single-cell force spectroscopy experiments are performed *in vivo* on different model substrates in various experimental conditions. The work focuses on the model organism *Chlamydomonas reinhardtii*, but other species of the family Chlamydomonadaceae are also studied. The main goal is divided into four individual objectives that address specific aspects necessary to understand the adhesion strategies of microalgae:

1. Develop a protocol for quantitative force spectroscopy experiments with microalgae.
2. Characterize the adhesion forces of *Chlamydomonas reinhardtii* to silicon model substrates.
3. Determine the biological mechanisms and strategies that trigger microalgal adhesion and surface colonization.
4. Identify the predominant intermolecular interactions that mediate microalgal adhesion to substrates.

The first objective (chapter 4) validates the force spectroscopy approach and seeks to identify important experimental parameters for performing reliable *in vivo* force spectroscopy experiments. The second objective (chapter 5) intends to elucidate the general adhesion mechanism of microalgae by performing a comprehensive statistical analysis of the adhesion forces to a model substrate. The third and forth objectives aim to identify strategies that microalgae have developed to effectively colonize surfaces in their natural habitats. Chapter 6 focuses on the biological aspects that trigger microalgal surface-association, whereas chapter 7 aims at dissecting the contributions of different intermolecular interactions to the adhesion forces of *Chlamydomonas reinhardtii* to surfaces. Chapter 8 seeks to expand the most important findings from the model organism *Chlamydomonas reinhardtii* to other soil-dwelling microalgae.

---

These chapters are accompanied by an overview of the state of the art in chapter 2, which includes a discussion of the ecological and technological relevance of microalgae and biofilms. This chapter also contains an introduction to the model organism *Chlamydomonas reinhardtii*, and intermolecular interactions and surface forces. Chapter 3 provides a detailed overview of the materials and methods: the micropipette force spectroscopy technique, the force spectroscopy setup, the experimental settings and protocols, and the model substrates.

A concluding summary of the findings and a brief outlook is given in chapter 9. Additional projects related to microalgae in confined geometries are presented in Appendix B.



## 2. State of the Art

### 2.1. Ecological and Technological Relevance of Microalgae

Algae are phototrophic eukaryotes, i.e. they are organisms that perform photosynthesis to produce energy, that exist in various forms and complexities. There are many unicellular microalgae, but there are also species that form colonies of thousands of cells. Some macroscopic algae even grow to sizes of tens of meters in length like kelp found in coastal regions. It is assumed that terrestrial plants, which grow on land and not in water, evolved from freshwater green algae [Kenrick and Crane, 1997; Wellman et al., 2003], and algae in turn appear to share common ancestors with present-day cyanobacteria [Deusch et al., 2008; Cavalier-Smith, 2000; Ochoa de Alda et al., 2014]. All algae are associated with wet environments, as water is a prerequisite for their sexual reproduction, which often happens via flagellated, haploid gametes<sup>1</sup>. In addition, most algae inherit zoospores, which are unicellular, flagellated, and free-swimming cells that serve the dissemination of the organism. The zoospores are found in unicellular species, where the zoospore represents the organism itself (for example, *Chlamydomonas*), but also in macroscopic algae that form long filaments with hundreds of thousands of cells, for example.

The phytoplankton of salt- and freshwater ecosystems consists of a variety of microalgae. The phytoplankton contributes to global nutrient cycles and is the basis of food chains [Porter, 1977; Finlay and Esteban, 1998; Bidle and Falkowski, 2004; Arrigo, 2005]. This role becomes apparent when looking at the net global primary production of organic carbon compounds. Although microalgae in the oceans make up less than 1 % of Earth's biomass, they are responsible for about 50 % of the annual global production of organic compounds of about  $104.9 \times 10^{15}$  g of C [Field et al., 1998]. This imbalance is due to a biomass turnover rate that is more than three orders of magnitude faster for microalgae (2 to 6 days) than for terrestrial plants (average 19 years) [Field et al., 1998, and references therein]. Thus, microalgae have a profound ecological importance as primary producers of organic carbon, as well as oxygen from their photosynthesis. Climate change and other anthropogenic influences on aquatic ecosystems immediately affect microalgae, which can be observed in the bleaching in coral reefs or the eutrophication of lakes and coastal marine ecosystems from excessive nutrient run-off from farms to water bodies [Smith, 2003; Hughes et al., 2003; Slezak, 2016; McGuirk, 2017].

---

<sup>1</sup>The gametes fuse to form a zygote that grows to the mature organism that produces new gametes. In unicellular algae, such as *Chlamydomonas*, gametogenesis transforms vegetative cells in sexually active gametes (see section 2.3.3). In other species, the mature organism produces the haploid gametes.

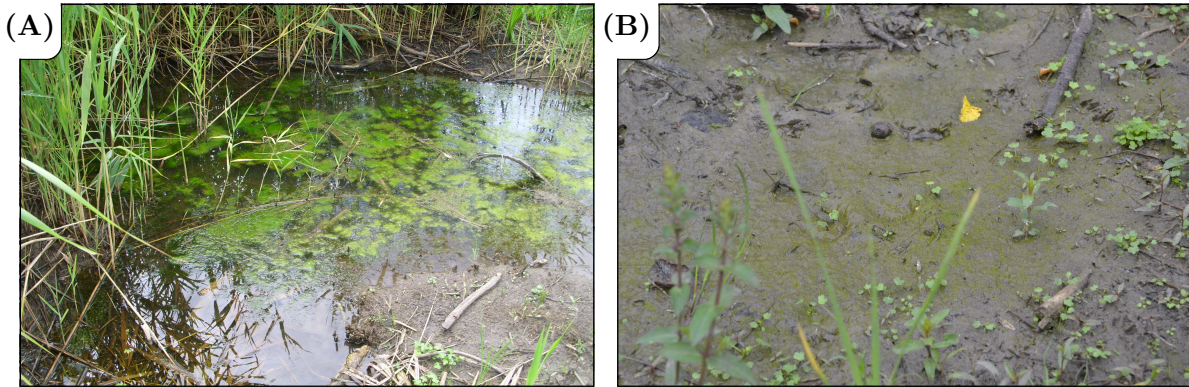


**Figure 2.1.: Photographs of algae in their natural habitats.** The photographs were taken by Christian Titus Kreis at the beginning of August 2017 after a couple days of rain at the Étang des Marais, 57510 Rémering-lès-Puttelange, France. **(A)** Reed and algae at the lakeshore. **(B)** Algae on moist ground close to the lake.



**Figure 2.2.: Photosynthetic activity of algal biofilms.** The photograph was taken by Christian Titus Kreis at the beginning of August 2017 after several days of rain at Étang des Marais, 57510 Rémering-lès-Puttelange, France. Algal biofilm at the bottom of a puddle. The air bubbles indicate regions of high photosynthetic activity.

Although often associated with open water bodies, microalgae colonize various light-exposed surfaces in moist habitats, like soil, puddles, temporary pools, or streams (see Figure 2.1 and Figure 2.2). Many biofilms encountered in natural environments, such as on rocks, wood or other biotic materials, often contain a community of algae, bacteria, and other microorganisms. Microalgae are also found in symbiotic relationships, such as lichen, which are microalgae (or cyanobacteria) living in a fungal network. The versatility of microalgal biofilms enables their use in many technological applications, for example, in water purification systems and waste



water treatment [Kesaano and Sims, 2014]. The quick turnover rate of microalgae gives rise to their potential in photobioreactors as a sustainable method to produce biofuel, drugs, and food components [Chacón-Lee and González-Mariño, 2010; Guedes et al., 2011; Siaut et al., 2011; Singh and Sharma, 2012; Hamed, 2016; Wells et al., 2017]. In contrast, microalgal biofilms lead to biofouling on surfaces in moist environments, like on ship hulls, aquaculture systems, heat exchangers and oceanographic sensors [Chambers et al., 2006; Callow and Callow, 2011; Landoulsi et al., 2011].

## 2.2. Microbial Adhesion and Biofilm Formation

Microbial adhesion strategies have been widely studied for bacteria due to their consequences in biomedical settings [Donlan, 2001; Hall-Stoodley et al., 2004]. Bacterial adhesion is generally mediated by membrane proteins and cellular appendages, like pili and fimbriae, which are often tailored to attach to extracellular material in a host organism or biofilm, but may also lead to remarkable adhesion to abiotic substrates [Abraham et al., 1988; Hultgren et al., 1993; Pizarro-Cerdá and Cossart, 2006; Beloin et al., 2008; Proft and Baker, 2008]. Atomic force microscopy was widely employed to study the adhesion-mediating proteins and underlying intermolecular interactions that mediate the adhesion [Bos et al., 1999; Busscher et al., 2008; Loskill et al., 2012b; Dufrêne, 2015; Sullan et al., 2015; Thewes et al., 2014, 2015b]. Differences in the intermolecular interactions on each substrate result in varying adhesion capabilities of bacteria. For example, *Staphylococcus* adheres strongly to hydrophobic substrates, while the adhesion forces are at least on order of magnitude smaller on hydrophilic substrates [Thewes et al., 2014]. Furthermore, the substrate's stiffness and topography influence bacterial adhesion [Hsu et al., 2013; Perera-Costa et al., 2014; Song and Ren, 2014; Kolewe et al., 2015]. Although these studies are often hardly comparable due to different species, bacterial strains and varying several surface parameters at the same time, the overall message remains the same. The surface attachment of bacteria is influenced by the molecular properties of the adhesins and the substrate's surface parameters, such as surface charge, hydrophobicity, roughness, topography, chemistry, and rigidity.

After the initial surface colonization, the bacteria proliferate, accumulate in microcolonies, and ultimately secrete extracellular polymeric substances, which enclose the individual bacteria in a so-called biofilm [O'Toole et al., 2000; Watnick and Kolter, 2000; Flemming and Wingender, 2010; Flemming et al., 2016, see Figure 2.3]. The extracellular polymeric substances mainly consist of biopolymers such as polysaccharides, nucleic acids, proteins, and lipids that form a three-dimensional cohesive network to stabilize the biofilm [Beloin et al., 2008; Flemming and Wingender, 2010; Sheng et al., 2010]. Besides determining the morphology of the biofilm, this network glues the bacteria together, mediates substrate adhesion, serves as reservoir of nutrients, allows for cell-to-cell communication, enables horizontal gene transfer, etc. The extracellular polymeric substances can account for up to 90 % of the dry mass in a mature biofilm.

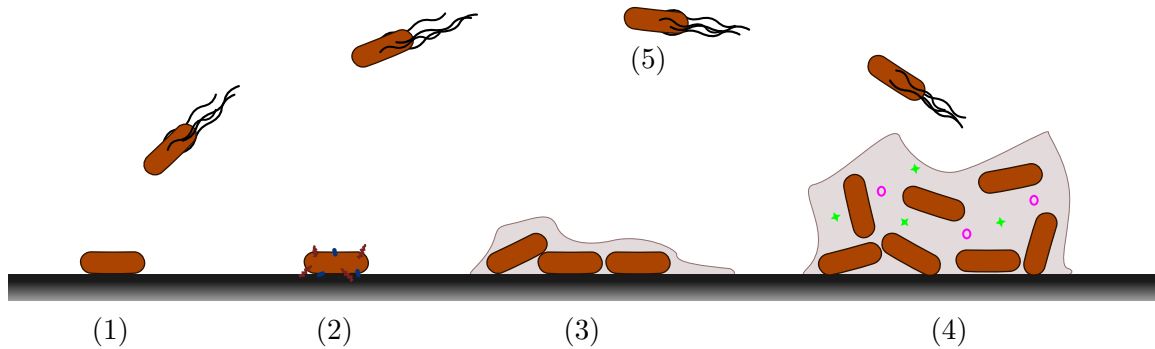


**Figure 2.3.: Sketch of the different steps in biofilm formation.** The sketch visualizes the formation of a biofilm from individual organisms to the mature biofilm. Each step shows characteristic features that are not shown in the following steps for reasons of clarity. (1): Biofilm formation starts with the reversible attachment of microorganisms on a substrate. (2): The initial adhesion triggers a signal pathway that results in the secretion of specific adhesins that irreversibly glue the microbe to the substrate. (3): Subsequently, the microorganism proliferates, individual cells accumulate in microcolonies, and the cells produce extracellular polymeric substances that embed the cells. (4): The mature biofilm provides a protected habitat that stores nutrients and allows bacteria to transfer genetic material in a process called bacterial conjugation, which enhances the development of resistances against antimicrobial treatments, among other functions. (5): Cells leave the biofilm and actively move or are passively transported to new locations, at which the biofilm formation processes are repeated.

This general biofilm composition reflects the importance of extracellular polymeric substance production for the transition from individual cells to a mature biofilm [Flemming and Wingender, 2010].

Although the implications of microalgal biofilm formation is widely recognized [Chambers et al., 2006; Callow and Callow, 2011; Landoulsi et al., 2011], adhesion studies of microalgae to surfaces are fairly limited. Surface interactions of microalgae, in particular *Chlamydomonas*, were studied in the context of gliding motility (see section 2.3.4). Whereas these studies show that algae do adhere to surfaces, the adhesion forces were rather studied qualitatively [Sekar et al., 2004; He et al., 2016]. Force spectroscopy has been performed on the diatom *Toxarium undulatum* [Dugdale et al., 2005] (diatoms are a major group of algae in the phytoplankton). Swimming spores of the green alga *Enteromorpha linza* exhibit adhesion forces of tens of nanonewton [Callow et al., 2000]. A study that quantifies forces between the flagella of *Chlamydomonas* and silicon substrates was performed by Ramaswamy et al. [Ramaswamy et al., 2013]. This study shows adhesion forces of approximately 1 nN; however, the authors used flagella extracted from *Chlamydomonas*, thus, this study cannot provide any *in vivo* adhesion force quantifications.

## 2.3. The Model Organism *Chlamydomonas reinhardtii*

The genus *Chlamydomonas* characterizes unicellular microalgae with two flagella attached to the anterior of the cell body. There are over 400 species in the genus *Chlamydomonas*, which Pröschold et al. grouped into 18 monophyletic lineages<sup>2</sup> in the class Chlorophyceae [Ettl, 1976; Pröschold et al., 2001]. While the taxonomic classification and relationships of individual *Chlamydomonas* species is still under debate, it is widely accepted that *Chlamydomonas reinhardtii* (*C. reinhardtii*) is the most prominent representative of the genus.

*C. reinhardtii* is the best-studied *Chlamydomonas* species, and many features of the cell architecture and behavior of *C. reinhardtii* can be generalized to the whole genus. This study focuses on the *C. reinhardtii* strain SAG 11-32b that was derived from an isolate taken from a potato field (Amherst, Massachusetts, 1945). In the following, I will refer to *C. reinhardtii* as *Chlamydomonas*. A review of the species *Chlamydomonas* is given in “The Chlamydomonas Sourcebook” [Harris et al., 2009], which serves as basis for the following description<sup>3</sup>. This book is recommended for more comprehensive insights of the alga’s cell architecture and behavior.

*Chlamydomonas* is a widely used model organism to study the molecular biology of eukaryotes, such as the photosynthesis-related cell metabolism, motility phenomena like phototaxis and gliding, microtubule-based axonemes, and intraflagellar transport [Harris et al., 2009, and the reviews included on these topics]. Physicists are interested in *Chlamydomonas* to study puller-type microswimmers and life at low Reynolds numbers<sup>4</sup>, and to quantify forces generated by molecular motors [Goldstein, 2015; Laib et al., 2009; Shih et al., 2013]. Bioengineers are interested in *Chlamydomonas* and other species of the class Chlorophyceae, like *Dunaliella* or *Haematococcus*, due to their potential use in photobioreactors.

### 2.3.1. The *Chlamydomonas* Cell Body and its Flagella

#### Cell Architecture and Major Organelles Inside the Cell Body

The cell body of *Chlamydomonas* is ellipsoidal to spherical, with a diameter of approximately 10  $\mu\text{m}$  (although it can vary significantly throughout the cell cycle). A sketch of the cell body and the main organelles is shown in Figure 2.4. The cell body is encased within the plasma membrane, which in turn is surrounded by a multilayered cell wall that has been intensively studied in electron microscopy studies [Harris, 2009a]. Roberts et al. found seven layers in the cell wall of vegetative *Chlamydomonas* cells with an estimated thickness of in

---

<sup>2</sup>A monophyletic group is a group of species that share a common ancestors.

<sup>3</sup>A shorter review by Harris [Harris, 2001] summarizes important information of the cell, and is more easily accessible than “The Chlamydomonas Sourcebook”.

<sup>4</sup>The Reynolds number is the ratio of inertial forces and viscous forces. At low Reynolds number, the viscous forces dominate and any motion stops immediately without propulsion. A net propulsion can solely be achieved by a time-invariant flagella waveform. See also [Purcell, 1977] for a short introduction in the field of “Life at low Reynolds number”.

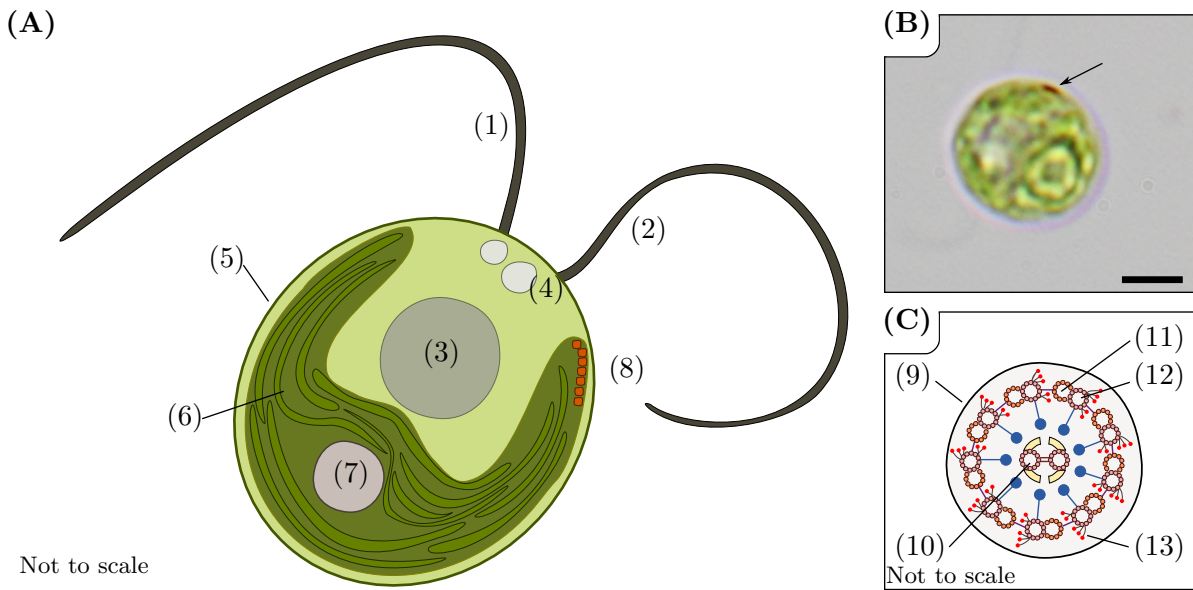


**Figure 2.4.: Architecture of the *Chlamydomonas* cell body and the flagella.**

(A) Sketch of a *Chlamydomonas* cell, including the: *trans*-flagellum (1), *cis*-flagellum (2), nucleus (3), contractile vacuoles (4), multi-layered cell wall (5) and chloroplast (6), which includes the pyrenoid (7) and the eyespot (8). The *cis*- and *trans*-flagellum correspond to the flagella position with respect to the eyespot. The *cis*-flagellum is located closer to the eyespot. Adapted from [Harris et al., 2009]. (B) Optical micrograph of a *Chlamydomonas* cell. The arrow indicates the location of the orange eyespot. The flagella at the cell apex are not visible. Scale bar: 5  $\mu\text{m}$ . (C) Internal structure of the flagellum including: flagellar plasma membrane (9), central microtubules pair (10), B microtubule containing 11 or 12 protofilaments (11), A microtubule containing 13 protofilaments (12), and outer and inner dynein arms (13). Adapted from [Lodish et al., 2004]. More information on flagella can be found in [Bloodgood, 1990a].

total 100 to 450 nm. The innermost and outermost layers of the cell wall can vary between 30 to 200 nm in thickness [Roberts et al., 1972]. For comparison, the plasma membrane has a thickness of a few nanometers (see the electron microscopy studies mentioned above).

Major organelles inside the cell body are the nucleus (making up approximately 10 % of the cell volume [Schötz et al., 1972]), the chloroplast ( $\approx 40\%$  [Schötz et al., 1972]), mitochondria, and contractile vacuoles (sometimes also called pulsating vacuoles). *Chlamydomonas* has two contractile vacuoles that pulsate alternately at intervals of tens of seconds to pump excessive water out of the cell body [Luykx et al., 1997; Komsic-Buchmann et al., 2014]. The water flows into the cell due to an osmotic pressure difference between the aqueous solution inside the cell (cytosol) and the surrounding fluid. Thereby, the contractile vacuoles regulate the osmotic pressure of the cell. The recurrent motion of the vacuoles can be used to determine the viability of the cell.

The chloroplast is located in the basal part of the cell body (i.e. opposite the flagella) and is the organelle where photosynthesis occurs. The chloroplast contains the pyrenoid and the orange eyespot, which is located directly beneath the plasma membrane. The pyrenoid consists of the protein RuBisCO and serves, amongst other functions, as an anchor for starch plates. The eyespot is composed of regularly arranged granules with a diameter of 80 to 130 nm diameter that shield the photoreceptors in the plasma membrane from light passing through the cell body (see Figure 2.4A+B). This carotenoid-rich structure enables the cell to detect the direction of incident light and locate a light source. By adapting the flagella beating pattern to the light incidence, the cell turns its cell body towards the light stimulus and swims in the direction of the light source, in a phenomenon called phototaxis, which is further described in section 2.3.3.

### The Flagellar Structure

One of the most characteristic features of the species *Chlamydomonas* are its two flagella, which can also be found in almost all microalgae Figure 2.4. A general review of flagellar organization and functions can be found in “Ciliary and Flagellar Membranes” [Bloodgood, 1990a] and “The Chlamydomonas Sourcebook” for *Chlamydomonas* more specifically. The two flagella of *Chlamydomonas* are equal in length and approximately 10 to 12  $\mu\text{m}$  long, with a diameter of 200 nm. The flagellar length is independent of the size of the cell body. The flagella are attached to the cell apex and anchored within the basal bodies inside the cell body. The structure of the flagella is characteristic of the structure of motile eukaryotic cell appendages (flagella and cilia): nine double microtubules surrounded by a central microtubules pair, which is often called a  $9 \times 2 + 2$  axoneme<sup>5</sup> (see Figure 2.4C). The microtubules are made out of protofilaments consisting of  $\alpha$ -tubulin and  $\beta$ -tubulin dimers. The side of the microtubules with exposed  $\alpha$ -subunits is the minus end and the side with the  $\beta$ -subunits the plus end [Lodish et al., 2004]. Each outer microtubule has associated dynein or kinesin molecular motors that are responsible for transport inside the flagellum and within the flagellar membrane.

The axoneme is encased in the flagellar plasma membrane that is a continuation of the cell body plasma membrane. Both membrane compartments are separated by the so-called flagellar bracelet and necklace, which can be seen in freeze-fractured *Chlamydomonas* cells [Weiss et al., 1977]. The flagellar bracelet and necklace serve as barriers for the free diffusion of membrane proteins [Bloodgood, 1988; Hunnicutt et al., 1990]. In contrast to the cell body plasma membrane, the flagellar membrane has direct access to the environment as it is not surrounded by any cell wall. For this reason, the flagellar membrane may serve as a sensory organ and allows for surface-associated motility that is further described in section 2.3.4.

In comparison, bacterial flagella have a completely different composition, as the prokaryotic

---

<sup>5</sup>Non-motile, primary cilia lack the central microtubules pair, therefore called  $9 \times 2 + 0$  axoneme, and dynein motors on the outer microtubules.

flagellum consists of the protein flagellin that forms an individual filament of 20 nm in diameter [Alberts et al., 2002]. The bacterial flagellum's motion is rotational and corkscrew-like, whereas the eukaryotic flagellum's motion is planar in a wave-like fashion (like sperm cells) or a beating with power and recovery stroke (like cilia and *Chlamydomonas*' flagella). The force generation that results in flagellar motion in both cases cannot be compared either: molecular motors drive the motion of the eukaryotic flagellum, whereas ions flowing through the stator drives the motion of a rotor connected to the prokaryotic flagellum. "The use of the same name to denote these two very different types of swimming apparatus is an unfortunate historical accident." (Molecular Biology of the Cell, p. 968 [Alberts et al., 2002])

### 2.3.2. Structures and Proteins in the Flagellar Membrane of *Chlamydomonas*

The *Chlamydomonas* flagellar membrane is comprised of a variety of proteins and protein structures, such as the major flagellar membrane glycoprotein FMG-1B, the mastigonemes, and the sexual agglutinins in gametes. A comprehensive overview of the flagellar membrane components can be found in "The *Chlamydomonas* Flagellar Membrane and Its Dynamic Properties" by Bloodgood, which is published in "The Chlamydomonas Sourcebook" [Bloodgood, 2009]. The following overview summarizes the key information of this review with regards to the aforementioned flagellar membrane protein structures.

#### The Major Flagellar Membrane Glycoprotein FMG-1B

The *Chlamydomonas*' flagella are covered with a glycocalyx of approximately 16 to 18 nm thickness, as seen in transmission electron microscopy (sometimes described as "fuzzy coat") [Bloodgood and May, 1982; Bloodgood, 2009]. The glycocalyx is made of the ectodomain of the major flagellar membrane glycoprotein FMG-1B (UniProt database: Q84X68<sup>6</sup>) and carbohydrates covalently-bound to FMG-1B (N-linked glycosylation, see below). The glycoprotein FMG-1B consists of 4149 amino acids (ectodomain over 4100 amino acids), predicted by the gene encoding the protein [Bloodgood, 2009]. The predicted amino acid sequence matches the amino acid composition determined by SDS-polyacrylamide gels [Bloodgood, 1990b]. Although the putative amino acid composition and sequence of FMG-1B were determined, the structure of the adhesion protein or individual domains remain unknown. The protein presumably forms dimers and tetramers in the flagellar membrane [Bloodgood, 2009].

FMG-1B is N-glycosylated on at least 15 out of 31 potential N-glycosylation sites [Bloodgood et al., 1986]. Glycosylation of a protein denotes a covalently binding of glycan oligosaccharides to the protein and N-glycosylation refers to glycosylation at a nitrogen atom in the amino acid asparagine [Lodish et al., 2004]. Protein glycosylation is a common concept amongst eukaryotes and the structure of the N-linked oligosaccharides is highly preserved amongst different species (see Figure 2.5 for the structure of the N-linked oligosaccharides). The monosaccharide

---

<sup>6</sup>[www.uniprot.org](http://www.uniprot.org), retrieved 19.07.2017.

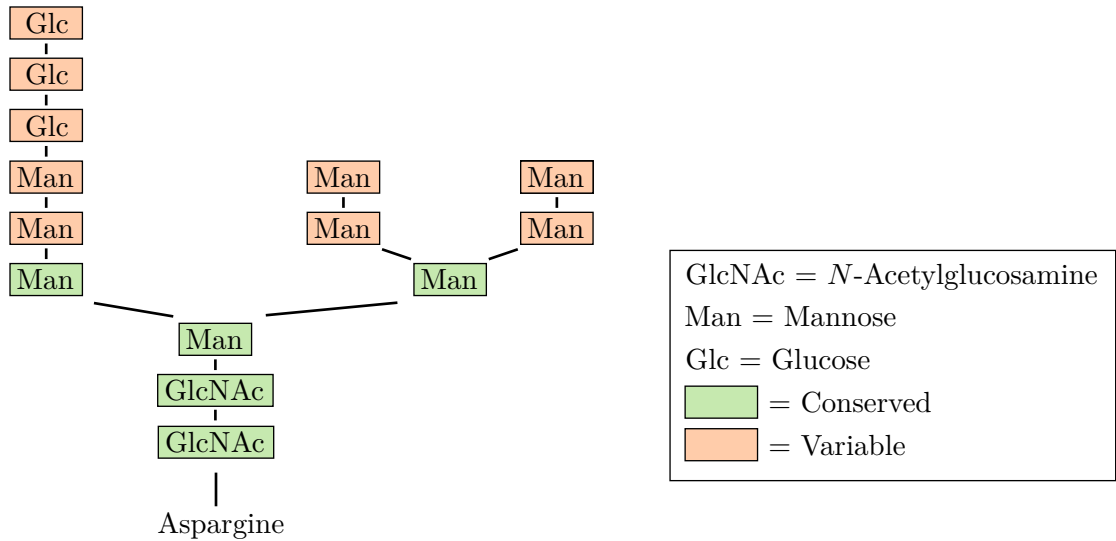


**Figure 2.5.: Structure of the N-linked glycosylation.** The N-linked oligossaccharides are added in the endoplasmatic reticulum to the protein at the amino acid asparagine after the protein synthesis. The depicted core structure is subsequently modified in the endoplasmatic reticulum and Golgi apparatus. The five core residues (highlighted in green) are retained, while the residues in red are replaced by other sugars, often other monosaccharides, like galactose or arabinose. Adapted from [Lodish et al., 2004].

composition of the FMG-1B glycosylation was determined and coincides with the composition of N-linked glycosylation [Bloodgood, 1990b]. The protein glycosylation prevents monoclonal antibodies to protein epitopes of FMG-1B from accessing the protein<sup>7</sup>, i.e. the protein is surrounded by a layer of carbohydrates that prevent the bonding of the antibody to the protein. Evidence of this compact carbohydrate layer on the flagellar membrane is a staining of the flagellar surface by the lectin concanavalin A<sup>8</sup> [McLean et al., 1981] and by antibodies to carbohydrates epitopes of FMG-1B [Bloodgood et al., 1986].

On each flagellum, there are approximately 90000 copies of FMG-1B (this number was estimated from polyacrylamide gel electrophoresis<sup>9</sup> [Adair et al., 1983]), which corresponds to a

<sup>7</sup>A protein epitope is a local region of the protein that is recognized by an antibody, which is specific to this region. Monoclonal antibodies are antibodies produced by clones of the same B lymphocyte parent cell. Different B lymphocytes in the same animal would produce different antibodies (polyclonal) to the same antigen (in this case a protein), as antigens consist of different epitopes. To produce a monoclonal antibody, the B lymphocytes are extracted from an animal (mostly mice), an individual lymphocyte is chosen, and this cell is subsequently cultured to obtain clones producing the same antibody [Alberts et al., 2002; Lodish et al., 2004].

<sup>8</sup>Concanavalin A is a protein that binds to carbohydrates and is used to stain glycoproteins, among other functions.

<sup>9</sup>Polyacrylamide gel electrophoresis is a very common technique in molecular biology to identify proteins by their molecular mass.

protein density of 12000 to 14000 proteins/ $\mu\text{m}^2$  flagellar surface (flagella: 10 to 12  $\mu\text{m}$  in length, 200 nm in diameter). The protein was identified as the adhesion-mediating flagellar membrane protein in a study where the flagella come into contact with a polystyrene microsphere or a glass surface coated with an iodination system [Bloodgood and Workman, 1984]. The flagella-surface contact led to the transfer of radioactive iodine  $^{125}\text{I}$  to the protein that mediated the adhesion, which was then used to identify the adhesion-mediating protein in polyacrylamide gel electrophoresis. The translocation of FMG-1B in the flagellar membrane allows for realizing the surface-associated gliding and transport of microbeads along the flagella that will be discussed below.

### Mastigonemes

Mastigonemes are filamentous structures that can be found on the flagella of protists<sup>10</sup>, and they are especially common among biflagellated algae. The mastigonemes found on *Chlamydomonas* flagella have a length of 0.9 to 1.0  $\mu\text{m}$  with a diameter of 16 nm [Ringo, 1967; Witman et al., 1972; Bernstein and Rosenbaum, 1993; Nakamura et al., 1996]. A single mastigoneme is comprised of approximately 50 identical subunits of a 200 kD glycoprotein of 20 nm in length [Bloodgood, 2009]. The mastigonemes cover the distal two-thirds of the flagella in two rows on opposite sites, with uniform spacing in between the individual polymer filaments [Bergman et al., 1975; Snell, 1976; Nakamura et al., 1996].

The function of flagellar mastigonemes is presumably to increase the flagellar surface area [Bouck, 1971; Nakamura et al., 1996], as cells without mastigonemes on the flagella swim 20 to 30 % slower, while their flagellar beat approximately 10 % faster. The mastigonemes do not mediate adhesion to surfaces, which is required to perform gliding motility [Nakamura et al., 1996] and to translocate beads along the flagellar surface [Bloodgood, 1977]. Furthermore, the mastigonemes are also not involved in the adhesion to another cell during mating [McLean et al., 1974].

### Sexual Agglutinins

The sexual agglutinins, which are termed plus and minus, are solely present in gametic cells and determine their mating type: plus and minus, respectively. Isolated agglutinins have a size of 200 to 250 nm [Adair et al., 1983; Goodenough et al., 1985; Ferris et al., 2005], while they extend approximately 225 nm from the flagellar membrane. The agglutinins are organized into linear rows on the gametic flagellum [Goodenough et al., 1985; Tomson et al., 1990] and have a characteristic cane shape, as seen in rapid-freeze/deep-etch preparations in transmission electron microscopy. The proteins have a large globular head (C-terminal end), a long shaft with a bend or kink, and a smaller globular end (N-terminus) associated with receptor proteins in the flagellar membrane [Adair et al., 1983; Goodenough et al., 1985; Ferris et al., 2005].

---

<sup>10</sup>Protists are unicellular eukaryotic organisms, like microalgae and protozoa. Protists do not form a taxonomic group, but are rather grouped together based on appearance.



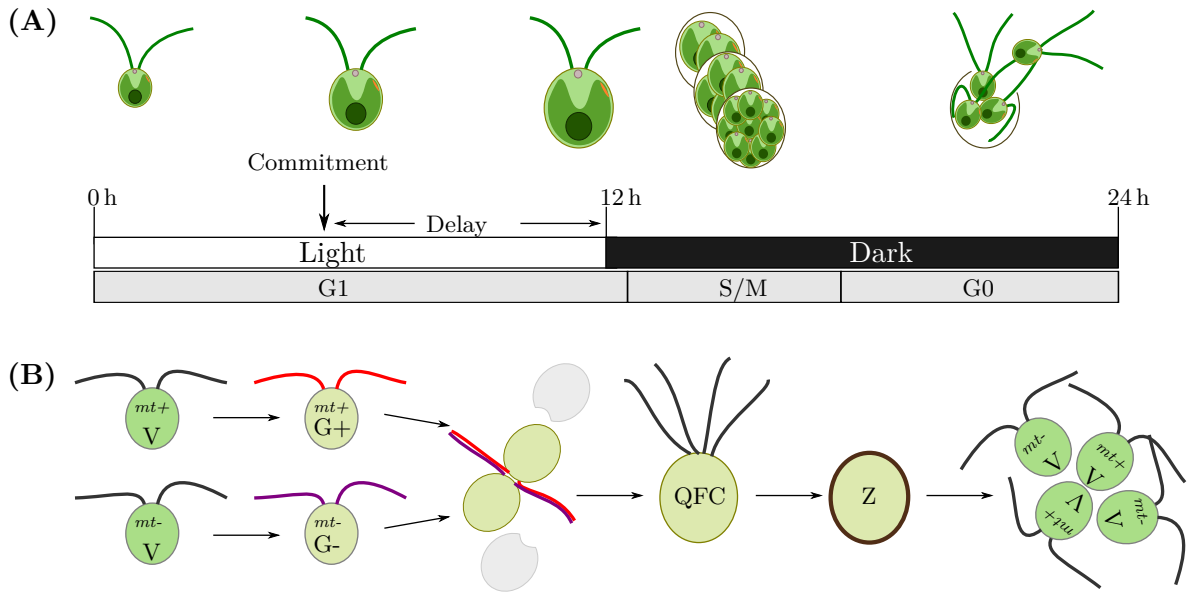


**Figure 2.6.: The two reproduction pathways of *Chlamydomonas*.** (A) Vegetative reproduction. The cell grows during the light period (day) and undergoes several consecutive divisions at the beginning of the dark period (night). After hatching, the cells remain “dormant” until growth starts again at the beginning of the light period, when the cells can perform photosynthesis. (B) Sexual reproduction. Vegetative cells transform to gametes in unfavorable conditions (for example, nitrogen-deprived medium) and express the sexual agglutinins on their flagella (see section 2.3.2). Cells of opposite mating types recognize each other via the plus and minus agglutinins, align their flagella so that the cell apices are in contact, shed the cell wall and fuse to a quadriflagellated cell. Subsequently, a non-flagellated zygote with a thick cell wall is formed, which undergoes meiosis to form four haploid cells once sufficient growth conditions are restored (in the laboratory, light and nitrogen-containing medium).

### 2.3.3. Cell Behavior and Motility

#### The Life Cycles of *Chlamydomonas* – Vegetative Reproduction

The reproduction of *Chlamydomonas* resembles the reproduction of many other microalgae and allows for two different pathways. *Chlamydomonas* cells can undergo vegetative reproduction, where a haploid mother cell divides during a fission phase into several identical haploid daughter cells (see Figure 2.6A). The vegetative reproduction appears under optimal growth conditions and is commonly used in the laboratory to cultivate *Chlamydomonas* cells. Cells in synchronous cultures grow in size during the day phase, when the cells can perform photosynthesis in light, and divide during the night phase in darkness. During vegetative growth, most of the characteristic phases of an eukaryotic cell cycle can be observed: the G1 phase, followed by several repetitions of the S and M phase (the G2 phase is undetected), and a G0 phase (see Figure 2.6A). In the G1 phase, the cell grows in size and multiplies its volume until the G1

phase is terminated at the end of the light period. Several hours before the dark phase (in the G1 phase), the cells commit to divide in the night phase. The commitment is based on a minimal cell volume, calculated to be  $178 \mu\text{m}^3$ , at the commitment point [Umen and Goodenough, 2001], though the cell might grow further after the division commitment. Shortly after the beginning of the dark phase, the cell undergoes multiple divisions (S and M phase<sup>11</sup>) inside the cell wall of the mother cell in quick succession resulting in  $2^n$  daughter cells. After each round of division the daughter cell size determines whether another division round is added, while the total number of division rounds  $n$  is related to the cell size of the mother cell. After completing recurrent division cycles, the daughter cells regrow the flagella. All daughter cells (of all mother cells in the culture) are simultaneously released into the medium shortly before the new day-phase (hatching, controlled by a vegetative lytic enzyme<sup>12</sup>). The growth is delayed in this G0 phase until the beginning of the G1 phase, where the cell can perform photosynthesis. The circadian rhythm of *Chlamydomonas* was studied in various growth conditions, like variations in light intensities and temperature, as well as the persistence of the circadian rhythm when cells were transferred to continuous illumination or darkness.

### The Life Cycles of *Chlamydomonas* – Sexual Reproduction

Another possibility is a sexual reproduction pathway, where two haploid *Chlamydomonas* gametes (of different mating type) fuse to form a diploid zygote that subsequently divides twice to form four haploid vegetative daughter cells (two of each mating type) [Snell and Goodenough, 2009; Harris et al., 2009] (see Figure 2.6B). Lack of nutrients, in particular nitrogen depletion, triggers gametogenesis. Gametogenesis is the transition from vegetative cells to gametes, which leads to an expression of the sexual agglutinins at the flagellar surface. Sexual reproduction promotes more mutations compared to vegetative division, which enhances adaptation to unfavorable environmental conditions. The sexual reproduction can be used to interbreed different strains, or to produce mutants by additional treatment, for example by treatment with ultraviolet light. It is assumed that the common ancestor of all eight groups of modern eukaryotes was sexual, engaging in haploid-diploid transitions. Other commonalities between *Chlamydomonas* and eukaryotes found in all other phylogenetic groups<sup>13</sup> encourage speculations that the “root” eukaryote was very similar to the modern *Chlamydomonas* (see corresponding discussion in [Snell and Goodenough, 2009]).

### Swimming Motility and Phototaxis

In an aqueous environment, the flagella of *Chlamydomonas* perform a breaststroke-like beating with approximately 50 Hz that propels the cell forward with a velocity of 100 to 200  $\mu\text{m/s}$ . During forward swimming, the cell rotates counterclockwise with a frequency of 1.2 to 2 Hz,

---

<sup>11</sup>S phase: DNA replication, M phase: Mitose.

<sup>12</sup>Lysis denotes the disruption of the cell membrane (used, for example, by viruses in their reproduction cycle to release new viruses). A lytic enzyme is an enzyme that controls this process [Lodish et al., 2004].

<sup>13</sup>A phylogenetic group is a group of organisms with common ancestors.

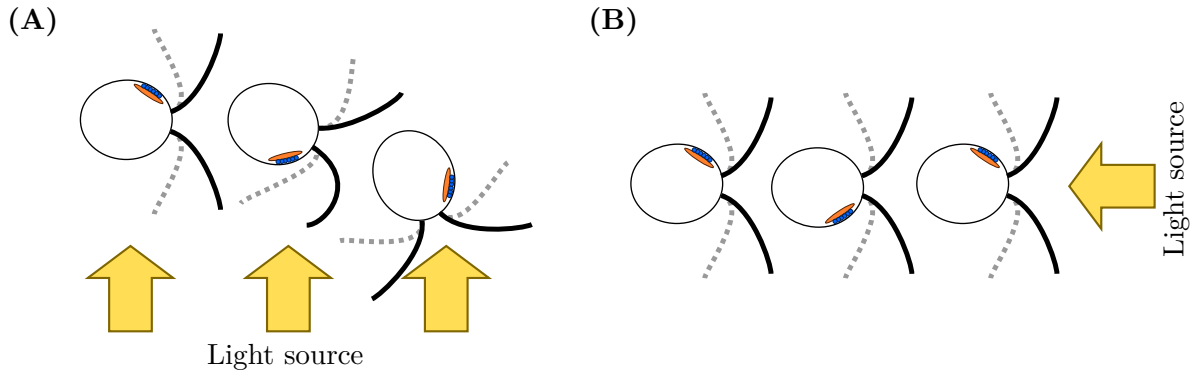


**Figure 2.7.: The work principle of phototaxis in *Chlamydomonas*.** (A) Cell swimming perpendicularly to a light source: the photoreceptors (indicated in blue) are exposed to light incidence solely when the photoreceptors face the light source. The granules in the eyespot, which give the eyespot the distinct orange colour, shield the photoreceptors from light incidence when the cell's photoreceptors face away from the light source. The light incidence triggers photocurrents that lead to changes in the beating waveform of the flagella. These changes in the beating pattern turn the cell towards the light source. (B) Cell swimming towards a light source: continuous light illumination does not trigger photocurrents. Hence, the beating pattern remains unaffected and the swimming direction does not change. The cell continues to swim towards the light source.

which is caused by a slight asymmetry in the beating of the *cis*-flagellum and *trans*-flagellum (see Figure 2.4): the waveform of both flagella differs marginally and the *trans*-flagellum beats transiently faster every 20 beats, whereas the beating of the *cis*-flagellum appears to be very stable, as seen in high-speed cinematography [Rüffer and Nultsch, 1985, 1987]. Besides the forward breaststroke swimming mode, *Chlamydomonas* cells swim backwards in response to sudden bright light exposure. In this swimming mode, the flagella exhibit an undulatory motion comparable to the motion of a sperm's flagellum [Ringo, 1967].

During swimming motion, *Chlamydomonas* exhibits phototaxis, i.e. the cell's swimming is directed by an external light stimulation, to optimize the photosynthesis efficiency. By rotating the cell body along the swimming axis, the eyespot with the photoreceptors scans the environment for the location of the light source [Foster and Smyth, 1980]. If the cell swims perpendicularly to the light source, the channelrhodopsin photoreceptors [Foster et al., 1984; Berthold et al., 2008], located in the eyespot, senses the light solely when the photoreceptors are facing towards the light source due to the permanent cell body rotation (see sketch in Figure 2.7). The photoreceptors trigger photocurrents in the eyespot that induces a flagella photocurrent, which ultimately results in a change in the beating pattern of the flagella [Harz and Hegemann, 1991; Rüffer and Nultsch, 1991]. This modulation of the beating pattern turns the cell orientation towards the light source. Continuous illumination of the eyespot, when the

cell swims towards the light source, does not trigger a photocurrent [Yoshimura and Kamiya, 2001], and the cell maintains its swimming direction.

The photoreceptor was identified by recording action spectra of a population of *Chlamydomonas* cells. A population of *Chlamydomonas* cells that exhibit negative phototaxis was suspended in a petri dish and illuminated from one side with light. As the cells swam away from the light source, the cell density at the edge of the petri dish closest to the light source decreased. The decrease of the cell density in the solution and the extend of the depleted area was quantified after 600 s. The distance the cells traveled, as indicated by the depleted area, was defined as the phototactic rate and quantified for different illumination wavelengths. As a lower absorption probability of the photoreceptor resulted in a smaller phototactic rate, the resultant action spectrum resembled the absorption spectrum of the photoreceptor. This adsorption spectrum was compared to known absorption spectra of other photoreceptors.

The phototactic behavior of an individual cell can either be positive (phototaxis towards the light source) or negative (swimming away from the light source). The transition between positive and negative phototaxis is not completely understood to date, but it is assumed that the efficiency of photosynthesis and the ion concentration in the medium contribute to the transition from positive to negative phototaxis and vice versa [Witman, 1993; Hegemann and Berthold, 2009, and references therein]. The phototactic behavior of cells adapt on short and long timescales to light of varying intensities, and the phototaxis shows a circadian rhythm [Mayer, 1968; Bruce, 1970; Mittag et al., 2005; Hegemann and Berthold, 2009].

### 2.3.4. Dynamic Properties of the Flagellar Membrane

#### Translocation of Microbeads and Gliding

Some of the most remarkable phenomena in *Chlamydomonas* are motility-related effects that are directly associated with glycoprotein dynamics in the flagellar membrane. The protein FMG-1B is actively transported by molecular motors in the plane of the flagellar membrane (i.e. no passive diffusion). This process is temperature-dependent and is induced by the crosslinking of the protein [Bloodgood et al., 1986]. The protein dynamics are visible as the translocation of microbeads along the flagella and the gliding motility of the cell on a substrate (see Figure 2.8). Note that FMG-1B mediates the adhesion between surfaces and the flagella [Bloodgood and Workman, 1984, see section 2.3.2]. Both effects were widely studied by Bloodgood and others; Bloodgood wrote comprehensive reviews on these effects and the underlying mechanisms that shall be recommended for further insights [Bloodgood, 1990b, 2009]. Both reviews serve as background for the following concise overview.

The translocation of objects along the flagellum was observed for microbeads of different surface chemistry (and also non-motile *Escherichia coli*) with velocities of 1.5 to 2.0  $\mu\text{m/s}$

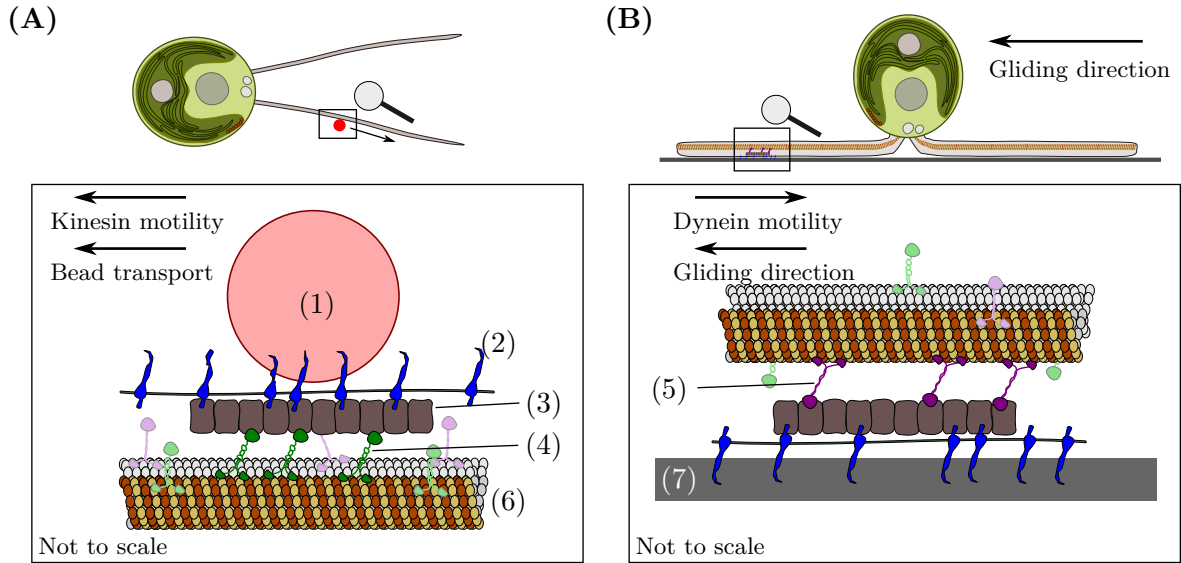


**Figure 2.8.: Flagellar membrane associated motility in *Chlamydomonas*.** The force transduction machinery of *Chlamydomonas* that leads to the translocation of a microbead (1) or gliding on a surface (7) includes: FMG-1B (2) and intraflagellar transport train (3), which are pulled by kinesin (4) or dynein (5). The molecular motors walk on the microtubule (6). (A) Translocation of microbeads: the microbead is attached via FMG-1B to an intraflagellar transport train. The intraflagellar transport train is pulled by molecular motors (in the sketch, kinesin) walking on microtubules, which results in a motion of the microbead in the same direction. (B) Gliding: FMG-1B mediates adhesion to a substrate; this adhesive contact fixates the position of the intraflagellar transport train. Therefore, molecular motors (dynein) connected to the intraflagellar transport train that walk along the microtubule do not move the intraflagellar transport train. Their position with regard to the adhesive contact remains fixed. Instead, the molecular motors pull the microtubules opposite to their walking direction. This microtubule motion leads to a motion of the cell body, as the microtubule is connected to the cell body. That is, the gliding direction is opposite to the walking direction of the dynein motors.

[Bloodgood, 1977]. These objects can travel along the entire length of the flagellum, but can also stop and restart its motion, as well as reverse the direction at any point of the flagellum. The bead motion appears to follow tracks indicated by linear arrays of intramembrane particles in the flagellar plasma membrane that are possibly associated with the outer double microtubules [Weiss et al., 1977]. The beads do not move circumferentially on the flagellar surface or spiral along the flagellum.

Gliding is the motion of *Chlamydomonas* on a substrate without any visible motility of the flagellum compared to the swimming motility. The exact function of gliding motility is not yet

revealed, but might be related to optimizing the photosynthetic yield during surface-association [Bloodgood, 2009, see the discussion about the function of gliding on page 356]. This motility mode has been observed in many other flagellated green algae and protists [Ettl, 1976; Saito et al., 2003], with extensive studies existing only for the *Chlamydomonas* species. During gliding, the *Chlamydomonas* cells spread their flagella in a characteristic gliding configuration  $180^\circ$  from one another. Both flagella can serve as the leading flagellum that determines the gliding direction. The direction of the gliding motion can be stopped and reversed at any time. Gliding occurs at the same speed as the microbead movement at approximately 1 to 2  $\mu\text{m/s}$  and non-gliding mutants do not exhibit microsphere movement [Lewin, 1982; Reinhart and Bloodgood, 1988]. Although this suggests that both processes have commonalities, there is evidence that gliding and microbead movement are distinct from one another. Firstly, some non-gliding mutants isolated by Kozmizki showed microsphere motility [Bloodgood, 2009]. Secondly, microspheres can move in both directions on every flagellum, whereas during gliding the cell is pulled by the flagella [Bloodgood, 1981, 1990b]. Finally, microbead movement involves retrograde and anterograde intraflagellar transport trains<sup>14</sup>, while gliding involves only retrograde intraflagellar transport trains [Shih et al., 2013].

Both motility modes associated with the flagellar membrane, gliding and microsphere movements, are induced by the crosslinking of FMG-1B [Bloodgood et al., 1986; Bloodgood and Salomonsky, 1998]. This crosslinking leads to a dephosphorylation of a phosphoprotein that binds to the cytoplasmic domain of FMG-1B<sup>15,16</sup> [Bloodgood and Salomonsky, 1994, 1998]. Thereby, the protein crosslinking triggers a signal pathway that leads to the directed movement of FMG-1B in the flagellar membrane by intraflagellar transport trains, which are pulled by molecular motors walking on the microtubules. The maximal forces that the intraflagellar transport trains can exert on microbeads in an optical trap are in the order of tens of piconewtons [Laib et al., 2009; Shih et al., 2013]. These forces exceed the stall forces of individual molecular motors (approximately 6 to 8 pN [Svoboda et al., 1993; Shingyoji et al., 1998; Toba et al., 2006]) by approximately one order of magnitude, showing that multiple molecular motors can coordinate to pull the intraflagellar transport trains.

---

<sup>14</sup>Intraflagellar transport trains are particles inside the flagellum that cluster to complexes that can be as large as several hundreds of nanometer. These particle complexes are moved by molecular motors either towards the plus (distal) end of the outer microtubules (kinesin-II motor, anterograde transport, towards the flagella tip of *Chlamydomonas*) or towards the minus (proximal) end (dynein 1b, retrograde transport, towards the cell body). The intraflagellar transport trains presumably transport material for the assembly and maintenance of the flagellar axoneme and membrane [Kozminski et al., 1993; Rosenbaum and Witman, 2002; Kozminski, 2012].

<sup>15</sup>Dephosphorylation: the removal of a phosphate group ( $\text{PO}_4^{-3}$ ) from the protein.

<sup>16</sup>Cytoplasmic domain: the domain inside the flagellar membrane of a receptor that relays signals.

### Flagellar Assembly and Protein Turnover in the Flagellar Membrane

After deflagellation, the flagella of *Chlamydomonas* regrow to full length within 1 to 2 hours, and fully grown flagella maintain a constant length [Rosenbaum et al., 1969; Lefebvre and Rosenbaum, 1986]. The assembly and maintenance of the flagella requires a constant transport of flagellar proteins inside the flagella via intraflagellar transport. At any time, the flagellar membrane is likewise subject to dynamic maintenance processes, termed flagellar membrane turnover, which is mediated by the intraflagellar transport. The turnover of flagellar membrane proteins enables a recovery of the flagellar membrane after treatments that modify or degrade flagellar membrane proteins. *Chlamydomonas* cells placed in a fresh medium after a pronase treatment, which degraded the adhesion-mediating protein, recovered the flagellar adhesiveness within approximately two hours [Bloodgood and May, 1982].

A study that visualizes this turnover process was performed by Bloodgood et al. [Bloodgood et al., 1986]: FMG-1B was labeled with a fluorescence marker, and the redistribution of the labeled proteins was observed. At the beginning, the whole flagellum was uniformly labeled, subsequently, the fluorescence label redistributed in the flagellar membrane and disappeared completely in the end. The fluorescence label visualized the motility of FMG-1B in this process: the proteins were cleared from the proximal end of the flagella (at the cell body) and aggregated at the flagella tips, then the protein aggregates moved from the tip towards the base of the flagellum, and finally new FMG-1B copies appeared on the flagella. The proteins are presumably shed into the medium from the flagellar base, as fluorescent aggregates could be observed in the medium at later stages. This protein turnover is temperature-dependent and occurs at 30°C within a couple of minutes, while at 15°C the same process is significantly slower. At 23°C, the previously described process took about 15 min.

## 2.4. Micropipettes as Tools in Biological Research

Micropipettes are thin, hollow glass capillaries with diameters ranging from several micrometers up to hundreds of micrometers (see Figure A.3 for two micropipettes of different size). They are a common tool in life sciences that enable precise manipulations in biological systems and good characterizations of processes in living systems ranging from individual cellular components, via unicellular organisms, to multicellular clusters. The micropipette's characteristics and geometry can be adapted to the research question allowing for many different applications, including force measurements.

### 2.4.1. Micropipettes as Object Support and Injection Needles

One of the most common applications of micropipettes is their use as an injection needle (see Figure 2.9A) or support for any kind of object. As the micropipette is hollow, applying suction pressure at the end allows the user to hold, for example, a cell without any type of glue.

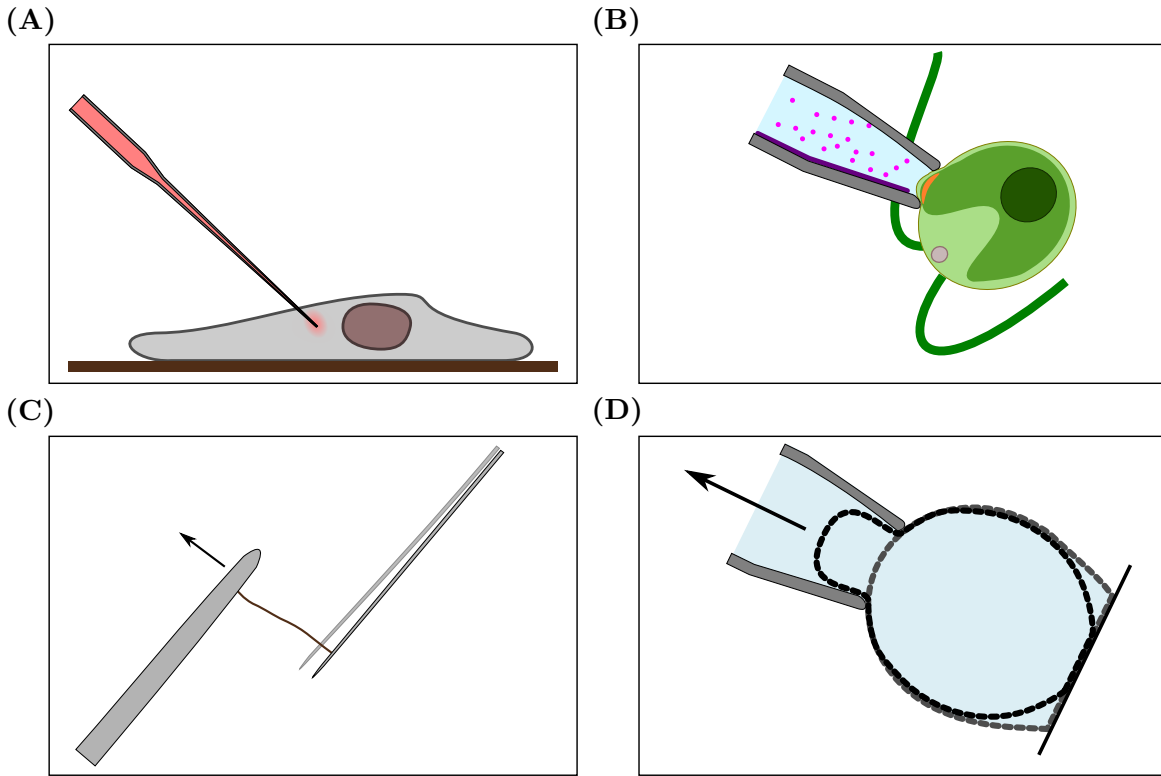


**Figure 2.9.: Sketch of different applications of micropipettes in the life sciences.**

(A) Micropipette as an injection needle: a thin, sharp micropipette is used to inject a drug (indicated in red) into a cell. (B) Micropipette in a patch-clamp system: the eyespot of a *Chlamydomonas* cell, indicated in orange, is sucked into a micropipette filled with an ion solution. A light stimulus triggers the photoreceptors in the eyespot, which opens ion channels. The ions flow into the cell, which results in a current that can be measured [Harz and Hegemann, 1991]. (C) Micropipette as force sensor: an actin filament is attached to the end of a thick, stiff micropipette and a thin, soft micropipette cantilever. The cantilever deflects, when the stiff micropipette is moved, until the actin filament ruptures [Kishino and Yanagida, 1988]. (D) Micropipette aspiration: A vesicle attached to a substrate is sucked in the micropipette. The applied pressure difference is correlated with the change in the contact area at the surface and the deformation of the vesicle to determine the membrane tension and adhesion energy to the substrate [Evans, 1980].



Using this approach, the beating pattern of the *cis*- and *trans*-flagellum of *Chlamydomonas* was monitored and analyzed after external light stimulation in order to understand the phototactic behavior [Rüffer and Nultsch, 1987, 1991]. With a *Chlamydomonas* cell held still by the micropipette, the flow field around the cell was computed from the trajectories of tracer particles that are moved by the flagella in the fluid [Drescher et al., 2010]. Finally, micropipettes as cell supports are employed to reconcile the debate whether the *Chlamydomonas* flagella are coupled via hydrodynamic interactions or whether the flagella synchronization originates from a direct mechanical connection in between the basal bodies of the flagella [Wan et al., 2014; Wan and Goldstein, 2016]. The latter study also shows that several micropipettes can be used in parallel, and in particular that a second micropipette can be used to physically manipulate a *Chlamydomonas* cell by removing a single flagellum [Wan and Goldstein, 2016].

These few examples from settings studying *Chlamydomonas* give only a glimpse of the possibilities of how micropipettes can be used in biological settings. Micropipettes are regularly employed in electrophysiology studies using the patch-clamp technique to measure receptor signals produced by ion channels in neurons and axons, muscle fibers, or the *Chlamydomonas* eyespot (see Figure 2.9B, [Neher and Bert, 1976; Sakmann and Neher, 1984; Harz and Hegemann, 1991]). The combination of two micropipettes is used in some *in vitro* fertilization methods, where one micropipette serves as support for the egg, while a second, thin and sharp micropipette is used as an injection needle to insert a sperm cell into the egg. Many more applications exist that employ micropipettes directly as support or indirectly to manipulate any kind of biological system.

#### 2.4.2. Micropipettes as Force Sensors

The physical properties of micropipettes can be used to study mechanical properties and forces in biological systems. The thin, tapered part of a micropipette with diameters of tens of micrometers and fewer has a low bending rigidity; this soft glass filament can be employed as a cantilever to measure forces. Thereby, the force acting on the glass cantilever is coupled via the filament's elastic modulus to its deflection. In the last decades, this application was used to measure forces and force transduction in systems of various size and complexity.

First attempts of this application were published in 1960 when Yoneda measured the torque applied by a single cilium on a flexible glass micro-needle [Yoneda, 1960]. Later, a micropipette cantilever technique was used to measure the forces of microtubules sliding in the flagellum of a sea urchin sperm cell (see Figure 2.9C, [Kamimura and Takahashi, 1981]), the rupture forces of actin filaments, and to estimate the forces generated by myosin motors [Kishino and Yanagida, 1988]. In these studies, the cantilever was monitored optically and the deflection was determined by an auto-correlation analysis of the cantilever's position from consecutive optical photographs. Due to the high magnification (100x oil immersion objective) and spring

constants of 1 to 10 pN/ $\mu\text{m}$ , a piconewton force resolution was achieved [Kishino and Yanagida, 1988].

Micropipette force spectroscopy was further used to study the tensile strength of biofilms, microbial flocs, and colloid-polymer flocs [Yeung and Pelton, 1996; Poppele and Hozalski, 2003]. A similar experimental configuration was used to study adhesion and mechanical properties of bacteria, vesicles and living cells [Tsang et al., 2006; Colbert et al., 2009], and the mechanical properties and propulsion forces of *Caenorhabditis elegans*, a small nematode of approximately 1 mm size [Backholm et al., 2013; Schulman et al., 2014]. Besides these direct force measurements, micropipette aspiration was used to determine the membrane tension of vesicles and cells and their adhesion energies to substrates (see Figure 2.9D [Evans, 1980; Hochmuth, 2000; Prechtel et al., 2002]).

## 2.5. Intermolecular Interactions and Surface Forces

From a macroscopic view, *Chlamydomonas* adheres with its flagella to substrates. On a mesoscopic scale, the adhesion of *Chlamydomonas* to substrates is mediated by the proteins on the flagellar surface that interact with the substrate (see Figure 2.8). At a microscopic level, the individual atoms that build the protein macromolecule interact with the atoms of the substrate and surrounding medium. These attractive and repulsive interactions add up to a resulting attractive adhesion force of the cell's flagella to the substrate.

From the four fundamental interactions, only interactions that are electromagnetic in origin are relevant for the description of the adhesion process<sup>17</sup>. The fundamental electromagnetic interactions between atoms and molecules arise as different intermolecular interactions that I briefly introduce in the following. Thereby, I consider the most important interactions and forces between surfaces and particles in aqueous environments: electrostatic interactions, van der Waals interactions, steric repulsion, and hydrogen bonds and hydrophobic forces. The overview is based on the textbook of Israelachvili [Israelachvili, 1991] and the review of Leckband and Israelachvili [Leckband and Israelachvili, 2001] that are recommended for a more detailed description.

### 2.5.1. Electrostatic Interactions

Electrostatic or Coulomb forces arise between all charged atoms, molecules, and surfaces in aqueous environment. The electrostatic interaction potential between macromolecules or sur-

---

<sup>17</sup>The four fundamental interactions are strong and weak interaction acting between elementary particles on a sub-atomic level, gravitational forces acting between atoms and molecules, and electromagnetic interactions likewise between atoms and molecules.

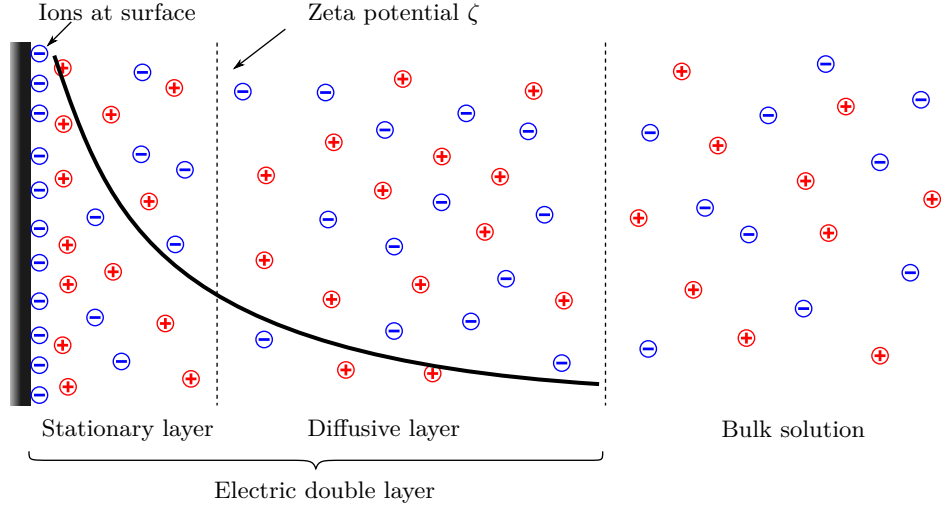


**Figure 2.10.: Surface charges and ion distribution in aqueous environment.** Any surface in aqueous solution carries charges that form a stable layer on the surface and a diffusive layer of ions in close proximity to the surface. The electrical potential indicated by the solid line, caused by the asymmetric ion distribution close to the surface, decays with the Debye length  $1/\kappa$ . The Zeta potential  $\zeta$  is the electrical potential at a slipping plane, i.e. the potential difference between the bulk solution and a stationary ion layer at the surface.

faces follows an exponential function of their separation distance  $d$ :

$$W(d) \approx C_{\text{ES}} e^{-\kappa d}, \quad (2.1)$$

where  $C_{\text{ES}}$  depends on the geometry of the interacting surfaces, their surface charge density and the ion solution. The Debye length  $1/\kappa$  describes the distance at which the electric potential of any net charge is reduced to  $1/e$ . The Debye length gives a measure for the interaction range and is related to properties of the solution via

$$\kappa^{-1} = \left( \frac{\epsilon \epsilon_0 k_B T}{I e^2} \right)^{\frac{1}{2}}, \quad (2.2)$$

whereby  $\epsilon$  is the relative permittivity or dielectric constant of the solution,  $\epsilon_0$  the vacuum permittivity or electric constant,  $k_B$  the Boltzmann constant,  $T$  the temperature,  $e$  the elementary charge, and  $I = \sum_i \rho_{\infty,i} z_i^2$  the ionic strength of the solution, which in turn depends on the concentration of a specific ion  $\rho_{\infty,i}$  and the ion's valence  $z_i$ . The Debye length in the Tris-Acetate-Phosphate (TAP) growth medium used as buffer solution in the experiments is  $1/\kappa_{\text{TAP}} = 1.80 \text{ nm}$  (see Table 3.1 for the TAP medium composition). The Debye length in the minimal medium used to differentiate cells into gametes is  $1/\kappa_{\text{NMM}} = 2.64 \text{ nm}$  (see section 3.2) [Berthold et al., 2008].

Although a surface or object might not be charged in air, in a liquid the ionization or dissociation of surface groups and the adsorption of ions from the solution lead to a net charge. In aqueous environments, the electrochemical properties of the surface or macromolecule, like proteins, ultimately determine the surface charge in conjunction with the ion concentration of the solution and its pH value. The sign and amount of the charge is described by the Zeta potential  $\zeta$  on the surface, which gives rise to the isoelectric point, the pH value at which the substrate has no net charge. Besides forming a stable layer at any surface in an aqueous environment, the ions further screen the electrostatic interactions by forming a second layer of diffusive ions. This phenomenon of an electrical double layer around any object in an ion solution was first described by Helmholtz [Helmholtz, 1853] and further advanced by Gouy and Chapman, Stern, and others [Gouy, M., 1910; Chapman, 1913; Stern, 1924]. The Zeta potential is the electric potential of the electric double layer with regard to a point with infinite distance to the charged surface. Consequently, the Zeta potential depends on the ion concentration and can only be compared for measurements performed with the same medium and technique.

In summary, surfaces and macromolecules carry charges in an aqueous solution. The amount and sign of the charges depend on the pH value of the solution and the ion concentration. The Coulomb forces between these charges lead to either attraction or repulsion between the surface and the macromolecule.

### 2.5.2. Van der Waals-Interactions

Van der Waals interactions encompass three types of interactions between electrical dipoles: Keesom interactions, Debye interactions and London dispersion interactions [Israelachvili, 1991]. Keesom interactions describe dipole-dipole interactions of permanent dipoles. Debye interactions characterize the forces between a permanent dipole and a dipole induced by the electric field of the permanent dipole. Finally, London dispersion forces arise from interactions between two instantaneously induced dipoles that exist for any atom or molecule even if their time-averaged dipole moment is zero, as the electrons are delocalized and constantly move in the electron cloud. All of these three interactions have in common that their interaction potentials scale with  $W(d) \sim d^{-6}$  for molecular systems.

Similar to electrostatic interactions, the interaction potential of the van der Waals interactions changes with the system's geometry. For macroscopic systems, for example, a macromolecule like a protein of radius  $r$  interacting with a substrate, the interaction potential in a distance  $r$  ( $r \gg d$ ) is:

$$W(d) = -A \frac{r}{6d}, \quad (2.3)$$

where  $A$  is the Hamaker constant. The value of the Hamaker constant can be derived from the static dielectric constants and refractive indices of the involved materials using the Lifshitz theory [Israelachvili, 1991, and references therein]. For heterogeneous biological materials, these

material properties are not accessible. Thus, the interaction potential of the van der Waals interactions can only be estimated.

A tool to study van der Waals interactions between microorganisms and substrates are multi-layered materials, where each layer has a different interaction strength with the object. Model substrates that represent such a multi-layered material are silicon (Si) wafers with a silicon dioxide (SiO<sub>2</sub>) layer of tunable thickness [Loskill et al., 2012a]. The van der Waals interactions between a silicon substrate with SiO<sub>2</sub>-layer and a protein can be written as:

$$W_{\text{vdW},\text{total}} = W_{\text{Si}} + W_{\text{SiO}_2}, \quad (2.4)$$

where  $W_{\text{Si}}$  denotes the interaction with the underlying silicon, and  $W_{\text{SiO}_2}$  denotes the interaction with the oxide layer on top of the bulk material. The interaction potential of FMG-1B in a distance  $d$  to a silicon substrate with an oxide layer with thickness  $d_{\text{SiO}_2}$  is:

$$W_{\text{Si native}} \sim \frac{A_{\text{Si-FMG-1B}}}{d + d_{\text{SiO}_2}} + \frac{A_{\text{SiO}_2\text{-FMG-1B}}}{d}, \quad (2.5)$$

where  $A_{\text{Si-FMG-1B}}$  denotes the Hamaker constant (see section 2.5) of the Si-FMG-1B interactions and  $A_{\text{SiO}_2\text{-FMG-1B}}$  the Hamaker constant of the SiO<sub>2</sub>-FMG-1B interactions. Equation 2.5 is valid for the interaction of a macromolecule with a surface (see Equation 2.3). In case of another geometry the argumentation holds true, whereas the interaction length may decrease (larger exponent in the denominator).

The contribution of the underlying silicon substrate (first term in Equation 2.5) to the overall van der Waals interactions can be altered by tuning the SiO<sub>2</sub>-layer thickness. It can be assumed that the interaction strength between FMG-1B and silicon is larger than the interaction strength between FMG-1B and SiO<sub>2</sub> [Sze and Ng, 2006; Loskill et al., 2012a]<sup>18</sup>. The interaction between FMG-1B and Si is negligible in case of a silicon wafer with thick oxide layer, due to the large distance between FMG-1B and the Si layer ( $d_{\text{SiO}_2} = 150 \text{ nm}$ ). Consequently, the total interaction strength between FMG-1B and a wafer with thin silicon oxide layer ( $d_{\text{SiO}_2} = 1.7 \text{ nm}$ ) is larger compared to a wafer with thick silicon oxide layer, as the “strong” interaction with the bulk silicon material is absent.

### 2.5.3. Steric Repulsion

On a microscopic atomic scale, the steric repulsion between atoms originates from the overlap of their associated electron clouds. There is no general description of the interaction potential, yet, there are three commonly used short-range repulsive interaction potentials: the hard sphere

---

<sup>18</sup>The properties that determine the interaction strength are the dielectric constant and refractive index of Si and SiO<sub>2</sub>, and FMG-1B. The van der Waals interactions between FMG-1B and these substrates differ, as the dielectric constant and refractive index vary significantly for Si and SiO<sub>2</sub>.

potential, the inverse power-law potential, and the exponential potential. On a molecular scale, the potential is often characterized with a  $r^{-12}$  power-law<sup>19</sup>. In combination with attractive Van der Waals interactions between atoms and molecules, this choice for the steric repulsion results in the Lennard-Jones potential:

$$W(r) = \frac{B}{r^{12}} - \frac{C}{r^6}, \quad (2.6)$$

where  $B$  and  $C$  include characteristics of the interacting atoms relevant for the steric repulsion and van der Waals interactions, respectively.

#### 2.5.4. Hydrogen Bonds and Hydrophobic Interactions

Hydrogen bonds are best-known for their appearance between water molecules, yet, in general hydrogen bonds may occur between electronegative atoms (e.g. O, N, F and Cl) and H atoms. A hydrogen atom that is covalently bound to an electronegative atom becomes positively polarized, thus allowing for attractive interaction with another electronegative atom. Although the hydrogen bonds are of electrostatic origin, they share some characteristics with covalent bonds. The hydrogen bonds are rather weak and directional, which may allow for building weak three-dimensional structures in solids or may lead to a significantly increased range of the short-range order in liquids. Hydrogen bonds can appear between atoms of the same molecule or between different molecules. Hydrogen bonds play an important structural role, especially in macromolecules like proteins.

The polarity of water and the affinity of water molecules to form hydrogen bonds immediately affect any object and surface immersed in water. As the water molecules cannot form hydrogen bonds with a nonpolar surface, the water molecules realign to maximize the amount of hydrogen bonds with neighboring water molecules. Bringing two nonpolar surfaces in contact decreases the total polar surfaces area, which results in an entropy increase in the system, as fewer water molecules realign in that case.

The strength of the hydrophobic interactions depends on the polarity of the two surfaces immersed in the aqueous solution. This type of interaction can be described as electron-acceptor–electron-donor interactions and the interaction strength depends on the electron-acceptor and electron-donor parameter of the involved materials. These parameters can be deduced from contact angle measured with three different liquids and determine the Lewis acid-base contribution of the surface energy  $\gamma^{AB}$  [van Oss, 1993]. For two nonpolar surfaces (hydrophobic) with  $\gamma^{AB} = 0 \text{ mJ/m}^2$ , the resulting hydrophobic interaction becomes attractive, while two polar (hydrophilic) substrates repel each other.

---

<sup>19</sup>The exponent is normally taken between 9 and 16.

## 3. Materials and Methods

The goal of this work is to quantify adhesion forces of microalgae to surfaces and to characterize the adhesion mechanism of microalgae in different experimental conditions. In the next sections, I first describe the general principle of the micropipette force spectroscopy technique that was employed to study the adhesion of *Chlamydomonas*, and the requirements of the experimental setup to perform force spectroscopy experiments. Then, I introduce the different microalgae strains studied in this work, their specific growth conditions and growth media, and the buffer solutions for the experiments in aqueous environment. Subsequently, I characterize the properties of the different substrates employed in the adhesion experiments, and I describe the experimental routines and protocols of the force spectroscopy experiments. Finally, the data analysis methods will be covered.

### 3.1. Micropipette Force Spectroscopy

Micropipette force spectroscopy is a force spectroscopy technique that employs the deflection of a micropipette cantilever to measure forces in biological systems (see section 2.4 for an overview of applications of micropipettes). The deflection of the cantilever is detected using optical microscopy, where the force sensor, the object, like a *Chlamydomonas* cell, and its proximity are monitored. This visualization allows for quantitative force-shape and force-deformation correlations. Due to this technique's adaptability, force ranging from piconewtons to millinewtons can be accessed for objects ranging in size from nanometers to millimeters. In this study, the force sensor holds the microalgae by a small suction pressure enabling non-invasive force-spectroscopy studies with living organisms.

The micropipette force sensor is a thin hollow glass filament, commonly referred to as micropipette, that was bent in a characteristic shape (see Figure 3.1A+B) with a long flexible cantilever. The deflection of the cantilever was extracted from optical micrographs of the force sensor via an auto-correlation analysis (compare Figure 3.1C-E). The cantilever's deflection translates linearly via the cantilever's spring constant into the corresponding force acting on the cantilever, i.e. there is a linear relation between the deflection and the force acting on the cantilever (Hooke's law, see the calibration of the cantilever in Figure 3.4). This general principle to measure forces by the deflection of a cantilever is identical to the work principle of an atomic force microscope, the most common technique to measure single-cell and single-molecule interactions with a substrate, for example. In the following sections, I further portray

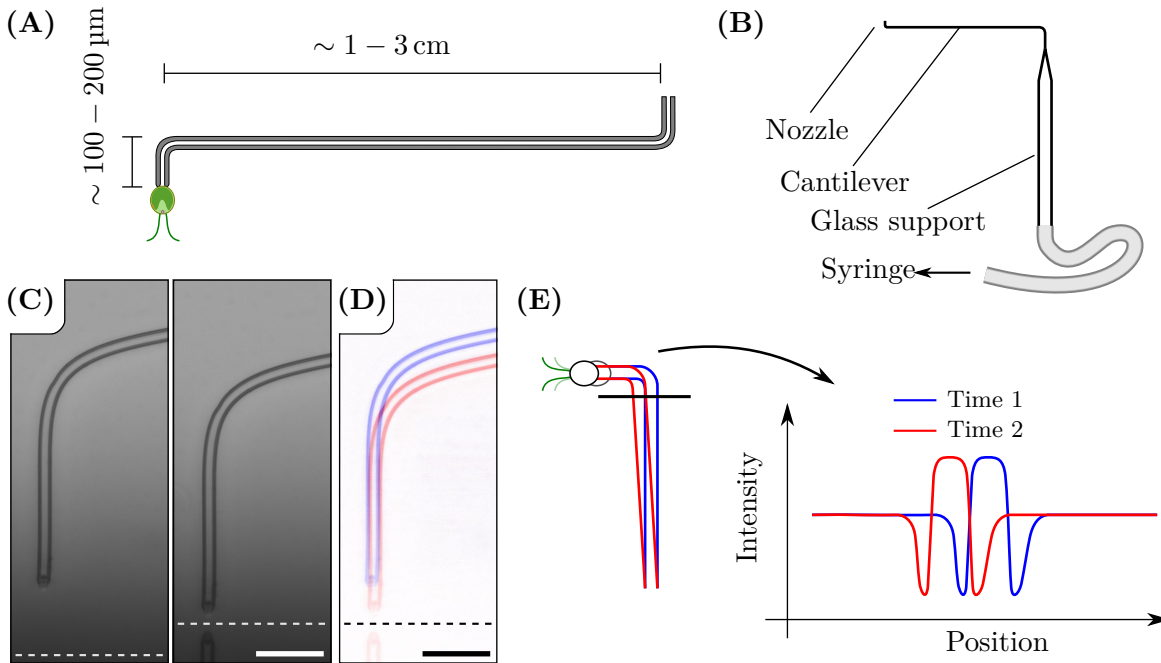


**Figure 3.1.: Work principle of micropipette force spectroscopy.** (A) Sketch of the micropipette cantilever exhibiting the double-L shape. (B) Sketch that shows an overview of the whole force sensor. (C) Unprocessed optical micrographs from an experiment showing the force sensor at the zero-force position (left-hand side) and the deflection of the force sensor at a later timepoint (right-hand side). The dashed line indicates the substrates's position. Scale bar:  $50 \mu\text{m}$ . (D) Overlay of the micropipette force sensor positions from the panels in (C) extracted with an edge detection algorithm. (E) Detection of the cantilever's deflection via an auto-correlation analysis, where the intensity profile of the cantilever is extracted from optical micrographs. The spatial shift of the intensity profiles at different timepoints provides the deflection.

the characteristics and calibration of the micropipette force sensor, followed by an introduction in the detection of the cantilever's deflection, and a full summary of the experimental setup. I will refer to different parts of the micropipette force sensor throughout this work using the following terminology (see Figure 3.1B):

- **Micropipette:** A thin hollow glass filament, which was produced from a glass capillary.
- **(Micropipette) force sensor:** A force sensor made out of a micropipette.
- **(Micropipette) cantilever:** The flexible part of the force sensor that deflects during force spectroscopy, i.e. the part that detects the force.
- **Nozzle:** The opening of the micropipette at the cantilever's end.



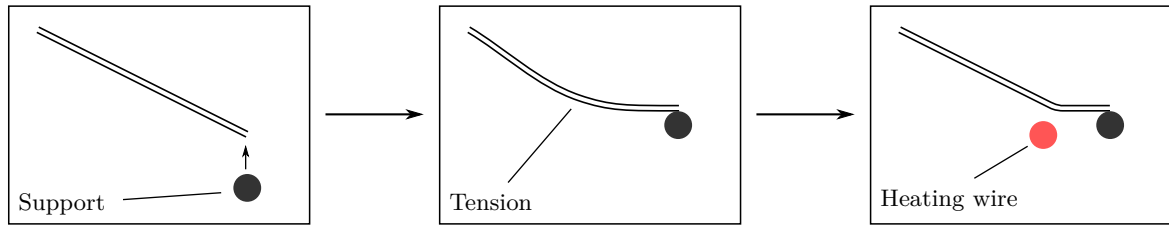


**Figure 3.2.: Sketch of the steps employed to bend a micropipette.** A support is pushed against the straight micropipette, which creates a reversible, elastic bending of the micropipette. Subsequently, the micropipette is locally heated, which releases the tension and results in an irreversible kink. These steps are repeated until the desired bending angle is achieved.

### 3.1.1. A Micropipette Cantilever as Force Sensor

The micropipette force sensors were made from borosilicate glass capillaries with initial outer diameter of 1 mm (World Precision Instruments, Inc., Sarasota, Florida, USA; TW100-6)<sup>20</sup>. These glass capillaries were clamped in a pipette puller (Sutter Instrument, Novato, California, USA; P-97) and heat was applied at the center of the capillary with the heating filament of the pipette puller. When the glass was melting, the ends of the glass capillary were pulled apart resulting in a tapered, straight micropipette of tens of micrometer in diameter and several centimeter in length. Subsequently, the end of the micropipette was cut to obtain a straight opening, the edges of the opening may be rounded by applying heat. Then, this straight micropipette was bent with a microforge (Narishige Group, Tokyo, Japan; MF-900) into the final shape of the force sensor. Therefore, the flexible part of the micropipette was held under tension (by pushing the nozzle against a support, such as a metal wire) and locally heated, which resulted in the release of the tension by the formation of a kink (see Figure 3.2). I repeated this process until the kink formed an angle of  $90^\circ$ , subsequently, the second kink was forged in the same manner.

The final force sensor consisted of three different parts: the glass capillary support, the micropipette cantilever, and the nozzle (see Figure 3.1B). The glass support was used to hold the micropipette with a pipette holder (Narishige Group, Tokyo, Japan; H-7) that was mounted on a three-axis micromanipulator (see below). At the end of the support, the glass capillary tapered from an initial diameter of 1 mm to the micropipette: a glass filament of tens of micrometer diameter that further tapered to a final diameter of approximately  $10\text{ }\mu\text{m}$  at the nozzle (over the course of several centimeters). This thin part was bent by  $90^\circ$  to create a flexible cantilever. At the end, the cantilever was bent a second time by  $90^\circ$  (in the same plane like the first kink) to create a nozzle that was oriented normal to the cantilever. The nozzle of

<sup>20</sup>Other experimental configurations might require glass capillaries with a different outer diameter or wall thickness.

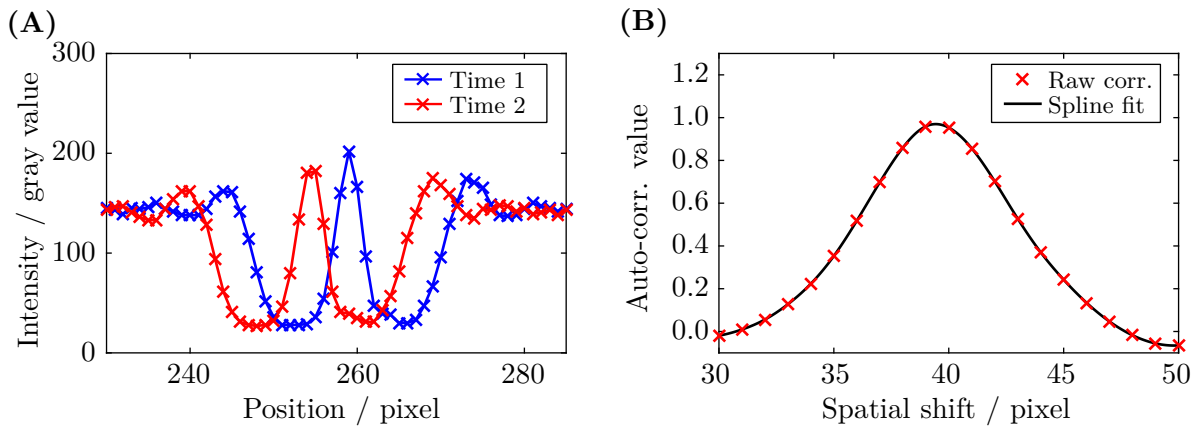


**Figure 3.3.: Auto-correlation analysis to detect micropipette deflections.** (A) Intensity profiles of the exact same micropipette cantilever at two different times. (B) Auto-correlation profile of the cantilever's intensity profile between two different timepoints.

the micropipette had a diameter of about 5  $\mu\text{m}$ , so that it could hold a *Chlamydomonas* cell<sup>21</sup>. At the nozzle, the microalgae was held in place with a suction pressure created by a syringe (more fragile objects, like vesicles, can be held with a fluid pump) that was connected to the glass capillary support via tubes<sup>22</sup>.

### Detection of the Cantilever's Deflection via an Auto-Correlation Analysis

In the experiments, I measured the cantilever's deflection, which was converted into forces created by the object attached to the cantilever using the cantilever's spring constant. The micropipette cantilever's deflection is the spatial displacement of the cantilever at the nozzle (see Figure 3.1C+D). This spatial shift was detected with an auto-correlation analysis of the cantilever's intensity pattern in different optical micrographs. To obtain the cantilever's intensity pattern, I extracted the intensity values along a single line perpendicular to the cantilever in the optical micrographs, which were grayscale digital images<sup>23</sup> (see the black line in Figure 3.1D+E). These intensity profiles show a distinct pattern at the cantilever's position in each individual image (see Figure 3.3A). As the position of the line remains fixed, the spatial shift in the micropipette's position translates to a displacement of the micropipette signature in the intensity profiles. The auto-correlation analysis spatially shifts the intensity profiles extracted from two images with regard to each other and returns a measure of the overlap as a function of the shift. This correlation value corresponds to the match between the intensity profiles

<sup>21</sup>The diameter of the nozzle and cantilever were adapted to the size of the object, for example, they are larger for *Volvox* colonies with a diameter of several hundreds of micrometer (see Figure B.1).

<sup>22</sup>The suction pressure is created by lowering the syringe below the level of the micropipette. This hydrostatic pressure difference can be calculated by  $\Delta p = \rho g \Delta h$ , where  $g$  is the gravitational acceleration,  $\rho$  the fluid density, and  $\Delta h$  the height difference between the syringe and the micropipette's nozzle.

<sup>23</sup>In this work most images exhibit a depth of 8 bits, i.e. 256 different intensity values from zero (black) up to 255 (white).

of the two lines, with a larger value indicating a better match. Consequently, the correlation value is maximal when the shifted intensity profiles exhibit the best match. The spatial shift required to maximize the correlation function corresponds to the deflection of the cantilever (see Figure 3.3).

I performed the auto-correlation analysis in MATLAB with the in-build *xcov*-function. This function returns raw correlation values as a function of the shift in pixels, as the digital image information is exclusively stored at discrete locations. The maximum of the correlation function normally lies in between two pixels, as the optical micrographs store the cantilever's intensity signal at discrete locations, whereas the underlying cantilever's intensity signal is a continuous function in space. The analytical auto-correlation of the underlying cantilever signal would yield a continuous correlation function with a precisely defined global maximum. That is why the resolution of the discrete raw auto-correlation could be improved by determining a function that resembles the shape of the raw MATLAB analysis output. The experimental equivalent would be to improve the resolution, for example, by objectives with a higher magnification. I extracted the functional shape of the underlying analytical auto-correlation function by fitting the raw correlation function using a non parametric *spline*-function. The maximum of this function yields a sub-pixel resolution of the auto-correlation analysis. For a further discussion on the choice of the *spline*-fit see the discussion in section A.1.

### Micropipette Cantilever Calibration

To determine the cantilever's spring constant, I correlated the change in the cantilever's deflection with the change in the forces acting on the cantilever. Therefore, I measured the force and the corresponding cantilever's deflection simultaneously from a time series of optical micrographs. The "known" force acting on the cantilever was either the gravitational force of a water droplet (added mass method) or the restoring force of another cantilever (reference cantilever method).

In the **added mass method**, the cantilever was deflected by the gravitational force of a water droplet. The water droplet is created by pushing liquid through the micropipette's nozzle. During the calibration, the micropipette force sensor was oriented such that the glass capillary support is parallel to the direction of the gravitational force (see above, compare Figure 3.1B). In this configuration, the direction of the cantilever's deflection during the calibration was identical with the deflection in the force spectroscopy experiments (see Figure 3.4A+B). The calibration was performed by monitoring the temporal evolution of the cantilever's deflection and the water droplet's volume (see Figure 3.4C), which I converted into the gravitational force acting on the cantilever. The gravitational force as a function of the micropipette's deflection yielded a linear force-deflection relation for deflections up to several hundreds of micrometer (see Figure 3.4D). Thus, the cantilevers were Hookean springs with the proportionality constant of the force-deflection relation being the spring constant of the cantilever.

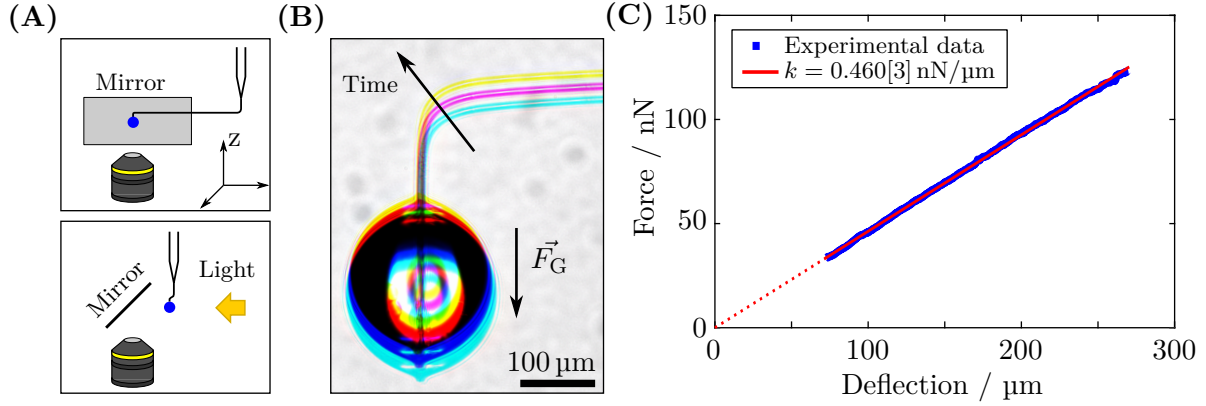


**Figure 3.4.: Force sensor calibration with a variable added mass.** (A) Experimental setup to calibrate the micropipette with an added variable mass. The lower panel is rotated by  $90^\circ$  around the  $z$ -axis. (B) Optical micrographs of the calibration of a reference cantilever. The gravitational force of a water droplet added on the micropipette deflects the micropipette. (C) Force and deflection extracted from optical micrographs as seen in (B). The micropipette cantilever yields a linear force-deflection relation.

The crucial part of this calibration method was the calculation of the gravitational force using the volume of the water droplet. To measure the volume of the droplet, I detected the outline and area of the water droplet's two-dimensional projection in the optical micrographs. Subsequently, the volume of the droplet was determined by rotating the two-dimensional projection around the droplets symmetry axis. The symmetry axis is an axis through the centroid of the droplet's area parallel to the direction of the gravitational force. Note that this method assumes a rotational symmetric water droplet (compare Figure 3.4C). The size of the water droplets was smaller than the capillary length of water ( $\approx 2.7 \text{ mm}$  at  $25^\circ\text{C}$ , see Figure 3.4B), i.e. gravitational forces did not deform the droplets. The error in the water droplet method was predominantly determined by the error in the volume of the water droplet. The method assumed a rotational symmetric water droplet, which was not always the case when the droplet was pinned at the kink of the cantilever (see Figure A.4B+C). Independent calibration runs with the same cantilever yield an error below 10 to 20 %, while the error of the individual measurement was much smaller (compare the confidence interval of the fit in Figure 3.4C).

In the **reference cantilever method**, a reference cantilever pushes against the uncalibrated cantilever deflecting both cantilevers according to Newton's third law. In this process, the ratio of the deflection change of both cantilevers is equal to the ratio of the inverse spring constants (i.e. the stiffer cantilever deflects less). In this method, the reference force sensor can be an atomic force microscope cantilever of known spring constant, or a second micropipette, which was calibrated, for example, with the previously described added mass method. In this

work, I used carefully calibrated micropipettes as reference force sensors (see Figure 3.4B for snapshots from a reference cantilever’s calibration). The error between several calibration runs with the same reference cantilever was as large as 20 % consistent with the error of the spring constant reported for atomic force micropipette cantilevers calibrated with the reference cantilever method [Gibson et al., 1996; Gates et al., 2011].

The micropipette cantilevers used in this study were usually calibrated using the water droplet method with three individual calibration runs for the same force sensor. Independent validations of the calibration with the reference cantilever method yielded consistent spring constants; the difference of the spring constants resulting from both methods was smaller than the error of the calibration methods itself. In the case of suboptimal water droplet configurations (see Figure A.4B+C), I did not observe any systematic deviations from independent calibrations of the same cantilever with the reference cantilever method.

In conclusion, the design of the micropipette force sensor guarantees a precise measurement of *Chlamydomonas* adhesion forces. The location of the first kink, directly after the tapered part, ensured that there was only one flexible part of the force sensor that deflected in the experiments. The spring constants of the force sensors varied between 0.1–2 nN/ $\mu\text{m}$ , depending on the length and diameter of the cantilever. Most experiments were performed with cantilevers exhibiting spring constants below 0.5 nN/ $\mu\text{m}$ , which is up to three orders of magnitude softer than cantilevers employed in atomic force microscopy single-cell adhesion studies [Thewes et al., 2015a]. In conjunction with a sub-pixel resolution of the deflection detection, these spring constants enabled a force resolution in the order of tens of piconewtons. The deflection accuracy of the sub-pixel resolution was better than 100 nm (resolution using a 20x objective: 0.278  $\mu\text{m}$ /pixel, see Table A.1) which results in a force resolution better than 50 pN for a spring constant of 0.5 nN/ $\mu\text{m}$ . This force resolution is comparable to the force resolution achieved with an atomic force microscope in single-cell adhesion studies.

### 3.1.2. Experimental Setup

Micropipette force spectroscopy relies on high-resolution optical microscopy to determine the force sensor’s deflection, as described in the previous section. Optical microscopy allows additionally to correlate the measured forces with certain characteristics of the object interacting with a substrate. Thus, the whole micropipette force spectroscopy setup was build around an optical microscope (see Figure 3.5)<sup>24</sup>. As microalgae commonly live in aqueous environments, I performed all experiments in a liquid medium in a custom-built liquid cell mounted on the microscope stage. The work with individual microalga required precise positioning of the force sensor and the substrate employed for force spectroscopy experiments; the precise control of

<sup>24</sup>Most parts of the setup’s scaffold and the liquid cell’s frame were designed by Dr. Marcin Michal Makowski and manufactured in the workshop of the Max Planck Institute for Dynamics and Self-Organization (Göttingen, Germany).

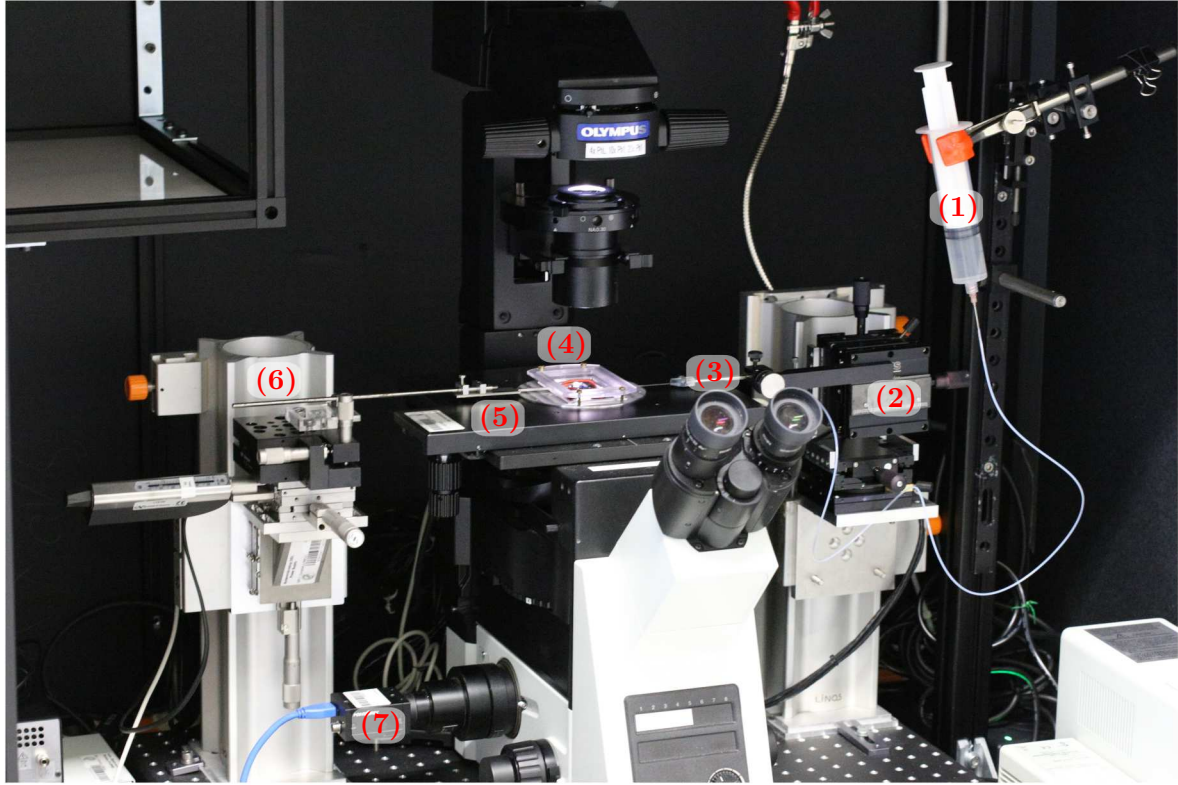


**Figure 3.5.: Micropipette force spectroscopy setup.** The micropipette force spectroscopy setup is built around an inverted optical microscope. The whole setup is placed on an active anti-vibration table inside a box to precisely control the light conditions. (1) Syringe connected to micropipette to create suction pressure. (2) Micromanipulator set: Control of the micropipette force sensor position. (3) Micropipette holder. (4) Liquid cell (see Figure 3.7). (5) Stainless steel substrate holder. (6) Set of linear stages: Control of the substrate position. (7) Camera.

the force sensor's and substrate's positions and their movements were achieved by several micromanipulators.

The experiment itself was vibration sensitive, as unsuppressed concussions, for example from closing a door, lead to oscillations of the cantilever and the substrate holder that would cause severe implications in the detachment process during a force-distance curve. These vibrations could lead to premature rupture of the adhesive contacts between the alga and the substrate. Thus, the micropipette force spectroscopy setup including the microscope and the micromanipulators were placed on an active anti-vibration table (Accurion GmbH, Göttingen, Germany; Halcyonics i4-large) to minimize vibrations. This active vibration isolation suppressed cantilever oscillations after external shocks and reduced the noise level of the experiment by more than one order of magnitude, as seen in Figure 3.6. I defined the noise level of the cantilever's

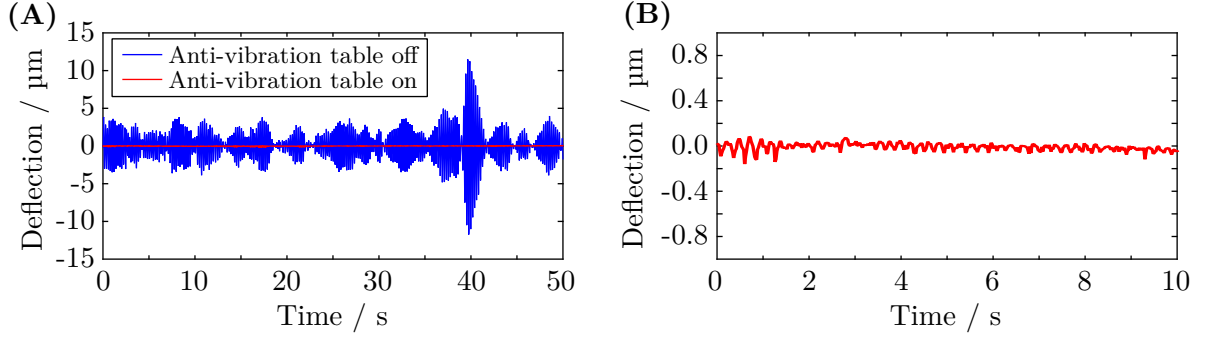


**Figure 3.6.: Effect of the active anti-vibration table on the noise level.** Deflection signal of a micropipette cantilever freely suspended in the liquid cell. In this comparison the box surrounding the experiment was open. **(A)** Direct comparison of the effect of the active anti-vibration table: active anti-vibration table switched off (blue) and switched on (red). **(B)** Active anti-vibration table switched on. In this data set, the root mean square of the deflection is 34.0 nm (maximal deflection: 160 nm, average of the absolute deflection with regard to the cantilever’s equilibrium position: 25.5 nm), which results in a noise-level of approximately 7-17 pN assuming a typical spring constant of 0.2–0.5 nN/ $\mu\text{m}$ .

deflection as the standard deviation of the deflection signal from the equilibrium position with a *Chlamydomonas* cell attached to the micropipette. The noise level was typically in the order of 10 to 20 pN (see Figure 3.6).

Microalgae are photoactive organisms; hence, a crucial parameter was the light exposure of the organism during an experiment. To control the light conditions, I built a box around the whole experimental setup that enclosed the anti-vibration table and the microscope setup. This box allowed for exposing the organism to tailored light conditions, for example, light of a specific wavelength, during experiments. The light conditions during the experiments were a crucial parameter, and are described separately in the section 3.4.4.

### Optical Microscopy and Imaging

This study employed two inverted microscopes (Olympus Corporation, Tokyo, Japan; IX-73/IX-83) for the force spectroscopy experiments. I monitored the micropipette cantilever’s deflection using bright field imaging with long-distance objectives of 10x to 40x magnification. Force-distance experiments employed objectives with 20x or 40x magnification; the calibration was done using objectives with 10x or 20x magnification. To image the flagella configuration during force spectroscopy 40x objectives, or oil immersion objectives with 60x or 100x magnification were used. Most force-distance experiments were performed using 20x magnification with a resolution of approximately 0.278  $\mu\text{m}$  per camera pixel. A list of the objectives and the conversion factors from pixel to micrometers can be found in Table A.1.



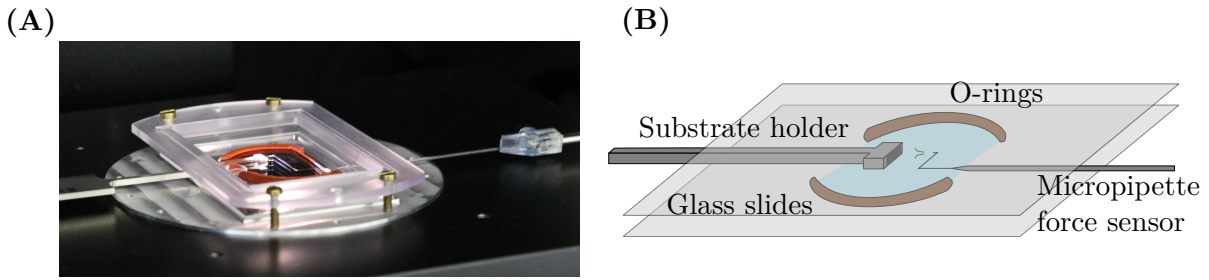


**Figure 3.7.: Design of the liquid cell.** (A) Picture of the liquid cell that was used during the experiments. (B) Sketch of the liquid cell. Adapted from [Kreis et al., 2017].

The optical micrographs for the detection of the cantilever’s deflection were recorded using scientific grayscale cameras. The micrographs to track the cantilever’s deflection during force-distance curves and during calibration (see section 3.1.1) were taken at 10 frames per second (FLIR Integrated Imaging Solutions Inc. Richmond, BC, Canada; Grashopper, GS3-U3-41C6M-C)<sup>25</sup>. The experiments that study the rupture kinetics of force-distance curves require a higher frame rate of at least 200 frames per second. The flagella dynamics in close proximity to a substrate, during the auto-adhesion experiments, (see below and section 6.3, Figure 6.7) were visualized at approximately 400 or 800 frames per second (PCO AG, Kelheim, Germany; pco.edge 4.2). Likewise, the flagella dynamics after rupture of the adhesive contact were observed at the same frame rates (see Figure 4.4).

### Liquid Cell

I performed all experiments in aqueous solution in a custom-build liquid cell (see Figure 3.7). The buffer solutions in the experiments were the aqueous-based undiluted growth media of the microalgae (see section 3.2 below).

The liquid cell consisted of a bottom and a top glass slide, which were separated by two pieces of an O-ring. In between the two O-ring pieces, there were two openings at both sides of the liquid cell, so that the substrate and the force sensor could enter the liquid cell from opposite sides. The liquid cell’s height was adapted to the experiment and was varied by choosing O-rings with a different diameter. In standard force-distance experiments, the liquid cell’s height was 3.4 mm so that the substrate holder of 2 mm height can fit in the liquid cell; in experiments that image the flagella during force spectroscopy the liquid cell’s height was approximately 1.4 mm. The glass slides were fixated with a custom-made frame out of polymethylmethacrylat (PMMA) and/or metal (stainless steel/aluminum).

<sup>25</sup>In experiments that varied the substrate velocity during force-distance curves frame rates up to 50 frames per second were employed (see Figure 4.5). The experiments in Figure 3.6 were likewise recorded at 50 frames per second.



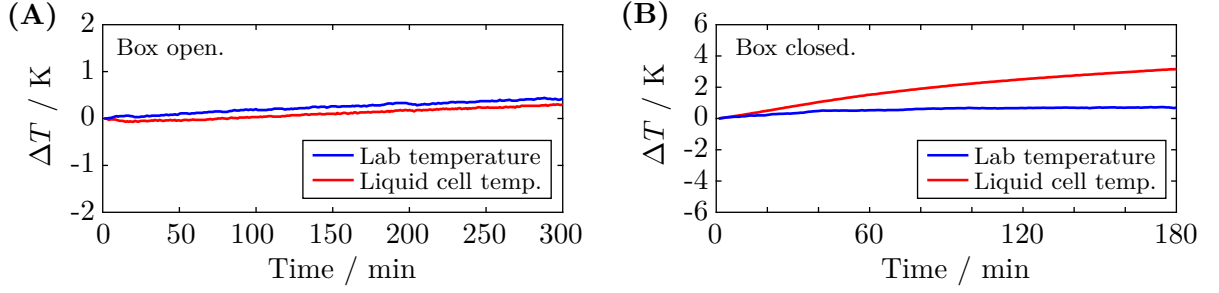


**Figure 3.8.: Temporal evolution of the temperature inside the liquid cell.** The change in the temperature during an experiment is measured in the laboratory (blue) and in the liquid cell (red). The temperature in the liquid cell was measured with a temperature sensor glued to the bottom glass slide of the liquid cell, directly underneath the liquid volume. The laboratory temperature was measured outside the box enclosing the experiment. **(A)** Box open. **(B)** Box closed. The long-term temperature profile is shown in Figure A.5.

Before assembling the liquid cell, I rinsed the glass slides and O-rings with ethanol (CAS 64-17-5; Carl Roth GmbH+Co. KG, Karlsruhe, Germany; ROTISOLV<sup>®</sup>, HPLC Gradient Grade, Purity (GC)  $\geq 99.9\%$ ), dried them with wipes and a nitrogen gas stream. Subsequently, I placed the glass slide in the bottom frame and the two O-rings on top of this glass slide. The O-rings were placed several centimeters apart, so that a micropipette cantilever can fit in the liquid cell. The O-rings were aligned such that the micropipette penetrated the water meniscus in between both O-rings normal to the plane of the meniscus (see Figure 3.7). This alignment guaranteed that the water meniscus did not exert a net force on the micropipette<sup>26</sup>. Next, I closed the liquid cell with the top glass slide and top frame, fixated the frames with screws, and placed the liquid cell on the microscope stage. Finally, I filled the liquid cell with approximately 2 to 3 ml liquid (for a liquid cell's height of 3.4 mm and diameter of 3 cm) before starting an experiment.

I performed all experiments at room temperature (approximately 24-26 °C) without any external temperature control. I measured the temporal evolution of the temperature inside the liquid cell in a control experiment with thermistors, which are electrical resistors whose resistance changes with temperature (McShane, Inc., Medina, Ohio, USA; TR 136-32 and TR 136-170, temperature controller/read out: 5R7-001H3). The temporal evolution of the temperature inside the liquid cell followed the temperature profile of the laboratory temperature during an experiment when the box enclosing the setup was kept open. This experimental configuration was chosen for all experiments in white-light conditions (see section 3.4.4). In cases of a closed box, the temperature inside the liquid cell increased approximately by 3 K over a time of three hours, and by 5 K in about ten hours (see Figure 3.8). This temperature increase

<sup>26</sup>A net force of the meniscus complicates the force sensor alignment and may contribute to drift in the experiment.

inside the closed box and liquid cell is due to electrical devices inside the box radiating heat (for example, the light source of the microscope). During the experiments, the temperature never reached a critical value (for example, *Chlamydomonas* cells start to deflagellate at temperatures above 40 °C [Quarmby, 2009]), as the box was kept closed for a periode of two hours at maximum (for example, in the proteolysis experiments).

#### Micromanipulators and Linear Actuators

The micropipette and substrate position were controlled by micromanipulators and linear stages, respectively (see Figure 3.5). The micromanipulator set (Thorlabs Inc., Newton, New Jersey, USA; Burghleigh PCS-5400) was a manual three-axis mechanical micromanipulator for coarse alignment with integrated piezoelectric-driven fine alignment unit. The piezoelectric alignment had an accuracy better than 120 nm without any backlash and low drift according to the supplier (below 1  $\mu\text{m}$  per hour at constant temperature). This combination allows for precise handling and positioning of the micropipette.

The substrate position was controlled with a motorized linear actuator (Newport Corporation, Irvine, California, USA; LTA-HS) that allowed for cyclic substrate motions. In this micropipette force spectroscopy setup, the cantilever was stationary and the substrate is moved relative to the cantilever during an experiment. The linear actuator featured a position repeatability of approximately 200 nm, an average hysteresis of about 500 nm, and a backlash of about 7  $\mu\text{m}$  (inferred from the control reports of the actuators). The substrate motion was controlled with the graphical user interface provided by the supplier of the linear stages. Additional multi-axis tilt platforms (Newport Corporation, Irvine, California, USA; M-36) enabled a parallel alignment between the cantilever and the substrate corresponding to a perpendicular alignment between the cantilever's nozzle and the substrate.

## 3.2. Microalgae Strains

All experiments in this work were performed using unicellular green microalgae. The algae strains and some of the growth media were kindly provided by the Culture Collection of Algae (SAG) in Göttingen, Germany. The buffer solution used in the experiments was fresh culture medium of the respective organism. Unless stated otherwise, I performed experiments with vegetative wild-type *Chlamydomonas reinhardtii* cells strain SAG 11-32b. *Chlamydomonas reinhardtii* gametes and other microalgae species (see below) were exclusively studied in chapter 8. The incubator temperature of 24 °C was chosen such that the cultures were grown approximately at the temperature that was found inside the lab. The day/night cycle settings (see below) lead to synchronized cultures, i.e. all cells in the culture were in the vegetative growth stage of the life cycle during the day (see Figure 2.6).

Major components (mM)			
NH <sub>4</sub> <sup>+</sup>	7.15 (7.48)	K <sup>+</sup>	1.63 (1.94)
Na <sup>+</sup>	- (0.27)	Ca <sup>2+</sup>	0.34 (0.34)
Mg <sup>2+</sup>	0.41 (0.41)	Cl <sup>-</sup>	8.46 (8.22)
SO <sub>4</sub> <sup>2-</sup>	0.74 (0.51)	PO <sub>4</sub> <sup>3-</sup>	1.00 (1.00)
TRIS	20.0 (20.0)	Acetate	18.3 (17.4)

Tracer components (μM)			
Fe <sup>2+</sup>	18.0 (17.9)	Zn <sup>2+</sup>	69.6 (76.5)
Cu <sup>2+</sup>	8.01 (6.3)	Co <sup>2+</sup>	8.41 (6.8)
Mn <sup>2+</sup>	25.3 (25.6)	Mo <sup>6+</sup>	48.5 (6.2)
BO <sub>3</sub> <sup>3-</sup>	162 (184)	EDTA	123 (134)

**Table 3.1.: Composition of the TAP growth medium.** The composition of the TAP medium is determined from the media formulations of the supplier. The composition in parentheses is taken from “The Chlamydomonas Sourcebook” [Harris et al., 2009]. TRIS is an abbreviation for tris(hydroxymethyl)aminomethane (C<sub>4</sub>H<sub>11</sub>NO<sub>3</sub>), EDTA for ethylenediaminetetraacetic acid (C<sub>10</sub>H<sub>16</sub>N<sub>2</sub>O<sub>8</sub>), and acetate is a salt from acetic acid.

### 3.2.1. *Chlamydomonas reinhardtii*

*Chlamydomonas reinhardtii* strain SAG 11-32b were grown axenically<sup>27</sup> in Tris-Acetate-Phosphate (TAP) medium (Thermo Fisher Scientific, Waltham, Massachusetts, USA; Gibco™ TAP growth medium)[TAP, 2017] in a Memmert IPP 100Plus incubator (Mettler GmbH+Co. KG, Schwabach, Germany, IPP 100Plus; light module cold white 6500K, spectrum see Figure A.9). The TAP medium has a well-established composition with pH 7 optimized for *Chlamydomonas* cultivation. A pH of 7.03 was measured with a pH-meter (Thermo Fisher Scientific, Waltham, Massachusetts, USA; Eutech Instruments; Eutech pH 2700). Synchronous cultures were achieved by growing the cells on a 12h-12h day-night cycle. The daytime temperature was 24 °C with light intensity of 0.3 to 6 × 10<sup>20</sup> photons/m<sup>2</sup>s, which was reduced to 22 °C and zero light intensity during the night time. The light intensity in the center of the incubator was 3 × 10<sup>19</sup> photons/m<sup>2</sup>s, at maximal distance to the light source (from both sides); directly next to the light source: 6 × 10<sup>20</sup> photons/m<sup>2</sup>s. The culture container were placed rather in the center of the incubator. The day cycle started at 7:00 in the morning and ended at 19:00 in the evening. I performed experiments with vegetative cells taken from cultures in logarithmic

<sup>27</sup>Axenically describes cultures that only include a single strain of a species, i.e. the cultures do not contain other organisms or strains of the same species.

Species	SAG strain number	SAG Medium
<i>Chlamydomonas noctigama</i>	35.72	+V
<i>Oogamochlamys gigantea</i>	44.91	+V

**Table 3.2.: Overview of other species and their culture media.** The culture media were kindly provided by Dr. Maike Lorenz (SAG, Göttingen, Germany). A preparation guide for the specific media can be found in [SAG, 2017a,b].

growth phase during the daytime on the second to fourth day after incubation.

To differentiate vegetative cells into gametes (see section 2.3.3), I transferred the cells into nitrogen-free minimal medium (NMM: 80  $\mu$ M  $\text{MgSO}_4$ , 100  $\mu$ M  $\text{CaCl}_2$ , 3.1 mM  $\text{K}_2\text{HPO}_4$ , and 3.4 mM  $\text{KH}_2\text{PO}_4$ , pH 6.8[Berthold et al., 2008; Harris et al., 2009]). Therefore, the cells were centrifuged into a pellet at 100 g for ten minutes, the excessive medium was removed, and replaced with the nitrogen-free minimal medium. This procedure was repeated three times so that the final TAP concentration was below 0.1 %. The success of the differentiation into gametes was judged by mixing both *Chlamydomonas reinhardtii* mating types together (SAG 11-32a and SAG 11-32b). In this cell mixture, I could observe the agglutination and formation of zygotes, indicating that the differentiation into gametes was successful.

### 3.2.2. Other Microalgae Strains

*Chlamydomonas noctigama* strain SAG 35.72 and *Oogamochlamys gigantea* strain SAG 44.91 were grown in culture medium provided by the Culture Collection of Algae in Göttingen (SAG) using the same incubator settings as given above (see Table 3.2). The cultures grew slower than *Chlamydomonas reinhardtii* cultures, so experiments with these algae were performed up to one week after incubation.

### 3.3. Substrates

This work studies the adhesion of *Chlamydomonas* and other microalgae to various model substrates. In experiments that aim at characterizing adhesion forces, I used small substrate pieces that were attached to the stainless steel substrate holder. In this configuration, the substrate was oriented perpendicular to the focal plane of the microscope and the adhesion force was measured normal to the substrate. Although the substrate’s surface was visible in these experiments, the flagella remained invisible in close proximity to the substrate (compare Figure 3.1C). The scattered light from the surface concealed the flagella as the flagella diameter is only about 200 nm. In fact, the flagella contact area and the flagella dynamics during the adhesion process were not accessible with this substrate configuration.

For this reason, I chose another substrate type to qualitatively study the flagellar dynamics close to a substrate. In these experiments, I employed the outer surface of a micropipette cantilever, with a diameter of tens of micrometers and without a nozzle, as a substrate. Although bent in the same shape as the micropipette force sensor, these substrate cantilevers did not deflect in the experiments as they were much stiffer than the force sensor. This configuration suppressed light scattering problems caused by the substrate, which allowed for imaging the flagella (see Figure 4.4 for an example, Figure A.3 shows an overview of the experimental configuration). The micropipette substrates were mounted in a micropipette holder.

### 3.3.1. Overview of the Model Substrates

As substrate I used non-functionalized and functionalized silicon wafers, as well as magnesium oxide and gold substrates. Non-functionalized silicon wafers with thin SiO<sub>2</sub>-layer were employed as the standard and reference substrate. The silicon wafers with native, thin SiO<sub>2</sub>-layer of 1.7 nm thickness (called Si native, type P/Bor, orientation  $\langle 100 \rangle$ , resistivity 1 to 20  $\Omega\text{cm}$ , unilateral polished) and the silicon wafers with thermally grown, thick SiO<sub>2</sub> layer of 150 nm thickness (Si thick, type P/Bor, orientation  $\langle 100 \rangle$ , resistivity 10 to 20  $\Omega\text{cm}$ , unilateral polished) were purchased from Si-Mat (Kaufering, Germany). The SiO<sub>2</sub>-layer thicknesses of the Si substrates were inferred from earlier studies employing the same type of substrates from the same supplier [Loskill et al., 2012a]. Magnesium oxide substrates (MgO, CAS 1309-48-4; Purity  $\geq 99.9\%$ , single crystal substrate) were purchased from Sigma-Aldrich (Germany). I functionalized silicon wafers (type native SiO<sub>2</sub>-layer) with a self-assembled silane monolayer (molecules with a CH<sub>3</sub> tailgroup; octadecyltrichlorosilane, OTS, CAS 112-04-9; Sigma-Aldrich, Germany) to obtain hydrophobic substrates (OTS) following a standard procedure [Lessel et al., 2015]. Additionally, I performed experiments on gold substrates (Ted Pella, Inc., Redding, California, USA; Prod No. 260156-G), glass cover slips, and on silicon wafer pieces coated with polydimethylsiloxan (PDMS; Dow Corning, Midland, Michigan, USA; Sylgard<sup>®</sup> 184 silicon elastomer kit) and Teflon<sup>®</sup> AF1600 (Poly[4,5-difluoro-2,2-bis(trifluoromethyl)-1,3-dioxole-co-tetrafluoroethylene], CAS 37626-13-4; Sigma-Aldrich, Germany).

In the experiments, I used small substrate pieces of approximately  $6 \times 2$  mm of the enumerated bulk substrates. These substrate pieces were glued with PDMS to a stainless steel substrate holder. After attaching the substrate to the holder, I immersed the substrate holder and substrate for three minutes in an ethanol ultrasonic bath in preparation for experiments (ethanol: CAS 64-17-5; Carl Roth GmbH+Co. KG, Karlsruhe, Germany; ROTISOLV<sup>®</sup>, HPLC Gradient Grade, Purity (GC)  $\geq 99.9\%$ ). All experiments, except the quantitative substrate comparison in chapter 7, employed Si native substrates that were prepared and cleaned following this procedure. The micropipette cantilever substrates were also cleaning for three minutes in an ethanol ultrasonic bath prior to experiments.

In the experiments reported in chapter 7 (surface forces that mediate the adhesion of microalgae), I attached two substrates next to each other on the substrate holder (see Figure 3.10). Afterwards, I cleaned the substrate holder and substrates as described above. Note that in experiments featuring substrates cleaned with piranha solution, one substrate was cleaned with piranha solution, a second substrate was cleaned with ethanol; then both substrates were attached to the substrate holder. The piranha solution contained sulfuric acid ( $\text{H}_2\text{SO}_4$ , varying suppliers, CAS 7664-93-9; Purity 96.5 %) and hydrogen peroxide ( $\text{H}_2\text{O}_2$ , varying suppliers, CAS 7722-84-1, 30 %, stabilized) in a 1:1 ratio. The residues of the piranha solution were removed over a period of 90 min by rinsing the substrate with ultra pure water, which was exchanged four times (ultra pure water: Merck KGaA, Darmstadt, Germany; Milli-Q® A10 Water Purification System, total organic carbon residues:  $\geq 5$  ppb, resistivity at 25 °C:  $18.2 \text{ M}\Omega\cdot\text{cm}$ ).

#### 3.3.2. Substrate Characterization

In order to compare the influence of intermolecular interactions on the adhesion forces, I performed a full substrate characterization. The root mean squared roughness (rms), calculated by  $R_{\text{rms}} = \sqrt{\frac{1}{n} \sum_{i=1}^n y_i^2}$ , where  $y_i$  is the deviation from the average surface level, was measured in  $1 \mu\text{m} \times 1 \mu\text{m}$  sections of the substrate using atomic force microscopy (Bruker, Billerica, Massachusetts, USA; Veeco diDimensionV) with a cantilever featuring a nominal tip radius of 7 nm (Olympus Corporation, Tokyo, Japan; Micro Cantilevers OMCL-AC160TS-W2). The surface energy was determined with a three liquid method [van Oss, 1993; Mykhaylyk et al., 2003] using ultra pure water, glycerol (CAS 56-81-5; Sigma-Aldrich, Germany) and bromonaphthalene (1-Bromonaphthalene, CAS 90-11-9; Sigma-Aldrich, Germany) as probe liquids. This method allows to determine the total surface energy  $\gamma$ , as well as its Lifshitz-van der Waals ( $\gamma^{\text{LW}}$ ) and the Lewis acid-base ( $\gamma^{\text{AB}}$ ) component from the static contact angle. The contact angles (shown in Table 3.4) were determined from at least ten independent measurements (DataPhysics Instruments GmbH, Filderstadt, Germany; OCA 20). The isoelectric point IEP, the pH-value at which the substrate carries no mean net charge, is inferred from zeta-potential measurements from literature [Robinson et al., 1964; Bousse et al., 1991; Loskill et al., 2012b]. The relevant substrate properties of the substrates are summarized in Table 3.3.

Substrate	$\gamma^{\text{tot}}$ (mJ/m <sup>2</sup> )	$\gamma^{\text{LW}}$ (mJ/m <sup>2</sup> )	$\gamma^{\text{AB}}$ (mJ/m <sup>2</sup> )	rms (nm)	IEP
Si native (Piranha)	64(2)	43(1)	21(2)	0.15	3
Si native (Ethanol)	35(4)	32(1)	3(3)	0.17	3
Si thick (Ethanol)	37(3)	32(1)	5(3)	0.19	3
OTS (Ethanol)	23(1)	23(1)	$\leq 0.2$	0.16	$\leq 4$
MgO (Ethanol)	41(1)	39(1)	2(1)	0.23	12.5

**Table 3.3.: Overview of the Substrate properties of the substrates employed in the adhesion measurements.** The substrate and its cleaning method are given. The surface energy is measured with a three liquid method. The uncertainty (values in parentheses) in the Lewis acid-base component of the surface energy measurements are estimated from a control measurement employing ethylene glycol (CAS 107-21-1; Sigma-Aldrich, Germany) instead of glycerol. Additionally, the error in the experimentally derived acid-base and Lifshitz-van der Waals components of the probe liquids contribute to the error in the surface energy. The roughness is determined from atomic force microscopy topography maps. The error in the roughness measurement is estimated to be below 10 %. The isoelectric point is inferred from literature.

Substrate	$\theta_{\text{Water}}$ (°)	$\theta_{\text{Glycerol}}$ (°)	$\theta_{\text{Bromonaphthalene}}$ (°)
Si native (Piranha)	< 10	< 10	15(1)
Si native (Ethanol)	68(3)	71(2)	47(1)
Si thick (Ethanol)	66(2)	67(1)	47(2)
OTS (Ethanol)	113(3)	101(1)	65(2)
MgO (Ethanol)	57(6)	60(2)	30(1)

**Table 3.4.: Contact angles for three probe liquids on the used substrates.** The contact angle  $\theta$  of a sessile drop is measured from at least ten individual measurements (standard deviation given in parentheses).

## 3.4. Force Spectroscopy Experiments

I performed micropipette force spectroscopy experiments to quantify the adhesion of microalgae to substrates. In the next sections, I introduce the experimental routines that all force spectroscopy experiments have in common, describe the important experimental parameters, and individual experimental protocols.

### 3.4.1. Preparation of the Experiment

#### Assembling of the Experimental Setup

As a first step, I cleaned and assembled the liquid cell, placed the liquid cell on the microscope stage, and filled the liquid cell with the buffer solution. Subsequently, the force sensor and substrate holder with substrate were inserted in the liquid cell and positioned in the center of the liquid cell and the field of view of the microscope and the camera. Afterwards, I brought the micropipette force sensor in the proximity to the substrate (hundreds of micrometers distance), and I aligned the cantilever and substrate such that the cantilever is parallel to the substrate. This alignment minimized lateral shear forces during the experiment and guaranteed that the adhesion forces of the cell are measured normal to the substrate. Finally, I prepared the imaging of the cantilever and the data analysis code for a real-time view of the cantilever's deflection during force-distance cycles. For more details on the liquid cell, buffer solution, and substrates see the specific sections above.

After executing the aforementioned steps, I injected the microalgae into the liquid cell to create a dilute algae suspension. The algal cell concentration inside the liquid cell was not controlled, yet chosen small enough that algae swimming in the liquid cell and algae colonizing any existing surface inside the liquid cell (for example, the substrate and also the force sensor) did not interfere with the experiment.

#### Attaching a Living Motile Microalgae to the Micropipette

The force spectroscopy experiments require the attachment of an individual, living (and motile) microalga to the cantilever's nozzle in a controlled configuration. The cell's configuration was important as only the flagella exhibit adhesion (see section 4.2.1). The cell's configuration was controlled by monitoring the flagella beating or by identifying the pyrenoid at the anterior part of the cell body.

To fixate a cell at the nozzle of the cantilever, I used a trick that allows for grasping cells reliably in a configuration at which the flagella face the substrate and the flagellar adhesiveness is probed; this "flagellar adhesion" configuration is shown in Figure 3.1. This method exploits the fact that the microalgae start to colonize the substrate after injecting them into



the liquid cell. The *Chlamydomonas* cells always adhere to the substrate with their flagella in the characteristic gliding configuration (see section 2.3.4), which ultimately determines their orientation with regard to the force sensor. The cells adhering to the substrate were picked up with the micropipette. Therefore, I brought the micropipette either in direct contact with a cell or in close proximity to a cell. Then, I created a small suction pressure at the cantilever's nozzle. This suction pressure fixated the cell at the opening of the micropipette, and was constantly applied to hold the cell at the force sensor. Finally, I manually detached the cell from the substrate by retracting the cantilever with the piezoelectric micromanipulator. Using this approach, I could reliably grasp *Chlamydomonas* cells in the configuration needed to study the flagellar adhesion<sup>28,29</sup>. I did not observe any deflagellation or cell damage using this method; all cells harvested from the substrate could be used for experiments.

The cells' viability was checked during and after the experiment in different ways. With a high-speed camera, I observed the regular beating of the flagella, which indicated a living cell with fully functional flagella. Another method of checking the cell's viability was by observing the pulsing vacuole at the cell apex close to the flagellar basal bodies (see Figure 2.4). The pulsing vacuole regulates the osmotic pressure of *Chlamydomonas* by pumping excessive water out of the cell body. This recurrent process could be optically observed and implied that the cell was alive.

### Final Substrate Positioning and Reference System in Force Spectroscopy

After grasping a microalgae, I finalized the substrate positioning with regard to the micropipette cantilever's position. In force-distance experiments, I had to manually define the limits of the substrate movement (reversal points of the substrate motion), as there was no closed-loop system based on the cantilever's deflection that would limit the substrate movement. The limits of the substrate motion were chosen such that the substrate was pressed by 5  $\mu\text{m}$  against the cell, respectively that the substrate was retracted far enough to detach the cell. Pressing the substrate by 5  $\mu\text{m}$  against the cell directly translates in a cantilever deflection of 5  $\mu\text{m}$ , as the cantilevers were much softer than the cell body; the microalgae were not deformed during an experiment (see the discussion in section 4.1). The point at which the cell came into contact with the substrate and entered the repulsive force regime was defined as the zero distance position in the coordinate system of the force-distance curves (see the sketches and explanations in Figure 3.9). Conclusively, this reversal point (limit of substrate motion, subsequently substrate motion in opposite direction) in the repulsive regime was at a distance

---

<sup>28</sup> Another method to grasp a cell was to apply a small suction pressure at the nozzle and to wait until a cell that swam close enough past the nozzle was sucked to the cantilever's opening. This method fixated the cell in an uncontrolled configuration to the cantilever and is rather time consuming, as the process had to be repeated until a cell attached in the desired configuration.

<sup>29</sup> The cell body adhesion configuration (see Figure 4.2B) was achieved either by the method described in footnote 28 or by pushing the cell with the micropipette to the side and subsequently applying the suction pressure. The procedure was repeated until a cell was grasped in the correct configuration, which often took several attempts as the configuration was determined randomly.

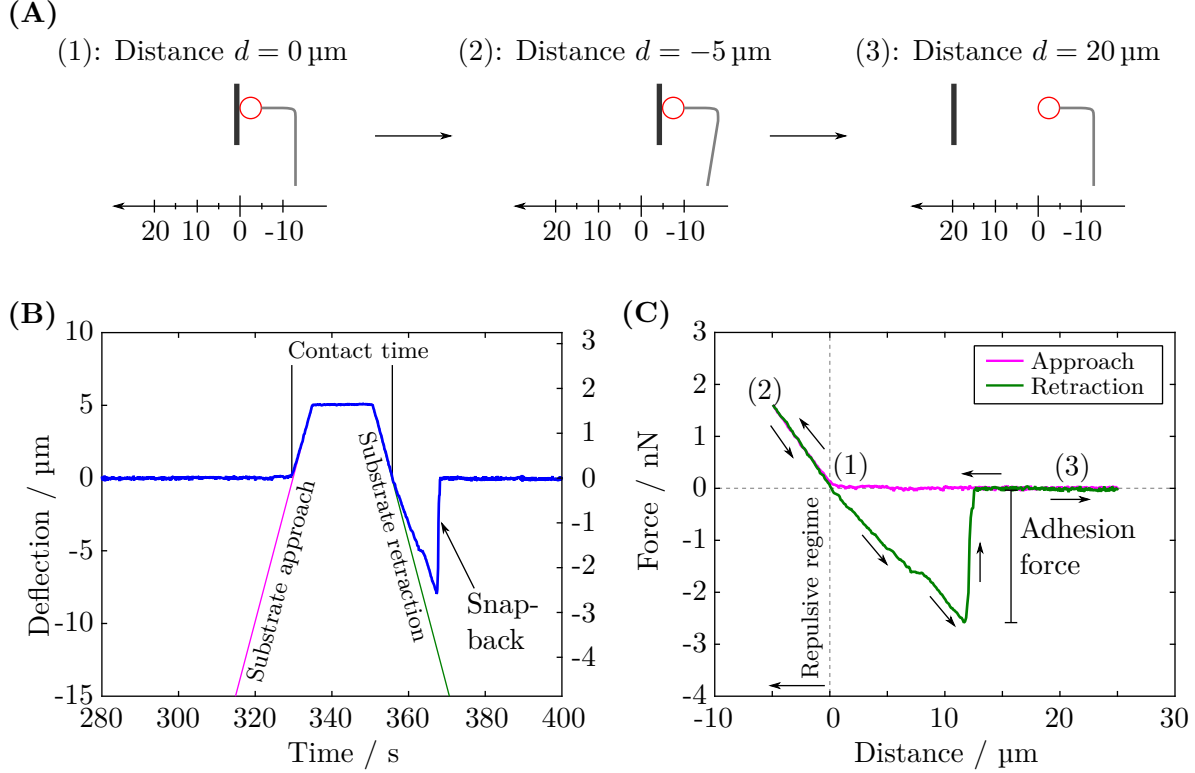


**Figure 3.9.: Introduction to micropipette force spectroscopy.** (A) Coordinate system during force spectroscopy. The cell-substrate distance and cantilever's deflection is given at three different times (see also the force-distance curve in panel (C)). (1): The zero substrate-cell distance is defined as the point at which the cell (sketched in red) comes into contact with the substrate. All other distances are given with regard to this zero point. (2): Repulsive regime. (3): Cell not in contact with substrate. (B) Deflection of the cantilever (blue) and cell-substrate distance during approach (pink) and retraction (green). The right-hand axis shows the force acting on the cantilever calculated from the cantilever's deflection and spring constant. The cell-substrate contact time was defined as the time during which the cell experiences a positive force (repulsive regime, substrate pressed against the cell). The rupture of the adhesive contact is seen as snap-back of the cantilever in the zero-force position. The different slopes during the detachment process are a feature that is discussed in section 5.2. (C) Final force-distance curve. The repulsive regime is the part of the force-distance curve at which a repulsive force is acting on cell (the cell-substrate distance is negative).

of  $-5\text{ }\mu\text{m}$ , while the second reversal point was at a cell substrate distance of several tens of micrometers.

### 3.4.2. Force-Distance Experiments

Adhesion forces are commonly measured in force-distance experiments that dissect the interactions between an object attached to a force sensor and a substrate. This procedure allows for quantifying repulsive and attractive interactions between a substrate and the microalga, characterizing the structures that are involved in interaction processes, and determining deformations of the object and the substrate. The force-distance experiments performed with the micropipette force spectroscopy followed an identical procedure like the force-distance experiments performed with an atomic force microscope in the force spectroscopy mode. The object, in this study a microalga, was brought into contact with the substrate and was subsequently detached. During this process, the deflection of the cantilever was monitored, while the experimentally controlled position of the substrate was known. In the following paragraphs, I describe the procedure of an individual force-distance experiment, followed by the procedure that was used to extract the force-distance curves from the raw deflection data, and the protocol of a complete force spectroscopy experiment consisting of several force-distance cycles.

Each individual force-distance cycle consisted of a substrate-cell approach, a time delay during which the cell was in contact with the substrate, and the retraction of the substrate from the cell. These different parts can be identified in the cantilever's as a function of time (see Figure 3.9B). From these raw deflection data, I extracted the force-distance curves commonly used to characterize the adhesion process. Therefore, I correlated the distance between cell and substrate, shown in Figure 3.9B as the pink and green line, with the force acting on the cantilever, which was calculated from the cantilever's deflection. The coordinate system in analysis of the force spectroscopy was chosen such that a zero distance corresponds to the point when the cell comes into contact with the substrate during the cell-substrate approach. At this point, the cantilever's deflection enters the repulsive force regime (positive deflections/forces in Figure 3.9B/C). The adhesion force of the cell can be either calculated from the raw deflection versus time data or can be extracted from the force-distance curve. In this study, I define the adhesion force as the maximal force measured during the detachment process of the alga, which corresponds to the minimal force in the retraction cycle of the force-distance curve (see Figure 3.9C).

A complete force spectroscopy experiment consisted of several sets of individual force-distance cycles (also abbreviated as sets in the following) with the same microalga. Each set consisted of five consecutive force-distance cycles with the same experimental conditions and parameters at the same substrate position. In experiments using *Chlamydomonas noctigama* and *Oogamochlamys gigantea* a set consisted of two force-distance cycles. If at all, the experimental parameters (for example, light conditions and contact time) were varied between different sets.

Each set was performed at a different location on the substrate.

#### 3.4.3. Standard Parameters in Force-Distance Experiments

In most force-distance experiments, I consistently employed the same standard parameters that I want to introduce in the following.

The substrate moved at a constant velocity of  $1\text{ }\mu\text{m/s}$  during the approach and retraction part of the force-distance cycle. During the approach and retraction cycle, I normally set the limits of the substrate motion 30 to  $40\text{ }\mu\text{m}$  apart, depending on the cantilever's spring constant and the expected adhesion forces of the microalgae<sup>30</sup>. In exceptional cases the substrate movement during approach and retraction could be as large as  $100\text{ }\mu\text{m}$  for cells exhibiting high adhesion forces in combination with a soft cantilever.

Between periods of substrate motion, the substrate remained stationary for approximately 15 seconds<sup>31</sup>. Additionally, the cell was in contact with the substrate for about 10 seconds while the substrate was moving<sup>32</sup>, which consequently resulted in a total cell-substrate contact time of approximately 25 seconds (see Figure 3.9B)<sup>33</sup>. The contact time was chosen such that the flagella of *Chlamydomonas reinhardtii* can realize the gliding configuration on the substrate, which was achieved after less than 15 seconds of contact (see Figure 4.3 and the corresponding discussion).

The time in between two contact periods of two consecutive force-distance cycles was about 50 to 60 seconds, which was long enough so that the flagella restored a regular beating after detaching. This time consisted of the time in between two force-distance cycles of 15 seconds, the time when the substrate was approaching the cell at the beginning of a force-distance cycle, and the time when the substrate was further retracted after the cell detached. The latter two times add up to approximately 40 to 50 seconds, depending on the movement range during a force-distance cycle. This time was long enough that the cells recovered the regular beating of the flagella (see Figure 4.4 and the corresponding discussion).

---

<sup>30</sup>I estimated the expected adhesion force from the manual force-distance cycle that I performed while determining the limits for the substrate motion (see above).

<sup>31</sup>The time delay consisted of a dwell-time, which was directly entered in the graphical user interface of the linear actuators, and an additional backlash time delay of approximately five seconds (at substrate velocity of  $1\text{ }\mu\text{m/s}$ ). This additional time delay originated from the mechanical backlash of the gear wheels of the linear actuators. To compensate the backlash, the gear wheels moved for five seconds without resulting in a net motion of the linear actuators. Both times added up to the total time delay in between phases when the substrate is moving during one force-distance cycle. I chose a dwell-time of 10 seconds, which added up with the backlash compensation delay to a total time at which the substrate was stationary of approximately 15 seconds.

<sup>32</sup>The substrate was pushed by  $5\text{ }\mu\text{m}$  against the cell body at a velocity of  $1\text{ }\mu\text{m/s}$ .

<sup>33</sup>The contact time was increased to 45 seconds for experiments with *Chlamydomonas noctigama* and *Oogamochlamys gigantea*.

One set of five force-distance curves took in average 10 minutes with the chosen experimental parameters. I chose to include five force-distance cycles in one set as this choice was a good compromise between a minimal statistical robustness at the same experimental parameter and the possibility to probe several experimental parameters within a time frame of 1 to 2 hours. Furthermore, it minimized the amount of force-distance cycles at the exact same substrate spot.

#### 3.4.4. Light Conditions

Microalgae are photoactive microbes whose behavior is strongly affected by the exposure to different light conditions, for example, they may swim towards a light source in an aqueous environment (phototaxis, see section 2.3.3). Consequently, I controlled the light conditions by using different light sources and filters during all experiments (see Appendix C for a story of the time before I controlled the light conditions). The light intensities were adjusted by the power of the light source and optical density filters. The individual emission spectra for the light sources and the transmission spectra of the filters are shown in Figure A.6 to A.8. The filters are classified by the center wavelength of transmission and the width at which the transmission is reduced to 50 %, i.e. the full width at half maximum (FWHM). For example, 672/11 nm specifies a red filter around 672 nm with a full width at half maximum (FWHM) of 11 nm.

In the following, I classify the standard light conditions that I used throughout the experiments. Any deviations from these configurations are explicitly mentioned in the description of the experiment itself. The three main light conditions are:

1. **White illumination or white light conditions:** Standard microscopy illumination at approximately  $5$  to  $10 \times 10^{20}$  photons/m<sup>2</sup>s (Olympus, Halogen light bulb JC 12V100W; see Figure A.6A and Figure A.7A).
2. **Red illumination/red light conditions:** Standard white illumination with an added red filter: 672/11 nm at approximately  $1.5$  to  $3 \times 10^{19}$  photons/m<sup>2</sup>s (see Figure A.6D and Figure A.7D).
3. **Blue illumination/blue light conditions:** Aforementioned red illumination for imaging and an additional blue-light LED as additional light source with variable intensities (470/18 nm; see Figure A.8).

In experiments shown in chapters 4, 5, and 7, I employed exclusively white-light conditions. In chapter 6 and 8, I studied the influence of light on the adhesion of microalgae using the previously enumerated different light conditions. In the experiments in Figure 6.1A-C, I employed a bandpass filter (665/65 nm, spectrum see Figure A.6, Figure A.7). In the red-light experiments in Figure 6.4B, I employed a high-pass red filter ( $\lambda_{\text{cutoff}} = 550$  nm, see Figure A.6B and Figure A.7B); otherwise red illumination with the displayed intensities could not be achieved

Light exposure	Microscope	Filter	Spectrum	Comments
White light	IX-73	none	Figure A.6A	Halogen light bulb
White light	IX-83	none	Figure A.7A	Halogen light bulb
Red light	IX-73	672/11	Figure A.6D	Halogen light bulb with red filter
Red light	IX-83	672/11	Figure A.7D	Halogen light bulb with red filter
Blue light	IX-83	672/11	Figure A.8	Red light, additional blue LED

**Table 3.5.: Overview of the different main light conditions used in the experiments.** The nomenclature of the illumination is given in the first column. The setup refers to the microscope used for the experiment and the corresponding spectrum of the light source.

with the halogen lamps of the microscopes.

In the experiments in white-light conditions, the box enclosing the setup was open; in all other experiments the box was closed. An overview of the illumination conditions is shown in Table 3.5. I measured the white-light and red-light irradiance with a photometer (LI-COR® Biosciences, Lincoln, Nebraska, USA; Light Meter LI-250A) with radiation sensor (Quantum Sensor LI-190, Serial number Q49966). The blue-light intensities were calibrated using a power meter (Thorlabs Inc., Newton, New Jersey, USA; PM100D, sensor: S130C) and converted into a photon density flux (photons/m<sup>2</sup>s) by optically determining the spatial extent of the illuminated area. The spectra were determined using a UV-Vis spectrometer (OceanOptics, Inc., Dunedin, Florida USA; USB-650 Red Tide).

### 3.4.5. Experimental Protocols

#### Experiments Probing the Adhesion Forces to Different Substrates

To probe the influence of the substrate properties on the adhesion force (for example, the surface charge), I performed experiments with the exact same cell (*Chlamydomonas* strain SAG 11-32b) on two different substrates in white light conditions (as described in section 3.4.4). The two substrates were attached next to each other onto the same substrate holder (see above, see Figure 3.10). On both substrates, I carried out two sets of five individual force-distance curves, resulting in a total of ten measurements with the same cell on each substrate. The order of the four sets was varied randomly to avoid any bias in the measured adhesion forces caused by the experimental procedure. For the same reason, I selected approximately the same number of cells from each substrate for direct adhesion force comparisons, so that the statistics is not affected by any adaptation to the respective substrate. For example, in the experiment comparing the influence of the surface charge on the adhesion force, the overall statistics includes experiments with in total 18 cells: 10 cells were picked from the MgO substrate and 8 cells from Si substrate.

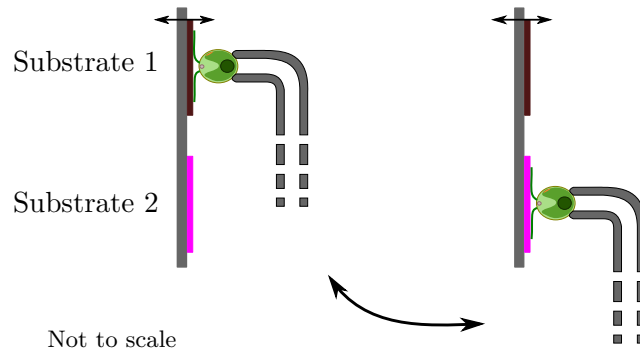


**Figure 3.10.: Force spectroscopy on two different substrates.** The adhesion forces is probed with the same cell on two different substrates. On each substrate, two sets with five force-distance cycles are performed. The order of the four sets is chosen randomly.

### Experiments with Different Light Intensities and Illumination Wavelengths

In the experiments probing different light intensities, I examined the threshold at which the adhesion force of *Chlamydomonas* was reduced to zero (see section 6.1). Therefore, I probed the adhesion force of the same cell from high blue-light intensities (irradiance:  $3 \times 10^{19}$  photons/m<sup>2</sup>s) to low blue light intensities (irradiance:  $1 \times 10^{17}$  photons/m<sup>2</sup>s). Reversing the order of the force-distance sets (from low to high light intensities) would yield an inconsistent force-intensity relation. This effect would occur after switching the flagellar adhesiveness on, as in some cases the adhesion force of a *Chlamydomonas* cells was observed to increase for about 30–60 minutes before it saturated (Figure 6.5).

In experiments with different illumination wavelengths, the same *Chlamydomonas* cells were exposed to different wavelengths of constant light irradiance of  $3 \times 10^{19}$  photons/m<sup>2</sup>s (see spectra in Figure A.8): 410/20 nm, 470/18 nm, 550/19 nm, 638/16 nm, and 672/11 nm. For these experiments, all light irradiances were calibrated using the Thorlabs power meter (see above). The cantilever's deflection was imaged in red light conditions throughout the experiment. For the same reason as mentioned above, these experiments were performed in a specific order: Firstly, the smaller wavelengths (400 and 470 nm) at which adhesion was observed were probed. Secondly, I performed experiments at the wavelengths above the threshold wavelength, where no adhesion was observed.

### Proteolysis Experiments

In proteolysis experiments, I studied the influence of an enzymatic digestion of proteins by pronase on the adhesion forces of *Chlamydomonas* cells (strain SAG 11-32b; pronase from *Streptomyces griseus*, CAS 9036-06-0). An aqueous solution containing pronase (10 mg/ml) was added directly to the TAP medium in the liquid cell, resulting in a pronase concentra-

tion of 0.1 mg/ml. The temporal evolution of the adhesion force for the exact same cell was subsequently monitored in two different situations. First, the influence of pronase treatment in white light conditions was monitored. During this treatment in white light, I performed adhesion experiments every 15 minutes for a total of two hours. Secondly, the same pronase treatment was performed under red illumination. After exposure of the cells to pronase in red light for two hours, the adhesion force was determined immediately after turning on the white light illumination without flushing the liquid cell with fresh TAP medium. Note that in both cases, the cell was held by the micropipette in solution and was not in contact with the substrate during pronase treatment.

#### 3.4.6. Auto-Adhesion Experiments

Auto-adhesion experiments required the same preparations as mentioned above, namely the assembly of the setup and grasping of the microalgae. The auto-adhesion experiments were solely performed with *Chlamydomonas reinhardtii* strain SAG 11-32b. Here, the cell body was brought in close proximity to the substrate (approximately 4-8  $\mu\text{m}$  distance between the substrate and the cell body) at the beginning of the experiment in red light conditions. After turning on an additional white/blue light source<sup>34</sup>, the flagella of the cell adhered to the substrate and started to pull the cell body into full contact with the substrate. A full description of the light response of the cell, which is seen as the auto-adhesion process is given in section 6.3.

### 3.5. Surface Colonization Experiments of Cell Populations

Besides the quantitative adhesion force characterization in force spectroscopy experiments, I qualitatively monitored the surface colonization of microalgae in adsorption experiments. These experiments were performed in an “open” liquid cell of about 150  $\mu\text{m}$  thickness, between two microscope glass slides with cover slips as spacers (cover slips No. 1; thickness: 130 – 160  $\mu\text{m}$ ). To create this liquid enclosure, I placed a droplet containing the microalgae on the bottom glass slide and subsequently closed the liquid cell with a second glass slide on the top. The algae samples were directly taken from the cultures; the algae concentration inside the liquid cell was not controlled systematically.

The surface-association of the algae and their flagellar adhesiveness was quantified by measuring adsorption and desorption kinetics in response to changing light conditions, adsorption after turning from red to white illumination and desorption from white to red illumination. Therefore, I recorded optical micrographs at 5 and 10 frames per second, respectively, with a grayscale camera (Grashopper, see above) with objectives of 4x or 10x magnification. From these micrographs, the amount of microalgae in contact with the substrate was determined by

---

<sup>34</sup>The first experiments were performed with an external white-light LED (type P585E, 2V/DC luminous intensity 6800 mcd, at approximately  $2 \times 10^{19}$  photons/ $\text{m}^2\text{s}$ ) mounted in close proximity to the liquid chamber. Most experiments were performed with the blue LED integrated in the microscope, which is described above.



counting the number of adhered cells with a self-made MATLAB code. These cells were non-motile (besides of subtle gliding motility) and could be distinguished from the cells in bulk, as the cells in bulk solution were swimming and traveled over a longer distance in the same time period.

### 3.6. Statistical Analysis of the Experimental Data

An overview of statistical tools can be found in statistics and data analysis textbooks, for example, [Sachs and Hedderich, 2006; Lista, 2016]. In the following, I describe the methods and tools relevant for this work. I performed the data analysis with MATLAB and its built-in analysis tools and fit functions, for example, *mean()*, *boxplot()*, and *fitdist()*.

For the data points comprised of several individual adhesion measurements, the mean of all force-distance cycles is plotted with the errorbars representing the standard deviation of all force distance curves. The standard deviation of the mean is given in parentheses (round) after the average value, for example, a mean force of 1.75(5) nN means that the computed mean adhesion force is 1.75 nN with a standard deviation of 0.05 nN, while 1.75(15) corresponds to a mean adhesion force of 1.75 nN with a standard deviation of 0.15 nN. The nomenclature  $1.75 \pm 0.05$  nN is not used, as it implies a symmetric distribution of the dataset around the mean, which is not necessarily true for these data sets (see section 5.1).

Confidence intervals for fits are given for a confidence level of 95 %, with box brackets indicating half the width of the confidence interval. In this nomenclature,  $\alpha = 0.45[3]$  means that the fit yields a value of  $\alpha = 0.45$  with the 95 % confidence interval ranging from 0.42 to 0.48, while  $\alpha = 0.45[12]$  implies a confidence interval ranging from 0.33 to 0.57.

#### 3.6.1. Visualizations of Datasets

The statistical distribution of data points in this work is shown in three ways. In addition to the visualization with a histogram, I use so-called box plots, and I show the empirical cumulative distribution function (ECDF) of the sample. Each visualization has certain advantages that shall be briefly described in the following.

A histogram shows the distribution of the data points in the most intuitive way (see Figure 3.11A). From a histogram, special characteristics of the data set can be easily recognized, like the skewness of the distribution or a multi-modal distribution. However, for a reliable representation, a relatively large amount of data points is necessary (ideally more than 100 individual data points) such that the bin width can be chosen small, which gives the distribution a continuous appearance. Additionally, the histogram does not enable a direct quantification of some important characteristics of the distribution, like the spread, mean, and median.

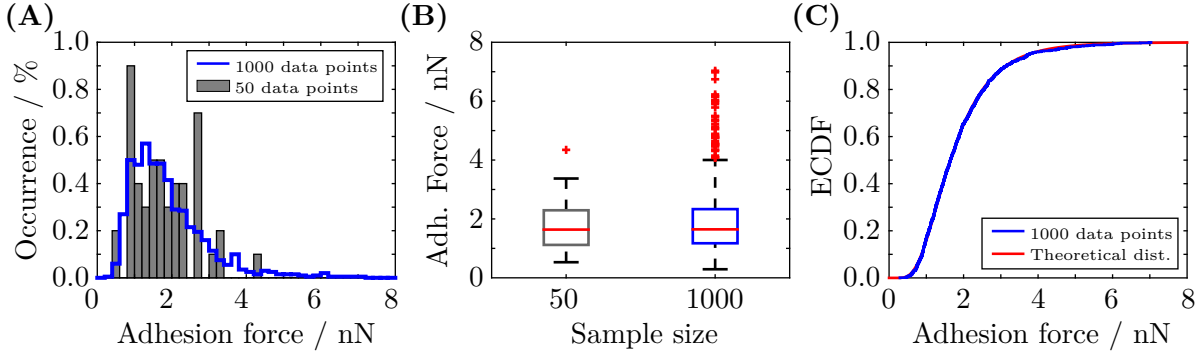


**Figure 3.11.: Statistical tools to analyze a sample set of data points.** Representations of two sample sets of different size drawn from a log-normal distribution with  $\alpha = 0.5$  and  $\beta = 0.5$ : 50 data points (gray), 1000 data points (blue). **(A)** Histograms. **(B)** Box plot. **(C)** Empirical cumulative distribution function ECDF and theoretical cumulative distribution function of the underlying log-normal distribution.

Box plots are often used to visualize samples that contain a relatively limited amount of data points (see Figure 3.11B). The advantage of a box plot is that it does not imply a specific distribution, while enabling the read out of certain characteristics of the distribution. A box plot includes the sample median, and the 25th and the 75th percentile. These values are indicated as a straight line (red) inside the box and the upper/lower limit of the box, while the box itself represents the middle 50% of the sample's data points. The difference between the 25th and 75th quantile of the sample is called the interquartile range and is a measure for the spread of the data points. The whiskers are lines vertically extending from the box (25th/75th percentile) to the furthest observations within 1.5 times the interquartile range, which are called lower and upper adjacent. Outliers are any data points that are more than 1.5 times the interquartile range away from the top or bottom of the box. Figure A.13 shows a comprehensive overview of a boxplot including all these features. Conclusively, a box plot is a simple representation of a data set, yet the information found in this representation give a good characterization of its distribution.

Finally, another visualization is the empirical distribution function of the sample (see Figure 3.11C). The empirical distribution function is the discrete version of a cumulative distribution function. For any value  $x_0$ , the empirical distribution function gives the fraction of data points that are smaller than the given  $x_0$ . This visualization enables to read of the median ( $x_0$  for which  $\text{ECDF} = 0.5$ ), any percentile, or an interval that contains a desired fraction of the data set (for example, the 25th/75th percentile); the fraction of data points above and below a given value can be directly read out of the representation of the data. Additionally, differences in the distribution of two sample sets can be easily detected by comparing their empirical distribution functions. The Kolmogorov-Smirnov statistical significance test employs this comparison of the empirical distribution functions of the data sets as discussed below.

### 3.6.2. Logarithmic-Normal Distribution

The logarithmic-normal distribution or log-normal distribution is a distribution of a random variable whose logarithm is normally distributed. The random variable created from the product of positive independent random variables follows a log-normal distribution, while the random variable created from the sum of independent random variables follows a normal distribution (central limit theorem). The probability density function of the log-normal distribution is:

$$f(x) = \frac{1}{\sqrt{2\pi}\beta x} \exp\left(-\frac{(\ln(x) - \alpha)^2}{2\beta^2}\right). \quad (3.1)$$

The distribution yields a median of  $\exp(\alpha)$ , a mean of  $\exp(\alpha + \beta^2/2)$ , a standard deviation of  $\exp(\alpha + \beta^2/2) \cdot \sqrt{\exp(\beta^2) - 1}$ , and a positive skewness<sup>35</sup> of  $(\exp(\beta^2/2) + 2) \cdot \sqrt{\exp(\beta^2) - 1}$ . The log-normal distribution often characterizes biological phenomena as they cannot yield negative outcomes, for example, the adhesion force to a substrate, or the weight of a human being.

### 3.6.3. Statistical Significance Testing: the Kolmogorov-Smirnoff Test

A statistical significance test evaluates the null hypothesis  $H_0$ , which assumes a specific relation of the distributions of two data sets. The data sets were potentially obtained from different experimental conditions, thus the significance test evaluates whether the experimental conditions significantly influence the data. The significance test gives a quantitative measure for the certainty that the null hypothesis  $H_0$  can be rejected, at a given significance level. In this work, I used a significance level of 5 %. This significance level means that the probability of rejecting the null hypothesis even though it is true is 5 %, which is commonly referred to as a type I error. As a significance test quantifies the certainty that the null hypothesis can be rejected, the failure to reject the null hypothesis is not equivalent with the null hypothesis being true. Yet, the failure to reject the null hypothesis is a strong indication that the null hypothesis resembles the true relation between the two data sets.

The Kolmogorov-Smirnov test examines the null hypothesis that two distribution of data sets (for example, adhesion forces obtained with the same cell from different substrates) were drawn from the same underlying distribution:

$$H_0 : F_1 = F_2, \quad (3.2)$$

where  $F_1$  and  $F_2$  are the empirical cumulative density functions of the two data sets. A rejection of the null hypothesis means that the two sample sets were from different distributions, i.e. the adhesion forces to the two substrates are different (95 % certainty at a significance level of 5 %). In contrast, if the test fails to reject the null hypothesis, it can be assumed that there

---

<sup>35</sup>The skewness of a sample  $X$  is given by  $S(X) = E\left[\left(\frac{X-\mu}{\sigma}\right)^3\right]$ , where  $\sigma$  is the standard deviation,  $\mu$  the mean, and  $E[\cdot]$  the expectation operator.

is no (significant) difference between the adhesion forces to the two different substrates.

To test the null hypothesis, the Kolmogorov-Smirnov significance test quantifies the difference between the empirical cumulative distribution functions of the first sample  $F_1$  and the second sample  $F_2$ . The test statistic is calculated as:

$$T_{KS} = \sup_x |F_1(x) - F_2(x)|, \quad (3.3)$$

with the empirical distribution functions  $F_1$  and  $F_2$  of the first and second sample with size  $n$  and  $m$ , respectively. The null hypothesis that the distributions are equal ( $H_0 : F_1 = F_2$ ) is rejected if

$$T_{KS} > c(\alpha) \sqrt{\frac{n+m}{n \cdot m}}, \quad (3.4)$$

with  $c(\alpha = 0.05) = 1.36$  and  $c(\alpha = 0.01) = 1.63$ , which correspond to a significance level of 5 % and 1 %, respectively. The Kolmogorov-Smirnov test statistic is the maximal absolute difference (residuals) of the two empirical distribution functions (see Figure 7.2D for an example). In MATLAB, a two sample Kolmogorov-Smirnov statistical test can be performed using the function `kstest2()`.

A one-sided Kolmogorov-Smirnov test is used to evaluate whether the empirical distribution function  $F_1$  is significantly larger or smaller than the empirical distribution function  $F_2$ . The test statistic for the alternative hypothesis  $H_0 : F_1 > F_2$  is:

$$T_{KS} = \max_x (F_1(x) - F_2(x)), \quad (3.5)$$

for the alternative hypothesis  $H_0 : F_1 < F_2$ :

$$T_{KS} = \max_x (F_2(x) - F_1(x)). \quad (3.6)$$

The alternative hypothesis is accepted at a given significance level if Equation 3.4 is true, with  $c'(\alpha = 0.05) = 1.22$  and  $c'(\alpha = 0.01) = 1.36$  correspond to a significance level of 5 % and 1 %, respectively. Note that the smaller empirical distribution function belongs to the data set with the larger values and vice versa.

## Results



## 4. Conceptual Aspects of Microalgal Single-Cell Force Spectroscopy Experiments

Studying the adhesion strategies of microbial life is a research direction that aims at controlling biofilm formation and biofouling, for example. Numerous single-cell force spectroscopy studies on bacterial adhesion have led to a comprehensive knowledge regarding experimental methods to quantify bacterial adhesion. However, bacteria are not the only form of microbial life that is of interest to humans. Recently, microalgae have raised considerable interest due to their potential in technological applications, such as in photobioreactors. Although microalgae are of profound ecological and technological importance (see section 2.1 and section 2.3.3), there are only a few force spectroscopy studies on microalgae and there are no *in vivo* studies on flagella-mediated microalgal adhesion. Consequently the expertise on quantitative adhesion measurements with microalgae is fairly limited. Yet, systematic, quantitative force spectroscopy experiments are necessary to dissect the mechanisms that govern the adhesion of microalgae to substrates (see the objective and individual task of this work as defined in chapter 1).

The aim of this chapter is to validate the force spectroscopy approach chosen to study *Chlamydomonas* adhesion and to optimize the experimental parameters to resemble a natural situation. Thereby, I provide important insights on the adhesion of *Chlamydomonas*, which will serve as a basis for the experiments and results shown in the following chapters.

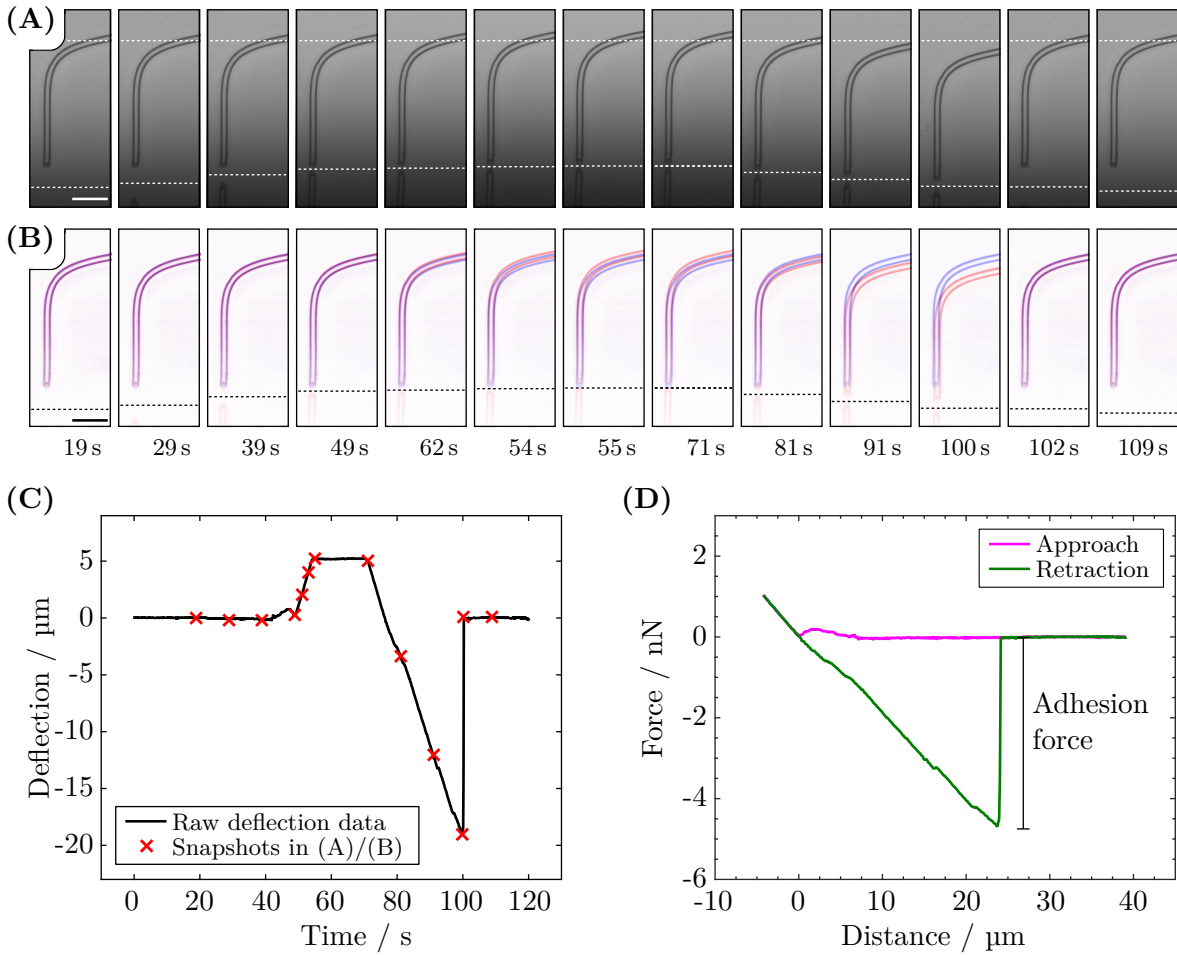


**Figure 4.1.: A representative force-distance experiment.** (A) Optical micrographs of an adhesion experiment at different time points. The dashed lined at the top represents the cantilever's zero-force position. The dashed line at the bottom indicates the substrate's position. Scale bar:  $50\mu\text{m}$ . (B) Micropipette extracted with an edge detection analysis from the images in (A). Red: current micropipette position. Blue: undeflected micropipette. (C) Raw deflection data of the optical micrographs shown in (A). (D) Corresponding force-distance curve of the raw deflection data shown in (C).



## 4.1. Adhesion Experiments with Micropipette Force Spectroscopy

Micropipette force spectroscopy promised to be an appropriate tool to study microalgal adhesion, as it was already employed in studies probing forces generated by molecular motors [Kamimura and Takahashi, 1981; Kishino and Yanagida, 1988], the adhesion of individual bacteria [Tsang et al., 2006], HeLa cells<sup>36</sup> and vesicles [Colbert et al., 2009]. In *Chlamydomonas* research, micropipettes were used to study the alga’s photoresponse as well as the flow field generated by the flagella beating [Rüffer and Nultsch, 1990, 1991; Harz and Hegemann, 1991; Drescher et al., 2010]. These studies suggested that adhesion experiments are feasible. Nevertheless, the first step in the project was to develop a reliable experimental routine to perform force spectroscopy experiments with *Chlamydomonas*.

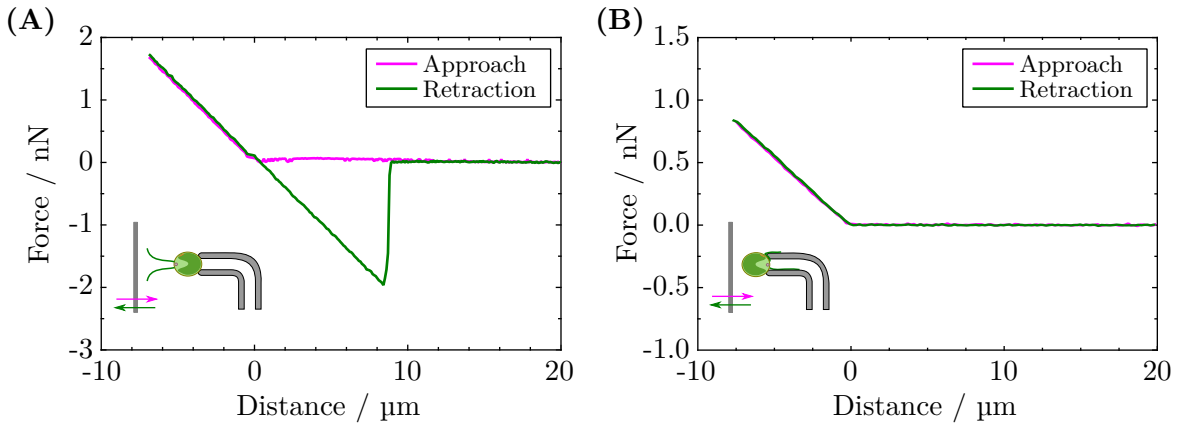
I developed a procedure to attach living *Chlamydomonas* cells to the micropipette cantilever in a controlled configuration (described in section 3.4). An optimal diameter of the micropipette’s nozzle guaranteed that the cell did not move and did not rotate during the course of an experiment. Afterwards, I brought a substrate in contact with the cell, and subsequently I measured the force that is required to detach the cell from the substrate. For detaching the cell, the substrate was retracted to its initial position, which caused the micropipette cantilever to deflect. The cantilever deflection generated a restoring force that pulls on the cell. The cell detached when the restoring force of the cantilever was larger than the cell’s adhesion force to the substrate.

Figure 4.1A+B shows a series of optical micrographs at distinct times during a force spectroscopy experiment; a video of this experiment is available in [Kreis et al., 2017, Supplemental Movie 1]. These images show the nozzle of the micropipette cantilever and the cantilever’s deflection during a typical force-distance cycle. The substrate was pushed against the cell body (from below), and retracted again with the cell adhering to the substrate. The rupture of the adhesive contact between the cell and the substrate can be identified in the optical micrographs as a snap-back of the cantilever to the equilibrium zero-force position (at time  $t \approx 100$  s). From these optical micrographs, I extracted the cantilever’s deflection and subsequently correlated the corresponding force acting on the cantilever with the substrate position. This correlation yielded the force-distance curve that characterize the interaction of *Chlamydomonas* with the substrate (see Figure 4.1C+D and section 3.4.2 for further details). The alga’s adhesion force to the substrate is the maximal absolute force during the detachment process, corresponding to the maximal negative cantilever deflection in the raw deflection data. In this particular force-distance experiment, the cell adhered with a force of approximately 4.2 nN to the substrate.

The repulsive (positive) force regime of the force-distance curves yields information of the cell

---

<sup>36</sup>HeLa cells are human epithelial cancer cells from Henrietta Lacks. These cancer cells are the oldest “immortal” human cell line that do not die after several cell divisions, which is the case for other human cells.



**Figure 4.2.: Flagella-mediated cell adhesion of *Chlamydomonas* to solid substrates.** Force-distance curves for two different cell configurations provide evidence that only the flagella and not the cell body adhere to the substrate. The cell configuration is controlled optically. **(A)** Flagella configuration. **(B)** Cell-body configuration. Adapted from [Kreis et al., 2017].

body’s deformation during an experiment. The force-distance curves always exhibited a linear force-distance relation in the repulsive regime (Figure 4.1D), which can be translated back into a linear relation between the cantilever’s deflection and the substrate’s motion (dividing the force by the spring constant). In all experiments, the cantilever’s deflection was equal to the amount the substrate was pushing against the cell, which becomes apparent when looking at the slope in the force-distance curve in the repulsive regime. The force-distance curve exhibited a slope of  $0.241 \text{ nN}/\mu\text{m}$ , which translates to a cantilever deflection of  $0.984 \mu\text{m}$  for each micrometer the substrate was pushed against the cell (the spring constant was  $0.245 \text{ nN}/\mu\text{m}$ ). Hence, the cell body was not deformed significantly. This finding is in line with the optical micrographs that also did not show a deformation of the cell body. In fact, this indirectly shows that the cell body is much stiffer than the cantilever.

Compared to bacteria, the *Chlamydomonas* cell body is enclosed within a thick, multilayered proteinaceous cell wall [Bloodgood, 2009], which is why, one might expect the cells to be stiffer than bacteria, such as *Escherichia coli* or *Staphylococcus aureus* [Cayley et al., 2000; Deng et al., 2011; Loskill et al., 2014]. These bacteria feature a spring constants of several  $\text{nN}/\mu\text{m}$ , while the spring constant of the cell membrane itself can be as large as several tens or even hundreds of  $\text{nN}/\mu\text{m}$ <sup>37</sup>. In contrast to the wild-type strain SAG 11-32b, *Chlamydomonas* mutants that lack the cell wall were mechanically more unstable (see section 6.5.2). With these cells, force spectroscopy tests were not successful so far, as the cells got destroyed during the experiment<sup>38</sup>.

<sup>37</sup>The cell’s spring constants were estimated from the reported elastic moduli, and the geometry of the bacteria and their cell wall.

<sup>38</sup>These tests were performed with photoreceptor deletion-mutants of the *Chlamydomonas reinhardtii* CC-3403 parent strain, which were kindly provided by Prof. Hegemann and co-workers (Humbolt-Universität, Berlin, Germany).

## 4.2. Flagellar Dynamics During Flagella-Mediated Cell Adhesion

Many microorganisms have developed flagella to explore their habitats, interact with surfaces, and form adhesive contacts with surfaces. In *Chlamydomonas*, the flagella presumably serve important sensory functions, mediate cell-cell interactions during the sexual mating, propel the cell forward during swimming, and provide adhesive contacts during gliding [Bloodgood, 2009; Harris et al., 2009, see also section 2.3]. The following three sections describe several experimental aspects of the flagella dynamics during the adhesion process. The first section compares the adhesion forces of the flagella with the adhesion forces of the cell body. The second section examines the flagella configuration when in contact with the substrate. Finally, the third section studies whether the flagella recover the regular breaststroke beating after the cell was detached from the substrate during the force-distance curves.

### 4.2.1. Flagella Adhesion versus Cell Body Adhesion

The optical control in the micropipette experiments allows for determining the adhesion forces of specific domains of the organism *Chlamydomonas*. The two different cell domains of interest are the cell body, which is enclosed by the cell wall, and the two flagella attached to the cell apex. I probed the adhesion forces of both domains separately by grasping cells in two different configurations (see section 3.4 for the individual steps).

In the “flagella configuration”, the cell was held at the anterior of the cell body, so that the flagella touched the substrate during the force-distance curve. Force-distance curves in this configuration yielded adhesion forces of several nanonewtons (see Figure 4.2A). In the “cell-body configuration”, I held the cell at the cell apex and probed the adhesion force of the cell body (the flagella could not touch the substrate and might have even been partially aspirated into the micropipette). In contrast to the flagella, the cell body did not exhibit any detectable adhesion (see Figure 4.2B). These quantitative findings agree with previous observations in gliding studies that only the flagella mediate the adhesion to surfaces [Bloodgood, 2009]. Henceforth, *Chlamydomonas* adhesion refers to the adhesion of the *Chlamydomonas* flagella to substrates.

### 4.2.2. Flagellar Dynamics During Flagella-Substrate Contact

In a natural situation where the cell established surface contact by itself, the flagella exhibit the gliding configuration. In this configuration, the flagella are spread out from the cell body and form an angle of approximately  $180^\circ$  between themselves. However, the flagella were forced into contact by being pushed against the substrate during the force spectroscopy studies. This procedure might result in an unpredictable configuration of the flagella when in adhesive contact with the substrate. As a random flagellar configuration does not represent the natural situation, a comparison to the natural situation would be difficult. Thus, the flagella configuration

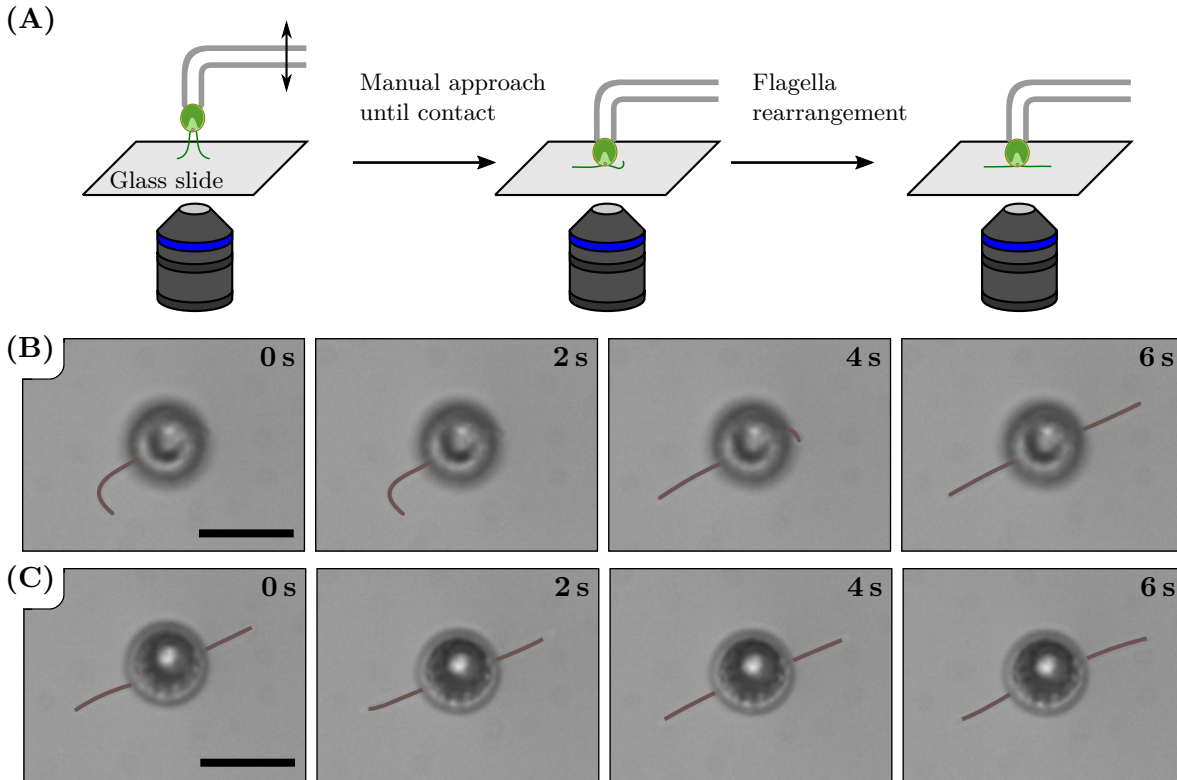


**Figure 4.3.: Visualizing the flagella configuration of *Chlamydomonas* on the substrate during the force spectroscopy experiments.** Force-distance experiments in a modified experimental configuration allow for visualizing the flagella configuration. The flagella of *Chlamydomonas* establish the gliding configuration within a few seconds. **(A)** The cell is manually brought into contact with a glass slide in the focal plane of the microscope. Note that the force sensor's geometry is modified such that the nozzle faces towards the glass slide. **(B)** Series of optical micrographs of a cell at different times after surface contact. The cell establishes the gliding configuration after 6 s. The solid line represents a guideline to the eye to visualize the flagella (raw images, see Figure A.11). Scale bar: 10 μm. **(C)** The flagella exhibit the characteristic gliding configuration immediately after surface contact. Scale bar: 10 μm.

when in contact with a substrate was studied during the force spectroscopy experiments<sup>39</sup>.

In the standard experimental design, the substrate was oriented perpendicular to the focal plane of the microscope, and the flagella were not visible on the substrate (see Figure 4.1A). As the focal plane of the microscope could not be rotated, I modified the experimental setup such that the cell was pressed against a glass substrate in the focal plane of the microscope (the bottom glass slide of the liquid cell). In contrast to the “normal” force sensor’s geometry, the nozzle was bent downwards and out of the focal plan to face the bottom glass slide of the liquid cell in this configuration. To bring the cell into contact with the glass substrate, the micropipette was moved manually up and down with a micromanipulator. This recurrent micropipette motion resembled a force-distance curve (see Figure 4.3A).

The flagellar dynamics when in contact with the substrate are shown in Figure 4.3B+C. These micrographs illustrate that the flagella contact dynamics can be separated into two different cases. The flagella either formed an adhesive contact directly in the gliding configuration (Figure 4.3B), which was observed in 6 out of 16 individual experiments, or the flagella established contact in a random configuration and rearranged into the gliding configuration afterwards (Figure 4.3B). The experiments yielded an average rearrangement time of 7.4(4.6) s, with a maximal rearrangement time of 15.2 s. Once the flagella had achieved the natural gliding configuration, the flagella remained straight and spread at approximately 180° relative to one another. Only subtle motions (“wiggling”) of the flagella tips were observed, which has been described before [Bloodgood, 1981]. It was hypothesized that this wiggling motion allows the cell to change its gliding direction in response to external stimuli such as light [Bloodgood, 1990b].

To ensure that the cells established the natural flagellar configuration during the force spectroscopy experiments, the cell-substrate contact time was set to 25 seconds.

#### 4.2.3. Flagellar Dynamics After Cell Detachment

During the force spectroscopy experiments, the flagella are detached from the substrate, which possibly injures the flagella and might affect subsequent adhesion experiments. Thus, I checked whether the cells recovered the regular flagella beating, as indicative of fully functional flagella after detachment, and I measured the timescale of the recovery process.

These experiments show that immediately after the detachment the flagella remained quiescent. The flagella resumed their motion over a time periode of several seconds. The optical micrographs in Figure 4.4 (recorded at approximately 400 fps) yielded a recovery time of the regular, synchronous breaststroke beating of about 1.7 s. The same experiment with nine cells

---

<sup>39</sup>The experiments were initiated by Christian Titus Kreis and performed by Christine Linne during her work as a master student tutored by Christian Titus Kreis [Linne, 2017].

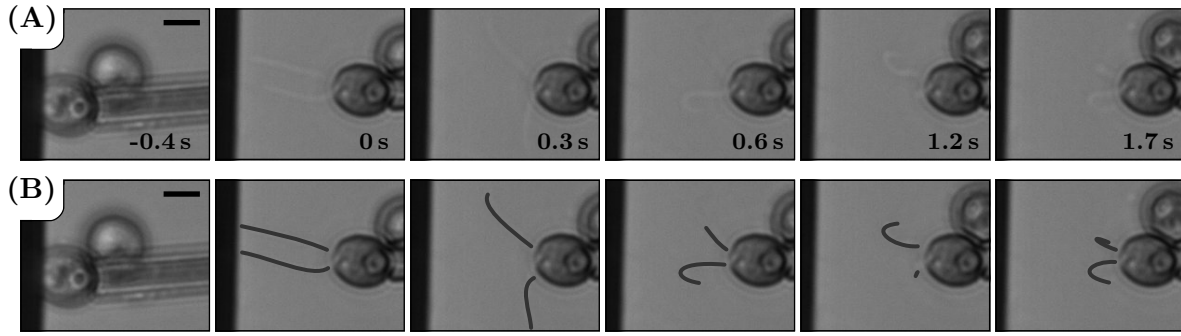


**Figure 4.4.: Flagella dynamics after detachment.** (A) Series of optical micrographs of the flagellar dynamics after detachment. (B) Series of optical micrographs shown in (A) with guidelines to the eye. Note that the flagella are not always perfectly aligned in the optical plane. The time is given relative to the time when the flagella were completely detached from the substrate. Scale bar: 5  $\mu\text{m}$ .

(43 individual measurements) yielded recovery times from 2.04 to 15.2 s (25th/75th percentile, median: 9.25 s, mean: 14.2 s). In 85 % of all cases, I measured a recovery time of less than 30 s. In general, I did not observe a correlation between consecutive experiments, since the recovery times of the regular beating could differ by tens of seconds for the same cell. Furthermore, the recovery times of the two flagella appeared to be independent from one another, i.e. both flagella started beating with the breaststroke waveform at different times (up to tens of seconds difference). The findings are in line with previous gliding studies. These studies suggest a signal pathway that presumably inhibits flagella motion, which is triggered by the flagella-substrate contact [Mitchell et al., 2004; Bloodgood, 2009]. In fact, I observed this transition from regular beating to quiescent flagella after the flagella adhered to a substrate (see Figure 6.7 and the corresponding discussion on page 107).

In conclusion, the flagella recovered their breaststroke beating after detachment. In combination with the flagellar membrane turnover (see section 2.3.4), which repairs any damage in the flagellar membrane, I expect the flagella to remain fully functional after force spectroscopy experiments. The time in between two contact periods of consecutive force-distance cycles was set to approximately 50 to 60 seconds, which is much longer than the typical recovery time of the breaststroke beating pattern.

### 4.3. Consistency Checks in Force Spectroscopy Studies

In the force spectroscopy experiments, the experimentally accessible parameters were the cell-substrate contact time, the substrate velocities during approach and retraction, and the pushing force at cell-substrate contact (see section 3.4.3). In previous studies, these parameters showed a significant influence on the adhesion forces of bacteria, cells, and vesicles [Thomas, 2008; Yakovenko et al., 2008; Colbert et al., 2009; Loskill, 2012; Apetrei and Sirghi, 2013]. Therefore, I studied the effect of the contact time, the substrate velocity, and the force at contact on the adhesion of *Chlamydomonas* to substrates.

#### 4.3.1. Temporal Evolution of the Adhesion Force

Systematic adhesion force studies require several force-distance cycles with the same cell that took about one hour in a typical experiment with *Chlamydomonas* (four sets of five force-distance cycles). Furthermore, each force-distance experiment might cause fatigue in the flagellar membrane that would influence the measured adhesion forces. In this context fatigue would mean that the flagellar membrane gets damaged during the force spectroscopy, for example, proteins remain at the substrate, and the cell is not able to repair any appearing damage quick enough. Consequently, I evaluated whether *Chlamydomonas* flagella showed any fatigue during the force spectroscopy studies by probing the temporal evolution of the adhesion force.

With the same cell, I performed one set of five force-distance curves every fifteen minutes over the course of two hours. On the single-cell level, the temporal evolution of the adhesion force showed subtle trends, and relatively large variations between two consecutive sets were possible (see Figure 4.5A, for example, the dataset drawn in yellow). These observations are likely related to the “dynamic” properties of the flagellar membrane, such as the turnover of the adhesion-mediating protein in the flagellar membrane [Bloodgood et al., 1986, see also section 2.3.4]. The turnover allows *Chlamydomonas* to recover the flagellar membrane and to replace flagellar membrane proteins within several minutes, which could lead to subtle fluctuations of the cell’s flagellar adhesiveness on a timescale of two hours (see also the results and discussion in chapter 5). In contrast, the average adhesion force of several cells stayed constant within the tested time frame, while signatures of individual cells were still visible due to the small sample size.

In addition, adhesion forces obtained from ten individual force-distance curves recorded within one hour ( $N = 127$  cells) did not yield any trend. The adhesion forces obtained from the last force-distance curve were found to be consistent with the forces recorded in the first force-distance curve (see Figure 4.6).

In summary, these results give evidence that the mean adhesion force of the same cell does not change significantly within the tested time frame of two hours. In particular, no fatigue

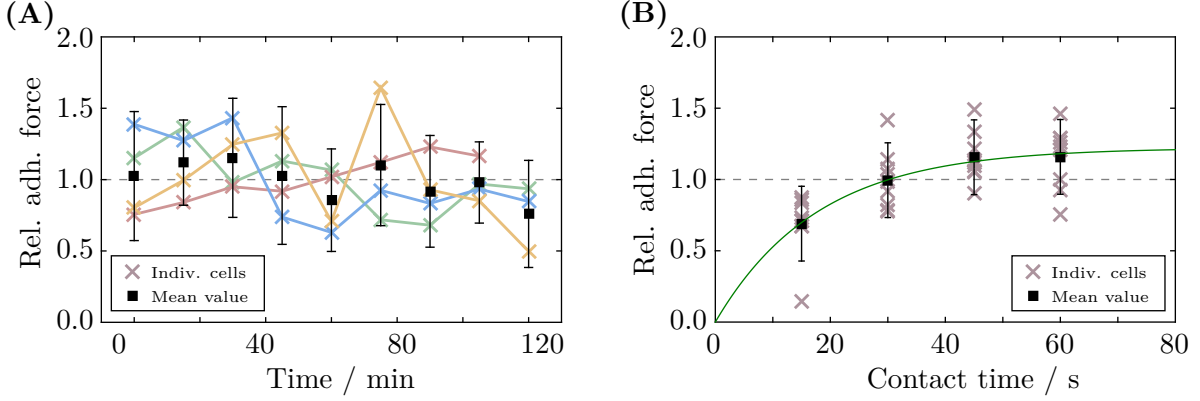


**Figure 4.5.: Consistency checks in force spectroscopy studies.** The adhesion force of several individual cells (crosses, mean of five force-distance curves) and the mean of all cells (squares) are shown (see section 3.4.3 for further information on the experimental parameters). The adhesion forces of each cell are normalized by the cell’s mean adhesion force of all individual force-distance curves. **(A)** Temporal evolution of the adhesion force. **(B)** Adhesion force as a function of the cell-substrate contact time. The solid green line represents a best fit to an exponential saturation (time constant of  $\tau = 5.65$  s).

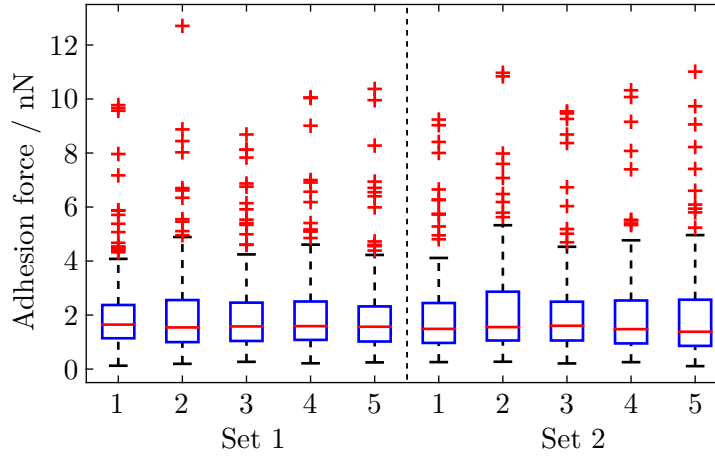


**Figure 4.6.: Temporal evolution of the adhesion force.** Adhesion forces of the individual force-distance curves performed with  $N = 127$  *Chlamydomonas* cells. The recorded adhesion forces of two sets of force-distance curves on a silicon substrate are displayed in chronological order. Before and in between the sets on the silicon substrate, experiments on other substrates might have been performed (see section 3.4.5 for the experimental routine when two substrates were involved).



was observed in any of the aforementioned experiments. The experiments indicate that any marginal damage caused by the force spectroscopy experiments, if present at all, was repaired by the flagellar membrane turnover without influencing the experimental outcome (see section 2.3.4). These findings allow for systematic force spectroscopy experiments with the same cell, which typically took less than 2 hours.

#### 4.3.2. Cell-Substrate Contact Time

A crucial parameter during the adhesion process is the contact time of the microorganism with the substrate. The contact with a substrate triggers signal pathways that regulate the transition from a reversible to an irreversible attachment and ultimately biofilm formation [O'Toole et al., 2000, see section 2.2]. In *Chlamydomonas*, the surface association presumably triggers flagella quiescence and gliding motility [Mitchell et al., 2004; Bloodgood, 2009, see also section 4.2.3]. Hence, I probed the adhesion force of *Chlamydomonas* as a function of the alga-substrate contact time.

With the same cell, I measured the adhesion force for contact times from 15 s up to 60 s (see the contact time definition in Figure 3.9), as for smaller contact times the flagella did not always exhibit the gliding configuration. The normalized mean adhesion force ( $N = 9$  cells) increased by about 68 % when the contact time was increased from 15 s to 45 s ( $F(15\text{ s}) = 0.690$  to  $F(45\text{ s}) = 1.16$ ), and saturated afterwards (see Figure 4.5B).

The adhesion force increase was less pronounced and occurred on a larger timescale compared to the adhesion force increase in similar experiments with bacteria. For example, viable *Staphylococcus aureus* showed an adhesion force increase of 500 % in a few seconds. In these living systems (*Chlamydomonas*, bacteria), the adhesion force increased much slower than in a passive system, like in adhesion force experiments with atomic force microscope cantilever tips interacting with pure lipid bilayers [Apetrei and Sirghi, 2013]<sup>40</sup>.

The observed adhesion force increase with the contact time for *Chlamydomonas* cells might be caused by a relocalization of adhesion-mediating proteins to the flagella-substrate contact points. This relocalization could be either a passive process driven by long-range interactions, a passive accumulation of adhesion-mediating proteins through diffusion in the membrane, or an active process driven by molecular motors inside the flagellum to enhance the adhesion strength of the flagellum-substrate contact. The observed timescale suggests an active relocalization of the adhesion promoting protein FMG-1B by molecular motors, as the described passive processes and protein diffusion of FMG-1B happen much quicker [Laib et al., 2009; Loskill,

---

<sup>40</sup>The timescale in the lipid bilayer experiment is rather comparable to the timescale of the adhesion force increase of inactive *Staphylococcus aureus* and viable *Staphylococcus carnosus* that lack adhesins. The smaller but faster increase, in this case, was attributed to hydrodynamic or equilibration effects [Loskill, 2012].

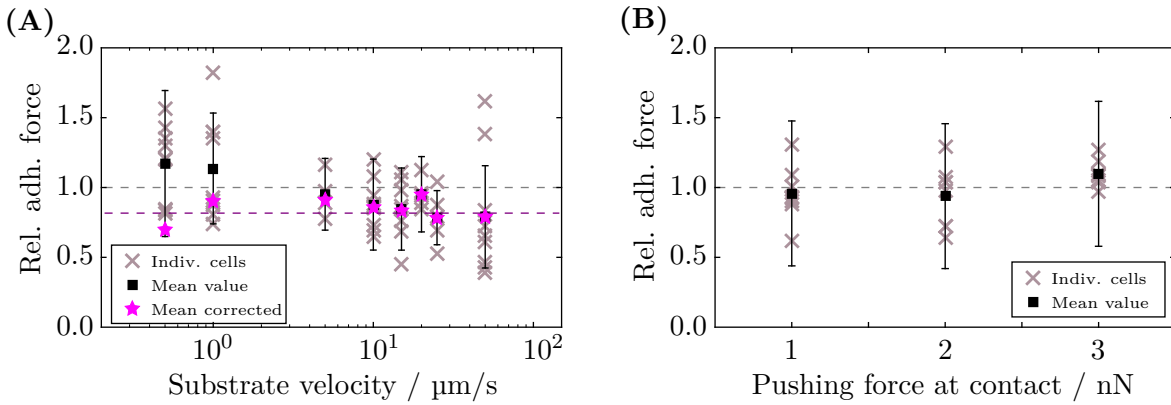


**Figure 4.7.: Consistency checks in force spectroscopy studies.** The adhesion force of several individual cells (crosses, mean of five force-distance curves) and the mean of all cells (squares) are shown (see section 3.4.3 for further information on the experimental parameters). The adhesion forces of each cell are normalized by the cell’s mean adhesion force of all individual force-distance curves. **(A)** Adhesion force as a function of the substrate velocity. Pink stars represent mean values corrected for the force increase with the contact time (linear correction, see text for explanations). **(B)** Adhesion force as a function of the pushing force at contact.

2012; Apetrei and Sirghi, 2013]. In fact, active protein motility associated with the adhesion protein FMG-1B was observed by Bloodgood and others, for example, as the translocation of microbeads along the flagellum and the flagellar membrane turnover (see section 2.3.4). The aforementioned hypothesis of a relocation of adhesion proteins causing the increase in the adhesion force, as well as the underlying mechanisms remains to be tested. Follow up experiments could study the hypothesis of an active accumulation process driven by molecular motors by inhibiting molecular motor motion, for example, by lidocaine or ciliobrevin D [Snell et al., 1982; Miyamoto et al., 2000; Firestone et al., 2012; Shih et al., 2013].

### 4.3.3. Substrate Velocity – Force Ramp Rate

The substrate velocity during the retraction of the substrate determined the force ramp rate acting on the cell until the adhesive contact ruptured. The force ramp rate has been shown to influence the adhesion strength of so called “catch bonds”. For example, the type 1 fimbrial FimH adhesin of *Escherichia coli* shows increased adhesion forces at higher ramp rates [Thomas, 2008; Yakovenko et al., 2008]. Whereas the force ramp rate may affect the adhesion process, the substrate velocity was the directly accessible quantity in the experiment. Yet, a constant substrate velocity translates into a varying force ramp rate in different experiments, as the ramp rate also depends on the cantilever’s spring constant. Keeping the substrate velocity constant was more practical, thus in this work, the force ramp rate varied in between the force spectroscopy experiments. To quantify the influence of the ramp rate on the adhesion forces, I quantified the adhesion force as a function of the force ramp rate by probing the adhesion

force with the same cantilever and *Chlamydomonas* cell at different substrate velocities.

For the same cells, the measured mean adhesion force decreased with increasing substrate velocity (see Figure 4.7A). However, the substrate velocity also influenced the cell-substrate contact time, which was not constant in these measurements<sup>41</sup>. A linear correction of the adhesion force with the contact time yields a substrate-velocity independent mean adhesion force. Hence, I can exclude any influence of the force ramp rate on the adhesion forces of *Chlamydomonas* in the tested range. At substrate velocities above 50  $\mu\text{m/s}$ , the cells deflagellated and no adhesion was observed afterwards at any substrate velocities. In fact, using mechanical shear stress is a commonly used method to purposely deflagellate *Chlamydomonas* cells [Rosenbaum et al., 1969].

The force ramp rates in the experiments shown in Figure 4.7A were between 0.1 to 30  $\text{nN/s}$  depending on the substrate velocity and the cantilever's spring constant. In all other experiments, I applied force ramp rates of 0.2 to 1  $\text{nN/s}$  (resulting from spring constants of 0.2 to 1  $\text{nN}/\mu\text{m}$  and a substrate velocity of 1  $\mu\text{m/s}$ ). These ramp rates are several orders of magnitude smaller than the ramp rates applied in single-cell bacterial atomic force microscopy studies (e.g. 12 to 200  $\text{nN/s}$  in [Thewes et al., 2015a,b]).

#### 4.3.4. Force Trigger – Force at Contact

In previous studies on vesicles, the force at contact showed a positive correlation with the adhesion force due to an increased contact area [Colbert et al., 2009]. In all experiments of the present study, the contact force of the cell with the substrate was proportional to the cantilever's spring constant, as the substrate was generally pushed by 5  $\mu\text{m}$  against the alga. The spring constants were mostly between 0.2 to 0.5  $\text{nN}/\mu\text{m}$  and up to 1  $\text{nN}/\mu\text{m}$  in rare instances; thus, the contact force in this study varied between 1 to 3  $\text{nN}$ . To quantify the influence of the force at contact on the adhesion of *Chlamydomonas* cells, I probed the adhesion force as a function of the pushing force at contact with the same cantilever (the contact time was kept constant at 25 s).

Force spectroscopy experiments with 8 cells did not show any effect of the pushing force at contact on the adhesion force; the mean adhesion force is constant in the tested range of contact forces between 1 to 3  $\text{nN}$  (see Figure 4.7B). As the cell body does not contribute to the adhesion, which is solely mediated by the flagella (see section 4.2), the contact area between cell body and substrates does not affect the adhesion process. The flagella always exhibit the gliding configuration (see section 4.2.2), thus the result of a contact force-independent adhesion force is reasonable.

<sup>41</sup>The contact time consists of ten seconds dwell time and a substrate velocity-specific time (cf. section 3.4.3). This velocity-dependent time is approximately  $t(v) = 15 \mu\text{m}/v$ , where  $v$  is the substrate velocity. Thus, the total contact time is given by  $t_{\text{total}} = 10 \text{ s} + 15 \mu\text{m}/v$ .

## 4.4. Summary

The aim of this chapter was to verify the quality of the *Chlamydomonas* force spectroscopy experiments, and to determine crucial experimental settings that guarantee comparable adhesion force studies. I studied the relevance of the flagella for the adhesion and their dynamics during the adhesion process. Subsequently, I quantified the influence of crucial force spectroscopy parameters on the adhesion force. These experiments yielded five main results:

1. The adhesion of *Chlamydomonas* was solely mediated by the flagella.
2. The flagella exhibited the natural gliding configuration in the force spectroscopy experiments in less than 15 s.
3. After the detachment, the flagella recovered the regular breaststroke beating within tens of seconds.
4. The force spectroscopy experiments did not lead to any fatigue in the *Chlamydomonas* flagella.
5. The adhesion force was independent of the force ramp rate and the pushing force at contact, while the adhesion force increased with contact time.

In summary, micropipette force spectroscopy is an appropriate method to characterize the flagella-mediated adhesion of *Chlamydomonas* to substrates. The second, third, and forth result validate that the force-distance curves are non invasive and can probe adhesion in the natural flagellar configuration found in surface-associated *Chlamydomonas* cells. The last two results provide insights in the force spectroscopy parameters that need to be controlled to obtain comparable adhesion forces. As the contact time influences the adhesion force, it was kept constant throughout the experiments. To allow the *Chlamydomonas* cells to establish the natural gliding configuration, I performed all experiments with a contact time of 25 s. Any other accessible force spectroscopy parameters (force ramp rate and pushing force at cell-substrate contact) did not affect the measured adhesion forces. In conclusion, the developed experimental routine allows for reliable adhesion measurements, which are necessary to quantify the adhesion forces of the *Chlamydomonas* flagella in different experimental conditions. Variations in the experimental conditions will elucidate mechanisms that trigger microalgal adhesion and dissect the underlying intermolecular interactions that govern the adhesion.

## 5. Quantitative Characterization of *Chlamydomonas* Adhesion Forces

Understanding the adhesion of microorganisms is necessary to control microbial biofilm formation in technological settings. Before studying biological mechanisms that trigger surface colonization (see chapter 6) and surface forces that govern the adhesion (see chapter 7), characterizing the fundamental aspects of the adhesion process and strategy is imperative.

The aim of this chapter is to elucidate fundamental details of the flagella-mediated adhesion of *Chlamydomonas* and to understand the typical adhesion force distributions on a model silicon substrate in a well-defined situation. Therefore, I quantify the adhesion force distribution of a population of *Chlamydomonas* cells and the force distributions of individual cells on silicon substrates. Subsequently, I characterize the signatures of individual force-distance curves. The chapter will be concluded by a discussion connecting the findings with each other and previous studies on the gliding motility of *Chlamydomonas*. Finally, the characteristics of *Chlamydomonas* adhesion will be compared to previous studies on bacterial adhesion.

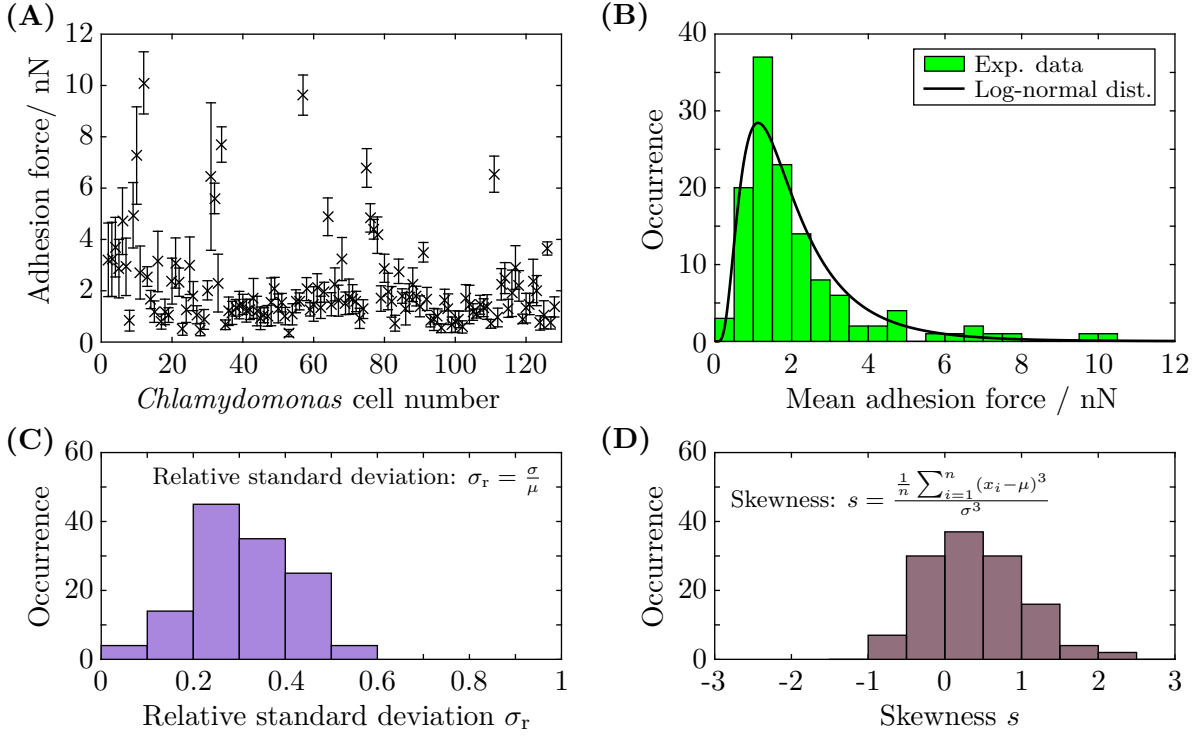


**Figure 5.1.: Adhesion force statistics of vegetative *Chlamydomonas* cells.** The adhesion force statistics of  $N = 127$  cells are shown. **(A)** Mean adhesion forces, error bars represent standard deviations. **(B)** Statistical distribution of the mean adhesion forces shown in (A). The solid line represents a best fit to a log-normal distribution. **(C)** Relative standard deviation for all cells shown in (A). The relative standard deviation is given as the standard deviation divided by the mean adhesion forces of the same cell. **(D)** Skewness of the force distributions of all individual cells shown in (A). The skewness is calculated using the displayed formula, with  $x_i$  being the ten individual force measurements of the cell,  $\mu$  the mean value, and  $\sigma$  the standard deviation of the forces  $x_i$ . A positive skewness indicates a distribution with a tail towards larger values.

## 5.1. Adhesion Force Statistics on Silicon Model Substrates

### 5.1.1. Statistical Distribution of Mean Adhesion Forces

I characterized the adhesion forces of vegetative *Chlamydomonas* cells on bare silicon substrates by *in vivo* force spectroscopy experiments in white light conditions (see the experimental routines and protocols in section 3.4.2 to 3.4.4). The reliability and comparability of these experiments was validated in chapter 4. With each *Chlamydomonas* cell, I performed ten force-distance curves with a substrate velocity of 1  $\mu\text{m/s}$  and a cell-substrate contact time of 25 s, to determine its adhesion forces. For each cell, I calculated the mean adhesion force, the spread of the adhesion forces, and the skewness of the data set.

The mean adhesion forces of 127 *Chlamydomonas* cells varied typically between 0.350 and 4.17 nN, but could be as large as 10 nN (Figure 5.1, upper and lower adjacent in a box plot, see Figure A.13). Individual force-distance curves exhibited adhesion forces up to 15 nN. The 25th and 75th percentile were 1.14 nN and 2.38 nN, respectively, yielding an interquartile range of 1.24 nN. Based on the upper adjacent, which is at maximum  $1.5\times$  the interquartile range extending from the 75th percentile, 13 cells were classified as outliers, which accounted for approximately 10 % of all cells. As a comparison, the lower and upper adjacent include approximately 99.3 % of the data in a normal distributed data set.

The measured adhesion forces were independent of the time of the day during the day cycle (see Figure A.12), yet in rare instances, cells did not exhibit any adhesion after about 15 to 17 o'clock (cells excluded from all analyses). This effect might be related to the cells starting to prepare the cell division after the commitment point, which is several hours before the start of the night cycle set to 19 o'clock (see section 2.3.3).

For the same cell, the adhesion forces measured in the individual force-distance cycles varied by 20 to 50 % around their mean adhesion force value, as described by the relative standard deviation (Figure 5.1C). This relatively large variation was not due to any fatigue of the flagella, as adhesion forces in the last force-distance cycle were consistent with adhesion forces recorded in the first cycle (see section 4.3 and Figure 4.6). In this context fatigue would mean that the flagellar membrane gets damaged during the force spectroscopy and the cell is not able to repair any appearing damage quick enough. In that case, I would expect the adhesion forces to decrease slowly over time, which is not the case.

The distribution of the skewness (Figure 5.1D), which was determined from the force distribution of each individual cell, was shifted towards positive values. As a comparison, the skewness of the distribution shown in Figure 5.3 was  $s = 1.22$ . Thus, for each cell the force distribution was rather asymmetric and featured a tail towards larger values (symmetric distribution: skewness  $s = 0$ ). The force distribution of each individual cell was less skewed (in

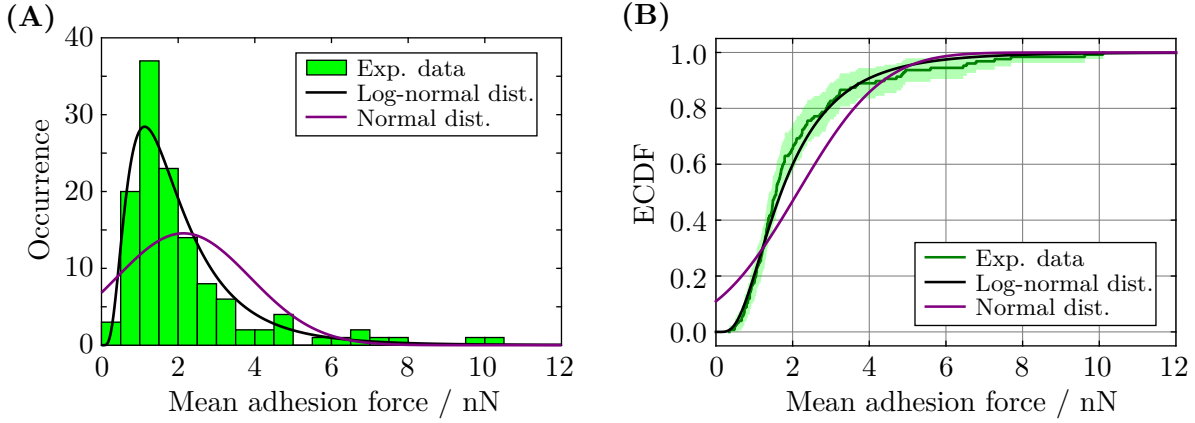


**Figure 5.2.: Distribution of adhesion forces of vegetative *Chlamydomonas* cells.** Analysis of the statistical distribution of adhesion forces shown in Figure 5.1. The force distribution is compared to a best fit to a log-normal distribution (black) and normal distribution (purple). **(A)** Histogram of mean adhesion forces and best fit to the data. **(B)** Empirical cumulative distribution functions of the mean adhesion forces and the fitted distribution models.

average) than the distribution including all individual measurements of all cells (see Figure 5.3).

The distribution of the mean adhesion forces followed a log-normal distribution (c.f. section 3.6.2):

$$F_{\text{adh}}(x) = \frac{1}{\sqrt{2\pi}\beta x} \exp\left(-\frac{(\ln(x) - \alpha)^2}{2\beta^2}\right) \text{ nN}, \quad (5.1)$$

where  $\alpha = 0.53$ [12] and  $\beta = 0.64$ [8] (see Figure 5.2). As shown in Figure 5.2, the adhesion force distribution did not follow a normal distribution. In light of the central limit theorem, this finding means that the adhesion forces of the individual cells were not independent and identically distributed, i.e. the adhesion forces of different cells had a different underlying distribution<sup>42</sup>. If the underlying adhesion force distribution of all cells would have been identical, i.e. the adhesion force distribution of all individual *Chlamydomonas* cells converge to the same underlying distribution for large numbers of measurements, then the mean adhesion force distribution in Figure 5.2 would follow a normal distribution. The histogram and empirical cumulative distribution functions show that this is not the case.

As elaborated in the previous paragraph, the difference in the mean adhesion forces seen for different *Chlamydomonas* cells originates from different underlying force distributions related

<sup>42</sup>The central limit theorem states that the distribution of means calculated for random samples drawn of independent and identically distributed random variables of the same underlying distribution follows a normal distribution. That is, independent of the functional form of the underlying distribution, the distribution of  $n$  sample means (in my case samples of cardinality 10) converges to a normal distribution for  $n \rightarrow \infty$ .



to (biological) characteristics of the *Chlamydomonas* cells. The adhesion of *Chlamydomonas* is mediated by the flagellar membrane glycoproteins FMG-1B [Bloodgood and Workman, 1984] (see also section 2.3.2). On each flagellum there are about 90000 copies of FMG-1B, which was estimated from polyacrylamide gel electrophoresis [Adair et al., 1983]. The flagellar surface area can be estimated to be constant with an area of about 6.3 to 7.5  $\mu\text{m}^2$  (flagella length: 10 to 12  $\mu\text{m}$ , diameter: 200 nm), as fully grown flagella conserve their length throughout the life cycle independent of the cell body size [Rosenbaum et al., 1969; Lefebvre and Rosenbaum, 1986]. Consequently, the average protein density in the flagellar membrane at the flagellar surface can be estimated to be 12000 to 14000 proteins/ $\mu\text{m}^2$ . This protein density represents a population average over approximately 5 millions of *Chlamydomonas* cells, as estimated from the methods used by Adair et al. [Adair et al., 1983]. On a single cell level, I assume that the protein density in the flagellar membrane depends on the expression of the gene that encodes the protein. In fact, it is well established that gene expression is a stochastic process that leads to variations in the amount of proteins in the cell and the protein density in the cell's plasma membrane [McAdams and Arkin, 1997; Elowitz et al., 2002; Newman et al., 2006; Sigal et al., 2006]. Hence, I attribute the cell-to-cell variability in the adhesion forces to a cell-to-cell variability in the amount of the adhesion-mediating protein FMG-1B on the flagellar surface (see section 2.3.2). That is, a higher mean adhesion force might have been caused by a larger average amount of FMG-1B in adhesive contact with the substrate.

The distribution of the FMG-1B density in the flagellar membrane in a population of *Chlamydomonas* cells is unknown and there is no information about the cell-to-cell variability in the FMG-1B transcription. Yet, Pazour et al. measured the changes in the transcription of flagellar proteins in *Chlamydomonas* upon deflagellation. They reported a five-fold increased FMG-1B transcription upon deflagellation in their study [Pazour et al., 2005]. An increased expression of the gene encoding FMG-1B could lead to an increased amount of adhesion promoting proteins on the flagellar membrane resulting in exceptionally high adhesion forces. A qualitative comparison of the mean adhesion forces shows that the adhesion forces of “outlier-cells” were about five times larger than typical mean adhesion forces (mean adhesion forces outliers: 4.5 to 10 nN, typical mean adhesion forces 1.14 to 2.38 nN). This estimation suggests that the amount of FMG-1B at the flagellar surface in the cells classified as outliers was increased about five-fold (under the assumption that the adhesion force scales linearly with the protein amount on the flagellum). Thus, a deflagellation-induced change in protein transcription could potentially explain the outliers. Explaining the outliers as cells that separated into gametes does not reconcile the “high” adhesion forces, as gametes exhibited adhesion forces which were consistent with the forces of vegetative “non-outlier” cells (see Figure 8.1A).

While Pazour et al. studied the deflagellation-induced protein transcription [Pazour et al., 2005], it might be possible that other kinds of flagella damage could also trigger an increased protein transcription, though experimentally probably difficult to study. Although, I did not

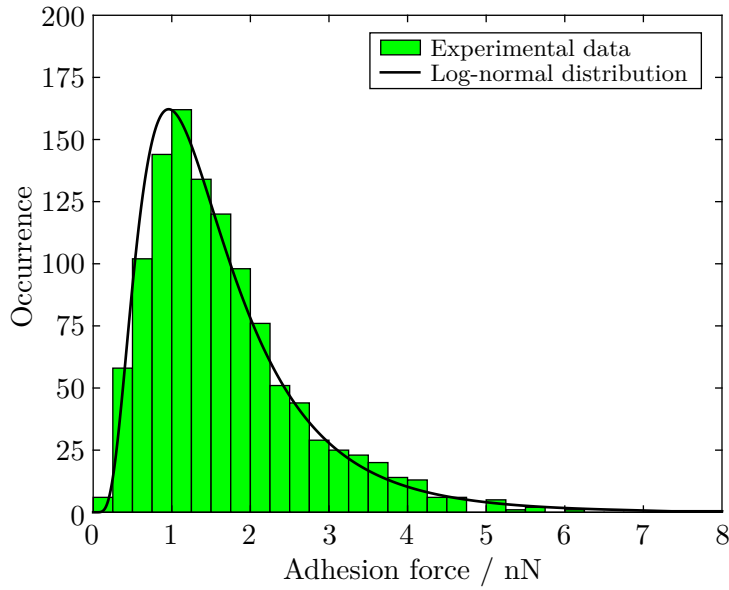


**Figure 5.3.: Statistical distribution of adhesion forces of vegetative *Chlamydomonas* cells.** The adhesion forces of 114 *Chlamydomonas* cells, each cell contributing ten individual measurements, are shown. The solid line represents the best fit of a log-normal distribution.

observe any damage of these “outlier-cells” or their flagella optically, an increased protein transcription after flagella damage appears to be a reasonable explanation for the high adhesion forces. Moreover, the finding from Pazour et al. supports the previously drawn conclusion that differences in the mean adhesion forces originated from differences in the protein density at the flagellar surface, which were presumably caused by differences in the FMG-1B transcription.

### 5.1.2. Adhesion Forces – Revised Statistics

I excluded the adhesion force data from the cells that were classified as outliers to avoid any influence on the following analyses from cells that might have experienced flagella damage in their history causing a higher FMG-1B expression (for example, in chapter 7). Furthermore, I include all force-distance curves of each cell (instead of the mean adhesion force), which improves the robustness and significance of the findings. The validity of this approach to include all force-distance curves of each cell in the statistic is discussed in section A.2. The resultant revised statistics of *Chlamydomonas* cells is shown in Figure 5.3. The force distribution was consistent with the functional form of the mean adhesion force distribution (see Figure A.2). The revised statistic yielded a mean adhesion force of 1.65 nN and a median of 1.43 nN, while 50 % of all adhesion forces were in the range of 0.951 to 2.09 nN (25th and 75th percentile). A log-normal distribution with  $\alpha = 0.33$ [4] and  $\beta = 0.61$ [3] described the functional form of the adhesion force distribution (see Figure 5.4). The Kolmogorov-Smirnov test statistic yields a difference of 0.029, which indicates an excellent agreement of the experimental data with the

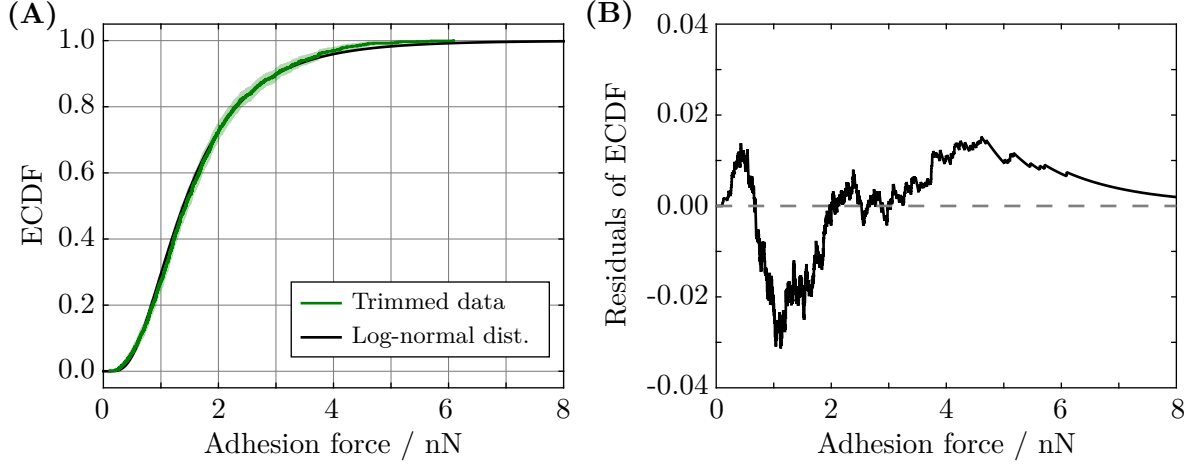


**Figure 5.4.: Empirical cumulative distribution function of the *Chlamydomonas* adhesion force distribution.** The empirical cumulative distribution function of the adhesion forces of 114 vegetative *Chlamydomonas* cells is shown (see also Figure 5.3). **(A)** Empirical cumulative distribution function ECDF (the shaded area represents the 95 % confidence interval) and best fit to a log-normal distribution. **(B)** Residuals of the cumulative distribution function of the fitted log-normal distribution and the empirical cumulative distribution function of the experimental data.

best fit to a log-normal distribution.

### 5.1.3. Discussion and Summary: Adhesion Forces

In summary, quantitative force spectroscopy experiments of 127 *Chlamydomonas* cells yielded log-normally distributed adhesion forces of several nanonewtons on a non-functionalized silicon substrate. The adhesion forces are consistent with forces reported in a study on purified and isolated flagella [Ramaswamy et al., 2013], yet any active process of the flagellar membrane could not be captured in this study. The flagella purification and modifications certainly also affected the properties of the flagellar membrane, which was evidenced by different signatures in the force-distance curves, and the main goal of the study [Ramaswamy et al., 2013]. Hence, the reported adhesion forces and drawn conclusions remain vague, and a direct comparison to my study seems difficult.

In contrast to this study on the adhesion forces, there are several studies on intraflagellar transport trains that transduce the forces necessary for the gliding motility (see section 2.3.4). These studies report that there are tens of intraflagellar transport trains in one flagellum, which are not all active at the same time [Stepanek and Pigino, 2016]. For geometry reasons, it can be assumed that only a fraction of these intraflagellar transport train can contribute to the force transfer between microtubules and the surface during gliding. The maximal force that

an individual intraflagellar transport train exerts on a microbead is in the order of tens of piconewtons [Laib et al., 2009; Shih et al., 2013]. This force magnitude seems to be at variance with the adhesion forces reported here, as a multiple of the existing intraflagellar transport trains were necessary to support adhesion forces in the order of nanonewtons.

The adhesion forces can be reconciled with the existing gliding literature, as outlined in the following. The forces reported by Laib et al. and Shih et al. represent stall forces of intraflagellar transport trains (driven by molecular motors) pulling on microbeads in an optical tweezers setup [Laib et al., 2009; Shih et al., 2013]. In these experiments, the microbeads were deflected in an optical trap by the motion of intraflagellar transport trains until a stall force of tens of piconewtons was reached, i.e. the maximal restoring force was equal to the the maximal force that the intraflagellar transport train can generate. At this point, one contact in the force transduction machinery between the microbead and the microtubules ruptured (bead – FMG-1B – intraflagellar transport train – molecular motors, see Figure 2.8 and the corresponding paragraph). Subsequently, the restoring force of the optical tweezers pulled the bead back into the center of the optical trap. Laib et al. analyzed the timescale of these return events in order to understand which part in the force transduction chain ruptured. The timescale found in the experiment was two orders of magnitude slower than the estimated timescale of a free return of the bead. A free return of the bead would have occurred if the adhesive contact between bead and FMG-1B would have ruptured. Instead, the timescale was rather comparable to a passive viscoelastic process, in which the bead–FMG-1B complex drags through the flagellar membrane (possibly, the intraflagellar transport train was also still connected to this complex). Although the exact origin of the drag was not resolved, the timescale of the return event strongly suggest that the adhesive contact between the bead and FMG-1B did not rupture. Consequently, the adhesion forces mediated by FMG-1B have to be larger than tens of piconewtons. Moreover, the adhesion forces reported here are conceptually different from the forces generated by molecular motors during gliding and should not be compared to these forces, but rather to forces measured in other single-cell adhesion studies.

The adhesion forces of *Chlamydomonas* are consistent with forces reported for individual bacteria [Sullan et al., 2014; Thewes et al., 2015b] and diatoms, a major group of algae in the phytoplankton [Dugdale et al., 2005]. The forces were slightly smaller than the adhesion forces of the microalga *Enteromorpha*, which secretes extracellular polymeric substances containing an adhesive glycoprotein [Callow et al., 2000].

Differences in the mean adhesion forces between cells were most likely due to a distinct cell-to-cell variability in the expression of the gene encoding the adhesion-mediating protein FMG-1B, which resulted in differences in the protein density in the flagellar membrane. This finding is in line with a distinct cell-to-cell variability in the previously mentioned bacterial adhesion studies, which is attributed to a spatial inhomogeneous protein distribution in the

bacterial cell wall. An unusually high FMG-1B density in the flagellar membrane, presumably caused by an increased FMG-1B transcription, appeared to be a reasonable explanation for cells that exhibited exceptionally high adhesion forces, as deflagellation and presumably flagella damage increases the FMG-1B transcription five-fold [Pazour et al., 2005].

For each individual *Chlamydomonas* cell, the variation in the adhesion force was about 20 to 50 % of the mean adhesion force value. In contrast, single-cell bacterial adhesion studies with *Staphylococcus carnosus* and *Staphylococcus aureus* yield a relative spread below 20 % [Thewes et al., 2014, 2015b, see the samples of multiple force-distance curves with the same bacterium and the corresponding spread in the adhesion force]. Consecutive force-distance curves of the same bacterium normally resemble the same shape, i.e. the same signatures appear in each force-distance curve, which indicates that the same individual adhesion proteins interact with the substrate in each force-distance cycle. Note that the bacterium is fixated at the cantilever and cannot rotate or move, consequently, the same portion of the cell wall is exposed to the substrate in every force-distance cycle. For another bacterium, the force-distance curves showed other sequences of signatures, rupture events, and another mean adhesion force, as the selection of adhesins interacting with the substrate had a different spatial distribution.

## 5.2. Adhesion and Characteristics of the *Chlamydomonas* Flagellar Membrane

In the previous section, I quantified the adhesion forces of a population of *Chlamydomonas* cells and presumably revealed the biological reason for the cell-to-cell variability in the adhesion forces. However, the reason for the force variation seen in multiple, consecutive force-distance curves performed with the same cell remains unclear. To elucidate the mechanism that causes the force variation for a single cell, I study the influence of the area of adhesive contact between the flagella and the substrate on the adhesion force and I characterize the individual signatures of the force-distance curves.

### 5.2.1. Contact Area in Adhesion Experiments

To study the influence of the area of adhesive contact between flagella and substrate on the adhesion forces, I varied the portion of the flagellum that can form an adhesive contact with the substrate<sup>43</sup>. Therefore, I combined force spectroscopy experiments with the auto-adhesion process, which allowed for adjusting the flagella length on the substrate without damaging the flagella. To perform these combined auto-adhesion and force spectroscopy experiments, a *Chlamydomonas* cell was held in close proximity to the substrate with a distance  $d_0$  smaller than the *Chlamydomonas*' flagella length  $l_f$  (see Figure 5.5). While the cell body was not in contact,

---

<sup>43</sup>The experiment was designed by Christian Titus Kreis and performed by Christine Linne for her Master's thesis [Linne, 2017], tutored by Christian Titus Kreis.

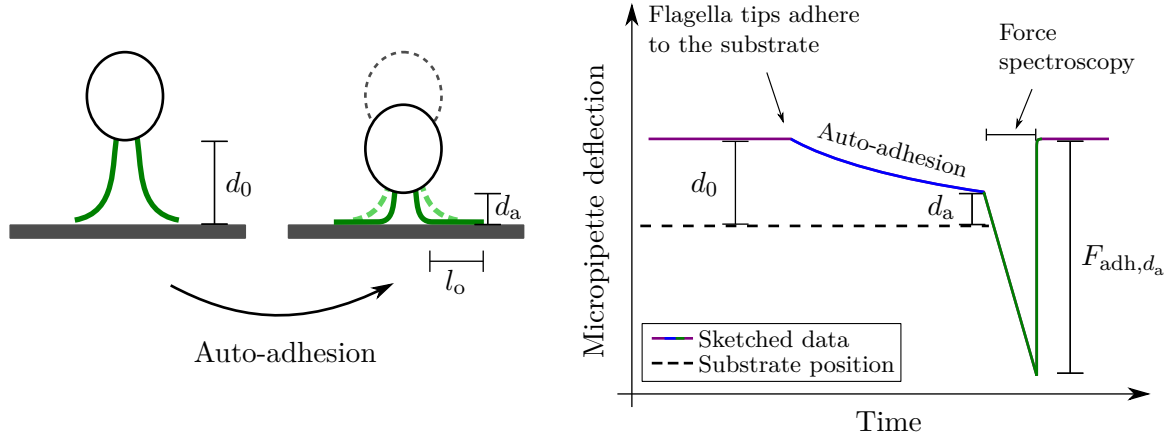


**Figure 5.5.:** Sketch of the setup to measure the adhesion force as a function of the flagella-substrate contact length. An auto-adhesion process (blue) is combined with force spectroscopy (green) to measure the adhesion force as a function of the flagellar length on the substrate. The *Chlamydomonas* cell is placed at an initial distance  $d_0$  to a substrate, so that the flagella tips can touch the substrate. After the flagella tips adhered to the substrate, the auto-adhesion process starts (see section 6.3 and section 3.4.6) and the flagella pull the cell body towards the substrate. At a cell-substrate distance  $d_a$  the substrate is retracted until the cell detaches, as in a force spectroscopy experiment, to determine the adhesion force. At this point the flagella length on the substrate is  $l_o$ .

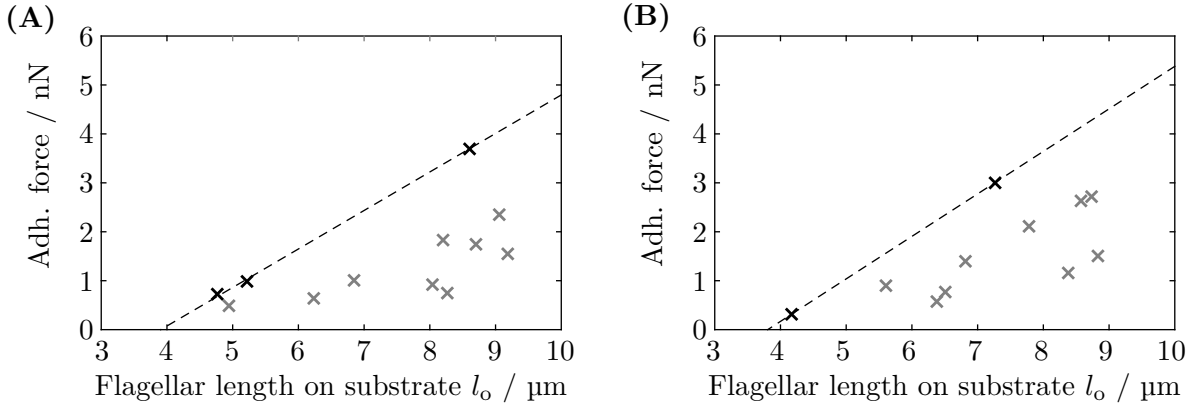


**Figure 5.6.:** Adhesion force as a function of the flagella length on the substrate. Two individual data sets of force measurements at different flagellar length on the substrate. The flagella length is determined from the cell-substrate distance by Equation 5.2 assuming a flagella length  $l_f$  of  $10\ \mu\text{m}$ . The data sets are shown in two separate figures for readability. An extended data set can be found in Figure A.10. The dashed lines envelope all data points (best fit to the dark data points (A):  $0.787\ \text{nN}/\mu\text{m}$ , (B):  $0.869\ \text{nN}/\mu\text{m}$ ).

the flagella tips touched the substrate during every cycle of their regular breaststroke beating. These recurrent interactions eventually led to an adhesive contact between the flagella and the substrate. Subsequently, the flagella tips started to glide on the substrate and pulled more of the flagella in contact and the cell body towards the substrate. During this process, termed auto-adhesion (discussed in more details in section 6.3), the flagella length on the substrate  $l_o$  increased as the cell-substrate distance  $d_a$  decreased:

$$l_o = l_f - \frac{d_a}{\sin \alpha}, \quad (5.2)$$

where  $\alpha$  is the angle between the flagella and the substrate. At a cell-substrate distance  $d_a$ , the substrate was retracted until the cell detached, which resembled the retraction cycle in a force spectroscopy experiment. Optical micrographs suggests that the angle between the flagella and the substrate was above  $75^\circ$  at the beginning of the auto-adhesion process (see the right-hand flagellum in Figure 6.7). The angle may become smaller at smaller cell-substrate distances, but was generally larger than  $45^\circ$ . For the following analysis, I assume that  $\alpha$  is constant  $90^\circ$  during the auto-adhesion process. This assumption results in an over estimation of  $l_o$  of  $0.25 \mu\text{m}$  at  $d_a = 7 \mu\text{m}$  and  $\alpha = 75^\circ$ ,  $0.62 \mu\text{m}$  at  $d_a = 4 \mu\text{m}$  and  $\alpha = 60^\circ$ , and  $0.83 \mu\text{m}$  at  $d_a = 2 \mu\text{m}$  and  $\alpha = 45^\circ$ . In conclusion, the combination of force spectroscopy experiments allowed for quantifying the adhesion force as a function of the cell-substrate distance, which can be used to estimate the flagella length on the substrate  $l_o$  (see Equation 5.2).

The measured adhesion forces were enveloped by a straight line, as shown for two representative datasets in Figure 5.6 (the complete data set is shown in Figure A.10). The slope of the envelope featured a distinct cell-to-cell variability from  $0.280$  to  $0.869 \text{ nN}/\mu\text{m}$  (see Table A.2). This result indicates that the adhesion force increases with the contact length of the flagellum. However, the same cell also exhibited adhesion forces that were just a small fraction of the adhesion force characterized by the envelope. For example, in the dataset shown in Figure 5.6A, adhesion forces of  $1 \text{ nN}$  were recorded at  $l_o = 8 \mu\text{m}$ , which is about  $1/3$  of the force characterized by the envelope. Furthermore, an increased flagella length on the substrate did not necessarily mean that higher adhesion forces were recorded. Adhesion forces of  $1 \text{ nN}$  were observed at a flagellar length on the substrate from  $5$  to  $8 \mu\text{m}$ . In general, for each cell there was always a fraction of data points that exhibited less than half of the force characterized by the envelope (see also Figure 5.6B and Figure A.10).

These findings suggest that the envelope can be understood as the maximal possible adhesion force at a given flagella length in contact with the substrate. Thereby, the slopes of the envelope characterizes the flagellar adhesiveness, which is presumably linked to the protein density in the flagellar membrane. The cell-to-cell variability in the slope pictures the previously described cell-to-cell variability of the protein density in the flagellar membrane. The data points “far” below the envelope suggest that an adhesive contact was not necessarily formed

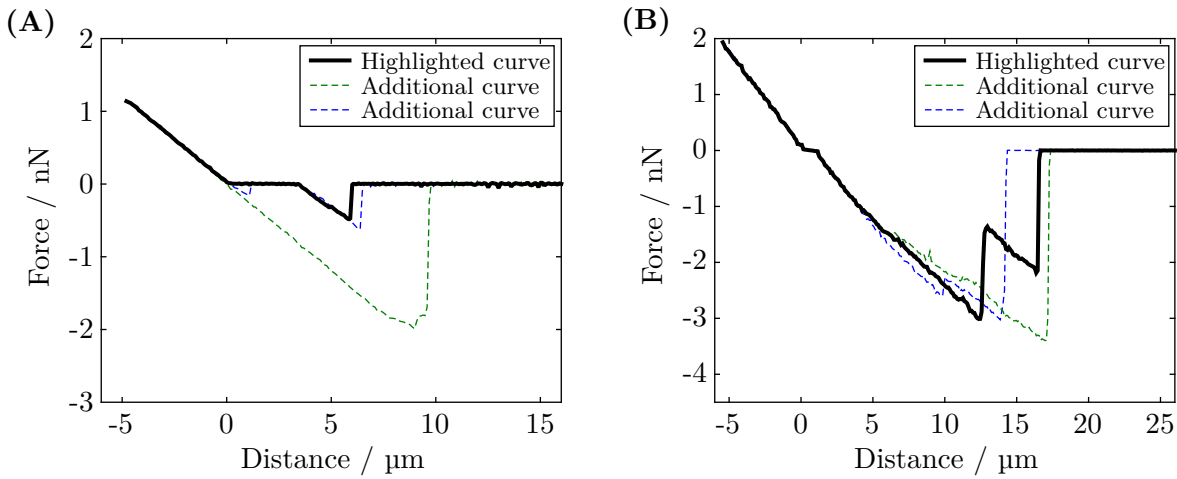


**Figure 5.7.: Signatures of force-distance curves.** A selection of representative force-distance curves of two different cells is shown. The black lines represent the force-distance curves with a specific signature, the blue and green dashed-lines are force-distance curves recorded in the same experimental set that visualize the variability in between different force-distance curves. **(A)** No adhesion at the beginning of the retraction cycle. **(B)** The force-distance curve exhibits two individual snap-back events.

between the substrate and the whole length of the flagellum apposed to the substrate. That is, in these experiments the flagella length that formed an adhesive contact was smaller than the flagella length on the substrate. Transferred to a regular force spectroscopy experiment, this interpretation suggests that the area of adhesive contact between flagellum and substrate is variable (even though the whole flagellum lies on the substrate). A previous interference reflection microscopy study on *Chlamydomonas* flagella during gliding supports this finding [Bloodgood, 1990b, unpublished results by Daniel and Kind]. The results of this study will be discussed below (see section 5.2.3).

In conclusion, the combined auto-adhesion and force spectroscopy experiments suggest that the area of adhesive contact between the flagella and the substrate differs in consecutive force-distance experiments. Thereby, the amount of adhesion-mediating proteins in adhesive contact may also vary, which ultimately contributes to the variation in the adhesion forces on a single-cell level.

### 5.2.2. Signatures of Force-Distance Curves

The force spectroscopy experiments comprise more information than the adhesion forces of the *Chlamydomonas* cells. In general, the rupture dynamics and signatures contain characteristics of the adhesive sites that can be used to extract valuable information of its structural properties [Sullan et al., 2015]. The optical micrographs and force-distance curves show the rupture of an



individual adhesive contact as snap-back of the cantilever (see Figure 4.1 and Figure 3.9B+C). Multiple snap-backs (in one single force-distance curve) indicate the rupture of several individual contacts. In the following, I analyze the rupture dynamics of the *Chlamydomonas* adhesive sites. Selections of several representative force-distance curves are shown in Figure 5.7 and Figure 5.8 (a larger selection of complete sets of force-distance curves is shown in Figure A.14).

In the sample force-distance curve shown in Figure 5.7A, the cantilever did not deflect up to a cell-substrate distance of approximately 4  $\mu\text{m}$ , at which the cantilever started to deflect. The force-distance curves did not exhibit any negative slope in this area, which suggests that the flagellum did not become stretched (see also the discussion on flagellar stretching below). This signature rather indicates that the proximal part of the flagella did not adhere to the substrate in this specific force-distance cycle. While often less prominent, I found this signature in other force-distance curves (for example, in Figure 5.7B and Figure 6.1A) and it was visible in the corresponding optical micrographs as a distinct flagella-substrate distance before rupture. In another force-distance cycle with the same cell, the proximal part of the flagella also adhered to the substrate (see Figure 5.7A, the dashed green line). This difference in between two force-distance curves of the same cell supports the finding that not necessarily the whole flagellum forms an adhesive contact.

Another prominent feature of the force-distance curves were two or more snap-back events in the same detachment process, where each snap-back event indicates the rupture of an individual adhesive site (Figure 5.7B). The appearance of two or more rupture events was found in many variations, for example, the individual snap-back could either be small or large compared to the current cantilever deflection (see Figure A.14). In some cases, the snap-back was (almost) as large as the current cantilever deflection with another subsequent adhesion event (see Figure 5.8). While the magnitude of the snap-back events was hardly comparable in different force distance curves, it seemed that in all cases at maximum two large snap-back events were observed, whereas many more small snap-back events could occur. As the cell has two flagella, this qualitative observation suggests that the major snap-back events are the detachment of the two flagella, whereas the small snap-back events are presumably related to several localized adhesive sites on each flagellum.

Whereas the snap-back events are presumably related to rupture events of the adhesive contacts, the force-distance curves feature other return events, where the cantilever deflection decreased on a much longer timescale. The snap-back of the cantilever could occur on a timescale of tens of milliseconds (see Figure 5.8A+B). The timescale and functional form of this snap-back was consistent with the over-damped step response of a cantilever in buffer solution (see Figure 5.9). Thus, this snap-back event was most like a free return of the cantilever in the zero-force position (or until the flagella are again under tension) after a localized adhesive contact between the flagellum and the substrate ruptured.

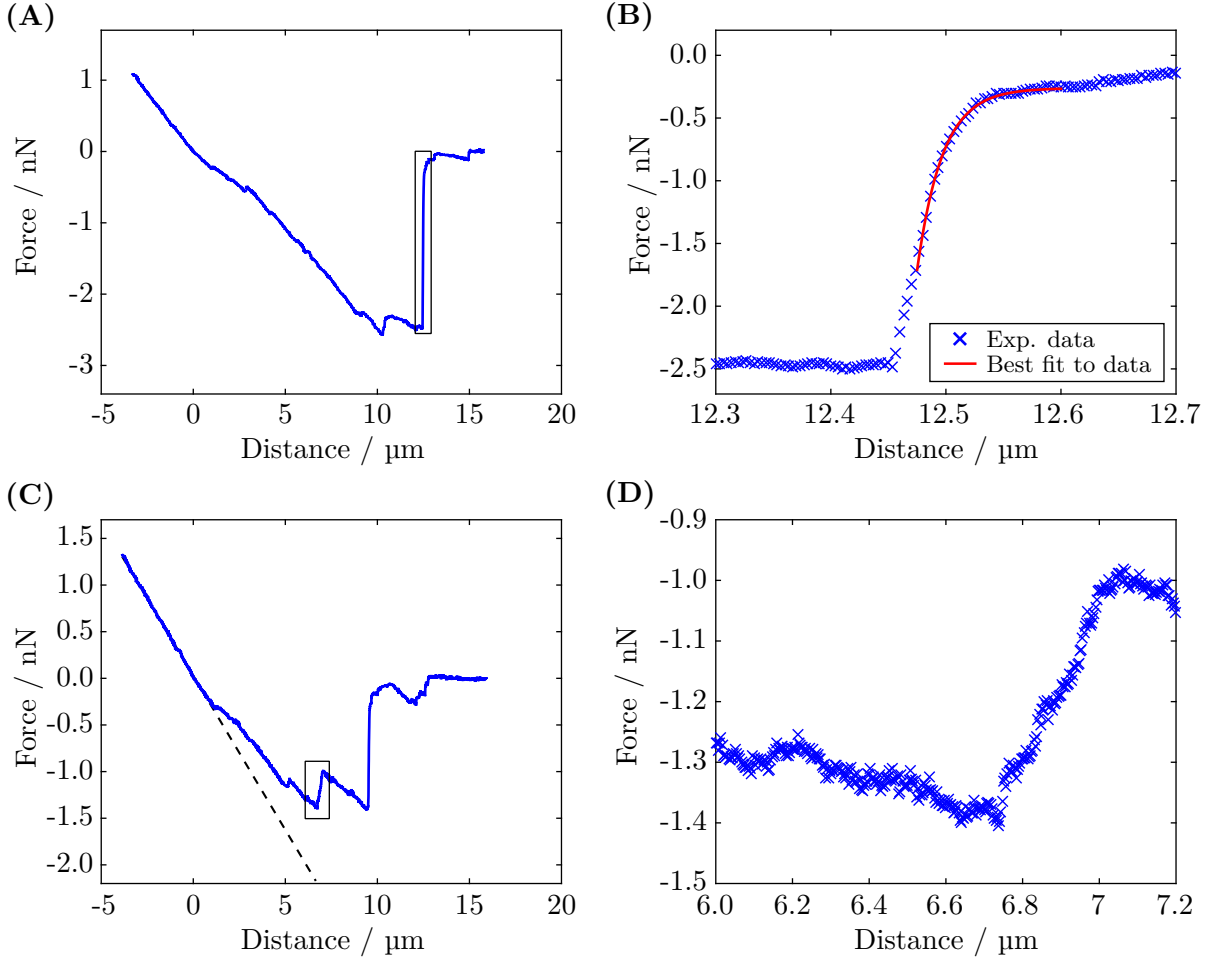


**Figure 5.8.: Signatures of force-distance curves at high time resolution.** Force-distance curves and representative sections recorded at high frame rates (300 frames per second). The force axis translates linearly back into the cantilever deflection ( $1 \text{ nN} \hat{=} 2.52 \mu\text{m}$ , as the spring constant was  $0.397 \text{ nN}/\mu\text{m}$ ), while the distance axis translates linearly into a time axis ( $1 \mu\text{m} \hat{=} 1 \text{ s}$ , as the substrate moved at  $1 \mu\text{m}/\text{s}$ ). **(A)** Force-distance curve, the box indicates the section shown in (B). **(B)** Section of the force-distance curve in (A) showing the main rupture event. The red line represents the best fit to an exponential decay  $F_{\text{adh}}(t) = a \cdot \exp(-b \cdot (t - 12.45 \mu\text{m})) - 0.26 \text{ nN}$ , where  $a = -4.5[2] \text{ nN}$ ,  $b = 45[1] \mu\text{m}^{-1}$ . This snap-back event has a time constant  $\tau = 22.2 \text{ ms}$ . **(C)** Force-distance curve, the box indicates the section shown in (D). The dashed line indicates the substrate position. **(D)** Section of the force-distance curve in (C) showing a decrease in the cantilever deflection, slower than the free snap-back shown in (B).

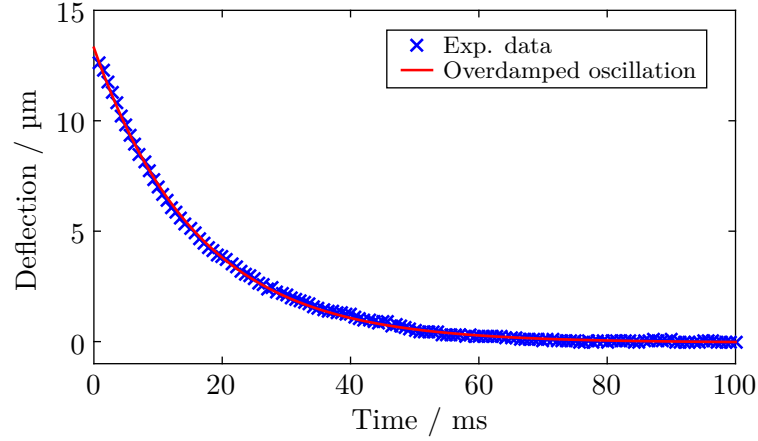


**Figure 5.9.: Step response of micropipette cantilever in aqueous medium.** The cantilever (spring constant:  $0.38 \text{ nN}/\mu\text{m}$ ) is deflected by another stiff cantilever in TAP growth medium. The snap-back is recorded at 1400 frames per second. The red line represents the best fit to an overdamped oscillation:  $f(t) = a \cdot \exp(-b \cdot t \text{ ms})$ , where  $a = 13.3[1] \mu\text{m}$ ,  $b = 0.0623[5] \text{ ms}^{-1}$ . The free snap-back has a time constant  $\tau = 16.1 \text{ ms}$ .

In contrast, there were gradual return events that featured a different functional form and happened on a much longer timescale of hundreds of milliseconds (see Figure 5.8C+D). The gradual return events were often characterized by a linear functional form compared to the exponential form of the free snap-back. This type of return event presumably indicates that the adhesive contact between substrate and flagellum was not lost. Instead, the adhesive site was presumably dragged through the flagellar membrane. As there seemed to be many flagella-substrate contact points, the motion through the flagellar membrane might be terminated either once the second flagellum is under tension or once the adhesive site was dragged to another adhesive site on the same flagellum that restricted any further motility. A similar phenomenon like the gradual return event has been reported before in studies with optical tweezers, although the magnitude of the return event is much smaller in the optical tweezers study [Laib et al., 2009]. Note that the timescale in this optical tweezer studies was different due to a different mass and spring constant of the overdamped oscillator (microbead in optical trap versus micropipette cantilever).

Finally, the slope of the force-distance curve during the detachment process characterizes two more signatures that could be observed in the force-distance curves. During the detachment process a slope of zero could potentially characterize two different phenomena: either the adhesive site was dragged through the flagellar membrane exactly at the speed of the substrate retraction, or the flagellum was slowly peeled of the substrate at a critical force (see Figure A.14, middle row, left-hand panel, the black curve, indicated by an arrow). A negative

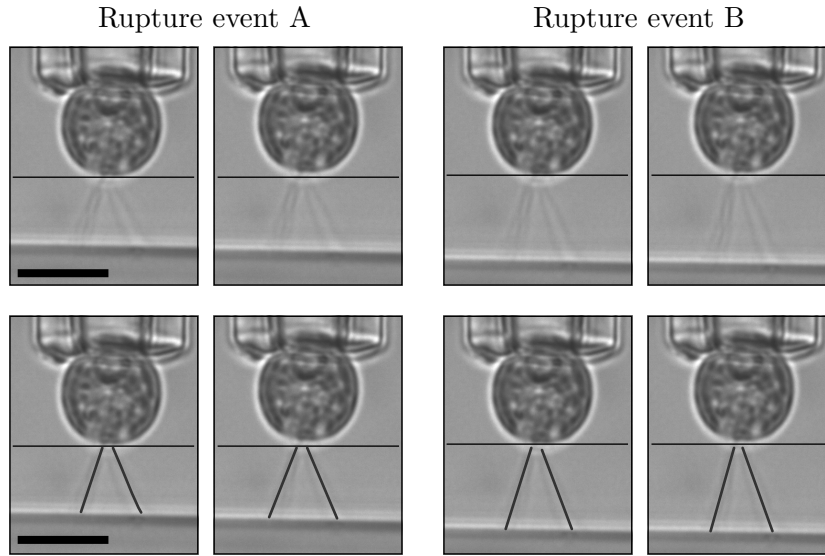


**Figure 5.10.: Visualizing the flagella during force spectroscopy.** Micrographs of two consecutive rupture events for the same cell (left-hand image: before the rupture, right-hand image: after the snap-back of the cantilever). The black line indicates the cantilever position before the rupture event (shifted downwards to the edge of the *Chlamydomonas* cell for a better visualization of the subtle snap-back, cantilever spring constant  $1.57 \text{ nN}/\mu\text{m}$ ). The flagella are attached to the substrate (bottom). The bottom row includes a guideline to the eye for the flagella. Scale bar:  $5 \mu\text{m}$ .

slope smaller than the substrate retraction speed can likewise indicate two different phenomena (see Figure 3.9B): either the adhesive site was slowly dragged through the flagellar membrane, or the flagellum was slightly stretched in the detachment process. The stretching of the flagella in the adhesion process can be estimated from the Young's modulus of the microtubules, which was estimated to be in the order of hundreds of Megapascal [Gittes et al., 1993; Kis et al., 2002]. A Young's modulus in this magnitude would approximately lead to an elongation of 2% at a force of  $1 \text{ nN}$  for a single microtubule (assuming a homogeneous elastic cylinder with  $25 \text{ nm}$  diameter and a Young's modulus of  $100 \text{ MPa}$ ). Consequently, the flagella of  $10 \mu\text{m}$  length would elongate at most by tens of nanometer at the applied forces (*Chlamydomonas* flagella consist of 20 microtubules), yet an elongation of at least  $3 \mu\text{m}$  would be required to explain the deviation from the substrate position seen in Figure 5.8C. Additionally, I would expect the difference in the slope compared to the force ramp rate to be visible in all experiments and to be consistent in between force-distance curves with the same cell (and also with different cells), as the mechanical properties of the underlying flagella scaffold do not change from one force-distance curve to another. However, I did not find a consistent difference between the substrate velocity for the same cell and the force-distance curve's slope, as well as the force ramp rate (for different cells and cantilevers) and the force-distance curve's slope. Hence, the

slopes that are smaller than the substrate retraction speed are presumably due to the adhesive site being dragged through the flagellar membrane.

Further elucidating these flagella rupture dynamics should incorporate the visualization of the flagella that allow for a correlation between the flagella rupture dynamics and the cantilever. Preliminary experiments enabled me to identify the flagella during the rupture of the adhesive contacts (see Figure 5.10)<sup>44</sup>. These experiments suggest that the cantilever snap-back events originate in localized areas of adhesive contact on both flagella.

In conclusion, an in detail inspection and analysis of individual force-distance curves yielded strong evidence for multiple flagella-substrate contact points. These contact points appear to be mobile and can be dragged through the flagellar membrane, while a flagella elongation can most likely be excluded. The variety of signatures that can be found in individual force-distance curves may lead to a plethora of different force-distance curves recorded with the same cell. Ultimately, this variety presumably contributes to the variation of the adhesion forces of a single cell.

### 5.2.3. Discussion: Signatures of the Detachment Process

In summary, experiments on the adhesion force as a function of the flagella length on the substrate suggest that not necessarily the whole flagellum forms an adhesive contact with the substrate. An in-depth analysis of the signatures of the detachment process indicates that a single flagellum can feature several individual adhesive sites.

The characteristics of areas of adhesive contact between *Chlamydomonas* flagella and substrates was already studied during gliding motility [Bloodgood, 1990b, unpublished results by Daniel and King]). This study employed interference reflection microscopy to estimate the distance between the flagellar membrane and the glass substrates. Thereby areas of closest contact could be identified. Daniel and Kind found that there may be several localized areas of closest contact on the same flagellum during gliding of *Chlamydomonas*. These areas appeared to be variable in size and were found independent of the gliding direction on the leading and trailing flagellum. As these areas of closest contact changed their position during gliding, they are presumably areas of adhesive contact between the substrate and the flagellum. These findings support the conclusions drawn from force spectroscopy experiments that explain the variations in the adhesion forces recorded for a single cell. The mobility of the contact points allow for a relative motion in the flagellar membrane (active and/or passive), which might be visible in some of the signatures discussed above.

In addition to these flagellar membrane characteristics, the adhesion promoting protein is

---

<sup>44</sup>This experiment was performed by Anni Röse as part of the work for her Master's thesis tutored by Christian Titus Kreis.

known to turnover in the flagellar membrane, i.e. proteins are constantly replaced with new copies of the protein [Bloodgood et al., 1986] (see also section 2.3.4). This protein turnover could lead to fluctuations in the amount of FMG-1B in the flagellar membrane, which would affect the adhesion forces. However, the timescale of the turnover is several minutes, thus, larger than the timescale in between consecutive force-distance cycles, which is in the order of tens of seconds. Hence, the turnover does not appear to be the predominant reason for the adhesion force variations seen in a single set of force-distance curves. Nevertheless, the turnover can potentially resolve mean adhesion force variations seen for the same cell over a course of two hours (see Figure 4.5).

The analysis of the rupture signatures suggests that the adhesive sites can be dragged through the flagellar membrane. In contrast, a stretching of the flagella appears to be incompatible to the mechanical properties of the microtubules. The force spectroscopy experiments can incorporate the visualization of the flagella during the rupture events. This force-flagella dynamics correlation should be employed in follow-up studies on the rupture dynamics, which are necessary to support the drawn conclusions.

### 5.3. Summary and Discussion

I carried out force spectroscopy experiments with *Chlamydomonas* cells and analyzed the recorded adhesion forces. Furthermore, I characterized different signatures that appear during the rupture of the flagella-substrate contact. These experiments yielded:

1. The *Chlamydomonas* adhesion forces were in the order of a few nanonewtons and their distribution is well-described by a log-normal distribution. The forces featured a cell-to-cell variability, which was presumably due to a cell-to-cell variability in the protein density in the flagellar membrane.
2. For each cell, the adhesion forces varied by tens of percent of the mean adhesion force, which was most likely due to a high variability in the area of adhesive flagella-substrate contact. Moreover, there can be several localized adhesive contacts between each flagellum and the substrate.

The order of the adhesion forces is in line with adhesion forces found in similar systems [Callow et al., 2000; Dugdale et al., 2005; Ramaswamy et al., 2013; Sullan et al., 2014; Thewes et al., 2015b]. These studies support the conclusions drawn on the cell-to-cell variability. In comparison to the bacterial adhesion studies, a single *Chlamydomonas* cell exhibited a relatively large force variation, which is most likely due to variations in the amount and total area of flagella-substrate contacts. This hypothesis is supported by earlier interference reflection microscopy studies [Bloodgood, 1990b]. These variabilities in the adhesive contacts and the possibility to move adhesive sites within the flagellar membrane led to remarkable signatures in the force-distance curves that make each force-distance curve unique. In contact with a surface, it is the

flagellar membrane dynamics driven by intraflagellar transport trains that allow microalgae to move on the substrate (see section 2.3.4). This activity in the adhesion-mediating structures represents the most substantial difference compared to the adhesion-mediating structures of bacteria.

In conclusion, the adhesion of *Chlamydomonas* shares features found in force spectroscopy studies of other microbes, whereas some characteristics of the adhesion process are remarkably different from bacterial adhesion. The findings from this chapter emphasize the unique characteristics of the microalgal flagella and the functionality of this complex organelle in the context of adhesion and surface interactions.





## 6. Light-Switchable Adhesion of Microalgae

The natural habitats of microorganisms are generally characterized by a heterogeneous distribution of locations with optimal growth conditions. Therefore, many microorganisms evolved strategies to locate areas that provide optimal conditions for survival and proliferation. As light is the main source of energy for algae, they have developed particular strategies to optimize the yield of their photosynthetic machinery. Mobile microalgae perform phototaxis, which is motility directed by light, that enables the organisms to find sun-drenched spots in their habitats. This optimization strategy generally requires the organism to be free-swimming in aqueous solution, however, many freshwater microalgae live associated with surfaces, such as in soil and puddles, or on rocks and on moss (see Figure 2.1B and Figure 2.2). Thus, interactions with surfaces play a major role in the dissemination process and life of these microalgae. Although microalgal responses to light have been widely recognized, any influence of light on cell-surface interactions remains unknown.

The aim of this chapter is to describe my discovery that the adhesion of microalgae to surfaces can be switched on and off by light (see Appendix C for the story of my discovery). This discovery is highlighted in [Kreis et al., 2017], which serves as the basis for this chapter. In this chapter, I study the influence of light on the adhesion of vegetative *Chlamydomonas* cells and their light-triggered transition from planktonic swimming to surface association. The chapter concludes with a discussion of the relevance of light-switchable adhesion for microalgae.

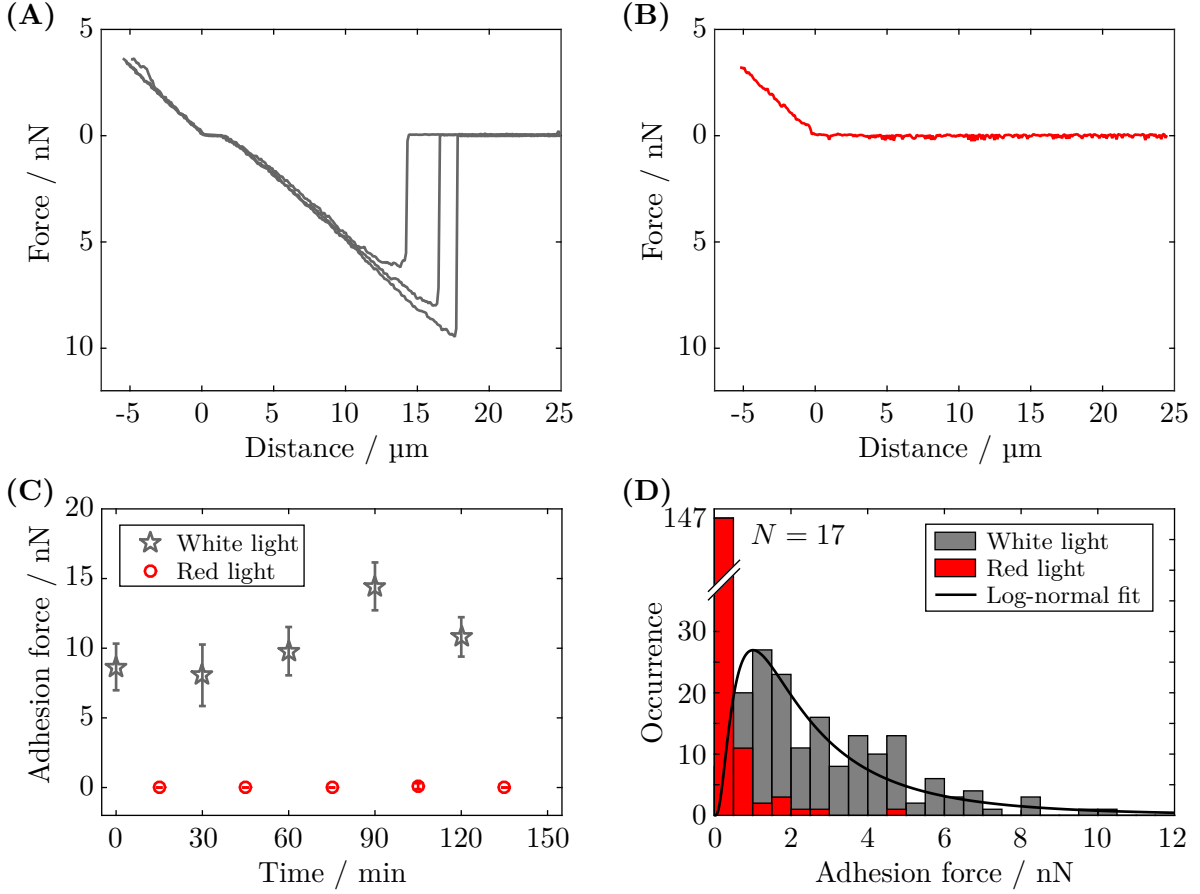


**Figure 6.1.: Force spectroscopy of vegetative *Chlamydomonas* cells in white and red light.** (A) Force-distance curves in white light; three individual retraction cycles are shown. (B) Force-distance curves in red light with the same cell as in (A); one retraction cycle is shown (for clarity reasons, no cycle shows adhesion, see first data point in (C)). (C) Adhesion force measurements for the same cell as in (A) and (B) in alternating light conditions. Each data point represents the mean adhesion force determined from five force-distance curves, and the error bars represent the standard deviation. This experiment employed non-standard red light conditions (see section 3.4.4). (D) Distribution of adhesion forces for cells in red and white light. The solid line represents the best fit of the white-light data set to a log-normal distribution ( $\alpha = 0.75[13]$ ,  $\beta = 0.86[9]$ ). Adapted from [Kreis et al., 2017].

## 6.1. Force Spectroscopy in Different Illumination Conditions

### 6.1.1. Light-Switchable Adhesion: A General Description of the Effect

I performed force spectroscopy experiments with vegetative *Chlamydomonas* cells in different light conditions (see section 3.4.4) to quantify the influence of light on the adhesion of *Chlamydomonas* to model substrates<sup>45</sup>. White-light experiments were performed using standard microscope illumination, whereas red-light conditions were realized by adding a bandpass interference filter (672/11 nm) to the white light source (see the spectra in Figure A.6 and A.7).

In white light, force-distance curves on silicon substrates yielded adhesion forces of several nanonewtons as described before, while experiments in red light did not exhibited adhesion. For the same cell that adhered with almost 10 nN to the substrate in white light (see Figure 6.1A), I did not measure any detectable adhesion in red light (see Figure 6.1B; for further examples see Figure 6.2). Videos of an adhesion process with the same cell in white light and red light are available in [Kreis et al., 2017, Supplemental Movie 1 and 2].

The light-switchable adhesion was reversible, as evidenced by a series of consecutive force-distance curves with the same cell in white-light and red-light conditions (see Figure 6.1C). Independent of the adhesion forces in white light, I could switch the adhesion to substrates off by switching from white illumination to red illumination. In white light, force spectroscopy experiments on silicon substrates ( $N = 17$  cells) yielded adhesion forces from 1.16 to 4.03 nN (25th/75th percentile, median: 2.34 nN, mean: 2.83 nN). The same cells exhibited adhesion forces from 0 to 0.170 nN (25th/75th percentile, median: 0 nN, mean: 0.190 nN) in red light (see Figure 6.1D). Comparing the force statistics of the exact same cells in different light conditions, I found that 95.2% of all force-distance curves recorded in red light exhibited adhesion forces that were more than one standard deviation smaller than the average adhesion force of the same cell in white-light conditions (see Figure A.15). This includes 72.4% of all measurements in red-light conditions without any detectable adhesion (typical noise level of approximately 10-20 pN, see Figure 3.6). In white light, 100% of the force-distance curves exhibited an adhesion peak.

The light-switchable adhesion was substrate unspecific, as evidenced by force spectroscopy experiments on different substrates that show the same effect. In white light, the cells adhered with forces of several nanonewtons to hydrophobized silicon substrates and magnesium oxide substrates. In contrast, the same cells did not exhibit adhesion to the same substrates in red light (see Figure 6.2). The influence of different surfaces forces on the adhesion of *Chlamydomonas* is further studied in chapter 7.

---

<sup>45</sup>Marine Le Blay (ESPCI, Paris, France), a summer student tutored by Christian Titus Kreis, contributed many data points to the figures presented in this chapter (Figure 6.1, 6.4B and 6.15) [Le Blay, 2016].

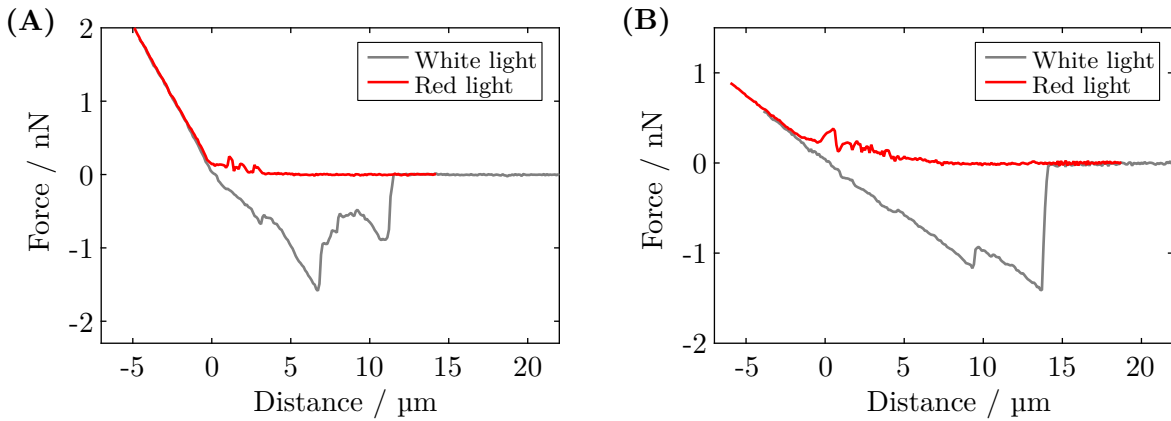


**Figure 6.2.: Light-switchable adhesion to different substrates.** Force spectroscopy of vegetative *Chlamydomonas* cells in white light and red light on different substrates (see section 3.3). An individual retraction cycle of the same cell is shown in white light (gray line) and red light (red line). **(A)** Experiment on a hydrophobized silicon substrate. **(B)** Experiment on a magnesium oxide substrate.

In conclusion, force spectroscopy experiments provided unambiguous evidence that the adhesion forces of *Chlamydomonas* to surfaces can be reversibly switched on and off by tailoring the illumination conditions.

### 6.1.2. Color Discrimination

Many processes in *Chlamydomonas*, such as phototaxis and gametogenesis, are controlled by light of a specific illumination wavelength. The light incidence triggers a photoreceptor that leads to a signal pathway that controls a specific cellular function. To identify the illumination wavelength that triggers light-switchable adhesion, I exposed the same cell to light of different wavelengths and quantified the adhesion forces (see the light conditions in section 3.4.4 and the experimental protocols in section 3.4.5). The irradiance (quantum flux density) was kept constant at  $3 \times 10^{19}$  photons/m<sup>2</sup>s. Note that red light was always on to monitor the cantilever deflection.

The illumination wavelength played a crucial role for the flagellar adhesiveness (irradiance  $3 \times 10^{19}$  photons/m<sup>2</sup>s): all cells exhibited adhesion in blue-light conditions (400 nm and 470 nm), whereas no significant adhesion was measured for green-light (550 nm) and red-light conditions (638 nm and 672 nm, see Figure 6.3). The adhesion forces in blue light at 470 nm (irradiance:  $1 \times 10^{19}$  photons/m<sup>2</sup>s) were in the range of 1.13 to 2.94 nN (25th/75th percentile, median: 1.51 nN, mean: 1.98 nN, see Figure 6.3C). Thus, the adhesion forces in blue light were consistent with the forces obtained in white light (see Figure 5.3). These experiments strongly suggest that a blue-light photoreceptor controls the flagellar adhesiveness in *Chlamydomonas*.

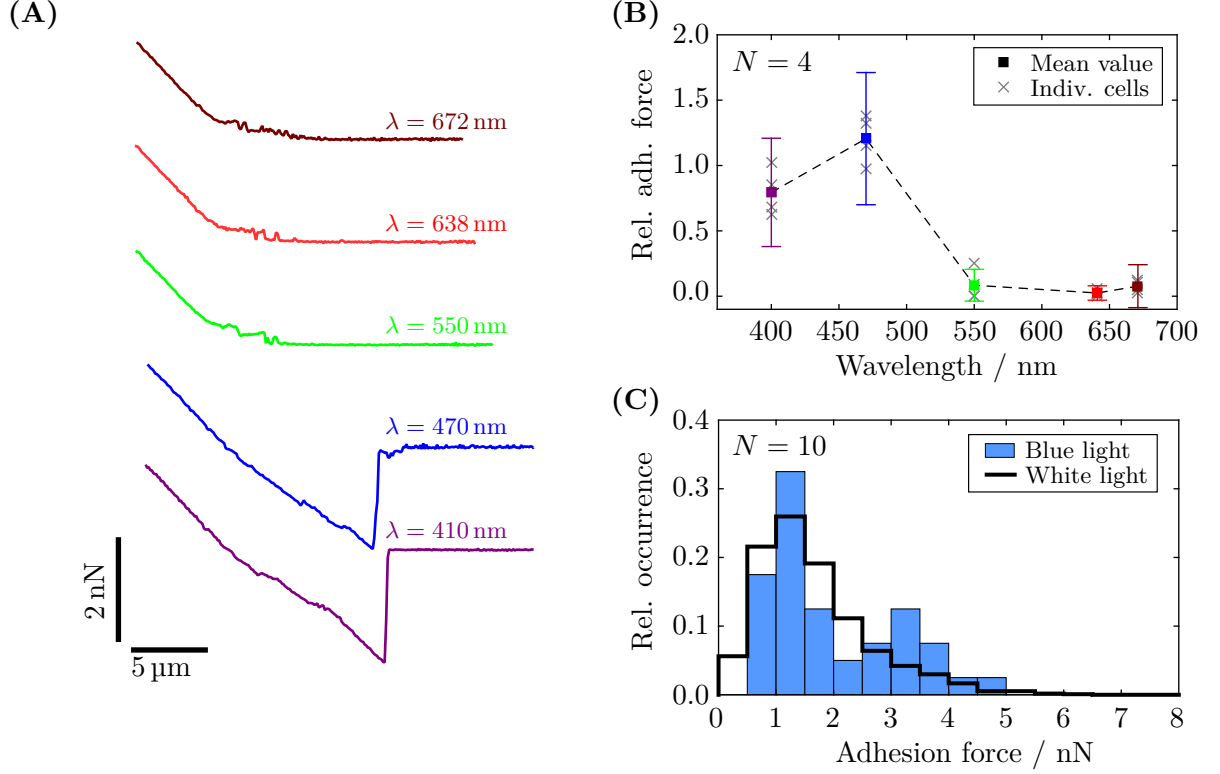


**Figure 6.3.: Force spectroscopy of vegetative *Chlamydomonas* cells at different illumination wavelength.** (A) Representative force-distance curves (retraction) for the same cell using different illumination wavelengths at a constant irradiance of  $3 \times 10^{19}$  photons/m<sup>2</sup>s (see section 3.4.4 and the spectra in Figure A.8). The cell exclusively adhered in blue-light conditions. (B) Mean adhesion forces of different cells ( $N = 4$  cells) in the same light conditions as in (A). At each wavelength, five individual force-distance cycles were performed with each cell. The mean adhesion forces of each cell are normalized to its adhesion forces in blue light (400 nm and 470 nm). (C) Distribution of adhesion forces for 10 cells in blue light (470 nm,  $1 \times 10^{19}$  photons/m<sup>2</sup>s). The black solid line represents the functional form of the histogram shown in Figure 5.3 with a different binning. Adapted from [Kreis et al., 2017].

Potential candidates for the blue-light photoreceptor that triggers the flagellar adhesiveness include channelrhodopsins and phototropin. Channelrhodopsins are responsible for the phototactic behavior of *Chlamydomonas* in aqueous environment [Foster et al., 1984; Berthold et al., 2008]. Phototropin can be found in the *Chlamydomonas*' flagella, controls the cell's life cycle, and governs several aspects of the mating process [Harris et al., 2009; Huang and Beck, 2003]. The photoreceptor that triggers phototaxis was identified by action spectra [Foster et al., 1984], i.e. the response of a population of *Chlamydomonas* cells was quantified for different wavelengths, in that case by measuring the phototactic rate (see section 2.3.3, page 18). Recording action spectra appears as a potential approach to identify the photoreceptor underlying light-switchable adhesion, however, this type of experiment requires an average over many *Chlamydomonas* cells. The number of individual measurements that are required to obtain an action spectrum from single-cell force spectroscopy measurements does not appear to be feasible on a reasonable timescale. Thus, another pathway has to be chosen to identify the photoreceptor. A promising approach is knock-out mutants that lack a specific photoreceptor. Preliminary experiments with channelrhodopsin and phototropin deletion-mutants are briefly discussed in section 6.5.2.

### 6.1.3. Photoreceptor Sensitivity and Light Intensity Dependence

The proliferation of microalgae depends on the light intensity, as they are mostly found in areas that provide optimal light intensities for their growth. In this process, the sensitivity of the photoreceptor that triggers light-switchable adhesion and the flagellar adhesiveness as a function of the light irradiance plays a crucial role in the surface colonization.

To quantify the sensitivity of the photoreceptor that triggers the light-switchable adhesion, I exposed the same *Chlamydomonas* cells to various blue-light intensities (at 470 nm) and measured the adhesion forces. As I gradually decreased the blue-light irradiance, the adhesion forces remained constant. Below a sharp threshold of less than half an order of magnitude in width, the same cells did not exhibit any significant adhesion (Figure 6.4A). In particular, I did not find that the adhesion forces increased with increasing blue-light irradiance in the tested range (above the threshold). The threshold was at different irradiances for different cells in a range of  $1 \times 10^{18}$  to  $5 \times 10^{18}$  photons/m<sup>2</sup>s. Three cells exhibited no adhesion below a blue-light irradiance of  $3 \times 10^{18}$  photons/m<sup>2</sup>s; for two cells the adhesiveness was reduced to zero at an irradiance of  $5 \times 10^{18}$  photons/m<sup>2</sup>s and  $1 \times 10^{18}$  photons/m<sup>2</sup>s, respectively.

The result in blue-light conditions was substantiated by adhesion experiments in white-light conditions at different illumination intensities. The adhesion forces likewise did not depend on the illumination intensities in a range of  $1 \times 10^{19}$  to  $1 \times 10^{21}$  photons/m<sup>2</sup>s (Figure 6.4B). In two cases, I did not measure adhesion in white light conditions at  $2 \times 10^{19}$  photons/m<sup>2</sup>s. However, the spectra of the halogen lamps change with increasing light intensity (i.e. the fraction of blue

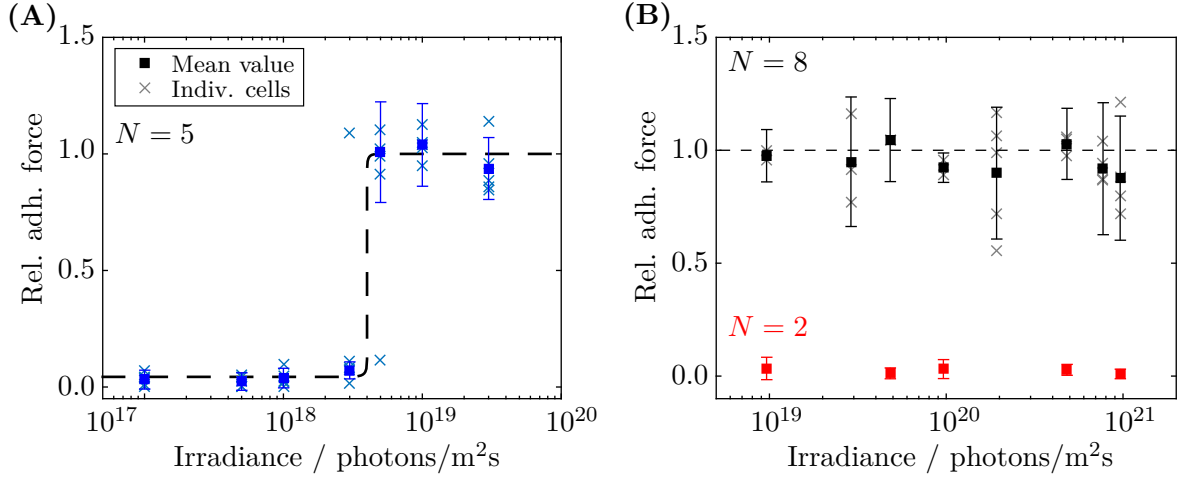


**Figure 6.4.: Force spectroscopy of vegetative *Chlamydomonas* at different illumination intensities.** The mean adhesion force of all cells (squares) and the mean adhesion force of the individual cells (crosses) are given as function of the illumination intensity in different illumination conditions (see section 3.4.4 and the spectra in Figure A.8). The dashed line represents a guide to the eye. **(A)** Adhesion forces in blue light (470 nm) at different illumination intensities ( $N = 5$  cells). The cells exhibit adhesion only above an intensity threshold of  $1 \times 10^{18}$  to  $5 \times 10^{18}$  photons/m²s. The forces are normalized to the adhesion forces above the intensity threshold. **(B)** Adhesion forces in white light ( $N = 8$  cells) and in red light ( $N = 2$  cells) at different illumination intensities. This experiment employed non-standard red light conditions (see section 3.4.4). The cells exhibit constant adhesion in white light and zero adhesion in red light in the tested intensity range. Two cells did not show adhesion below  $2 \times 10^{19}$  photons/m²s in white light (data not shown). The adhesion forces were normalized to the average adhesion force for the same cell. The adhesion forces in red light were normalized to a reference measurement with the same cell in white light. Adapted from [Kreis et al., 2017].

light increased with increasing lamp power, see Figure A.6A and Figure A.7A). Consequently, the light incidence at the photoreceptor cannot be as precisely controlled with this white light halogen source as with a blue light LED. Thus, the intensity threshold above which the flagella become sticky can be more reliably characterized in blue-light conditions. In red light, I did not observe adhesion at any illumination intensity. These experiments strongly suggest that the flagellar adhesiveness is independent of the photosynthetic yield in the tested range, as an increased light exposure of the photosystem did not lead to an increased adhesion force.

The blue-light irradiance threshold is consistent with the sensitivity of other photoreceptors of *Chlamydomonas*, as evidenced by a study that determined the sensitivity of channelrhodopsins [Harz and Hegemann, 1991]. In addition to the sensitivity of the photoreceptor, the study by Harz and Hegemann also showed that photoreceptors of *Chlamydomonas* can trigger binary effects. The photocurrents in the *Chlamydomonas* flagella, which ultimately regulate the varia-

tion in the beating waveform in the phototaxis process, appear only at photon exposures above a sharp threshold. Furthermore, the flagellar photocurrents are of constant magnitude independent of the illumination intensity [Harz and Hegemann, 1991]. This characteristic of the flagellar photocurrents is described by Harz and Hegemann as “all-or-none effect”. In contrast, the magnitude of the photocurrents in the *Chlamydomonas* eyespot that trigger the flagellar current increased with increasing irradiance [Harz and Hegemann, 1991].

The flagellar adhesiveness is presumably the result of a signal pathway that is triggered by a blue-light photoreceptor. In this context, the intensity dependence of the adhesiveness should not be compared to the immediate signal of the photoreceptors, but rather to the flagellar currents at the end of a signal pathway. The findings are in line with the flagellar photocurrents, which exhibit a sharp threshold and binary behavior. Consequently, the binary all-or-none effect of the flagellar adhesiveness seems reasonable.

### 6.1.4. Temporal Evolution of the Adhesion Force After Turning the Light on

I monitored the temporal evolution of the adhesion forces of vegetative cells after changing from red to white illumination. Therefore, I performed force-distance measurements with the same cell every fifteen minutes after switching from red to white illumination (see Figure 8.1A). Experiments of four cells showed an increase of the adhesion force for about 45 min until the adhesion force saturated (result type 1, see Figure 8.1A). In two experiments, the final adhesion forces were measured immediately after turning from white to red illumination (result type 2, see Figure 8.1A).

Additionally to the temporal evolution, I quantified the effect of a period of red light on the magnitude of the adhesion forces in white light. Therefore, the adhesion forces of the same cells were measured before the period of red light and approximately five minutes after turning back to white light (the red light period in between lasted for about 30 min). The adhesion forces after turning back to white light were significantly larger compared to the initial adhesion forces (see Figure 6.5). Note that the experiments in Figure 6.5B were performed with gametic cells, whereas the experiments in Figure 6.5A were performed with vegetative cells. Marginal behavioral differences in between the vegetative and gametic cells might explain the apparent discrepancy.

These experiments indicate that the adhesion forces measured in white light were influenced by switching from white to red to white illumination. Additionally, the adhesion forces exhibited a temporal evolution after turning to white light from red illumination. Consequently, the magnitude of the adhesion forces in white light might be affected by the experimental history, i.e. how long before a measurement the white light was turned on. Although the magnitude of the adhesion forces might be affected by the experimental history (times when light was turned on and off with respect to the measurement time), there was always significant adhesion in



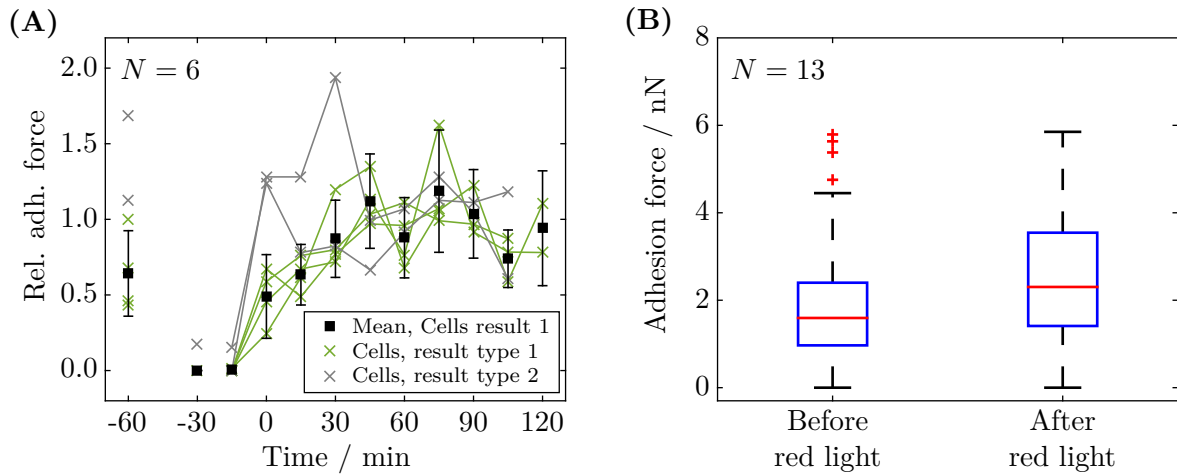


**Figure 6.5.: Temporal evolution of adhesion forces of *Chlamydomonas* after changing the illumination conditions.** (A) Temporal evolution of the adhesion forces ( $N = 6$  cells). For each cell, the initial adhesion force is measured in white light ( $t = -60$  min). Afterwards, the cells are kept in red light for 60 min. After switching back to white light, the adhesion forces are measured at intervals of 15 min (the data point at  $t = 0$  min was recorded immediately after switching back to white-light conditions). Each individual data point represents the mean of 5 force-distance cycles. The cells are divided into two categories based on the results (see text). The adhesion force of each cell is normalized to the average adhesion force of the cell after saturation ( $t > 30$  min). (B) Adhesion force measurements ( $N = 13$  gametic cells) in white light before red illumination (10 force-distance measurements for each cell) and approximately 5 min after (5 force-distance measurements for each cells) turning back from red illumination to white light. The cells were kept for 30 min in red light.

white light. In red light, the adhesion was reduced to zero as described before, independent of the experimental history. To avoid any bias by the previously described effects, the cells were normally exposed tens of minutes to white light (blue light) before the beginning of a new experiment, and the experimental routines of the experiments shown in Figure 6.3 and 6.4 were adapted (see section 3.4.5). In experiments unrelated to light-switchable adhesion (all experiments performed in chapter 4, 5 and 7), the cells were always exposed to white light of constant intensity during the complete experiment.

### 6.1.5. Concluding Remarks

In conclusion, I performed force spectroscopy experiments in various precisely controlled illumination conditions. These experiments prove that the flagellar adhesiveness can be reversibly switched on and off by light. The light-switchable adhesion is presumably triggered by a blue-light photoreceptor above a sharp irradiance threshold.

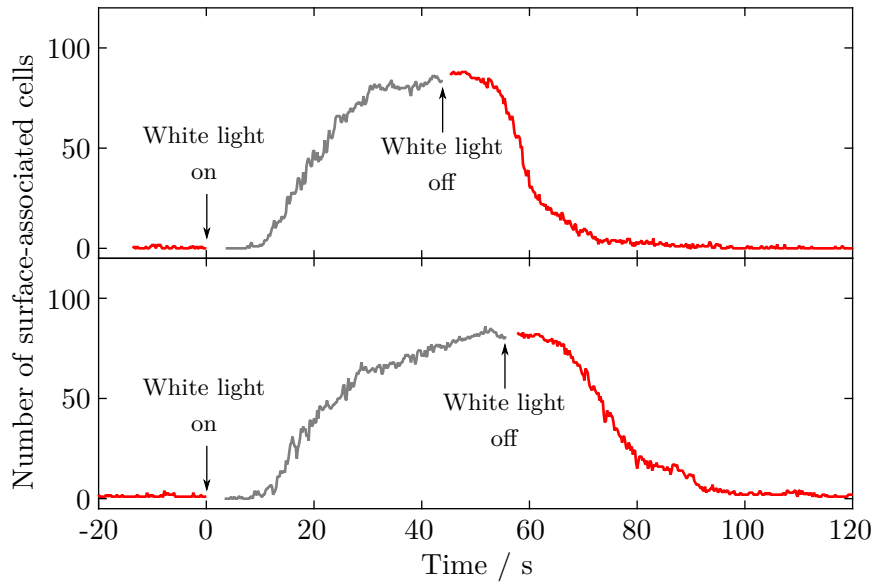


**Figure 6.6.: Surface colonization of *Chlamydomonas* controlled by light.** Adsorption and desorption of a population of *Chlamydomonas* cells from bulk solution to glass slides (see section 3.5). Both kinetics were recorded with the same population in consecutive experiments. The gaps in the kinetics are times of overexposure and underexposure after removing and adding a red filter, respectively, which inhibit any visualization of the cells on the substrate at these times.

## 6.2. Surface Colonization Experiments

Although the force spectroscopy experiments are non-invasive (see chapter 4), they cannot fully capture the transition from the planktonic state to the surface-association state. Therefore, I performed adsorption experiments with planktonic cells to corroborate the light-switchable adhesion found in force spectroscopy experiments (see section 3.5).

*Chlamydomonas* cells swimming in bulk liquid in red light attached to glass slides after turning to white illumination (“adsorption”, see Figure 6.6, the top kinetics was extracted from the video shown in [Kreis et al., 2017, Supplementary Movie 5]). The surface association was terminated by changing back from white light to red light: the cells adhering to the substrate detached and started to swim again (“desorption”). I found that the surface association started and was terminated approximately 10 s after switching to white and red illumination, respectively.

Phototaxis played an important role in the adsorption process by guiding the cells to the substrate (see the preliminary experiments with photoreceptor deletion-mutants in section 6.5.2). In contrast to the adsorption, the detachment is independent of any phototaxis, as the cells



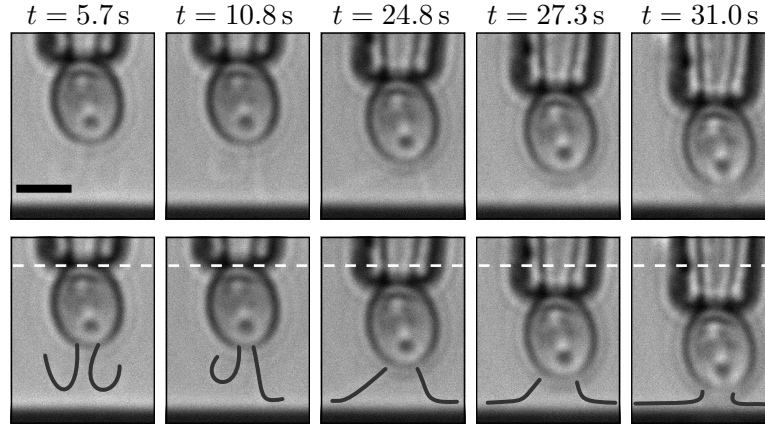


**Figure 6.7.: Optical micrographs of a cell at different times during an auto-adhesion experiment.** The *Chlamydomonas* cell is held with a micropipette cantilever in close proximity to a substrate (bottom, black). The time after turning on an external white-light LED is given at the top. After turning on the light stimulus, the flagella tips adhere to the substrate and pull the cell body towards the substrate. The top row shows the raw images. The bottom row includes guidelines to the eye (solid gray line: flagella, dashed white line: initial cantilever position). Scale bar: 5  $\mu\text{m}$ . Adapted from [Kreis et al., 2017].

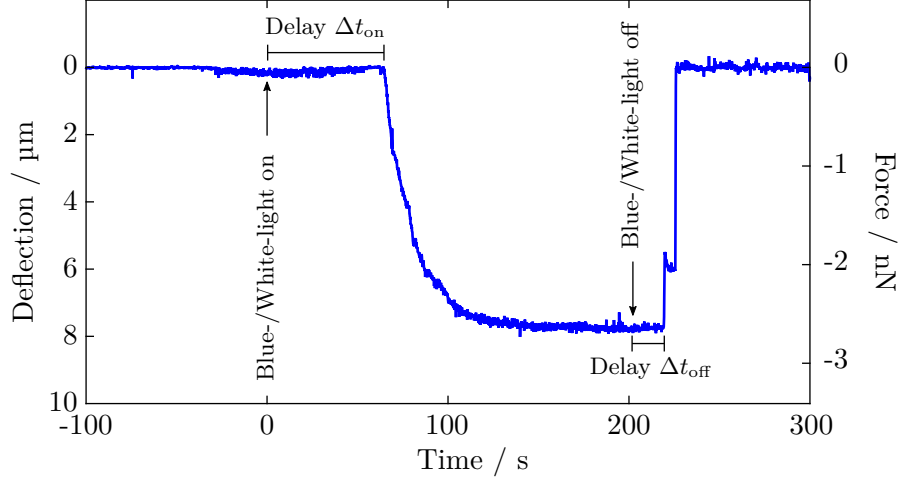


**Figure 6.8.: Cantilever deflection signal during an auto-adhesion experiment.** The micropipette cantilever deflection and corresponding restoring force are shown as a function of the time during an auto-adhesion experiment. The blue-/white-light stimulus is turned on at  $t = 0\text{ s}$ . After a delay time  $\Delta t_{\text{on}}$ , the cantilever deflects towards the substrate indicating that the cell body is pulled to the substrate. Turning off the light leads to a snap-back of the cantilever to the zero-force position after a distinct delay time  $\Delta t_{\text{off}}$ . Adapted from [Kreis et al., 2017].

flagella recovered the regular breaststroke beating afterwards.

A few seconds after the white-/blue-light stimulation was turned on, the flagella tips of one or both flagella adhered to the substrate, as seen in the high-speed optical micrographs (see the second panel in Figure 6.7, a video of this process is available in [Kreis et al., 2017, Supplementary Movie 3]). The immobilization of the tip of a flagellum, through its adhesion to a substrate, resulted in a drastic modulation of the flagellum’s beating pattern. Eventually, the adhesion terminated the beating and the flagellum became quiescence within tens of milliseconds (see [Kreis et al., 2017, Supplementary Movie 3]). This observation is in agreement with earlier studies, which suggest that flagellar adhesion to substrates presumably induces a signal pathway that suppresses the regular beating and activates the gliding motility [Mitchell et al., 2004; Bloodgood, 2009]. In some instances, exclusively one of the two flagella adhered at the beginning (see Figure 6.7, the second flagellum attaches at  $t = 24.8\text{ s}$ ), which was most likely due to the cell and flagella alignment with respect to the substrate. Whereas the adhered flagellum became quiescent, the non-adhered flagellum continued the regular beating. This observation suggests that the adhesion-induced signal pathway is limited to the flagellum that adheres to the substrate.

### Cell-Substrate Approach

After the flagella tips adhered to the substrate, the flagella started to pull the cell body towards the substrate. The cell-substrate approach deflected the cantilever that was holding the *Chlamydomonas* cell (see Figure 6.7 and Figure 6.8). This process, which I termed “auto-adhesion”, was terminated as soon as the cell had achieved a stationary configuration on the substrate. Turning off the blue-/white-light stimulation resulted in a snap back of the micropipette to the equilibrium zero-force position, as the adhesive contact between flagella and substrate ruptured. The detachment did not necessarily occurred as a single event, but sometimes in several steps, which indicates the rupture of multiple localized adhesive sites (see Figure 6.9).

### Further Aspects of Auto-Adhesion

The auto-adhesion process was completely reversible, as evidenced by a series of consecutive individual auto-adhesion experiments with the same cell (see Figure 6.9). In some instances, the approach stopped already before the cell body touched the substrate, as the restoring force of the cantilever became presumably too large for the cell to overcome (for example, caused by a large cantilever spring constant). During auto-adhesion, the adhesive contact was sometimes partially ruptured, seen as snap-backs of the cantilever (see section 5.2.2). Afterwards, the cell-substrate approach resumed (see Figure 6.9).

The adhesion forces of the cells after an auto-adhesion process were determined by retract-

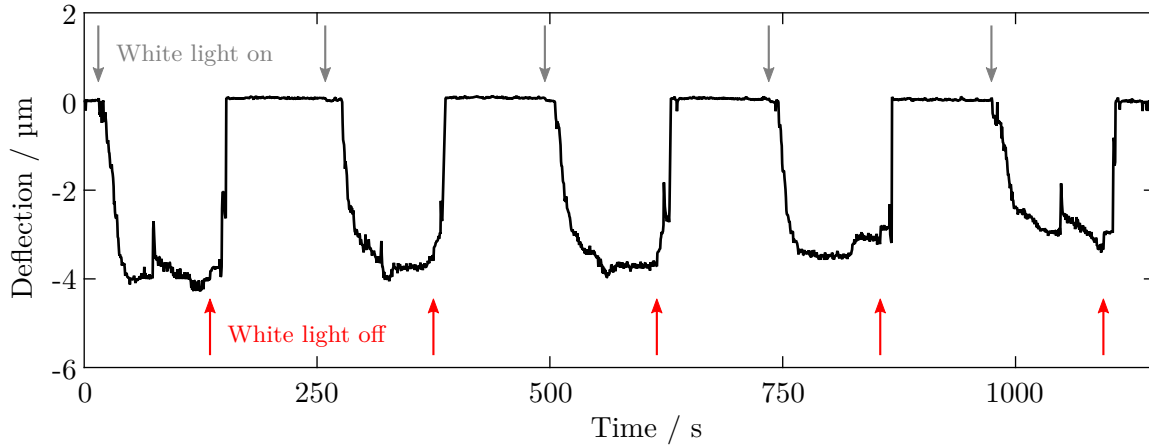


**Figure 6.9.: Cantilever deflection signal during several auto-adhesion cycles.** Several consecutive auto-adhesion experiments with the same cell. At time points indicated by gray arrows, an external white-light stimulus was switched on, and at times indicated by red arrows, white light was switched off. This series of auto-adhesion experiments shows several typical features, for example in cycle one and five, the adhesive bond partially ruptures and the auto-adhesion process is resumed. This dataset was kindly provided by Christine Linne [Linne, 2017].

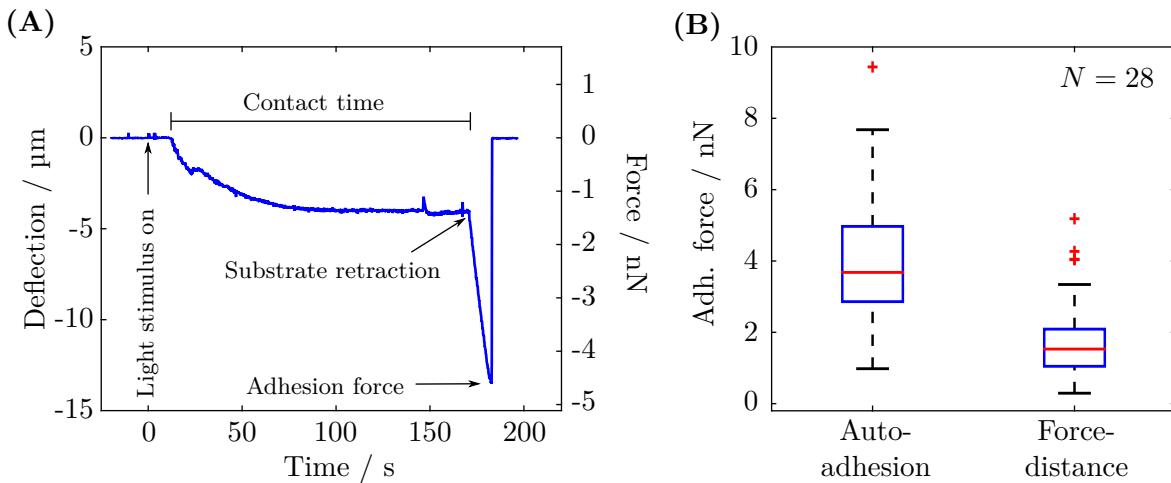


**Figure 6.10.: Auto-adhesion combined with force spectroscopy.** A cell is allowed to establish contact with a substrate by an auto-adhesion process. After the cell body is in contact with the substrate, the substrate is retracted, which resembles a force spectroscopy experiment. (A) Cantilever deflection and corresponding force during an auto-adhesion process immediately followed by a force spectroscopy experiment. (B) Adhesion forces ( $N = 28$  cells) measured by force spectroscopy after auto-adhesion (131 data points, 3 to 5 individual data points per cell) and adhesion forces measured by conventional force-distance curves with the same cells (140 data points, 5 data points each cell).

ing the substrate once the cell had achieved an equilibrium configuration in contact with the substrate (see Figure 6.10A)<sup>46</sup>. These force spectroscopy measurements after an auto-adhesion process yielded adhesion forces of 2.86 to 4.97 nN (25th/75th percentile, median: 3.68 nN, mean: 3.89 nN). In regular force-distance measurements, the same *Chlamydomonas* cells exhibited adhesion forces of 1.05 to 2.09 nN (25th/75th percentile, median: 1.53 nN, mean: 1.64 nN), which were in good agreement with the adhesion forces reported before (see Figure 5.4 and the corresponding paragraph on page 80). The contact time in the auto-adhesion experiments was tens of seconds (on average 96(41) s), as compared to 25 s in the force-distance curves (see section 3.4.3). As the adhesion forces increased with contact time (see section 4.3, Figure 4.5B), higher adhesion forces as seen after an auto-adhesion process are in line with previous findings. However, the magnitude of the force increase is larger than the adhesion force increase expected from a comparison to results obtained in conventional force-distance experiments (see Figure 4.5B). A direct comparison between the adhesion forces obtained after an auto-adhesion process and conventional force-distance curves with the same cells yielded a force increase by more than 100 %, as estimated by the characteristic values of the force distributions (mean, median, 25th and 75th percentile). In contrast, previously reported force-distance experiments exhibited a 39 % increase of the adhesion force from a contact time of 25 s to the saturation force value (see Figure 4.5B). This discrepancy suggests that there was another mechanism that contributed to larger adhesion forces after an auto-adhesion event. Possible explanations for higher adhesion forces could be a larger area of adhesive contact between the flagella and the substrate after an auto-adhesion process or an active response of the cell to the restoring force of the cantilever during the auto-adhesion process. Another possible explanation could be related to light-switchable adhesion, as I observed higher adhesion forces after turning from red to white illumination than before (see Figure 6.5B). This effect could explain higher adhesion forces compared to the force-distance curves, as the auto-adhesion process was always triggered by switching on an external white-/blue-light stimulation.

### 6.3.2. Characterizing Timescales in the Auto-Adhesion Process

The timescales of (biological) processes allow for concluding on the involved underlying mechanisms. Therefore, I characterized the delay times between the different steps observed in the auto-adhesion process. From high-speed images, I measured the delay time  $\Delta t_{\text{adh}}$  and  $\Delta t_{\text{pull}}$ , whereas the kinetics give rise to the delay time  $\Delta t_{\text{on}}$  and  $\Delta t_{\text{off}}$ .

The delay time  $\Delta t_{\text{adh}}$  was defined as the delay time between blue-/white-light stimulation and the first adhesive flagella-substrate contact of one of the flagella that lasted longer than one full beating cycle (see Figure 6.7, first contact at  $t = 10.8$  s). Experiments with 11 cells (19 individual measurements) yielded a delay time  $\Delta t_{\text{adh}}$  of several seconds (see Table 6.1). The final adhesive contact between the substrate and the flagella tips was often established many sec-

---

<sup>46</sup>Most of these combined experiments were performed by Aina Ramamonjy (ESPCI, Paris, France) during his time as a summer student tutored by Christian Titus Kreis [Ramamonjy, 2017].

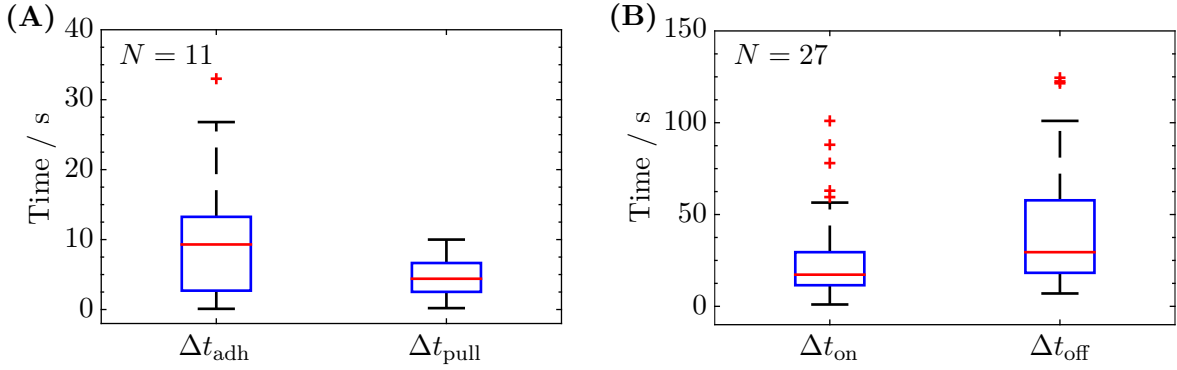


**Figure 6.11.: Delay times as determined from auto-adhesion experiments.** (A) Statistical distribution of delay times inferred from high-speed imaging (as shown in Figure 6.7, 400/800 frames per second) of 19 independent measurements ( $N = 11$  cells, each cell contributed 1 to 3 data points).  $\Delta t_{\text{adh}}$ : delay time between turning on the light stimulus and the first adhesive flagellum-substrate contact.  $\Delta t_{\text{pull}}$ : delay time between the final adhesive contact and the approach of the cell body towards the substrate (see text for further explanations). (B) Statistical distribution of delay times as inferred from the auto-adhesion kinetics ( $N = 27$  cells, each cell contributed 3 to 5 individual measurements, see Figure 6.8).  $\Delta t_{\text{on}}$ : delay time between turning on the light stimulus and the onset of the active approach.  $\Delta t_{\text{off}}$ : delay time between turning off the light stimulus and the snap-back of the cantilever to the zero-force position.

Delay time	$\Delta \bar{t}$ [s]	$\Delta t_{\text{median}}$ [s]	$\Delta t_{25\text{th}}$ [s]	$\Delta t_{75\text{th}}$ [s]
$\Delta t_{\text{adh}}$	10.6	9.3	2.7	13.3
$\Delta t_{\text{pull}}$	4.8	4.4	2.5	6.7
$\Delta t_{\text{on}}$	21.6	17.3	11.5	29.5
$\Delta t_{\text{off}}$	39.3	29.5	18.5	57.8

**Table 6.1.: Timescales in the auto-adhesion process.** The delay times are characterized by the mean delay time  $\Delta \bar{t}$ , the median  $\Delta t_{\text{median}}$ , and the 25th and 75th percentile  $\Delta t_{25\text{th}}$  and  $\Delta t_{75\text{th}}$ , respectively. The definition of the individual delay times is given in the text. See also Figure 6.11.



onds after the first contact, as the flagella could detached again. Although the flagella-substrate alignment and cell-substrate distance appeared to marginally influence the magnitude of the delay time, the delay time  $\Delta t_{\text{adh}}$  provides an estimation of the timescale of the light-switchable adhesion. The high-speed images suggest that the onset of flagellar adhesiveness occurred after several seconds, which is in line with the adsorption experiments shown in the previous section (see Figure 6.6).

In the experiments resolving the flagella dynamics and their surface attachment, there was always a significant delay time  $\Delta t_{\text{pull}}$  of a few seconds between the final adhesive contact of the flagella and the onset of the cell-substrate approach (see Table 6.1). The delay time  $\Delta t_{\text{pull}}$  was defined as the time between the final adhesive contact of the flagellum that adhered last and the onset of the cell-substrate approach. As the flagellum that drives the process might have attached first, the time reported here represents a lower boundary for the delay time  $\Delta t_{\text{pull}}$ . In rare instances, the cell-substrate approach was initiated before the second flagellum attached (most likely due to the flagella-substrate alignment), while the second flagellum kept beating regularly. This observation supports the previous finding that the flagella are independent from each other in the sense that the triggered signal pathway is localized to the adhered flagellum. In these cases, the delay time  $\Delta t_{\text{pull}}$  was taken as the time between the adhesive contact of the attached flagellum and the onset of the cell-substrate approach. The delay time  $\Delta t_{\text{pull}}$  of several seconds indicates that the auto-adhesion process is an active process, as a passive process would have started immediately after the flagella adhered to the substrate. Such a passive process could realize a protein-substrate attachment in a zipper-like fashion by forming more and more adhesive contacts between the flagella and the substrate (energy minimization of the system, which consists of the substrate and the adhesion-mediating proteins on the flagellar surface).

The delay time  $\Delta t_{\text{on}}$ , after turning the light stimulus on until the onset of the cell body approach, was in the order of tens of seconds (see Table 6.1 and Figure 6.8,  $N = 27$  cells, 131 individual measurements<sup>47</sup>). The delay time  $\Delta t_{\text{off}}$ , after turning the light stimulus off and until the first signature of a cantilever snap-back, was likewise about tens of seconds, yet significantly larger (see Table 6.1,  $N = 27$  cells, 130 individual measurements).

In conclusion, the flagella dynamics in close proximity to a substrate allowed for estimating the timescale of the light-switchable adhesion. The flagella became sticky several seconds after turning on an external blue-/white-light stimulus. The delay time between the final flagella-substrate contact and the onset of the cell-substrate approach indicates that the auto-adhesion process is an active process initiated by the *Chlamydomonas* cell. As gliding is an active process, which is driven by intraflagellar transport trains inside the flagellum, my findings suggest

---

<sup>47</sup>Most of the delay time data were contributed by Christine Linne as part of the work for her Master's thesis tutored by Christian Titus Kreis [Linne, 2017].

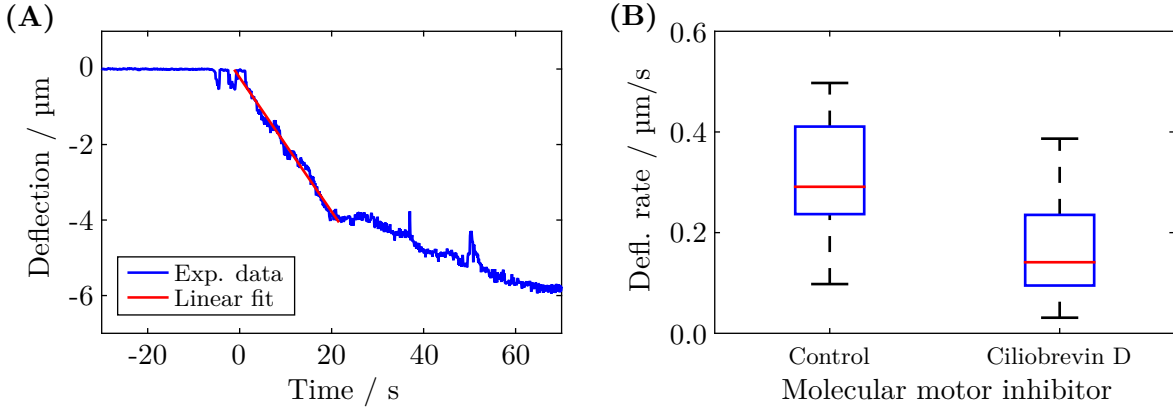


**Figure 6.12.: Effect of ciliobrevin D on the auto-adhesion process.** *Chlamydomonas* cells are incubated with ciliobrevin D that inhibits retrograde intraflagellar transport trains [Shih et al., 2013]. **(A)** The cantilever deflection rate at the beginning of the auto-adhesion process is determined as the best fit to the linear regime of the auto-adhesion process. In case of a non-linear regime, I define the deflection rate as the tangent to the onset of the auto-adhesion. The linear fit yields a slope of  $v = 0.207 \mu\text{m/s}$ . **(B)** The cantilever deflection rates are determined after incubation with ciliobrevin D for 1h ( $N = 12$  cells, 24 individual measurements, details see paragraph). As a control, the cantilever deflection rates are measured without incubation with ciliobrevin D ( $N = 11$  cells, 20 individual measurements).

	$\bar{v}$ [ $\mu\text{m/s}$ ]	$v_{\text{median}}$ [ $\mu\text{m/s}$ ]	$v_{25\text{th}}$ [ $\mu\text{m/s}$ ]	$v_{75\text{th}}$ [ $\mu\text{m/s}$ ]
Control	0.303	0.291	0.237	0.410
Ciliobrevin D	0.171	0.141	0.0949	0.235

**Table 6.2.: Effect of ciliobrevin D on the auto-adhesion process.** The initial cantilever deflection rate  $v$  in the auto-adhesion process is given without a molecular motor inhibitor and after incubating cells with a dynein inhibitor. The velocities are characterized by the mean velocity  $\bar{v}$ , the median  $v_{\text{median}}$ , and the 25th and 75th percentile  $v_{25\text{th}}$  and  $v_{75\text{th}}$ , respectively.

that the auto-adhesion might be connected to the same molecular machinery. The cell body is pulled by the flagella [Bloodgood, 1981] during gliding (driven by retrograde intraflagellar transport trains [Shih et al., 2013]), which coincides with my observations of the cell being pulled towards the substrate. Shih et al. further report that intraflagellar transport train were coupled to an adhesive site approximately every 8.5 s, which resulted in the onset of gliding, i.e. a quiescent cell would start moving in average after a few seconds. This timescale is comparable to the delay time  $\Delta t_{\text{pull}}$  extracted from the auto-adhesion study, which indicates a connection between intraflagellar transport and auto-adhesion.

### 6.3.3. Auto-Adhesion and Gliding Motility

The previously introduced auto-adhesion process is presumably an active process that is linked to the gliding motility. To test whether retrograde intraflagellar transport (dynein-1b) drives the auto-adhesion process, the influence of a dynein inhibitor on the auto-adhesion was studied [Ramamonjy, 2017]<sup>48</sup>. The activity of cytoplasmic dynein can be inhibited by ciliobrevin D, which does not affect kinesin [Firestone et al., 2012]. In previous studies on *Chlamydomonas* gliding, 150  $\mu\text{M}$  of ciliobrevin D in the buffer solution reduced the retrograde intraflagellar transport frequency by 92 %, their speed by 60 %, and the gliding velocity by 79 % [Shih et al., 2013].

I incubated *Chlamydomonas* cells with ciliobrevin D at a concentration of 200  $\mu\text{M}$  (Cytoplasmic Dynein Inhibitor, Ciliobrevin D: Merck KGaA, Darmstadt, Germany). The ciliobrevin D was dissolved in a pure water-dimethylsulfoxid (DMSO) solution at a ration of 9:1, as ciliobrevin D is insoluble in water (DMSO: CAS 67-85-5; Sigma-Aldrich, Germany, Purity  $\geq 99.9\%$ ). During the incubation and experiment, the DMSO volume fraction in the TAP medium was about 3.6 %, as a higher DMSO concentration is lethal to the cell<sup>49</sup>. After 30 minutes of incubation, the culture was centrifuged at 100  $g$  for ten minutes to concentrate dead cells at the bottom of the incubation flask. Subsequently, the culture was rested in the incubator for at least 30 minutes. Prior to an experiment, the upper part of the culture was suspended in the liquid cell. A second population of *Chlamydomonas* cells was incubated with DMSO and exposed to the same experimental routine to serve as a control group (without adding ciliobrevin D to the DMSO).

To quantify the effect of ciliobrevin D, I performed auto-adhesion experiments and measured the cantilever deflection rate at the onset of the auto-adhesion process (see Figure 6.12A). Cells that were incubated with ciliobrevin D exhibited a significantly decreased cantilever deflection rate at the onset of the auto-adhesion process (see Figure 6.12B). The cantilever deflection rate decreased by approximately 50 %, as estimated from the characteristic values of the distributions of the measured deflection rates (see Table 6.2). Thus, the flagella pulled the cell to the substrate with a lower velocity. These results strongly suggest that the auto-adhesion process is powered by dynein motors, which pull the retrograde intraflagellar transport trains. Consequently, the auto-adhesion is presumably linked to the same molecular machinery as the gliding motility.

### 6.3.4. Concluding Remarks

The light-switchable adhesion observed in the force spectroscopy experiments can be used to trigger an active process that brings a cell in close proximity to a substrate into adhesive

---

<sup>48</sup>These experiments were performed by Aina Ramamonjy (ESPCI, Paris, France) during his time as a summer student tutored by Christian Titus Kreis.

<sup>49</sup>DMSO increases the cell membrane permeability and reduces the membrane rigidity [Gurtovenko and Anwar, 2007].

contact with the substrate. The timescale of the auto-adhesion process indicates an active mechanism that pulls the cell body towards the substrate. This finding is substantiated by experiments that strongly suggest a direct connection between auto-adhesion and gliding [Ramamonjy, 2017]. A process that resembles the auto-adhesion was described by Daniel and King [Bloodgood, 1990b, Figure 3], who studied the transition from planktonic swimming to surface association. However, this study focused on the areas of the flagellum that generate the force necessary for gliding and did not provide a controlled manipulation of the cell-substrate interactions. Moreover, Daniel and King did not measure forces during the transition from swimming to gliding and did not report that light can be used to trigger surface-association.

The forces recorded during the auto-adhesion process are significantly larger than the stall forces of individual intraflagellar transport trains, which generate forces in the order of tens of piconewtons [Laib et al., 2009; Shih et al., 2013]. This difference suggests a cooperative effort of intraflagellar transport trains as a single intraflagellar transport train cannot overcome restoring forces of several nanonewtons. A cooperative effort is well-established for individual molecular motors, as otherwise the stall force of intraflagellar transport trains could not be generated [Klumpp and Lipowsky, 2005; Laib et al., 2009; Shih et al., 2013]. In the context of force generation in the flagellum, the auto-adhesion might open new pathways to study molecular motor and intraflagellar transport coordination in a whole flagellum. First steps in this direction have been performed by Christine Linne in her Master's thesis (tutored by Christian Titus Kreis) [Linne, 2017].

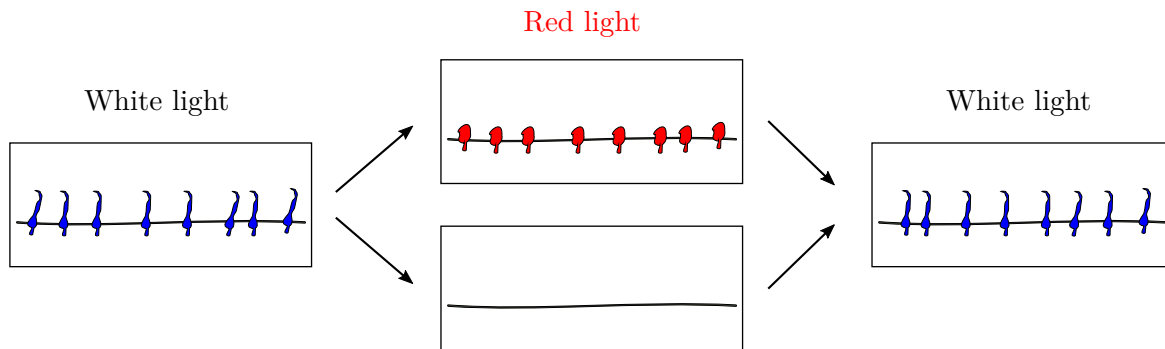


**Figure 6.13.: Sketch of two possible mechanisms underlying light-switchable adhesion.** In white light conditions, the adhesion-mediating protein FMG-1B (blue) is exposed at the flagellar surface. In red light, two possible pathways are sketched: either the protein is in a non-sticky conformation (top row, red proteins) or there are no proteins on the flagellar surface (bottom row). When turning back to white light, FMG-1B either changes back to its sticky conformation or reappears at the flagellar surface.

## 6.4. Unraveling the Molecular Mechanism of Light-Switchable Adhesion

### Introduction and Working Hypothesis

In the last sections, I demonstrated that the adhesiveness of the *Chlamydomonas*' flagella can be reversibly switched on and off by light. The onset of flagellar adhesiveness was found to be several seconds after blue-/white-light stimulation, as extracted from adsorption kinetics (see Figure 6.6) and high-speed imaging (see Figure 6.7). Whereas several characteristics of the light-switchable adhesion were found, the underlying mechanism that allows flagella to adapt their adhesiveness to different light conditions remains unclear and requires further inquiries. Two possible mechanisms to switch flagellar adhesiveness on and off are (sketched in Figure 6.13):

1. **Conformational changes of the adhesion-mediating protein:** The adhesion-mediation protein (FMG-1B, see section 2.3.2) has two different conformations. In white light, the protein is in a sticky conformation, whereas in red light the protein is in a non-sticky conformation. The conformational change could be triggered by a protein binding to the cytoplasmic domain of FMG-1B.
2. **Relocalization of the adhesion-mediating protein:** The adhesion-mediating protein relocates in the flagellum. In white light, FMG-1B can be found on the flagellar surface and renders the flagella sticky. In red light, FMG-1B is not present at the flagellar surface leading to non-sticky flagella.

In order to distinguish between these two suggested mechanisms, I tested the effect of proteolysis on the adhesion forces in controlled light conditions (see the experimental protocols in section 3.4.5). A pronase treatment is not specific to a certain protein, but rather degrades all proteins at the surface of the flagellar membrane into individual amino acids (proteolysis). At the applied concentrations, the flagellar membrane is not damaged [Bloodgood and May, 1982]. Thus, proteolysis can elucidate whether FMG-1B is present at the flagellar membrane in red-light conditions. The effect of the proteolysis on two suggested mechanisms is sketched in Figure 6.14.

### Proteolysis Experiments

In white illumination, force spectroscopy experiments ( $N = 3$  cells) showed that the exposure to pronase resulted in a gradual decrease of the adhesion force (see Figure 6.15A)<sup>50</sup>. After two hours of proteolysis, the adhesion force was less than 5 % of the initial adhesion force of the same cell. This finding is in agreement with earlier studies reporting the effect of pronase treatment on the flagellar adhesiveness, which was qualitatively judged by counting microspheres

---

<sup>50</sup>About half of the data points in the proteolysis study were contributed by Marine Le Blay (ESPCI, Paris, France), a summer student tutored by Christian Titus Kreis [Le Blay, 2016].

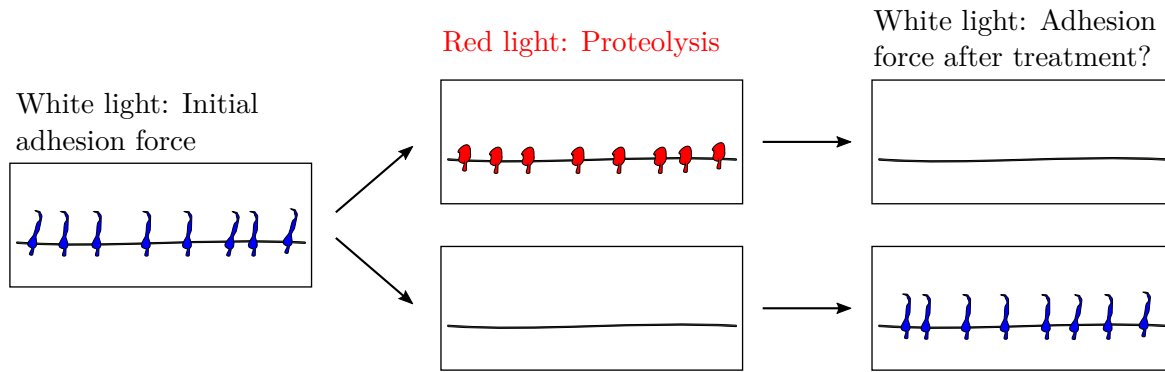


**Figure 6.14.: Proteolysis to identify the underlying mechanism.** Turning from white to red light either changes the conformation of FMG-1B (middle picture, top row) or relocates the protein from the flagellar surface (middle picture, bottom row; see Figure 6.13). These two cases can be distinguished with a pronase treatment, as pronase degrades all proteins that remain on the surface of the flagellar membrane. In the first case (top row), all adhesion-mediating proteins are degraded and I do not expect to record adhesion. In contrast, in the second case the proteins reappear at the flagellar surface and I expect to detect significant adhesion (bottom row).

bound to the flagella [Bloodgood and May, 1982]. The same effect was quantitatively reported on the adhesion-mediating membrane proteins of bacteria [Thewes et al., 2015b]. In a reference experiment, the adhesion forces remained constant in the absence of any pronase treatment during the same time frame (see Figure 4.5A).

I applied the same proteolysis treatment to cells in red light for two hours and quantified their adhesion forces immediately after switching to white illumination (the experiment was started at the latest 5 min after white light was turned on). Note that the cells were held with the micropipette in solution (and not pressed against the substrate) during proteolysis. In contrast to the white-light proteolysis, all cells ( $N = 8$  cells) still exhibited significant adhesion forces in white light after the treatment. Force spectroscopy experiments yielded adhesion forces of 32.5 to 69.9 % (25th/75th percentile, median: 49.6 %, mean: 53.9 %) compared to the initial adhesion forces of the same cells (see Figure 6.15B). In a control experiment with some of the cells, I did not measure adhesion in red light conditions during the proteolysis shortly before white light was turned on.

Force-distance experiments with cells that were incubated with pronase for two hours in red light conditions ( $N = 3$  cells) yielded significant adhesion forces in white light. The adhesion forces of these cells were consistent with the forces reported after proteolysis in red light. The data of these cells were not included in the analysis, as the cells were free swimming in the growth medium during proteolysis and no initial adhesion forces were recorded.

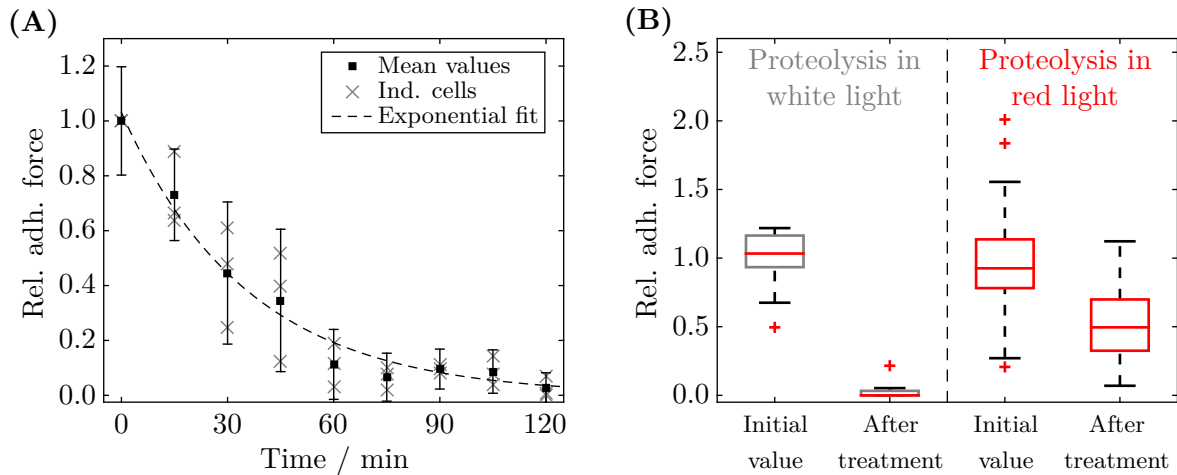


**Figure 6.15.: Effect of proteolysis on the adhesiveness of *Chlamydomonas* flagella in different light conditions.** (A) The adhesion forces ( $N = 3$  cells) are shown during a proteolysis treatment in white light. The pronase is added after the initial data point. The adhesion forces decrease to less than 5 % of the initial value within two hours of the pronase treatment. The dashed line represents an exponential fit to the data with a characteristic time constant of  $\tau = 35.7$  min. The adhesion forces of each cell are normalized to the initial mean adhesion forces of the same cell. (B) Comparison of the adhesion forces before and after a treatment (120 min) with pronase in different light conditions. While the adhesiveness is lost after proteolysis in white light (three cells shown in (A)), cells still exhibit adhesiveness after proteolysis in red light ( $N = 8$  cells, each cell contributes five force-distance curves). Note that adhesion forces were measured in white light. In the case of red-light proteolysis, the adhesion forces were measured approximately 5 min after turning on the white illumination. The adhesion forces of each cell are normalized to the initial mean adhesion force of the same cell in white-light conditions (see Figure A.16 for the non-normalized values).

The previous experiments demonstrate that the pronase treatment in red light did not reduce the adhesion forces to values that were comparable to the adhesion forces seen after the same treatment in white light. Hence, the proteolysis in red light was not effective. The adhesion forces after proteolysis in red light (recorded in white light) were consistent with the initial adhesion forces after turning on a white light stimulus (see the temporal evolution in Figure 6.5A): immediately after turning the light on, the (vegetative) *Chlamydomonas* cells exhibited adhesion forces that were approximately 50 % of the saturation value. The proteolysis results indicate that the adhesion-mediating protein was not exposed on the surface of the flagellar membrane in red light. Otherwise, the pronase would have degraded the protein and no significant adhesion would have been measured. Thus, protein relocalization in different light conditions appears to be the most plausible explanation for the light-switchable flagellar adhesiveness.

## Concluding Remarks

Two potential mechanisms underlying light-switchable flagellar adhesiveness were suggested. By performing proteolysis experiments in different light-conditions, I could presumably identify the mechanism that leads to light-switchable adhesion to surfaces. These experiments strongly suggest that *Chlamydomonas* regulates its flagellar adhesiveness by relocating the adhesion-mediating protein in different light conditions. The adhesion mediating protein is presumably not found at the surface of the flagellar membrane in red-light conditions. An active protein relocalization appears to be a reasoned explanation for the light-switchable adhesiveness in the context of flagellar membrane turnover, the translocation of microbeads, and gliding. Preliminary experiments that further support an active relocalization mechanism can be found in section 6.5.1 [Ramamonjy, 2017].

## 6.5. Preliminary and Ongoing Work

### 6.5.1. Active Regulation of Flagellar Adhesiveness

Proteolysis experiments in different light conditions suggest that the light-switchable adhesion of *Chlamydomonas* is based on a relocalization of the adhesion-mediating protein. This relocalization could be connected to the active FMG-1B mobility in the flagella, which allows for the translocation of microbeads, surface-associated gliding, and the quick protein turnover in the flagellar membrane (see section 2.3.4). All these processes are driven by molecular motors and intraflagellar transport.

To test whether active protein relocalization underlies light-switchable adhesion, I inhibited the molecular motor activity with lidocaine (CAS 137-58-6; Sigma-Aldrich, Germany), which is known to reversibly inhibit the translocation of microbeads along the flagellum [Snell et al., 1982; Miyamoto et al., 2000]. Therefore, lidocaine was injected into the liquid cell to achieve a final concentration of 1 mg/ml. Subsequently, the adhesion forces were recorded in white-light and red-light conditions by force spectroscopy with the same cell.

A preliminary experiment indicates that the timescale of the light-switchable adhesion is affected after adding lidocaine in red-light conditions<sup>51</sup>. Without lidocaine, adhesion was observed immediately after turning from red to white light, whereas I found a significant delay time of approximately 40 min for the onset of adhesion after adding lidocaine (see Figure 6.16, cf. Figure 6.5A). After turning back from white-light to red light conditions, the adhesion forces did not reduce to zero.

---

<sup>51</sup>The experiment was suggested by Christian Titus Kreis. The first test was performed by Aina Ramamonjy (ESPCI, Paris, France) during his time as a summer student tutored by Christian Titus Kreis [Ramamonjy, 2017].



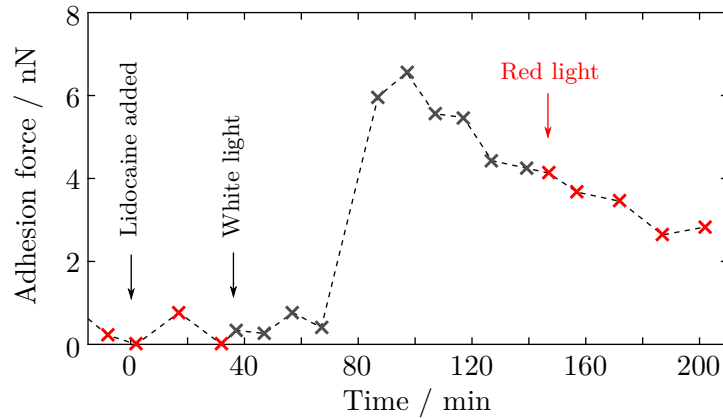


**Figure 6.16.: Effect of lidocaine on light-switchable adhesion.** The adhesion forces of a *Chlamydomonas* cell to a substrate are shown after adding lidocaine. Each data point includes two or three individual force-distance curves. The final lidocaine concentration in the liquid cell was 1 mg/ml. Turning white light on resulted in an increase of the adhesion force after a delay time of approximately 40 min. The adhesion force slowly decreased afterwards. Turning to red light did not reduce the adhesion force significantly.

Another approach to study the effect of lidocaine on the timescale of the light-switchable adhesion might be the previously shown adsorption experiments. Yet, lidocaine also inhibited the regular flagellar beating and the swimming of the cells at the applied concentrations, such that no adsorption experiments could be performed.

In summary, a preliminary experiment suggests that the light-switchable adhesion is governed by an active protein relocation. However, the data set shown here was recorded late in the afternoon and might not be representative. In rare instances, I did not measure adhesion in white light in the late afternoon (see the comment on page 77). Furthermore, the frequency of adhesion events recorded in red-light conditions seemed to be marginally higher (for cells that exhibited adhesion in white light) after 17 o'clock. In the presented experiment, lidocaine was added at approximately 14 o'clock. Nevertheless, lidocaine or another molecular motor inhibitor appears to be a promising pathway to verify the role of intraflagellar transport in light-switchable adhesion. Further experiments in more controlled experimental conditions are necessary to draw reliable conclusions.

## 6.5.2. Photoreceptor Deletion-Mutants

### Channelrhodopsin Deletion-Mutants

The influence of the blue-light receptors channelrhodopsin 1 and 2 on light-switchable adhesion was studied with a knockout mutant that lacks both channelrhodopsins. This channelrhodopsin mutant was generated from *Chlamydomonas reinhardtii* strain CC3403 using the protocols de-

scribed in [Sizova et al., 2013] (the second step of the procedure is not yet published)<sup>52</sup>. As the parent strain CC3404 lacks a cell wall, micropipette force spectroscopy experiments with these mutants were not successful, as of today (see section 4.1).

I performed “adsorption” experiments with the channelrhodopsin mutant as previously reported for the wild type strain (see the protocol in section 3.5 and the results in Figure 6.6). In contrast to the wild type cells, the cell number on the substrate did not change after turning on the white-light stimulus. As these mutants do not perform phototaxis<sup>53</sup> (experimental observation) [Berthold et al., 2008], I expect the cells to interacted less frequently with the substrate than the wild type cells, which were guided by the location of the light-source to the glass slides. This difference in the cell behavior could explain the absence of significant adsorption.

Instead of studying the light-switchable adhesion by the adsorption of cells to a substrate, the desorption could be characterized to show that the flagellar adhesiveness was switched off by turning off the white light. However, the desorption could not be studied due to the lack of adsorbed cells. As of today, the role of channelrhodopsins on the light-switchable adhesion could not be identified. Although this deletion-mutant provides a promising system to study the role of channelrhodopsins, the experimental design needs to be adapted to overcome the existing phototaxis barrier.

Adapting the cell density in the solution and/or the experimental geometry could significantly increase the number of cell-surface interaction events. A possible method is to use microfluidic systems where individual *Chlamydomonas* cells were trapped in quasi two-dimensional compartments [Ostapenko et al., 2016]. Preliminary tests in these compartments indicate that the in-plane swimming of the cell inhibits frequent surface interactions, which are necessary to reliably study the transition from swimming to surface association. Marginally increasing the compartments height and trapping several cells in the compartment (cell-cell interactions) might promote out-of-plane rotations that lead to more cell-surface interactions.

In contrast to this qualitative approach, force spectroscopy experiments would yield a direct quantification of the flagellar adhesiveness in response to variable light conditions. Therefore, either the experimental protocol needs to be adapted to enable experiments with more mechanically unstable cells or a channelrhodopsin mutant from a different parent strain needs to be generated. The experimental setup could be adjusted to these mechanically unstable cells by using a microfluidic pump to regulate the suction pressure at the micropipette’s nozzle (see page 32). This method has been already successfully integrated in the experimental setup to study polymersomes with tunable adhesive properties [Petit et al., 2017]. Furthermore,

---

<sup>52</sup>The photoreceptor deletion-mutant was kindly provided by Prof. Hegemann and co-workers (Humboldt-Universität, Berlin, Germany).

<sup>53</sup>Personal communication, Prof. Hegemann.

the opening of the micropipette's nozzle could be modified to support more fragile objects by rounding off the edges of the nozzle. Thereby, the cell is supported by a larger cell-nozzle contact area, which was useful in studies on the mechanical properties of *Volvox* colonies (see section B.1).

### Phototropin Deletion-Mutants

Phototropin deletion-mutants were employed to study the influence of phototropin on light-switchable adhesion. These mutants were generated from *Chlamydomonas reinhardtii* strain CC-125 (unpublished procedure<sup>54</sup>). The adsorption and desorption of a population of these genetically modified *Chlamydomonas* cells was studied in white and red illumination (see section 3.5 and the results in Figure 6.6).

In comparison to the wild type cells, the phototropin mutants appeared to have an impaired motility, as judged by the swimming dynamics of planktonic cells. All previously generated phototropin mutants lacked flagella<sup>55</sup>, thus a strong influence on flagella functionality is not surprising.

In a preliminary experiment, I did not observe significant adsorption of cells to the substrate after switching from red to white illumination. In contrast to the phototaxis mutant, the cells appeared to interacted more frequently with the substrate, as in some instances a flagellum transiently adhered to the substrate. These interactions lasted for less than a few seconds and were not sufficient to immobilize the alga on the substrate. This qualitative observation suggests that the flagellar adhesiveness is strongly reduced in white light compared to the wild type *Chlamydomonas* cells. A comparison to the flagellar adhesiveness in red light conditions is still lacking (the cells are not interacting with the glass slide in red light, as the phototaxis is lacking). Indeed, the reduced flagellar adhesiveness could be a general characteristic of the phototropin mutant. Consequently, the preliminary adsorption experiment cannot elucidate the influence of phototropin on light-switchable adhesion.

### Concluding Remarks

Preliminary adsorption experiments with channelrhodopsin and phototropin mutants were not sufficient to identify the influence of these photoreceptors on light-switchable adhesion. Although populations of cells from both mutant-strains did not show light triggered surface colonization, the absence of adsorption might be caused by a lack of surface interactions (channelrhodopsin mutant) and a reduced flagellar adhesiveness (phototropin mutant). Hence, force spectroscopy experiments are necessary to dissect characteristics of the mutants from the light response.

---

<sup>54</sup>The phototropin deletion-mutant was kindly provided by Prof. Hegemann and co-workers (Humboldt-Universität, Berlin, Germany).

<sup>55</sup>Personal communication, Prof. Hegemann (Berlin, Germany).

As of today, it is unknown whether the flagella of the phototropin (and channelrhodopsin) mutants exhibit altered adhesive properties in white light conditions. Thus, a characterization of the adhesion forces in white light is necessary (as in chapter 5), in conjunction with a biomolecular characterization of the flagellar properties, for example, to identify FMG-1B at the flagellar membrane. While the current experimental data suggest that the phototropin mutants have reduced flagellar adhesiveness, phototropin might not be the photoreceptor that triggers the light-switchable adhesion. The importance of phototropin for the flagella development might also affect the general flagellar structure and FMG-1B exposure at the surface of the flagellar membrane.

## 6.6. Discussion, Conclusions, and Outlook

In the course of this work, I discovered that the adhesion of vegetative *Chlamydomonas* cells to solid substrates can be switched on and off by light. This phenomenon was further characterized by force spectroscopy experiments, auto-adhesion experiments, and biomolecular manipulations in precisely controlled light conditions. These experiments yielded four main results:

1. Independent of the adhesion forces in white-light conditions, the adhesion of *Chlamydomonas* flagella could be reversibly reduced to zero in red-light conditions on any tested substrate.
2. The light-switchable adhesion is most likely controlled by a blue-light photoreceptor that triggers flagellar adhesiveness above a sharp irradiance threshold.
3. I discovered an active process, termed auto-adhesion, that allows a *Chlamydomonas* cell in close proximity to a substrate to establish contact after flagellar adhesiveness was switched on. This process is presumably linked to the same molecular machinery as gliding motility.
4. Proteolysis experiments suggest that *Chlamydomonas* adapts its flagellar adhesiveness by an active protein relocalization in different light conditions. A preliminary experiment with an inhibitor of molecular motor activity supports this finding.

In summary, force spectroscopy experiments provide unambiguous evidence that the adhesiveness of vegetative *Chlamydomonas* flagella is switchable by light. Results from adsorption experiments corroborate the findings and suggest that light-switchable adhesiveness is a natural functionality of *Chlamydomonas* to regulate the transition between the planktonic and the surface-associated state. The light-switchable flagellar adhesiveness appears to be linked to an active protein relocalization within the flagella and the flagellar membrane. Active protein motility and protein relocalization in the flagella of *Chlamydomonas*, seen as the flagellar membrane turnover, the gliding and the translocation of microbeads, are driven by intraflagellar transport. Hence, the putative protein relocalization, which allows for light-switchable flagellar

adhesiveness, is presumably linked to the intraflagellar transport.

The light-switchable adhesion connects the adhesiveness of *Chlamydomonas*' flagella to the light conditions in the natural habitat of *Chlamydomonas*. Sufficient sunlight exposure triggers the blue-light photoreceptor that controls the flagellar adhesiveness. In conjunction with phototaxis, the coupling of sunlight exposure to the adhesion capability allows *Chlamydomonas* to locate and colonize surfaces that provide optimal light conditions for proliferation. Thus, the light-switchable adhesion yields an adhesive adaptation to optimize the photosynthetic efficiency. This flagella functionality seems beneficial for an organism that is exposed to many surfaces and variable light conditions in its natural habitat. Hence, light-switchable adhesion might have evolved as a biological advantage for this photoactive microalgae.

The auto-adhesion is presumably an active process that mimics the transition from planktonic swimming to surface association. This process allows *Chlamydomonas* to establish adhesive contact with a substrate once a small part of one flagellum, such as the flagellar tip, adhered to the substrate. Furthermore, auto-adhesion allows for re-establishing the gliding configuration, as long as a small part of one flagellum remains adhered to the substrate. Gliding might have evolved to explore surfaces and rearrange on surfaces, whereas auto-adhesion seems beneficial to cross small gaps, for example, in between sand grains, without completely losing the surface association. In aqueous environments, auto-adhesion appears to be useful after, for example, viscous drag from water currents or rain drops detached the cell partially from the surface. In this context, auto-adhesion and light-switchable adhesion might trigger new discussions and studies on the functionality of the gliding motility, which is still not found as of today [Bloodgood, 2009, discussion on page 356].

Light-switchable adhesion seems to have an immediate relevance for *Chlamydomonas* in its natural habitat. To fully understand the mechanism and its implication, further studies on the characteristics of light-switchable adhesion and the mechanism are necessary. These inquiries include verifications of the underlying protein relocalization mechanism that was inferred from the findings in this work. Furthermore, identifying the photoreceptor is necessary to understand the signal pathway, which is involved in the newly discovered flagellar functionality. As of today, I limited the light-reception mechanism to a blue-light photoreceptor and performed preliminary tests with photoreceptor deletion-mutants.

A follow-up study on the auto-adhesion process should continue the work performed by Linne on the kinetics of the auto-adhesion process [Linne, 2017]. Adsorption experiments should be performed in tailored geometries to elucidate the interplay between light-switchable adhesion and phototaxis. These experiments could include geometries that resemble, for example, soil, algal colonies on rocks, or biofilm networks to mimic the natural habitats of microalgae.

In the context of technological applications, light-switchable adhesion appears to be a promising tool to control microalgal adhesion in technological and research settings and to inhibit microalgal biofilm formation in photobioreactors. Possible pathways could either be new design principles of photobioreactors to permanently or temporally tailor the light conditions, or genetic modifications of the organism to hamper its adhesion capability. Both approaches could significantly contribute to enhance the efficiency of photobioreactors.

In conclusion, the discovery of light-switchable adhesion might stimulate further research in many directions and fields, from fundamental molecular biology, evolutionary and behavioral biology, to biophysics, bioengineering and technological applications.

## 7. Surface Forces Governing Microalgal Adhesion

The adhesion force of a microorganism to a substrate is ultimately determined by the intermolecular interactions between the substrate and the adhesion-mediating structures of the microorganism. In an adhesion processes in biological systems, the most relevant interactions and forces are electro-magnetic in origin: hydrophobic forces, van der Waals interactions, and electrostatic interactions (see section 2.5) [Autumn et al., 2000, 2002; Loskill et al., 2012c; Lee et al., 2006; Maier et al., 2015; Waite, 2017; Thewes et al., 2014, 2015b; Barthlott and Neinhuis, 1997; Ma and Hill, 2006]. Characterizing the surface forces that mediate the adhesion is imperative to understand microbial adhesion mechanisms. In a technological context, understanding microbial adhesion mechanisms is necessary to develop pathways to control microbial surface colonization. For example, non-toxic coatings are required for surface treatments in marine environments, as toxin-containing anti-microbial coatings are widely banned due to severe implications in marine ecosystems [Evans et al., 1995; IMO, 2017]<sup>56</sup>. Although microalgae are of profound relevance for biofouling in aqueous environments [Chambers et al., 2006; Callow and Callow, 2011; Landoulsi et al., 2011], quantitative experiments that characterize the influence of surface forces on microalgal adhesion are lacking.

This chapter seeks to identify the surface forces that mediate the adhesion of *Chlamydomonas* to substrates. Therefore, I performed force spectroscopy experiments with the exact same cell on two different substrates (in white-light conditions) and compared the measured adhesion forces (see section 3.4.5 and Figure 3.10 for a description of the experimental routine). In total, I quantified the adhesion forces to substrates of four substrate sets, with varying strength of hydrophobic forces, van der Waals interactions, and electrostatic interactions. *Chlamydomonas* cells that exhibited a mean adhesion force larger than approximately 4 nN on the silicon reference substrate were excluded from the analyses, as they might have experienced flagella damage (see section 5.1). The substrate characterization and substrate properties are described in section 3.3.

---

<sup>56</sup>For example, conventional anti-microbial coatings on ship hulls contained tributyltin, which are compounds that contain a  $(C_4H_9)_3Sn$  group. Tributyltin was banned by several resolutions due to the negative impact it has on ecosystems in close proximity to harbors and shipping lanes. More information can be found on the website of the International Maritime Organization (IMO): <http://www.imo.org>, retrieved 08.08.2017.

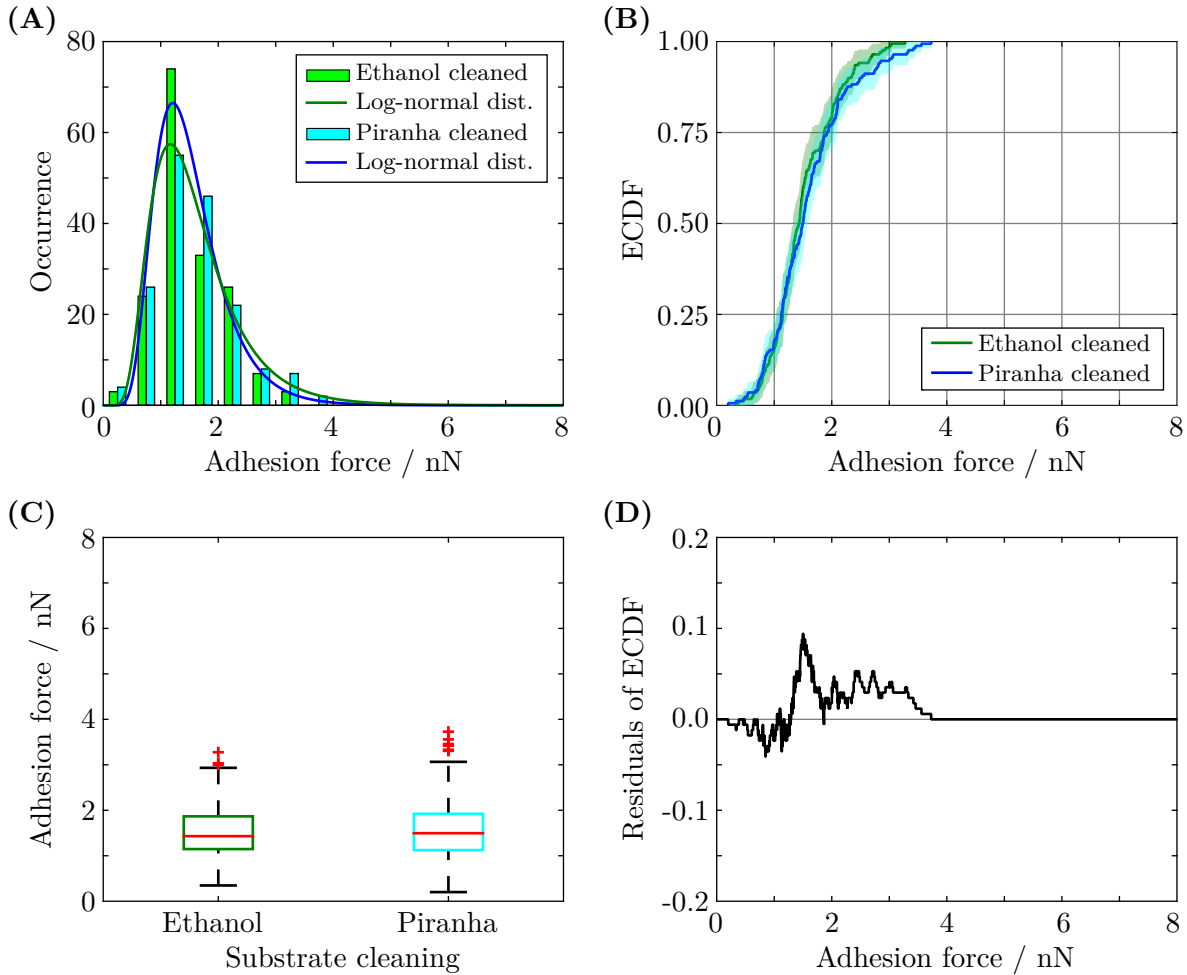


**Figure 7.1.: Influence of the surface cleaning on *Chlamydomonas* adhesion forces.** Distribution of adhesion forces to silicon substrates ( $N = 17$  cells) that were cleaned by ethanol (green) or piranha solution (teal). **(A)** Histograms of data sets; the solid lines represent best fits to log-normal distributions. Dark green line: best fit to ethanol data,  $\alpha = 0.34[6]$ ,  $\beta = 0.39[4]$ . Blue line: best fit to piranha data,  $\alpha = 0.36[7]$ ,  $\beta = 0.46[5]$ . **(B)** Empirical cumulative distribution functions (ECDF) of the data sets. The shaded area represents the 95 % confidence interval of the ECDF. **(C)** Box plots of the data sets. **(D)** Residuals of the ECDF of the ethanol and piranha data set.



## 7.1. Force Spectroscopy on Model Substrates with Tailored Properties

### 7.1.1. Hydrophobic Interactions: Surface Energy and Surface Hydrophobicity

The magnitude and sign (attraction or repulsion) of the hydrophobic interactions between the *Chlamydomonas* flagella and a substrate are determined by the polarity of the substrate and the adhesion-mediating protein FMG-1B. The polarity is determined by the Lewis acid-base component of the surface energy  $\gamma^{\text{AB}}$  (see section 2.5.4). A nonpolar surface has  $\gamma^{\text{AB}} = 0 \text{ mJ/m}^2$ , which generally results in a low total surface energy. To tune the hydrophobic interactions, I employed two substrate sets that consisted of substrates that differed in their surface energies. The other substrate properties, like the charge and roughness, were kept constant.

The first substrate set consisted of two pieces of silicon wafers that were cleaned with ethanol (reference substrate,  $\gamma_{\text{Ethanol}}^{\text{tot}} = 35(4) \text{ mJ/m}^2$ ) and piranha solution ( $\gamma_{\text{Piranha}}^{\text{tot}} = 64(2) \text{ mJ/m}^2$ ), respectively. The treatment with piranha solution removes organic residues, for example carbohydrates, and hydroxylates the surface (adds  $\text{OH}^-$ -groups), resulting in an extremely hydrophilic substrate (water contact angle  $< 5^\circ$ ). On both substrates, I performed force-distance experiments with the same cells ( $N = 17$  cells) and I compared the recorded adhesion forces (see Figure 7.1 and Table 7.1). The adhesion force distributions from both substrates were in good agreement, as evidenced by their characteristic values (the mean, median, and the 25th and 75th percentile, see Table 7.1). The difference between both adhesion force distributions was quantified by a Kolmogorov-Smirnov test (see section 3.6.3). The Kolmogorov-Smirnov test statistic yields  $T_{KS} = 0.100$ . Hence, the null hypothesis cannot be rejected at a significance level  $\alpha = 0.05$  (see Equation 3.4,  $n, m = 170$ ). Thus, there was no significant difference between the adhesion force distributions on both types of substrates.

Substrate	Varied	$\gamma^{\text{tot}} [\text{mJ/m}^2]$	$\bar{F} [\text{nN}]$	$F_{\text{median}} [\text{nN}]$	$F_{25\text{th}} [\text{nN}]$	$F_{75\text{th}} [\text{nN}]$
Si (Ethanol)	Cleaning	35(4)	1.51	1.43	1.15	1.87
Si (Piranha)		64(2)	1.58	1.50	1.12	1.92

**Table 7.1.: Adhesion forces to substrates with different cleaning procedures.** Differences in the cleaning method result in different surface energies  $\gamma^{\text{tot}}$ . The adhesion force distributions are characterized by the mean adhesion force  $\bar{F}$ , the median  $F_{\text{median}}$ , and the 25th and 75th percentile  $F_{25\text{th}}$  and  $F_{75\text{th}}$ , respectively.

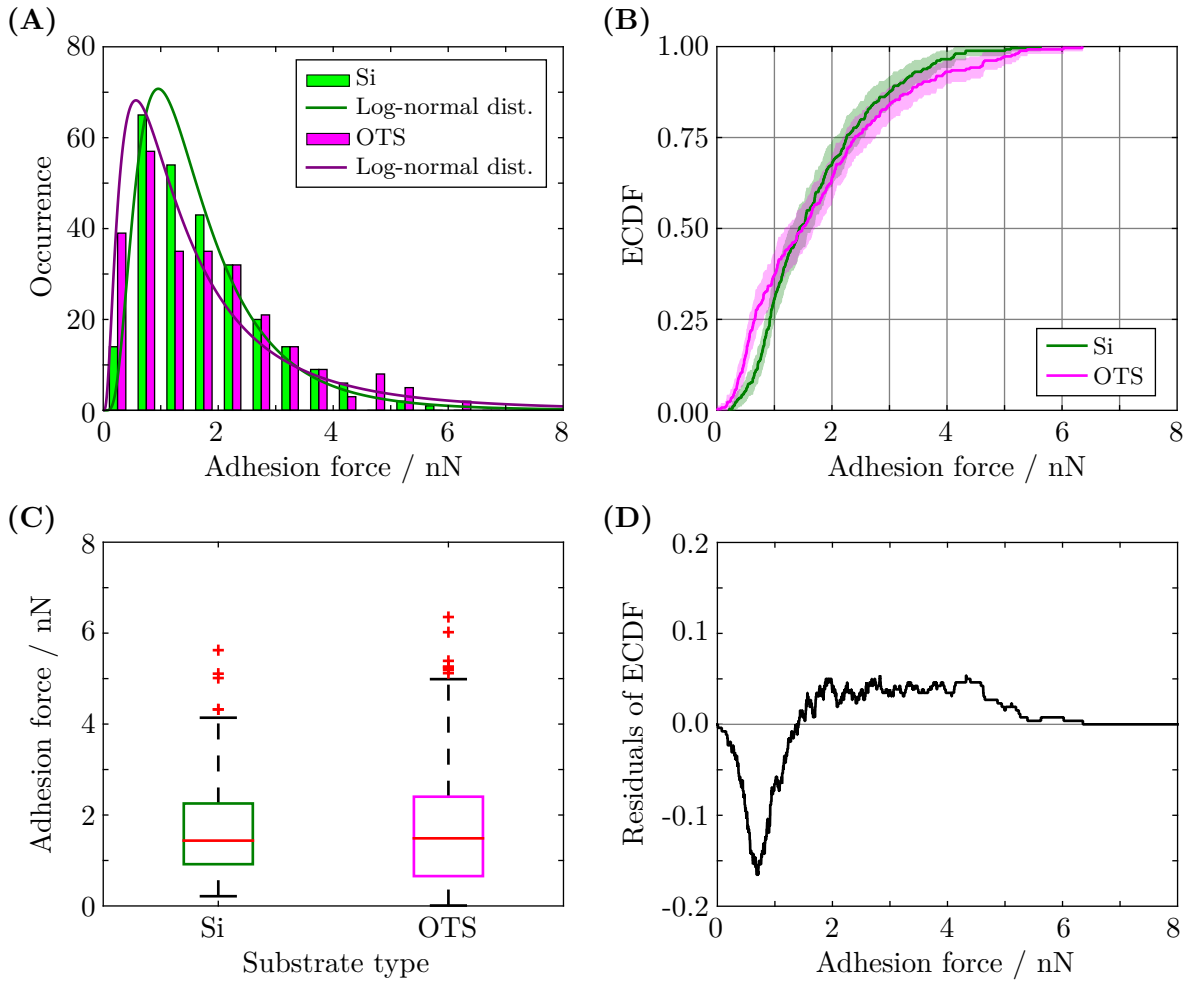


**Figure 7.2.: Influence of hydrophobic forces on *Chlamydomonas* adhesion forces.** Distribution of adhesion forces ( $N = 26$  cells) to a hydrophilic silicon substrate (Si, green) and a silicon substrate that was coated with a hydrophobic self-assembled silane monolayer (OTS, pink). (A) Histograms of data sets; the solid lines represent best fits to log-normal distributions. Dark green line: best fit to Si data,  $\alpha = 0.35[8]$ ,  $\beta = 0.63[2]$ . Purple line: best fit to OTS data,  $\alpha = 0.24[11]$ ,  $\beta = 0.90[8]$ . (B) Empirical cumulative distribution functions (ECDF) of the data sets. The shaded area represents the 95 % confidence interval of the ECDF. (C) Box plots of the data sets. (D) Residuals of the ECDF of the Si and OTS data set.

Substrate	Varied	$\gamma^{\text{tot}}$ [mJ/m <sup>2</sup> ]	$\bar{F}$ [nN]	$F_{\text{median}}$ [nN]	$F_{25\text{th}}$ [nN]	$F_{75\text{th}}$ [nN]
Si	Surface chemistry	35(4)	1.71	1.44	0.918	2.25
OTS		23(1)	1.75	1.49	0.657	2.40

**Table 7.2.: Adhesion forces to substrates with different functionalization.** A hydrophobic substrate coating decreases the surface energy  $\gamma^{\text{tot}}$  of the silicon substrate. The adhesion force distributions are characterized by the mean adhesion force  $\bar{F}$ , the median  $F_{\text{median}}$ , and the 25th and 75th percentile  $F_{25\text{th}}$  and  $F_{75\text{th}}$ , respectively.

The second substrate set contained a piece of a non-functionalized, hydrophilic silicon wafer (reference substrate, ethanol cleaned,  $\gamma_{\text{Si}}^{\text{tot}} = 35(4)$  mJ/m<sup>2</sup>) and a piece of a silicon substrate that was coated with a hydrophobic self-assembled silane monolayer (Octadecyltrichlorosilane (OTS), ethanol cleaned,  $\gamma_{\text{OTS}}^{\text{tot}} = 23(1)$  mJ/m<sup>2</sup>, [Lessel et al., 2015]). The mean and median of the adhesion force distributions ( $N = 26$  cells) were in good agreement (see Figure 7.2 and Table 7.2). However, there was a significant difference in the broadness of the adhesion force distributions, as characterized by the 25th and 75th percentile (see Equation 3.4,  $T_{KS} = 0.165$ , rejection of the null hypothesis at a significance level of 1 %,  $n, m = 260$ ).

In summary, I performed force spectroscopy experiments on two substrate sets to probe the influence of hydrophobic forces on the adhesion of *Chlamydomonas*. The experiments yielded adhesion forces of consistent magnitude (mean, median), whereas the distribution of the adhesion forces to the hydrophobic (OTS) substrate was broader compared to the distribution of the adhesion forces to the hydrophilic reference substrate (Si).

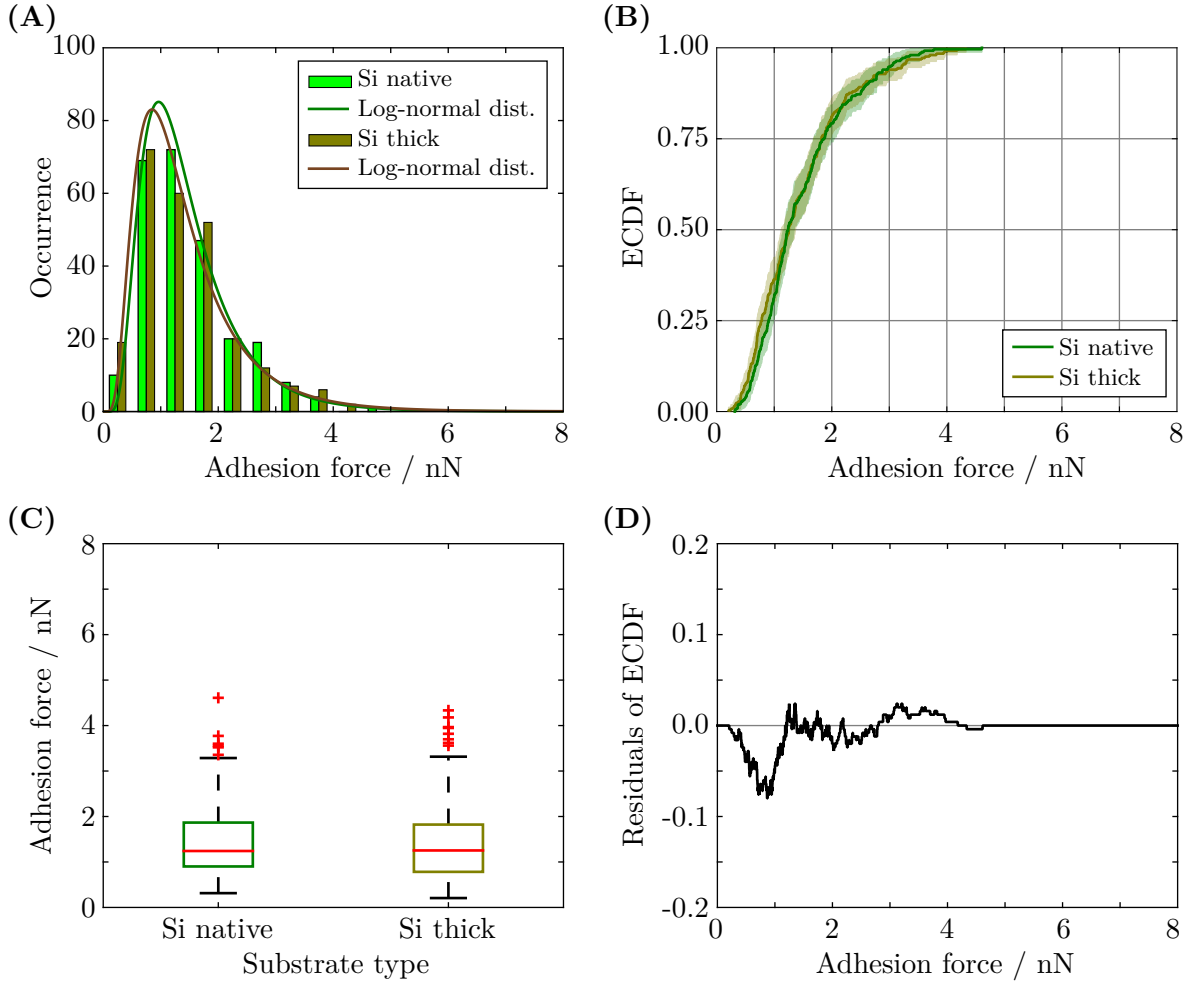


**Figure 7.3.: Influence of van der Waals interactions on *Chlamydomonas* adhesion forces.** Distribution of adhesion forces ( $N = 25$  cells) to a silicon substrate with a thin, native  $\text{SiO}_2$  layer (Si native, green) and to a silicon substrate with a thick, thermally-grown  $\text{SiO}_2$  layer (Si thick, olive). **(A)** Histograms of data sets; the solid lines represent best fits to log-normal distributions. Dark green line: best fit to Si native data,  $\alpha = 0.24[7], \beta = 0.53[5]$ . Brownish line: best fit to Si thick data,  $\alpha = 0.19[7], \beta = 0.59[5]$ . **(B)** Empirical cumulative distribution functions (ECDF) of the data sets. The shaded area represents the 95 % confidence interval of the ECDF. **(C)** Box plots of the data sets. **(D)** Residuals of the ECDF of the Si native and Si thick data sets.

### 7.1.2. Van der Waals Interactions

The interaction strength of the van der Waals interactions between two objects depends on the physical properties (polarizability) of the involved materials (see section 2.5.2). Van der Waals interactions between microorganisms and substrates can be varied by multi-layer materials, such as a silicon wafer with either a thin or a thick silicon dioxide ( $\text{SiO}_2$ ) layer on top. A protein interacts stronger with a silicon wafer with thin  $\text{SiO}_2$ -layer than with a silicon wafer with thick  $\text{SiO}_2$ -layer (see the derivation in section 2.5.2).

To vary the van der Waals interactions, I employed silicon wafers (ethanol cleaned) with different oxide layer thickness: a silicon wafer with native, thin oxide layer termed Si native ( $d_{\text{SiO}_2} = 1.7 \text{ nm}$ ), and a silicon wafer with thermally grown, thick oxide layer termed Si thick ( $d_{\text{SiO}_2} = 150 \text{ nm}$ ). This substrate set has proven to be a good system to study van der Waals interactions in biological systems, like geckos, bacteria, and proteins [Loskill et al., 2012a,b,c; Hähl et al., 2012].

Force spectroscopy experiments ( $N = 25$  cells) yielded consistent adhesion forces to both substrates, as evidenced by the characteristic values of the force distributions (see Figure 7.3 and Table 7.3). The force distributions did not exhibit a significant difference (see Equation 3.4,  $T_{KS} = 0.0800$ ,  $n, m = 250$ ).

Substrate	Varied	$d(\text{SiO}_2) \text{ [nm]}$	$\bar{F} \text{ [nN]}$	$F_{\text{median}} \text{ [nN]}$	$F_{25\text{th}} \text{ [nN]}$	$F_{75\text{th}} \text{ [nN]}$
Si native	SiO <sub>2</sub> -layer thickness	1.7	1.46	1.24	0.901	1.87
Si thick		150	1.42	1.25	0.783	1.82

**Table 7.3.: Adhesion forces to silicon substrates with different  $\text{SiO}_2$ -layer thickness.**

The  $\text{SiO}_2$ -layer thickness on a Si-wafer alters van der Waals interactions. The adhesion force is characterized by the mean adhesion force  $\bar{F}$ , the median  $F_{\text{median}}$ , and the 25th and 75th percentile  $F_{25\text{th}}$  and  $F_{75\text{th}}$ , respectively.

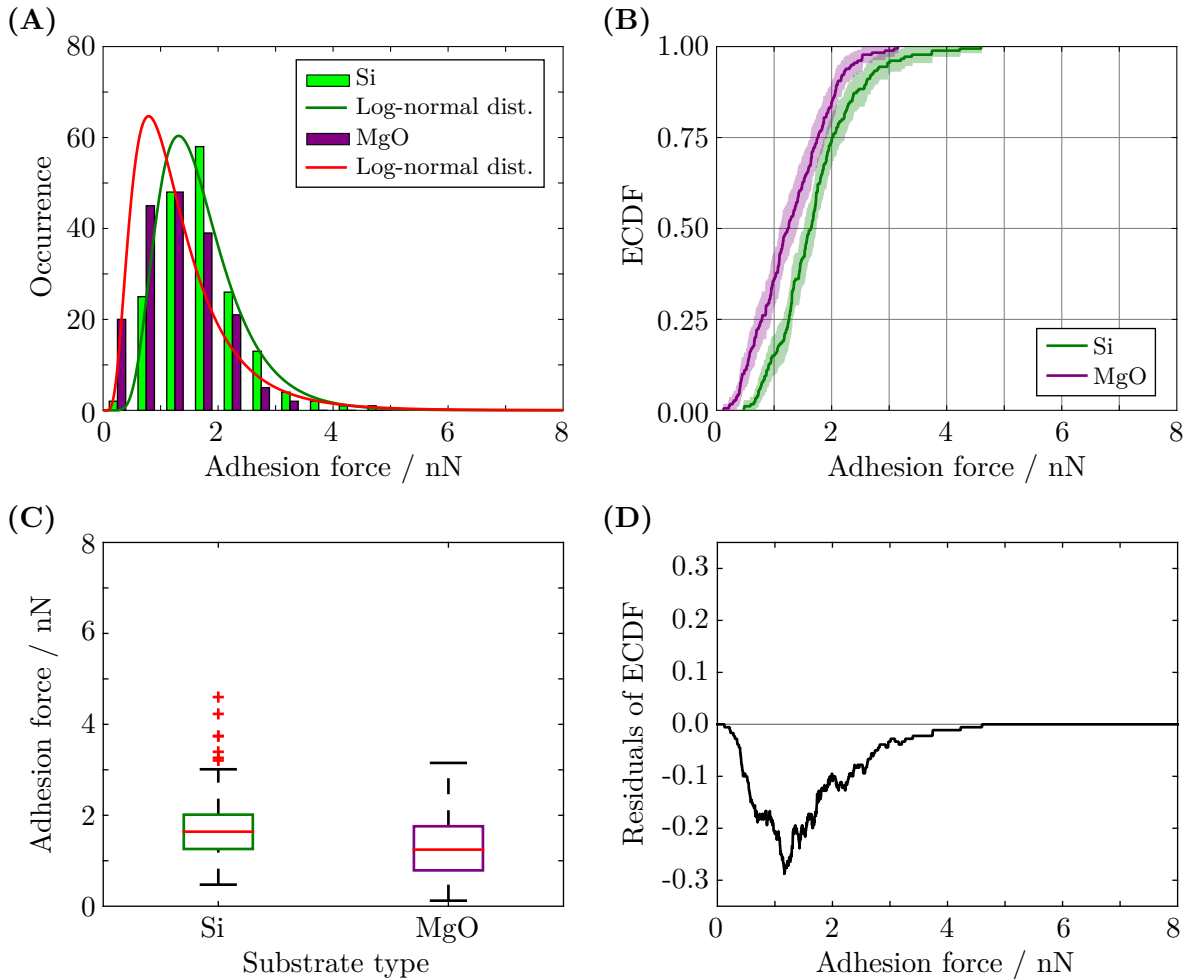


**Figure 7.4.: Influence of electrostatic interactions on *Chlamydomonas* adhesion forces.** Distribution of adhesion forces ( $N = 18$  cells) to a silicon substrate (Si, green) and on a magnesium oxide substrate (MgO, purple). **(A)** Histograms of data sets; the solid lines represent best fits to log-normal distributions. Dark green line: best fit to Si data,  $\alpha = 0.45[6]$ ,  $\beta = 0.42[4]$ . Red line: best fit to MgO data,  $\alpha = 0.11[9]$ ,  $\beta = 0.59[6]$ . **(B)** Empirical cumulative distribution functions (ECDF) of the data sets. The shaded area represents the 95 % confidence interval of the ECDF. **(C)** Box plots of the data sets. **(D)** Residuals of the ECDF of the Si and MgO data set.

### 7.1.3. Electrostatic Interactions

The net charge of the substrate and the adhesion-mediating protein FMG-1B determine the interaction strength and sign of their electrostatic interactions. In aqueous solution, the charge of substrates and proteins depends on their isoelectric point (IEP) and the pH-value of the solution (section 2.5). To probe the influence of electrostatic interactions on the adhesion, I performed force spectroscopy experiments on substrates that were oppositely charged due to different isoelectric points in the same buffer solution. In the TAP-buffer solution with  $\text{pH} \approx 7$ , the reference Si substrate is negatively charged (ethanol cleaned, isoelectric point of  $\text{pH} = 3$  [Bousse et al., 1991]), whereas a magnesium oxide substrate (MgO) substrate is positively charged (ethanol cleaned, isoelectric point of  $\text{pH} = 12.5$  [Robinson et al., 1964]). Consequently, this substrate set allows to alter the electrostatic interactions between the substrate and *Chlamydomonas* flagella, whereas the other substrate properties (surface energy, roughness) were comparable (see Table 3.3).

On both substrates, I performed force-distance curves with the same *Chlamydomonas* cells ( $N = 18$  cells) and I analyzed the adhesion force distributions (see Figure 7.4). The characteristic values of the force distributions were significantly smaller on the MgO substrate compared to the Si substrate (see Table 7.4). The difference in the adhesion forces was about 25 %, as estimated from the characteristic values and the shift of the ECDF (see Figure 7.4B). This finding is substantiated by a one-sided Kolmogorov-Smirnov test, which validates that the adhesion forces to Si are significantly larger than the forces to MgO (see Equation 3.6,  $T_{KS} = 0.289$ ,  $n, m = 180$ ).

Besides using substrates with different charges, the electrostatic interactions can be tuned by varying the concentration of ions in the buffer solution. A lower ion concentration reduces the screening of the electrostatic interactions, as indicated by a smaller Debye length. To vary the screening of the electrostatic interactions, I performed experiments in minimal medium (NMM, [Berthold et al., 2008]) that features a lower ion concentration compared to the TAP medium. The Debye length in the NMM is  $1/\kappa_{\text{NMM}} \approx 2.64 \text{ nm}$  compared to a Debye length in TAP medium of  $1/\kappa_{\text{TAP}} \approx 1.80 \text{ nm}$  (see section 2.5.1 and section 3.2). Whereas the concentration of

Substrate	Varied	IEP	$\bar{F}$ [nN]	$F_{\text{median}}$ [nN]	$F_{25\text{th}}$ [nN]	$F_{75\text{th}}$ [nN]
Si	Substrate charge	3	1.70	1.64	1.26	2.01
MgO		12.5	1.30	1.24	0.789	1.76

**Table 7.4.: Adhesion forces to substrates with different charge.** The isoelectric point (IEP) determines the substrate charge, which directly influences the electrostatic interactions. The adhesion force is characterized by the mean adhesion force  $\bar{F}$ , the median  $F_{\text{median}}$ , and the 25th and 75th percentile  $F_{25\text{th}}$  and  $F_{75\text{th}}$ , respectively.

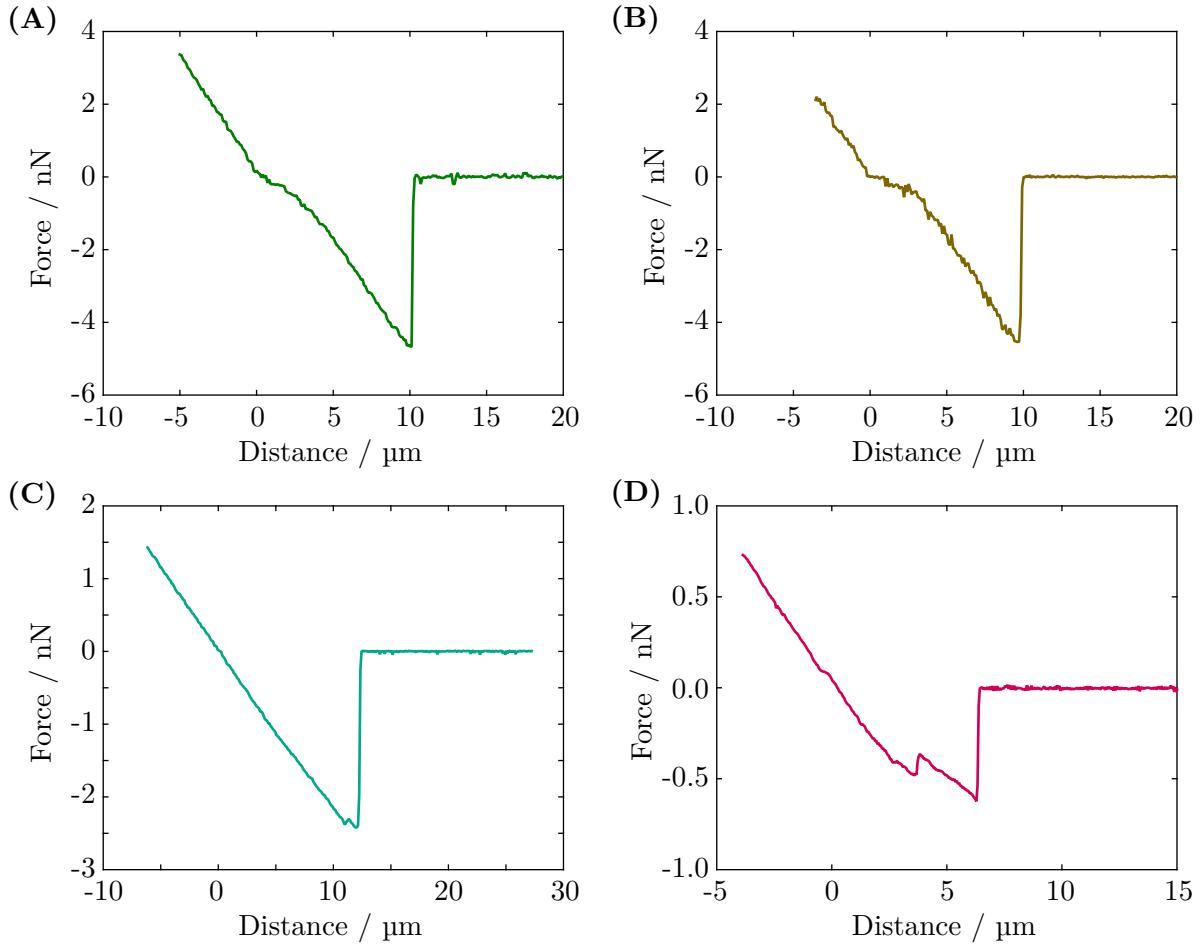


**Figure 7.5.: Force-distance curves on additional substrates.** Force spectroscopy on additional substrates: the retraction curves of one force-distance cycle is shown. For information on the substrates see section 3.3. **(A)** Glass substrate. **(B)** Gold substrate (same cell as in (A)). **(C)** PDMS-coated silicon wafer. Consistent adhesion forces were measured with the same cell to the reference silicon substrate. **(D)** Teflon<sup>®</sup> AF1600-coated silicon wafer. Consistent adhesion forces were measured with the same cell to the reference silicon substrate.



ions alters the strength of the electrostatic interactions, it also directly influences the biology and behavior of *Chlamydomonas*. In the NMM medium the vegetative cells transform into sexual active cells (gametes) that express additional sexual agglutinins on the flagellar surface, which are not involved in adhesion to substrates (see section 2.3.2 and section 2.3.3).

The gametes exhibited consistent adhesion forces with the vegetative cells ( $N = 29$  cells)<sup>57</sup>. In particular, I did not observe a change in the adhesion force due to the ion concentration (see Figure 8.1), which was probably due to the relatively small change in the Debye length by a factor of 1.5. Varying the concentration of ions such that the Debye length would change by, for example, one order of magnitude (ion concentration difference: two orders of magnitude) seems difficult, as the ion concentration modifies the biology and behavior of *Chlamydomonas*.

In summary, force spectroscopy experiments on substrates with different charge demonstrated that electrostatic interactions contribute to the interactions between *Chlamydomonas* flagella and a substrate. Further studying the electrostatic interactions by varying the concentration of ions in the buffer solution appears difficult, as the ion concentration directly influences the molecular biology of the *Chlamydomonas* cells.

## 7.2. Force Spectroscopy on Additional Substrates

Besides the systematic studies on the previously described substrates sets, the adhesion forces of *Chlamydomonas* cells were probed on glass and gold substrates, and on silicon wafers coated with Teflon® AF1600 and PDMS, respectively. Preliminary experiments show that the cells exhibited adhesion force of several nanonewtons to all substrates (see Figure 7.5). The forces were consistent with adhesion forces to the silicon reference substrate that were measured with the same cells.

---

<sup>57</sup>The experiments with gametes were mostly performed by Alice Grangier (ESPCI, Paris, France) during her time as summer student tutored by Christian Kreis [Grangier, 2017].

### 7.3. Discussion, Conclusions, and Outlook

I performed force spectroscopy experiments on substrates with tailored properties to dissect the influence of different intermolecular interactions on the protein-mediated adhesion of *Chlamydomonas* to substrates. Sample sizes of 170 to 260 individual force-distance curves on each substrate enabled a comprehensive statistical analysis of the adhesion force distributions, which yielded three main results:

1. The adhesion force distributions on hydrophobic and hydrophilic substrates were in good agreement and had equal mean and median values. The force distribution on the substrate with a hydrophobic coating was broader than on the hydrophilic reference substrate.
2. Van der Waals interactions did not show any significant influence on the adhesion force distributions.
3. Electrostatic interactions showed a significant influence on the adhesion force distributions. The adhesion forces decreased by about 25 % on a positively-charged substrate as compared to a negatively-charged substrate.

Ultimately, the force spectroscopy experiments demonstrated that the *Chlamydomonas* cells adhered to all tested substrates consistently with forces of several nanonewtons. This result suggests that *Chlamydomonas* has an universal adhesion mechanism that allows the alga to adhere to virtually all substrates. In conjunction with phototaxis and the light-switchable adhesion (see chapter 6), the possibility to adhere to any kind of surface that provides optimal growth conditions seems beneficial. Thus, the universal adhesion mechanism might have evolved as an evolutionary advantage for organisms that live in habitats with heterogeneous surfaces.

In contrast, the adhesion of bacteria to substrates depends often strongly on the molecular composition of the substrate. For example, single-cell force spectroscopy experiments with *Staphylococcus* showed adhesion forces of several nanonewtons to hydrophobic OTS substrates that were reduced to tens of piconewtons to hydrophilic Si substrates [Thewes et al., 2014]. In general, there are a plethora of adhesion studies with many different bacterial species that support the finding from the previously mentioned study on bacterial adhesion [Yongsunthon and Lower, 2006; Loskill et al., 2012b; Beaussart et al., 2014; Sullan et al., 2014; Zeng et al., 2014]. These differences on abiotic substrates are not surprising, as the adhesion-mediating structures of bacteria (pili, fimbriae, membrane proteins, etc.) are often tailored for attaching to certain biotic substances, for example the extracellular material in a host organism or biofilm [Abraham et al., 1988; Hultgren et al., 1993; Beloin et al., 2008; Proft and Baker, 2008; Sullan et al., 2014]. As the adhesion of *Chlamydomonas* is also mediated by proteins, the universality of the adhesion mechanism represents a remarkable difference compared to bacterial adhesion.

**Adhesion Mediated by Carbohydrates Bound to the Flagellar Membrane Protein FMG-1B**

In a more detailed view, the adhesion of *Chlamydomonas* is mediated by the major flagellar membrane glycoprotein FMG-1B, which is uniformly distributed on the flagellar surface (see section 2.3.2 for more details). Besides FMG-1B, no other protein has been identified to mediate substrate adhesion; in particular, the flagellar mastigonemes are not involved in the adhesion [Bloodgood, 1977; Nakamura et al., 1996]. The amino acid composition of FMG-1B suggests a similar amount of positively- and negatively-charged amino acids (at pH = 7.4), as well as a similar amount of polar and nonpolar amino acids. Since the structure of the protein and the structure of its individual domains are unknown, there is no information about hydrophobic and hydrophilic domains, as well as domains with any kind of net charge. Nevertheless, the iodination essay, which identified FMG-1B as the adhesion mediating protein, qualitatively showed that FMG-1B can bind to polar (glass beads) and nonpolar (polystyrene microspheres) surfaces [Bloodgood and Workman, 1984].

The ectodomain of FMG-1B is heavily N-glycosylated [Bloodgood et al., 1986, see also section 2.3.2]. The monosaccharide composition of the FMG-1B glycosylation was determined for two *Chlamydomonas* strains, which suggests that the carbohydrates do not carry a negative net charge, as there was no evidence of negatively charged sialic acid residues attached to the carbohydrates [Bloodgood, 1990b; Hermentin et al., 1996]. Although the general backbone structure of the N-linked glycosylation is known (see section 2.3.2, Figure 2.5), the structure of the glycosylation in *Chlamydomonas* remains unclear.

There is experimental evidence that the glycosylation might be responsible for the flagellar surface adhesiveness. A treatment with tunicamycin, which blocks protein glycosylation, led to a loss of flagellar adhesiveness, as judged by the lack of the ability to bind microspheres [Bloodgood, 1987]. The lack of glycosylation could affect the protein folding and the protein stability at the surface of the flagellar membrane [Lodish et al., 2004]. Although the glycosylation might thereby affect the adhesive properties of FMG-1B indirectly, there is evidence that the oligosaccharides mediate the adhesion directly. The carbohydrates normally extend at least 3 nm from the protein surface as flexible, hydrated branches [Helenius and Aebi, 2004], which is in line with the observation that monoclonal antibodies cannot access FMG-1B, presumably due to the glycosylation [Bloodgood et al., 1986]. That is, a carbohydrate layer presumably surrounds FMG-1B (at least partially). The adhesion-mediating function of protein glycosylation is supported by force spectroscopy studies on the glycosylation of yeast, where individual carbohydrates exhibited adhesion forces of tens of piconewtons to atomic force microscopy cantilever tips [Alsteens et al., 2008]. Note that the backbone structure of the glycosylation is the same in yeast and *Chlamydomonas*.

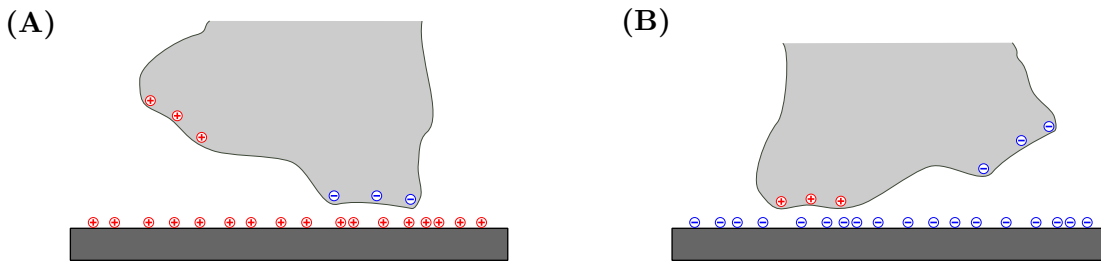


**Figure 7.6.: Sketch of a protein realignment mechanism.** The adhesion-mediating protein realigns due to interactions of the local charges on the protein and the substrate. Thereby, attractive electrostatic interactions dominate due to a shorter range, independent of the substrate's charge. **(A)** Positively charged substrate: the protein aligns such that negative charges at the protein surface are exposed to the substrate. **(B)** Negatively charged substrate: the protein aligns such that positive charges at the protein surface are exposed to the substrate.

### Perspectives on an Universal Adhesion Mechanism

In the context of glycoprotein-mediated adhesion, the first result of my experiments indicates that there are presumably no hydrophobic domains on the FMG-1B surface. Otherwise, an increased adhesion to the hydrophobized substrates would have been observed. The general characteristics of protein glycosylation corroborate this interpretation. The protein glycosylation potentially prevents a direct protein/surface interaction, so that any short range hydrophobic interactions are negligible. Furthermore, the glycan oligosaccharides are predominantly polar [Helenius and Aebi, 2004]. Nonetheless, variations in the protein glycosylation could explain the broader force distributions on hydrophobic OTS compared to hydrophilic Si, as most glycoproteins have a heterogeneous populations of glycans at each glycosylation site [Rudd et al., 1999]. A subtle cell-to-cell variability in the extent and composition of the protein glycosylation appears to be a reasonable explanation for a broader force distribution on the hydrophobic substrate.

The results from substrates that carry charges with different signs suggest that electrostatic interactions play an important role in the adhesion of *Chlamydomonas*, as changing the sign of the substrate charge resulted in a significant decrease in the measured adhesion forces. Although there was a significant influence of the substrate charge on the adhesion force, it is noteworthy that the difference in the adhesion force was only 25%. This difference is much smaller than the previously mentioned differences seen in bacterial adhesion, for example on OTS and Si. This observation points towards an adhesion mechanism that can mediate adhesion to positively- and negatively-charged substrates (or substrates with different substrate chemistry), which might be realized in one of the two following ways (inspired by [Waite, 2017]):

- 1. Conformational changes, or realignment of amino acids or carbohydrates:**

There might be protein domains (or individual amino acids) that carry charges of oppo-

site sign. Moreover, as glycan oligosaccharides are generally polar [Helenius and Aebi, 2004], they might feature local charges that can mediate electrostatic interactions. Due to electrostatic interactions between these charges on the protein and the substrate, the protein might realign and expose protein domains with a specific charge to the substrate (see Figure 7.6). These interactions could also result in conformational changes of the protein or individual protein domains. As conformational changes in proteins occur on timescales faster than the timescale of my force spectroscopy experiments, this mechanism appears to be a possible explanation for an universal adhesion mechanism based on electrostatic interactions [Henzler-Wildman and Kern, 2007].

2. **Adhesion-induced molecular modification of the protein:** Individual amino acids might be oxidized/reduced in contact with substrates. These chemical modifications would locally change the charge and or/chemistry of the protein. Potential candidates are the amino acids asparagine and glutamine, which can transform to aspartic acid and glutamic acid, respectively. In both forms, these amino acids account for approximately 8 % of the total number of amino acid in FMG-1B. Thus, protein modifications at adhesive contact sites seem possible [Bloodgood, 1990b].

In conclusion, FMG-1B represents a universal adhesion protein that can mediate adhesion to a variety of substrates. The adhesion mechanism is presumably based on electrostatic interactions between FMG-1B and the substrate. An adhesion mechanism based on electrostatic interactions seems beneficial, as surfaces are generally charged in aqueous environments. The structure of FMG-1B and its sugar residues remain important missing informations to fully understand the universal adhesion mechanism of *Chlamydomonas*, in which carbohydrates might play an important role.

### Outlook on an Universal Adhesion Mechanism in other Microalgae

On a more general perspective, N-linked glycosylation is extremely common amongst eukaryotes. As the structure of the glycosylation is highly preserved, it is likely that other microalgal species feature a very similar structure of carbohydrate residues on their adhesion-mediating proteins (see also the discussion on the “root” eukaryote in [Snell and Goodenough, 2009]). If carbohydrates are directly mediating the adhesion of *Chlamydomonas*, it is likely that other microalgae inherit a similar universal adhesion mechanism that allows them to adhere to virtually all substrates in aqueous environments. Future work should study the adhesion capability of other microalgae, starting with *Oogamochlamys gigantea* and *Chlamydomonas noctigama*, as force spectroscopy experiments with these microalgae have been already successfully implemented (see chapter 8). Subsequently, other close relatives of *Chlamydomonas* should be studied (see the taxonomic classification of these microalgae and the discussion in section 8.4).

In the context of biofouling, an universal adhesion mechanism implies that microbial adhesion cannot be prevented on any anthropogenic structures in wet environments by non-toxic surface

coatings. Thus, other approaches need to be found to prevent biofouling caused by microalgae. As the initial surface attachment is only the first step in biofilm formation, a pathway to prevent biofilm formation could be surfaces or surface coatings that alter or hamper the production of extracellular polymeric substances after surface colonization. Thereby, the structural stability of the biofilm could potentially be decreased and the maturation of the biofilm would be inhibited.

### 7.4. Summary

In summary, force-spectroscopy experiments on substrates with tailored intermolecular interactions with the *Chlamydomonas* flagella suggest that *Chlamydomonas* inherits an universal adhesion mechanism. Thereby, electrostatic interactions appear to play an important role for the adhesion of microalgae to surfaces in aqueous environments. The universal adhesion mechanism might be based on chemical modifications of the adhesion-mediating protein and/or its carbohydrates at adhesive protein-substrate contact. Future work should resolve the structure of the adhesion-mediating protein and verify the role of the carbohydrates in the adhesion mechanism.

## 8. Light-Switchable Adhesion: A Generic Trait of Soil-Dwelling Microalgae?

Microalgae appear in various shapes and forms with presumably hundreds of thousands of different species [Starckx, 2012]. Although microalgae are an extremely diverse, polyphyletic group, they share many features. One of the most remarkable features of microalgae are their flagella, which have the characteristic structure of the eukaryotic axoneme. There are microalgae, which are usually flagellated in aqueous environments, such as *Chlamydomonas*, whereas other species exclusively express flagella in a specific stage in their life cycle. This flagellated, free-swimming life stage can also be found in algae that form macroscopic structures, such as filaments, like the Oedogoniales [Hirn, 1900]. For these algae, the flagellated life stage (asexual zoospore) is usually linked to the dissemination of the organism to new locations. Hence, flagella-mediated adhesion to surfaces has a significant relevance for microalgae beyond typically flagellated species like *Chlamydomonas*.

The aim of this chapter is to study whether light-switchable adhesion to solid surfaces is a more generic trait of soil-dwelling, freshwater microalgae. Therefore, *in vivo* force spectroscopy experiments will be performed in precisely-controlled light conditions with sexual-active *Chlamydomonas reinhardtii* gametes and other species of the Chlorophyceae.

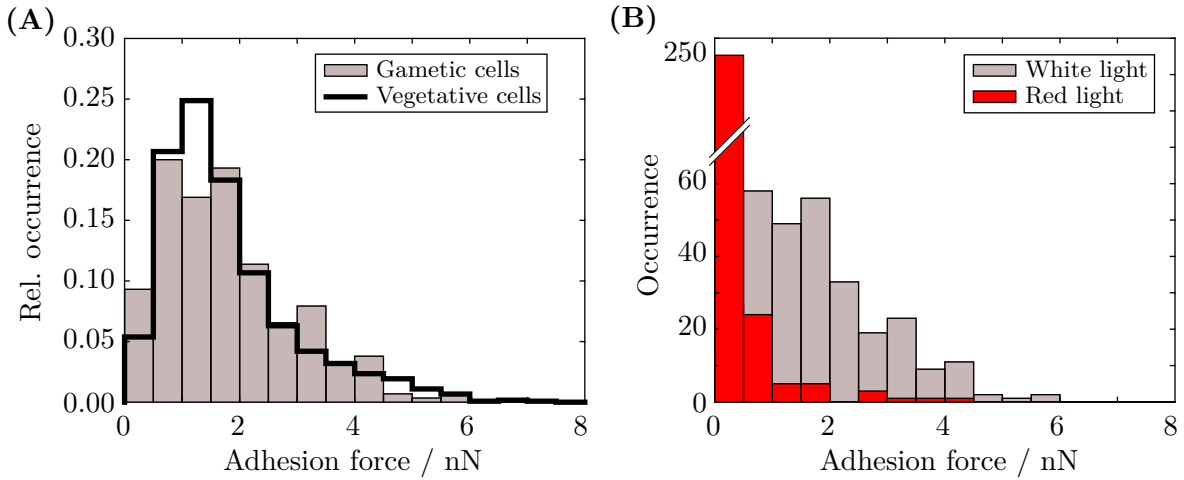


**Figure 8.1.: Force spectroscopy of gametic *Chlamydomonas reinhardtii* cells in white and red light conditions.** (A) Distribution of adhesion forces for gametic *Chlamydomonas reinhardtii* cells ( $N = 29$  cells) on a silicon substrate in white light. The black solid line represents the functional form of the adhesion force distribution of vegetative cells shown in Figure 5.3 with a different binning. (B) Distribution of adhesion forces for gametic cells in white light and red light ( $N = 29$  cells).

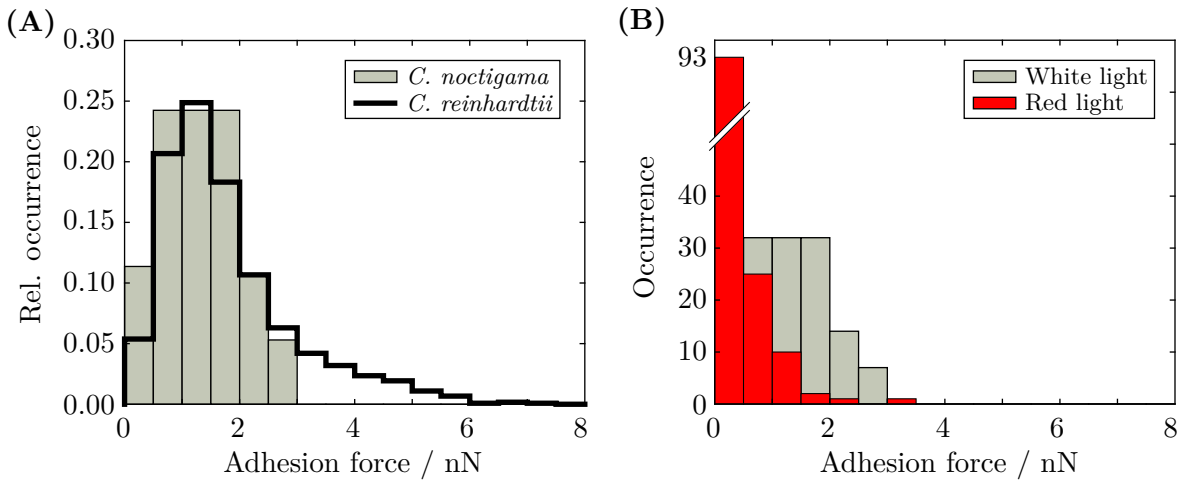


**Figure 8.2.: Force spectroscopy of *Chlamydomonas noctigama* cells in white and red light.** (A) Distribution of adhesion forces for *Chlamydomonas noctigama* (SAG 35.72) cells on a silicon substrate in white light ( $N = 33$  cells). The black solid line represents the functional form of the adhesion force distribution of vegetative *Chlamydomonas reinhardtii* cells shown in Figure 5.3 with a different binning. (B) Distribution of adhesion forces for *Chlamydomonas noctigama* cells in white light and red light ( $N = 33$  cells).



## 8.1. *Chlamydomonas reinhardtii* Gametes

The gametes of *Chlamydomonas reinhardtii* are indistinguishable from vegetative *Chlamydomonas reinhardtii* cells by conventional optical microscopy. The main difference on the flagella of gametes compared to vegetative cells are the sexual agglutinins that mediate the cell-cell interactions during the mating process (see section 2.3.3). In the laboratory, gametogenesis can be introduced by exposing the cells to a nitrogen-deprived medium, which mimics sub-optimal growth conditions. To identify whether the gametogenesis influences the flagellar adhesion properties and light-switchable adhesion, I performed force spectroscopy experiments with *Chlamydomonas reinhardtii* gametes (strain SAG 11-32b) on silicon substrates in white and red light<sup>58</sup>. The differentiation of vegetative cells into gametes is described in section 3.2. Gametes of both mating types (strain SAG 11-32a and SAG 11-32b) were mixed to observe sexual mating and to verify that gametes were formed.

Force spectroscopy experiments with gametic cells ( $N = 29$  cells) on silicon substrates yielded adhesion forces from 0.900 to 2.36 nN (25th/75th percentile, median: 1.56 nN, mean: 1.77 nN) in white light (see Figure 8.1A). The adhesion forces were consistent with the adhesion forces recorded for vegetative cells (see Figure 5.3 and the corresponding paragraph on page 77). For the same gametes, the adhesion forces were significantly reduced by switching from white to red illumination (25th/75th percentile: 0/0.256 nN, median: 0 nN, mean: 0.240 nN, see Figure 8.1B). In 59.3 % of all force-distance curves in red light, I did not measure any detectable adhesion, whereas 100 % of the force-distance curves of the same cells exhibited an significant adhesion peak in white light.

In summary, the gametic cells exhibited adhesion forces to solid substrates that were consistent with the adhesion forces of vegetative cells. Moreover, the gametes also exhibited light-switchable adhesion as seen for vegetative cells.

## 8.2. *Chlamydomonas noctigama*

*Chlamydomonas noctigama* is a unicellular green alga of the genus *Chlamydomonas* that is mostly found in broadleaf and coniferous forests [Ettl and Gärtner, 2014]. The cells are marginally larger and more ellipsoidal, and the flagella are slightly longer than in *Chlamydomonas reinhardtii*. The pyrenoid is located at the side of the cell body, whereas the pyrenoid of *Chlamydomonas reinhardtii* is found at the basal part of the cell body.

The force spectroscopy experiments with *Chlamydomonas noctigama* were performed with a cell-substrate contact time of approximately 45 s (see section 3.4.3). At a contact time of 25 s,

---

<sup>58</sup>The experiments with gametes were mostly performed by Alice Grangier (ESPCI, Paris, France) during her time as a summer student tutored by Christian Titus Kreis [Grangier, 2017].

as employed in experiments with *Chlamydomonas reinhardtii*, the cells did not always adhere to the substrate, whereas all cells adhered to the substrate after a contact time of 45 s in white light.

Force-distance curves with *Chlamydomonas noctigama* strain SAG 35.72 ( $N = 33$  cells, where each cell contributes four individual force-distance curves in red and white light) yielded adhesion forces of 0.855 to 1.80 nN (25th/75th percentile, median: 1.27 nN, mean: 1.33 nN) to a silicon substrate in white light conditions (see Figure 8.2A)<sup>59</sup>. In comparison to *Chlamydomonas reinhardtii*, the adhesion forces appeared to be marginally lower, in particular no force-distance curve exhibited an adhesion force larger than 3 nN. In contrast to white light, the adhesion forces of the same *Chlamydomonas noctigama* cells were significantly reduced in red light (25th/75th percentile: 0/0.606 nN, median: 0 nN, mean: 0.347 nN, see Figure 8.2B). For these cells, 52.3 % of all force-distance curves did not exhibit any detectable adhesion in red light, whereas 100 % of the force-distance curves of the same cells exhibited an significant adhesion peak in white light.

In summary, *Chlamydomonas noctigama* exhibited adhesion forces to substrates that were consistent with forces of *Chlamydomonas reinhardtii* in white light. Force spectroscopy experiments in different light conditions demonstrate unambiguously that the adhesion of *Chlamydomonas noctigama* to substrates is switchable by light. Thus, the light-switchable adhesion can also be found in other species of the genus *Chlamydomonas*.

### 8.3. *Oogamochlamys gigantea*

*Oogamochlamys gigantea*, previously known as *Chlamydomonas gigantea*, is a member of the family Chlamydomonadaceae and belongs to a different genus than *Chlamydomonas reinhardtii* and *Chlamydomonas noctigama* [Pröschold et al., 2001, see Figure 8.5]. The cells are cylindrical (the sides are flat or even concave) and about 20 to 40  $\mu\text{m}$  long, which is more than twice as long as *Chlamydomonas reinhardtii* cells [Ettl and Gärtner, 2014]. In contrast to the previously mentioned *Chlamydomonas* species, *Oogamochlamys gigantea* has many pyrenoids and contractile vacuoles distributed in the whole cell body. The most remarkable difference to species of the genus *Chlamydomonas* is the sexual reproduction via oogamy, i.e. the gametes of different mating types have a different size and the gametes of only one mating type are motile (the vegetative cells of both mating types are motile).

The cell-substrate contact time in the force-distance curves was 45 s (see section 3.4.3), for the same reason as in *Chlamydomonas noctigama* (see section 8.2). The adhesion forces of *Oogamochlamys gigantea* cells ( $N = 25$ , each cell contributes four individual force-distance curves

---

<sup>59</sup>The experiments with *Chlamydomonas noctigama* were initiated and tested by me. Most of the data were collected by Christine Linne, as part of the work for her Master's thesis tutored by Christian Titus Kreis [Linne, 2017].

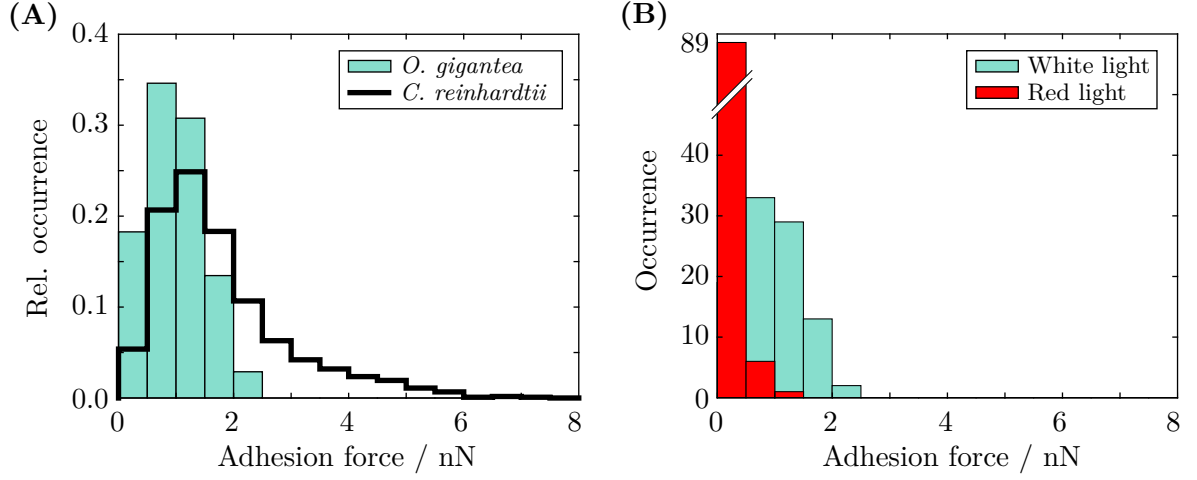


**Figure 8.3.: Force spectroscopy of *Oogamochlamys gigantea* cells in white and red light.** (A) Distribution of adhesion forces for *Oogamochlamys gigantea* (SAG 44.91) cells on a silicon substrate in white light ( $N = 28$  cells). The black solid line represents the functional form of the adhesion force distribution of vegetative *Chlamydomonas reinhardtii* cells shown in Figure 5.3 with a different binning. (B) Distribution of adhesion forces for *Oogamochlamys gigantea* cells in white light and red light ( $N = 25$  cells).

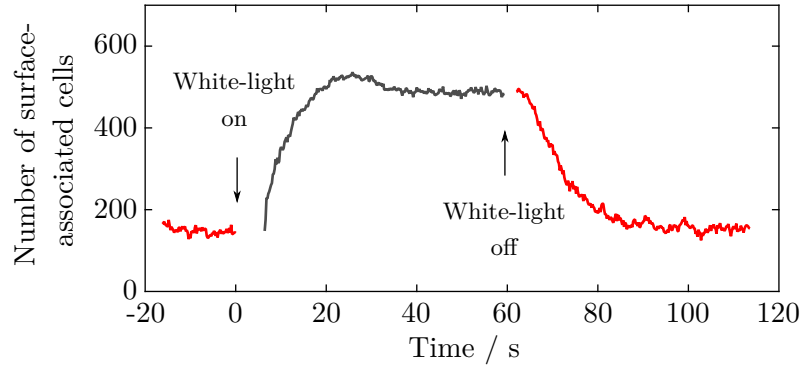


**Figure 8.4.: Surface colonization of *Oogamochlamys gigantea* controlled by light.** Adsorption and desorption of a population of *Oogamochlamys gigantea* cells from bulk solution to glass slides (see section 3.5). The gaps in the kinetics are times of overexposure and underexposure after removing and adding a red filter, respectively, which inhibit any visualization of the cells on the substrate at these time. The offset in red light represents cells that did not move, for example, as they were deflagellated.

in red and white light) to silicon substrates were in a range of 0.561 to 1.36 nN (25th/75th percentile, median: 0.963 nN, mean: 0.986 nN) in white light (see Figure 8.3A)<sup>60</sup>. The adhesion forces in white light appeared to be smaller than the forces recorded for *Chlamydomonas reinhardtii*. In red light, the same *Oogamochlamys gigantea* cells that adhered in white light exhibited significantly reduced adhesion. 77.1 % of all force-distance curves did not exhibit any detectable adhesion in red light (see Figure 8.3B), whereas 100 % of the force-distance curves of the same cells exhibited an significant adhesion peak in white light.

Adsorption experiments yielded the same outcome as for *Chlamydomonas reinhardtii*: *Oogamochlamys gigantea* cells started to attach to a glass slide after switching to white illumination and detached again in red light (see Figure 8.4, cf. section 6.2). The onset of the adsorption and desorption was approximately 5 seconds after the illumination was switched, which was marginally faster than in a comparable experiment with *Chlamydomonas reinhardtii*. After the initial surface attachment, a few cells appeared to detach again in white light conditions, as indicated by a small decrease in the number of surface-associated cells after approximately 25 s. This detachment was supported by the optical micrographs, in which more cells appeared to be motile again. The timescale of the onset of the detachment is too long to be attributed to a photophobic shock response that lasts less than hundreds of milliseconds (as seen in *Chlamydomonas reinhardtii*). In stead, it might be related to a phenomenon similar to the switching from positive to negative phototaxis at high light intensities in *Chlamydomonas reinhardtii* [Hegemann and Berthold, 2009].

In summary, force spectroscopy experiments with *Oogamochlamys gigantea* yielded smaller adhesion forces to silicon substrates compared to *Chlamydomonas reinhardtii*. As for the two *Chlamydomonas* species, *Oogamochlamys gigantea* adhesion to surfaces can be switched on and off by light. The surface-association of a population of cells could be triggered and terminated by switching the illumination condition. In conclusion, the light-switchable adhesion is not only limited to the genus *Chlamydomonas*, but was also found in a species of a different genus.

---

<sup>60</sup>The experiments with *Oogamochlamys gigantea* were initiated by me and tested by Christine Linne and me. Most of the data were collected by Alice Gagnier (ESPCI, Paris, France), during her time as a summer student, tutored by Christian Titus Kreis [Grangier, 2017; Linne, 2017].

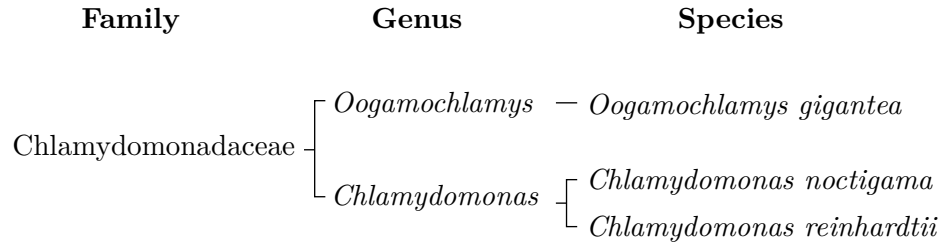


**Figure 8.5.: Taxonomic classification of the different species.** The relationship of the studied species are shown, for reasons of clarity other species of the genera and family are omitted. All studied species belong to the family Chlamydomonadaceae but to two different genera. As a comparison: the brown bear (*Ursus arctos*) and polar bear (*Ursus maritimus*) belong to the same genus *Ursus*, and the giant panda (*Ailuropoda melanoleuca*) belongs to the same family as the brown bear and polar bear, but to a different genus. The next higher taxonomic rank (suborder), includes weasels, wolves, seals, etc.

## 8.4. Summary and Outlook

I employed force spectroscopy to study the adhesion of other species of freshwater, soil-dwelling microalgae. The taxonomic classification of the different species is shown in Figure 8.5. These experiments yielded three results:

1. Vegetative and gametic cells of the species *Chlamydomonas reinhardtii* exhibited light-switchable adhesion.
2. The adhesion to substrates of cells from the species *Chlamydomonas noctigama* (same genus as *Chlamydomonas reinhardtii*) can be switched on and off by tailoring light conditions.
3. Cells of the species *Oogamochlamys gigantea* (same family as *Chlamydomonas reinhardtii*, but different genus) exhibited light-switchable adhesion to substrates.

In summary, light-switchable adhesion appears to be a more general trait of soil-dwelling microalgae in the family Chlamydomonadaceae.

In the context of light-switchable adhesion, actively controlled protein relocation in the flagellar membrane seems to play an important role, as suggested by the proteolysis experiments and preliminary lidocaine experiments (see section 6.4 and 6.5). These experiments suggest that the relocation of the adhesion-mediating protein in different light conditions is connected to the intraflagellar transport machinery that drives flagellar membrane turnover, gliding, and the translocation of microbeads along the flagellar membrane. A protein motility similar to *Chlamydomonas* can be presumably found in many other algae, as indicated by their ability to glide on substrates and translocate microbeads along the flagella [Bloodgood,

2009]. The occurrence of these motility phenomena linked to the flagellar membrane beyond *Chlamydomonas* suggests that a protein relocalization mechanism, which would be necessary for light-switchable flagellar adhesiveness, can be found in other microalgae beyond the microalgal family Chlamydomonadaceae. Moreover, the ability to glide on substrates and translocate microbeads highlights the relevance of flagella-mediated adhesion for microalgae.

On a more general perspective, the adhesion of algal zoospores and the influence of light on their surface-association might play a significant role in the dispersal of algae to locations that provide optimal light-conditions for survival and proliferation. Future work should expand on light-switchable adhesion and its evolutionary purpose by studying other microalgae from different families, orders, etc. A good starting point appear to be soil-dwelling microalgae that feature an active protein motility in their flagella, as indicated by flagellar membrane turnover and gliding.

## 9. Summary and Outlook

The main objective of this work was to reveal the biological mechanisms that trigger microalgal adhesion to surfaces and the surface forces that mediate the adhesion. Therefore, I developed and validated experimental routines and protocols for performing micropipette-based single-cell force spectroscopy experiments. Subsequently, *in vivo* force spectroscopy was employed to quantify microalgal adhesion forces in different environmental conditions and on different model substrates with tailored intermolecular interactions with *Chlamydomonas* flagella. These experiments yielded five main results:

1. The adhesion of *Chlamydomonas* is exclusively mediated by the flagella. The flagella establish the natural gliding configuration when in contact with a substrate during the force spectroscopy experiments.
2. The adhesion forces of *Chlamydomonas* are log-normally distributed with typical adhesion forces in the range of a few nanonewtons. The cell-to-cell variability in the adhesion force is most likely due to a cell-to-cell variability in the density of the adhesion-mediating protein in the flagellar membrane. For an individual cell, the variations in the adhesion forces in consecutive force-distance curves are presumably due to variations in the contact area between the flagella and the substrate. Moreover, multiple localized adhesive contacts between the flagella and the substrate may lead to characteristic signatures in the force-distance curves.
3. The adhesion of *Chlamydomonas* microalgae to surfaces can be reversibly switched on and off by exposing the algae to different light conditions. Thereby, the flagellar adhesiveness is actively switched on and off on a timescale of a few seconds. Adhesion is triggered by a blue-light photoreceptor when a sharp irradiance threshold is exceeded and the adhesion forces are independent of the light exposure above this threshold. The light-switchable adhesion appears to be based on a redistribution of the adhesion-mediating protein, which exclusively exposes the adhesion-mediating protein at the flagellar surface in blue/white illumination. The protein redistribution mechanism is presumably driven by the intraflagellar transport machinery. Auto-adhesion allows *Chlamydomonas* cells to establish adhesive contact to surfaces (and the gliding configuration) once a small part of one flagellum adhered to the surface. The auto-adhesion is an active process that is linked to intraflagellar transport.

4. *Chlamydomonas* features a universal adhesion mechanism that allows the alga to adhere to any kind of substrate with consistent adhesion forces. Model substrates with tailored intermolecular interactions with the adhesion-mediating protein on the surface of the *Chlamydomonas* flagella were employed to dissect the influence of hydrophobic interactions, van der Waals interactions, and electrostatic interactions on the adhesion forces. The force spectroscopy experiments indicate that electrostatic interactions mediate the adhesion.
5. The light-switchable adhesion seems to be a more generic trait of soil-dwelling microalgae. The flagellar adhesiveness is not only light-switchable for vegetative and gametic *Chlamydomonas* cells, but also for other representatives of the microalgal family Chlamydomonadaceae.

The adhesion forces found in this study are in line with forces reported earlier for microalgae and isolated flagella of *Chlamydomonas*. In contrast to these studies, the unique *in vivo* experiments presented in this work allow for identifying mechanisms that trigger flagella-mediated microalgal adhesion and for characterizing surface forces that mediate microalgal adhesion.

The adhesion forces of *Chlamydomonas* microalgae are on the same order of magnitude as the adhesion forces of bacteria. In contrast, microalgal adhesion features some remarkable differences compared to the well-studied bacterial adhesion strategies. Firstly, the characteristics of the flagellar membrane, which allow for gliding motility when in contact with a substrate, may lead to characteristic signatures in the rupture events in force-distance cycle. Secondly, microalgae inherit the ability to adapt their flagellar adhesiveness to optimal light conditions within seconds. Finally, microalgae appear to adhere to virtually all kinds of abiotic substrates with only marginally different adhesion forces. The light-switchable adhesion and the universal adhesion mechanism seem beneficial for photoactive organisms that seek to colonize surfaces that provide optimal growth-conditions. These adhesion strategies of soil-dwelling microalgae might have evolved as an evolutionary advantage for photosynthetic microbes that live in habitats with heterogeneous surfaces and variable light conditions.

The light-switchable adhesion appears to be linked to an actively controlled protein relocalization in the flagellar membrane that seems to be directly linked to intraflagellar transport. Translocation of microbeads along the flagella and gliding, which are driven by intraflagellar transport in *Chlamydomonas*, are also found in other microalgae and protists, such as *Peranema trichophorum* [Bloodgood, 1990b; Saito et al., 2003; Bloodgood, 2009]. Thus, these microalgae and protists might feature similar intraflagellar transport and protein relocalization mechanisms. These flagellar functionalities suggest the possibility that most microalgae (and other flagellated protists) might be able to adapt the adhesiveness of their flagellar membrane in different environmental conditions. Thereby, a direct coupling of the flagellar adhesiveness to the light exposure seems to be an enormous evolutionary advantage for photoactive organisms.



---

The evidence for the occurrence of light-switchable, flagella-mediated adhesion in species other than *Chlamydomonas* suggests an immediate relevance of this adhesion mechanism for microalgal life. As microalgae generally inherit a flagellated stadium (zoospore), flagella-mediated adhesion might also be of relevance for microalgae that do not have flagella during most of their life cycle. In this context, phototaxis of the zoospores could serve to locate areas with optimal sunlight exposure, while light-switchable adhesion presumably allows the zoospores to remain associated to surfaces in these locations. For these algae, surface-association in areas with optimal growth conditions might trigger the transition from the motile zoospore to the sessile mature organism. Hence, light-switchable adhesion would have an immediate effect on the survival and proliferation of algae, from permanently motile species to species, in which the mature organism is non-motile and macroscopic.

In the context of technological applications, light-switchable adhesion provides an easy tool to control microalgal adhesion and surface colonization in photobioreactors and research settings. In contrast, the finding that microalgal adhesion is substrate-unspecific implies that non-toxic surface coatings cannot prevent microalgal adhesion and biofouling in wet environments.

The fact that light-switchable and substrate-unspecific adhesion might have an enormous relevance for microalgal life and that both adhesion mechanisms have an immediate technological relevance raises the important question whether these adhesion mechanisms can be found in other microalgae. Experiments with different species of the family Chlamydomonadaceae substantiate the findings of light-switchable adhesion. The work should be expanded to other microalgae, starting with soil-dwelling species that feature gliding and flagellar surface motility. Future experiments on the universality of the adhesion mechanism should follow the same pathway, starting with the microalgae that were already successfully implemented in this work, *Chlamydomonas noctigama* and *Oogamochlamys gigantea*.

Regarding *Chlamydomonas reinhardtii*, future work should study the underlying mechanisms of the light-switchable and substrate unspecific adhesion. The photoreceptor that triggers light-switchable adhesion is not yet identified, as well as the signal pathway that ultimately switches the flagellar adhesiveness. The algae's ability to switch flagellar adhesiveness by a protein relocalization mechanism should be verified by further biomolecular tests, such as the lidocaine treatment, and direct visualizations of the protein relocalization. Follow-up work on the auto-adhesion kinetics could study cooperative force transduction of intraflagellar transport trains. In this context, the auto-adhesion and light-switchable adhesion might resolve the "mystery" of the function of gliding motility [Bloodgood, 2009]. Finally, the substrate-unspecific adhesion demands for further inquiries that include a structural analysis of the adhesion-mediating protein and its glycosylation.

In conclusion, the findings presented in this work may inspire research in many different directions and raise the interest from a broad audience. I anticipate that the discovery of light-switchable adhesion will stimulate the interest of molecular biologists to elucidate the underlying mechanisms and signal pathways, from the photoreceptor to the flagellar adhesiveness. The light-switchable adhesion might open new pathways to significantly enhance the yield of photo-bioreactors. Studying the generality of the findings of this study might be of particular interest for biologists working on behavior and evolution of microalgae and protists.

# **Appendices**



## A. Additional Material and Figures

### A.1. Auto-Correlation Analysis

The deflection of the micropipette cantilever was determined as described in section 3.1.1. In this method, the underlying correlation function is approximated by a nonparametric fit to the raw correlation data (*xcov*-function in MATLAB). I chose this approach for two reasons that should be shortly outlined in the following.

The functional form of the cantilever's intensity pattern (at the times that are compared with each other) determines the functional form of the underlying analytical auto-correlation function. However, the underlying functional form of the intensity pattern may vary during an experiment due to drift of the cantilever out of the focal plane of the microscope. Hence, the analytical auto-correlation function may vary in the same experiment and a universal functional form for the analytical auto-correlation function can not be determined. Moreover, the intensity pattern of each cantilever is unique. Thus, two different cantilever's feature a different form of the underlying analytical auto-correlation function in the auto-correlation analysis. Consequently, the optimal fit function would vary in between different experiments. Taken both arguments, the optimal fit function for the raw auto-correlation output appears to be the function that yields the best result in the sense that the analysis did not feature a systematic error.

Instead of using a nonparametric *spline*-function, another reasonable choice for the underlying continuous auto-correlation function appeared to be a Gaussian bell curve<sup>61</sup>. That is, the maximum of the raw correlation function would have been approximated by the maximum of the bell curve. To fit the raw correlation output, the MATLAB-code selected, for example, five data points on both sides of the maximum of the raw correlation analysis. These 11 data points (including the maximum) were fitted with a bell curve and the maximum of the bell curve determined the cantilever's deflection with a sub-pixel accuracy. This approach generally yielded good results, yet, the analysis featured an intrinsic systematic error that could be easily seen in some deflection analyses. In these cases, the data with sub-pixel resolution obtained

---

<sup>61</sup>This work was performed by Quentin Magdelaine (ESPCI, Paris, France), a summer student tutored by Christian Titus Kreis [Magdelaine, 2015].

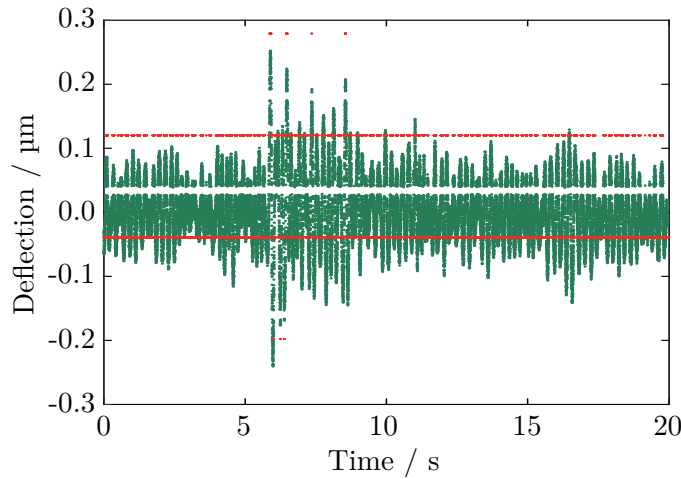


**Figure A.1.: Systematical error in the auto-correlation analysis using a Gaussian fit.** The deflection of a micropipette cantilever is shown as determined with the auto-correlation analysis. The red dots represent the maximum of the raw correlation output. The green dots represent the maximum of a Gaussian fit to the raw correlation output. The data obtained from the sub-pixel analysis exhibit a distinct gap of approximately  $0.05\ \mu\text{m}$  deflection (there are more gaps in the data points at approximately  $0.18\ \mu\text{m}$  and  $-0.16\ \mu\text{m}$ ). The data figure was kindly provided by Quentin Magdelaine [Magdelaine, 2015].

from the auto-correlation analysis exhibited a distinct gap (see Figure A.1). Each data point from the sub-pixel analysis was shifted towards the maximum of the raw correlation output. For data points that had the maximum in the raw correlation output at a different spatial location, for example, shifted by a single pixel, this shift ultimately led to the gap seen in the sub-pixel analysis. Ultimately, the gap indicates that the maximum of the fitted bell curve was shifted towards the maximum of the raw correlation function. This systematic error could not be completely resolved and using other fit functions, for example, a two-termed Gaussian fit ('gauss2' option in the *fit-function*) resulted in similar or other systematic errors. Thus, to avoid any bias the Gaussian bell curve was not used, even if a characteristic gap was not visible in the deflection output.

The nonparametric *spline*-fit did not show a systematic error, thus appeared to be the best choice. Moreover, any systematic error in the sub-pixel resolution can be neglected, as the recorded deflections are generally in the order of tens of pixels. The width of the gap can be used to estimate the error of the sub-pixel analysis, which appeared to be less than  $20\ \text{nm}$ , which corresponds to an error in the force of  $10\ \text{pN}$  at a typical spring constant of  $0.5\ \text{nN}/\mu\text{m}$ . Thus, the error is at least two orders of magnitudes lower than the typical adhesion forces reported in the study.

## A.2. Statistical Analysis of Data Sets

Statistical distributions of data points allow for a good characterization of a measured quantity and enable a good comparison between two sets of data points recorded in different experimental conditions (for example, adhesion forces to different substrates as in chapter 7). Any statement derived from the data set improves and becomes more informative, robust, and significant with increasing sample size. In statistical significance testing, the sample size directly affects the conclusions drawn from the significance test, as the same relation between data sets might lead to a rejection of the null hypothesis at larger sample sizes (see Equation 3.4). Consequently, a sample size as large as possible is desirable, but has to be balanced with the experimental effort.

In this study, the adhesion force of *Chlamydomonas* is characterized by the distribution of the mean adhesion forces, in the first place. Each mean adhesion force was calculated from ten individual force-distance curves (see chapter 7, for example)<sup>62</sup>, which could be potentially included in the analyses to increase the sample size. However, including ten force-distance curves of each cell in the analyses might affect the functional form and characteristics of the adhesion force distribution<sup>63</sup>. Thus, I compared the mean adhesion forces distribution to the adhesion force distribution that includes all individual force-distance curves.

The statistical distributions of the two different samples are shown in Figure A.2A+B. The statistical distribution of the mean adhesion forces yielded forces from 1.14 to 2.34 nN (25th/75th percentile, median of 1.57 nN, mean: 2.14 nN). The force distribution including all individual measurements exhibited the same mean force (per definition of the mean) and forces from 1.02 to 2.50 nN (25th/75th percentile, median: 1.55 nN). The empirical cumulative distribution functions (ECDF) of both distributions showed a good agreement (see Figure A.2C). A Kolmogorov-Smirnov test did not yield a significant difference ( $m = 1140, n = 114$ , see Equation 3.4). Thus, the functional form of the mean adhesion force distribution can be approximated by the distribution given by all individual cells. Therefore, I included all individual measurements in the analyses to improve the robustness of the drawn conclusions.

The marginal difference at small forces, i.e. small mean adhesion forces were measured with a lower probability than small forces in individual measurements, might be due to the selection procedure of the cells (see page 46). I expect that cells with a lower mean adhesion force (due to a lower protein density in the flagellar membrane) have a higher probability to scatter off from the substrate at contact interaction instead of getting attached. Moreover, I expect cells

---

<sup>62</sup>In some experiments, solely two or five force-distance curves were recorded, yet the argumentation remains the same.

<sup>63</sup>As an example that the distributions can be different: If the individual adhesion forces of all cells would be drawn from the same underlying distribution, then the mean adhesion force distribution would follow a normal distribution (central limit theorem).

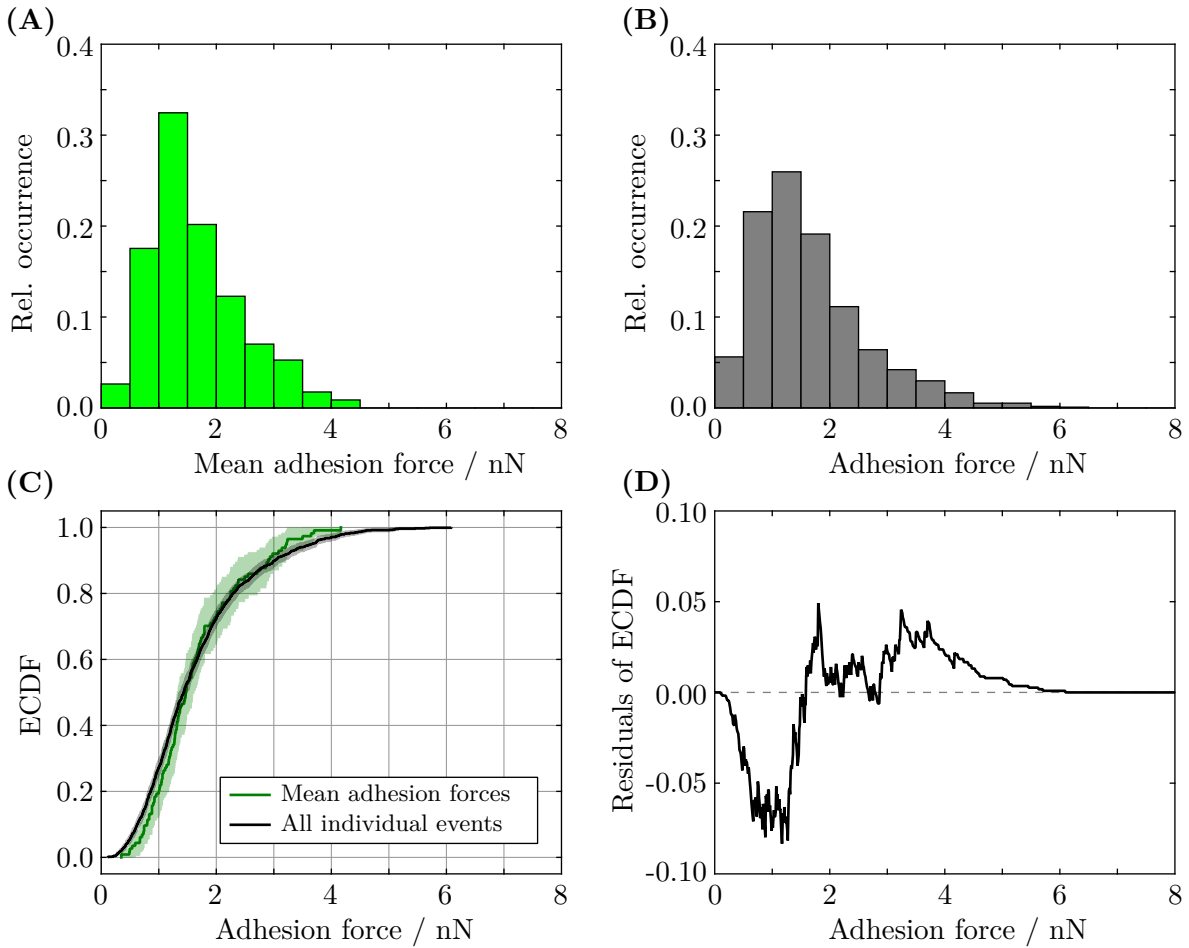


**Figure A.2.: Comparison between the statistical distribution of the mean adhesion forces and all individual events for the trimmed data set.** The force distributions of 114 vegetative *Chlamydomonas* cells are shown. **(A)** Statistical distribution of the mean adhesion forces. **(B)** Statistical distribution of all adhesion forces (each cell contributes ten individual measurements). This distribution is also shown in Figure 5.3 with a different binning. **(C)** Empirical cumulative distribution functions (ECDF) of both data sets. The shaded area represents the 95 % confidence interval. **(D)** Difference between the ECDF of both data sets.



that feature a lower flagellar adhesiveness to detach more frequently when associated with the substrate. It is well established that *Chlamydomonas* can briefly lift its flagella off the substrate during gliding [Bloodgood, 1990b, page 94], which might also lead to detachment from the substrate. The frequency of these events might be correlated with the flagellar adhesiveness, such that a cell that exhibit an extremely low flagellar adhesiveness would detach more often. Both effects combined would explain the marginal lower probability to find a cell with a small mean adhesion force, as seen in the empirical cumulative distribution function. In that case, the distribution that includes all individual forces measurements might represent the “true” adhesion force statistic of a population of *Chlamydomonas* cells better than the mean adhesion force statistics.

### A.3. Additional Material and Figures

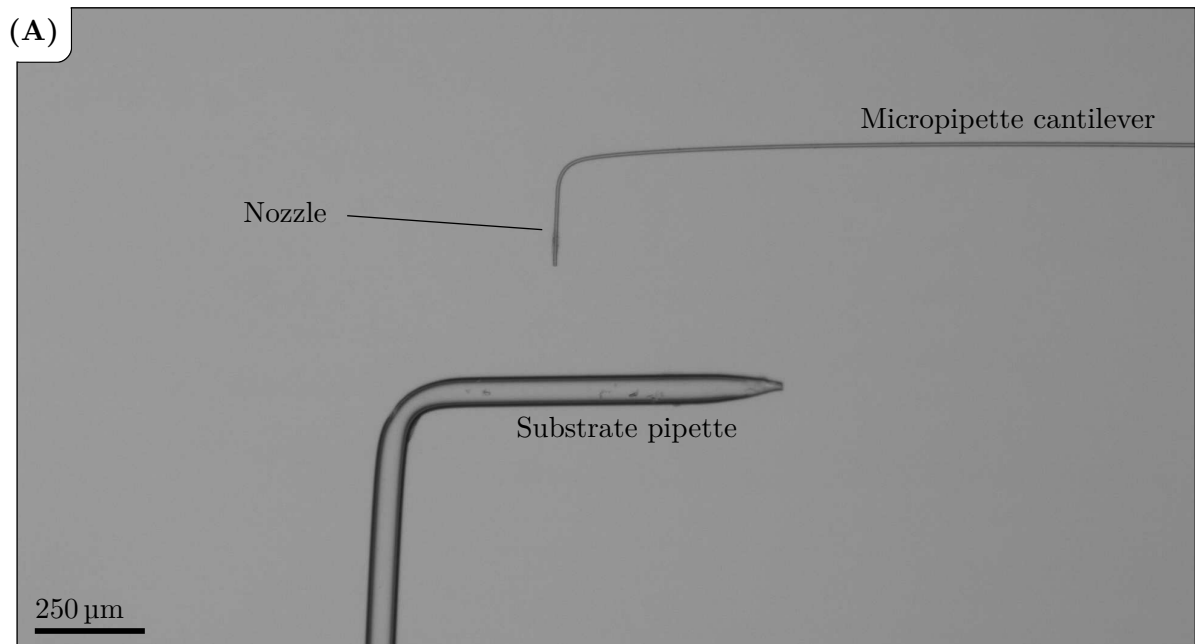


**Figure A.3.: Experimental geometry to visualize the flagella in close proximity to the substrate.** The flagella could not be visualized in the standard substrate geometry (see section 3.3). In all experiments that visualize the flagella (e.g. Figure 4.4 and Figure 6.7) a second micropipette was used as a substrate. The substrate micropipette was bent once as depicted in the figure.

Magnification	IX-73	1 pixel $\hat{=}$ $x$ $\mu\text{m}$	IX-83	1 pixel $\hat{=}$ $x$ $\mu\text{m}$
long-range objectives				
4x	UPlanFL N 4x/0.13 PhL $\infty$ /-/FN26.5	1.37	UPlanFL N 4x/0.13 $\infty$ /-/FN26.5	1.36 (-)
10x	UPlanFL N 10x/0.30 Ph1 $\infty$ /-/FN26.5	0.550	UPlanFL N 10x/0.30 $\infty$ /-/FN26.5	0.549 (-)
20x	LUCPlanFL N 20x/0.45 Ph1 $\infty$ /0-2/FN22	0.274	LUCPlanFL N 20x/0.45 $\infty$ /0-2/FN22	0.278(0.325)
40x	LUCPlanFL N 40x/0.6 $\infty$ /0-2/FN22	0.137	LUCPlanFL N 40x/0.6 $\infty$ /0-2/FN22	0.135(0.161)
60x	—	—	LUCPlanFL N 60x/0.7 $\infty$ /0.1-1.3/FN22	0.0903(-)
oil-immersion objectives				
60x	UPlanFL N 60x/1.25 Oil Iris $\infty$ /0.17	0.0913	UPlanFL N 60x/1.25 Oil Iris $\infty$ /0.17	0.0917
100x	UPlanFL N 100x/1.30 Oil P $\infty$ /0.17/FN26.5	0.0543	UPlanFL N 100x/1.30 Oil P $\infty$ /0.17/FN26.5	0.0546

**Table A.1.: List of objectives.** The microscope condenser has a numerical aperture NA of 0.30 in both cases (IX-73/IX-83). The conversion factor is given for the Grasshopper camera, in case of the IX-83 the conversion factor for the pco.edge camera is given in parentheses (see page 38). The conversion factors are exclusively given for objective and camera combinations that have been employed during this study.

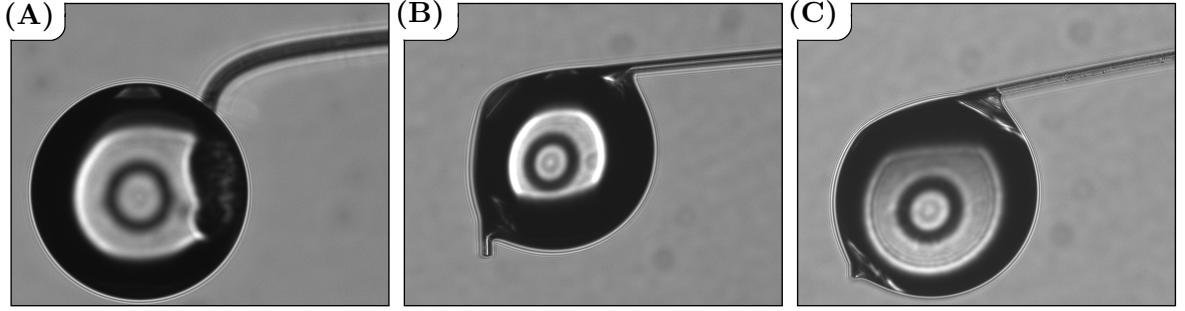


**Figure A.4.: Suboptimal droplet configurations during cantilever calibration.** The width of the micrographs is approximately 410  $\mu\text{m}$ . (A) Axial symmetric droplet pinned at the side of the micropipette's nozzle. (B)+(C) Droplet pinned in the kink between nozzle and cantilever leading to a non-axial symmetric droplet.

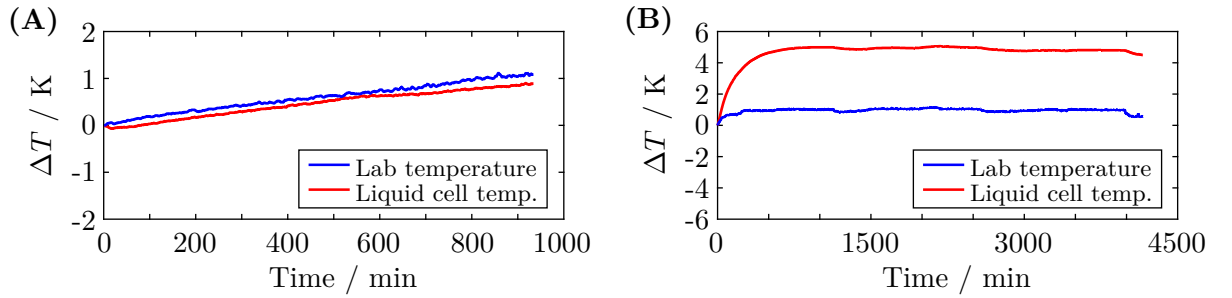


**Figure A.5.: Long-time temperature profile in the liquid cell.** The change in the temperature is shown in the lab (blue) and in the liquid cell (red) during an experiment (see Figure 3.8). (A) Box open. (B) Box closed.

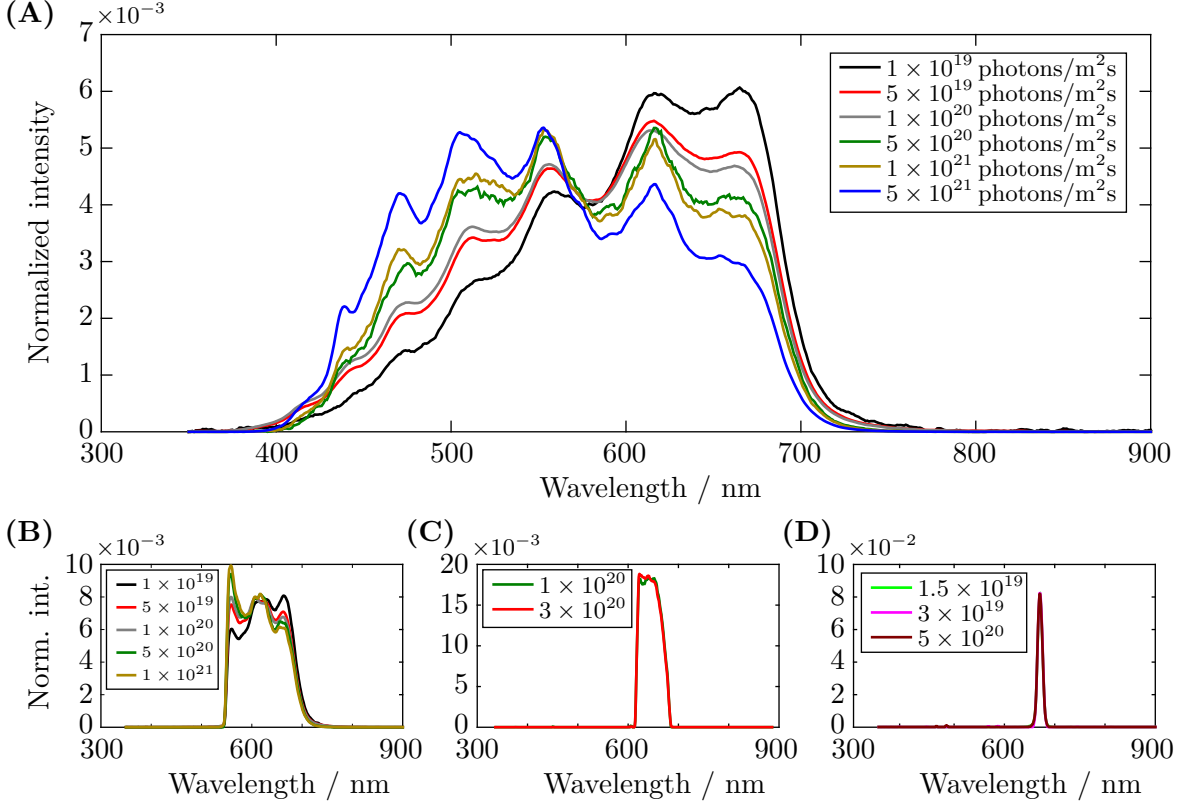


**Figure A.6.: Spectra of light conditions at the IX-73 microscope.** (A) Spectra of the halogen light bulb at different light intensities. (B) Spectra of the halogen light bulb with additional high-pass red filter ( $\lambda_{\text{cutoff}} = 550$  nm). (C) Spectra of the halogen light bulb with additional band-pass red filter 665/65 nm (see also section 3.4.4). (D) Spectra of the halogen light bulb with additional bandpass red filter 672/11 nm.

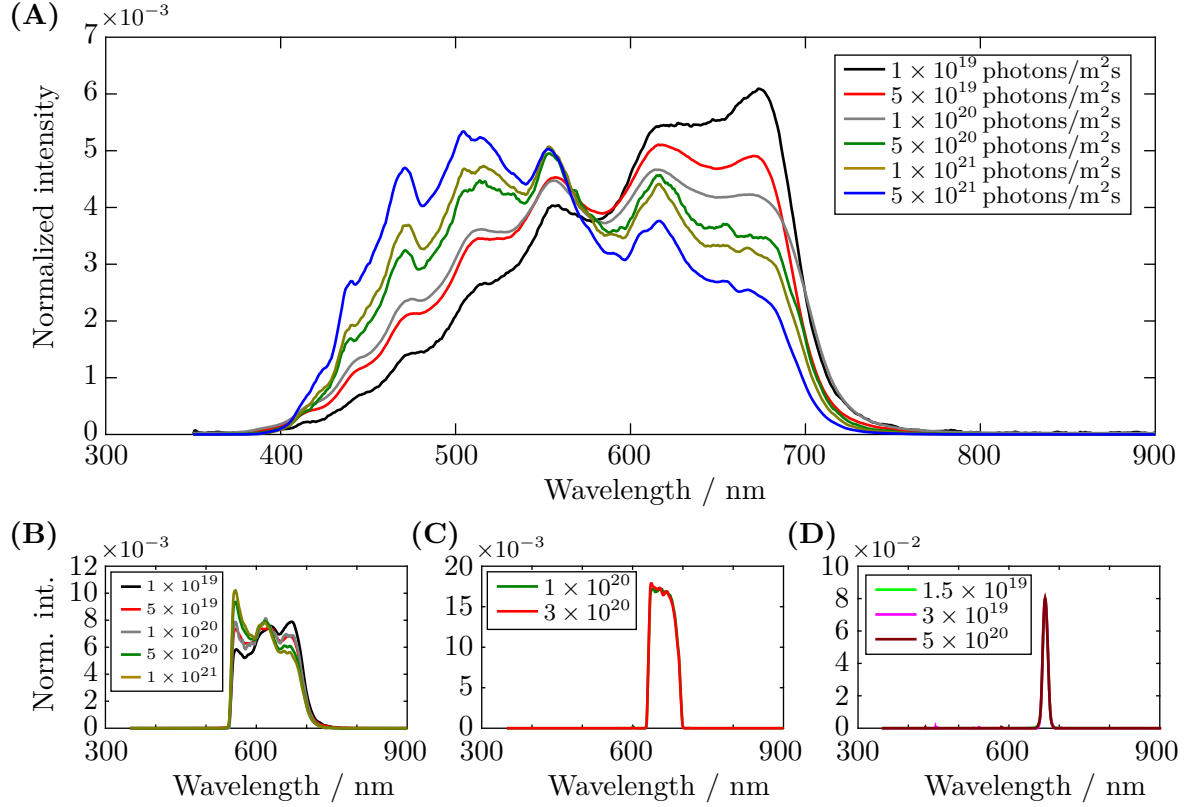


**Figure A.7.: Spectra of the light conditions at the IX-83 microscope.** (A) Spectra of the halogen light bulb at different light intensities. (B) Spectra of the halogen light bulb with additional high-pass red filter ( $\lambda_{\text{cutoff}} = 550$  nm). (C) Spectra of the halogen light bulb with additional band-pass red filter 665/65 nm (see also section 3.4.4). (D) Spectra of the halogen light bulb with additional bandpass red filter 672/11 nm.

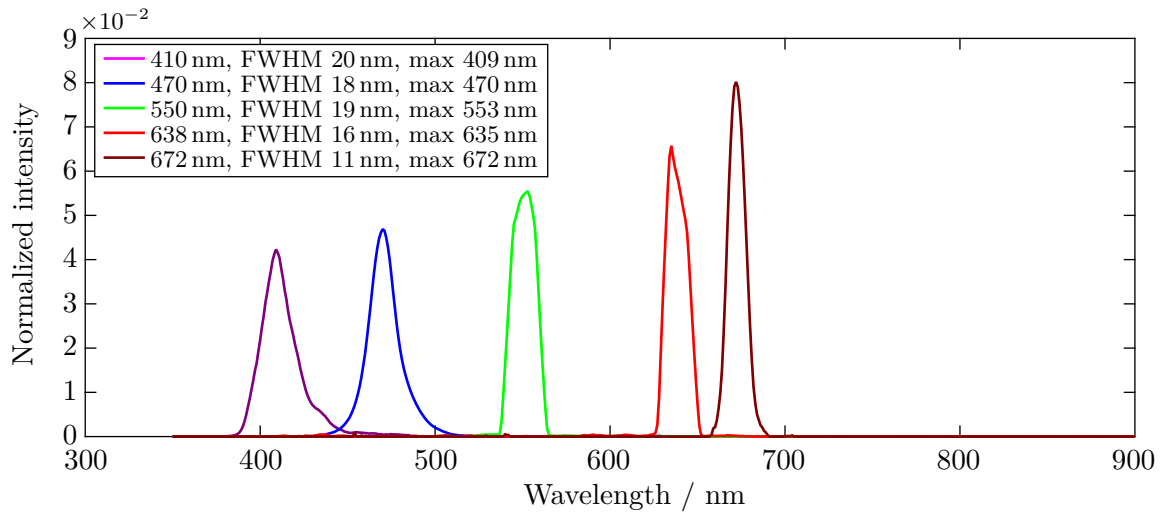


**Figure A.8.: Spectrum of different LED light conditions.** The spectra were recorded at a light intensity of  $3 \times 10^{19}$  photons/m<sup>2</sup>s. The wavelength denotes the center of the full width at half max (FWHM) interval, this does not necessarily correspond to the maximal emission wavelength. Additionally the wavelength of maximal intensity is given (max).

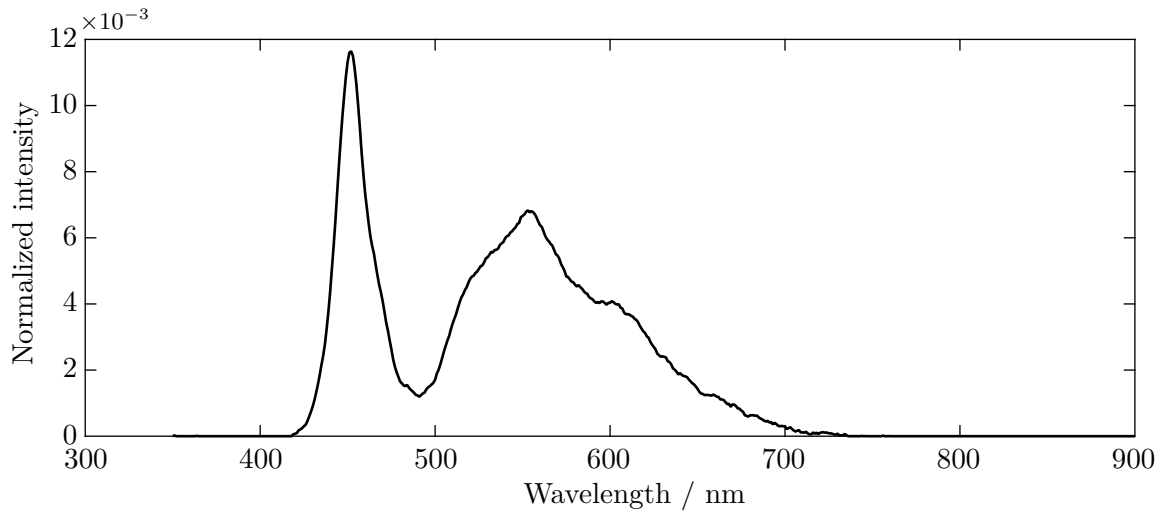


**Figure A.9.: Spectrum of the incubator's light source.** The spectrum was recorded in close proximity to the light source at a light intensity of approximately  $6 \times 10^{20}$  photons/m<sup>2</sup>s.

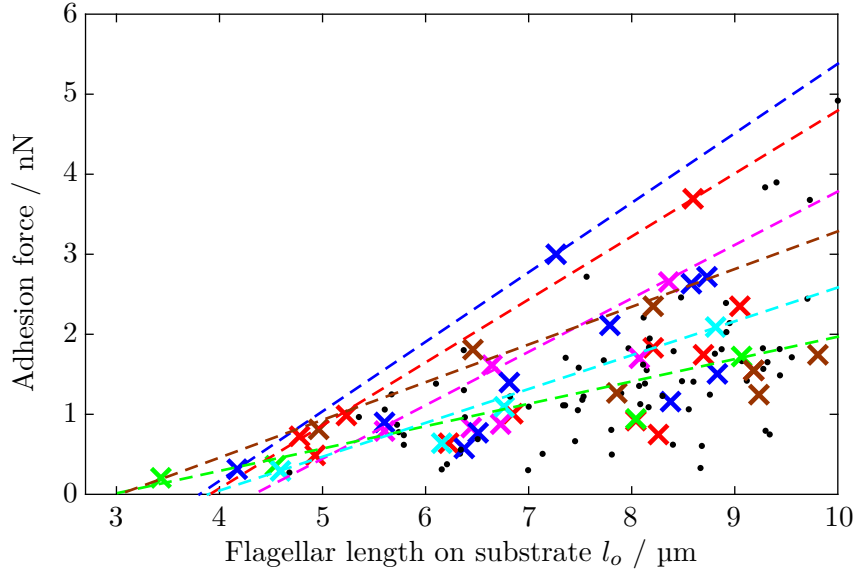


**Figure A.10.: Extended data: adhesion force as a function of the flagellar’s length on the substrate.** Individual force measurements at different flagellar length on the substrate ( $N = 28$  cells): different cells are represented by “crosses” in different colors, the dashed lines envelope all data points of the cell. The black dots represent cells that did not contribute enough data points to determine an enveloping straight line. The flagella length is determined from the cell-substrate distance by using Equation 5.2 and assuming a flagella length  $l_f$  of  $10\text{ }\mu\text{m}$ .

Cell	Slope [nN/ $\mu\text{m}$ ]	Force at $l_o = 10\text{ }\mu\text{m}$ [nN]
Blue	0.869	5.38
Red	0.787	4.80
Pink	0.668	3.78
Green	0.280	1.96
Teal	0.423	2.58
Brown	0.471	3.29

**Table A.2.: Analysis of the combined auto-adhesion and force/distance experiments.** The slopes of the envelopes in Figure A.10 and the extrapolated adhesion forces at full flagella length in contact with the substrate are given.

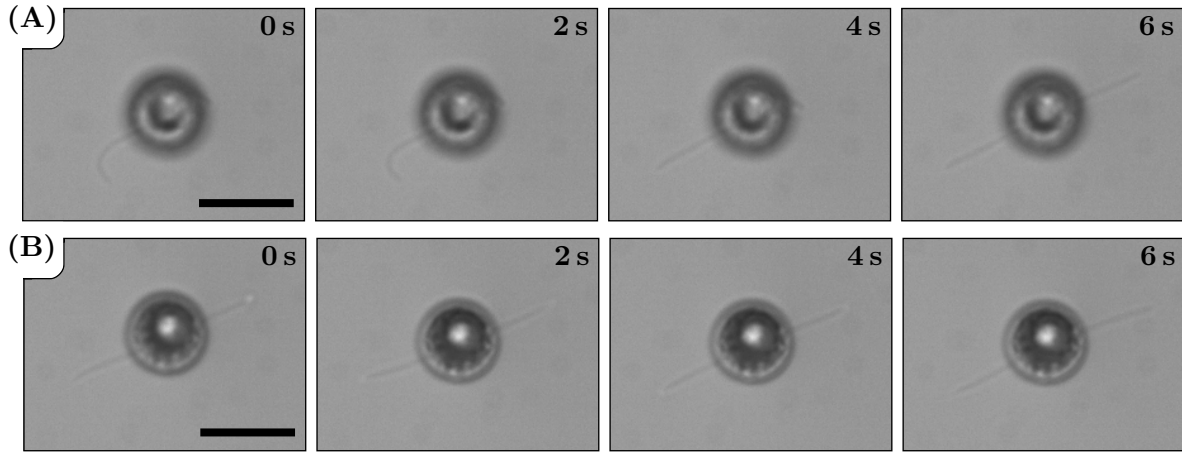


**Figure A.11.:** Visualizing the flagella configuration of *Chlamydomonas* on the substrate during force-distance experiments. See figure Figure 4.3 for guidelines to the eyes flagella and further comments. Scalebar 10  $\mu\text{m}$ .

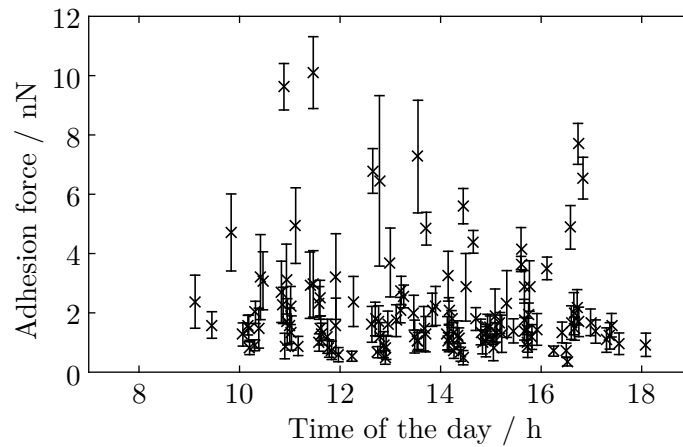


**Figure A.12.:** Extended data to single cell statistics in Figure 5.1. Mean adhesion forces of *Chlamydomonas* as a function of the time of the day ( $N = 127$  cells). The day cycle in the incubator (light on) lasts from 7 a.m. to 7 p.m. (see section 3.2).



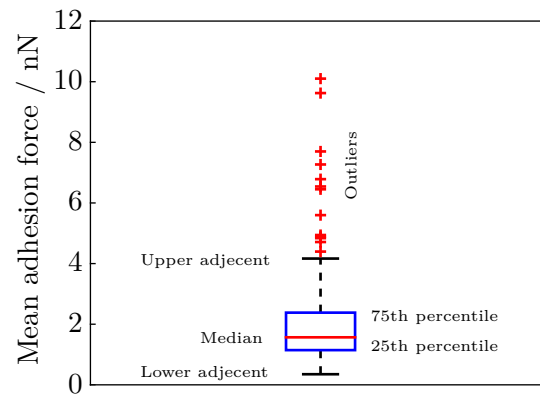


**Figure A.13.: Extended data to single cell statistics in Figure 5.1.** Box plot of mean adhesion forces indicating the outliers (red plus). See section 3.6.1 for further details.

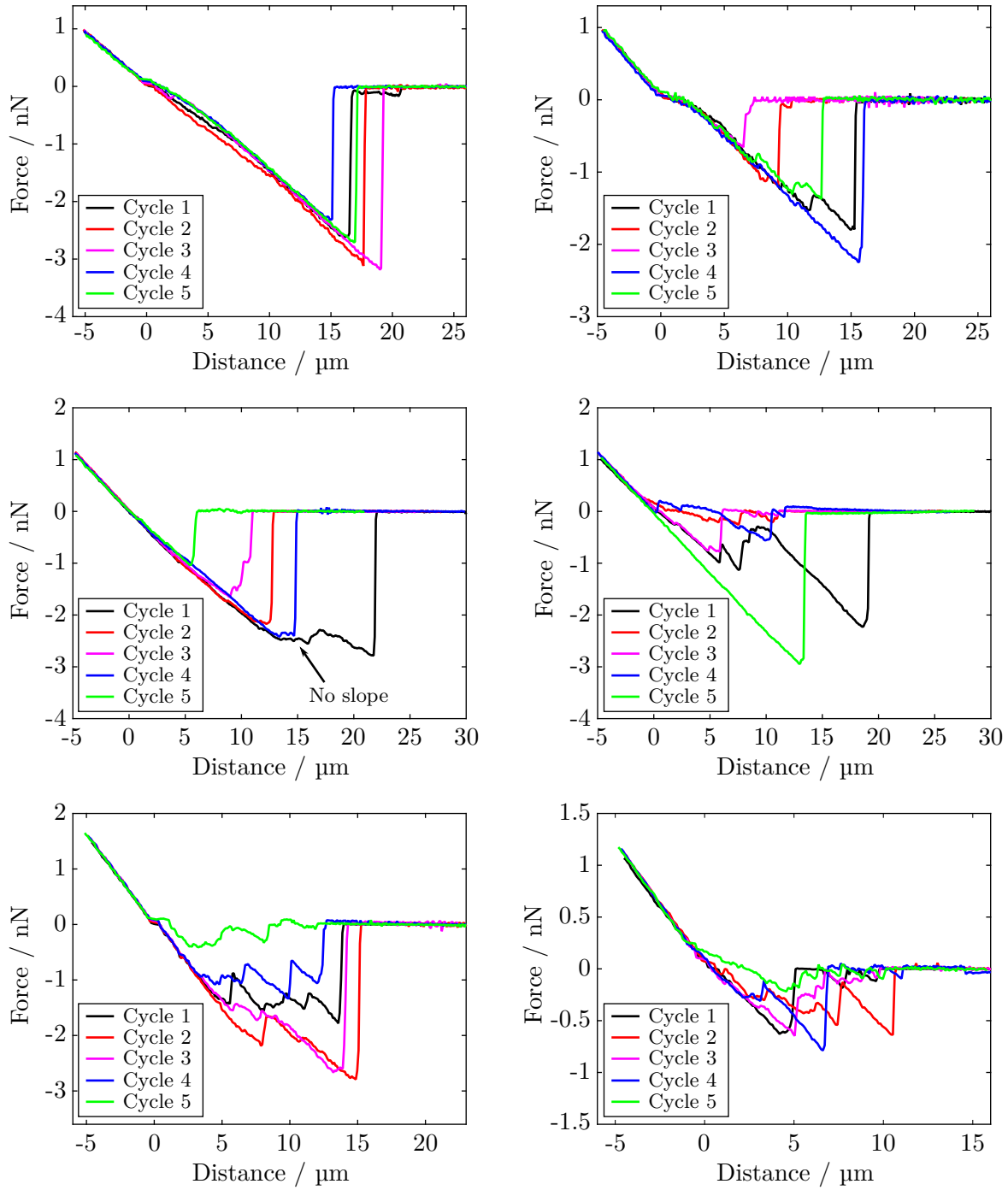


**Figure A.14.: Selection of force-distance curves.** Sets of five force-distance curves of six different cells recorded on silicon substrates in white light conditions. The individual force-distance curves show different signatures that explain the relative spread in the adhesion force of one cell (see Figure 5.1A+C). The origin of different signatures, like multiple rupture events, is discussed in section 5.2.

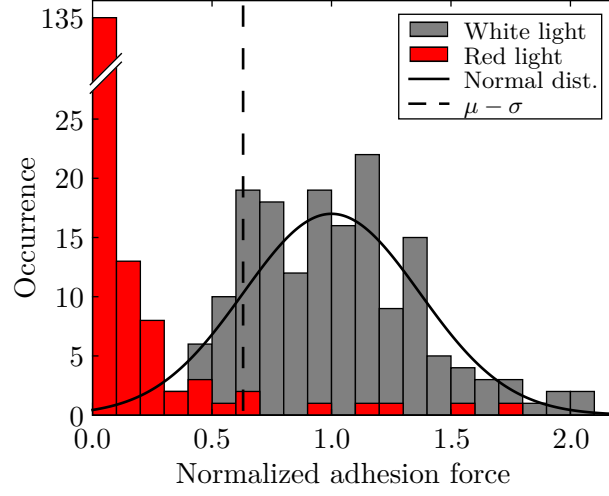


**Figure A.15.: Force spectroscopy of vegetative *Chlamydomonas* cells in white and red light.** Adhesion forces shown in Figure 6.1. The adhesion forces of each cell are normalized by the mean adhesion force of the cell in white light. The solid line represents a normal distribution with  $\mu = 1.00[6]$  and  $\sigma = 0.37[4]$ . The dashed line indicates forces that are one standard deviation smaller than the mean value.

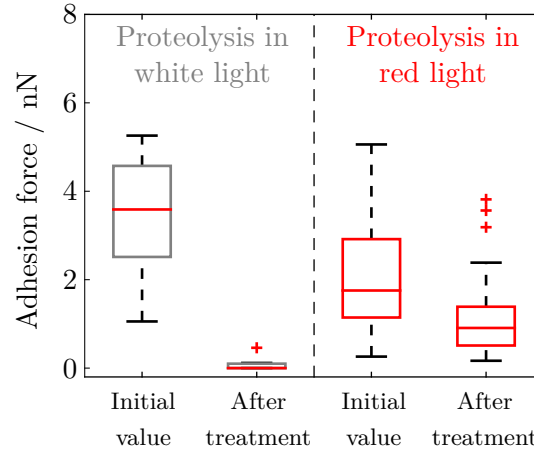


**Figure A.16.: Effect of proteolysis in different light conditions on the adhesiveness of *Chlamydomonas* flagella.** Comparison of the adhesion forces before and after a treatment (of 120 min) with pronase in different light conditions. While the adhesiveness is lost after proteolysis in white light (three cells shown in Figure 6.15A), cells still exhibit adhesiveness after proteolysis in red light ( $N = 8$  cells, each cell contributes five force-distance curves). Note that adhesion forces were measured in white light (in the case of red-light proteolysis approximately 5 min after turning on the white illumination).



## B. Further Work: Microalgae in Confined Geometries

### B.1. Mechanical Properties of *Volvox* Colonies: Deformation and Relaxation

*Volvox globator* (*Volvox*) colonies are freshwater green algae of hundreds of micrometers in diameter that can be found, for example, in ponds and lakes. An individual colony consists of ten thousands of *Chlamydomonas*-like cells that each have two flagella, a pyrenoid, a chloroplast, an eyespot, etc. The cells form a unicellular sheet filled by extracellular material that mostly consists of water [Kirk et al., 1986]. *Volvox* is widely studied to understand the transition from unicellular to multicellular life, as the colonies show coordinated behavior (flagella beating) and specialization of individual cells [Haas and Goldstein, 2015]. For example, the cells at the anterior of the colony are more sensitive to light than the cells at the posterior of the colony. At the beginning of the life cycle, the *Volvox* embryos consist of thousands of cells that form a spherical sheet like the mature colony. However, in contrast to the mature colony, the individual cells face inward and the flagella would be located at the interior of the organism [Haas and Goldstein, 2015]. Consequently, the cellular sheet needs to turn inside out so that the mature colony can swim. In this process, the mechanical properties of the colony play a crucial role.

I suspended *Volvox globator* colonies strain SAG 199.80 in +V growth medium (see Table 3.2). Subsequently, I attached a colony at the micropipette cantilever and pressed a substrate against the colony. The cantilever was deflected during this process and the restoring force of the cantilever deformed the *Volvox* colony (see Figure B.1B). From the optical micrographs, I measured the cantilever deflection, i.e. the force acting on the *Volvox* colony, and the deformation of the colony (see Figure B.1C+D). The cantilever deflection was correlated with the deformation to extract mechanical properties of the colony (see Figure B.2).

After the substrate motion was stopped, the colony relaxed and deformed further, as indicated by a decrease of the cantilever deflection (see Figure B.2A+B). The edge-detection analysis confirmed this behavior, yet yields a lower resolution (edge detection: pixel resolution at best, cantilever deflection: sub-pixel resolution). The colonies deformed less at higher

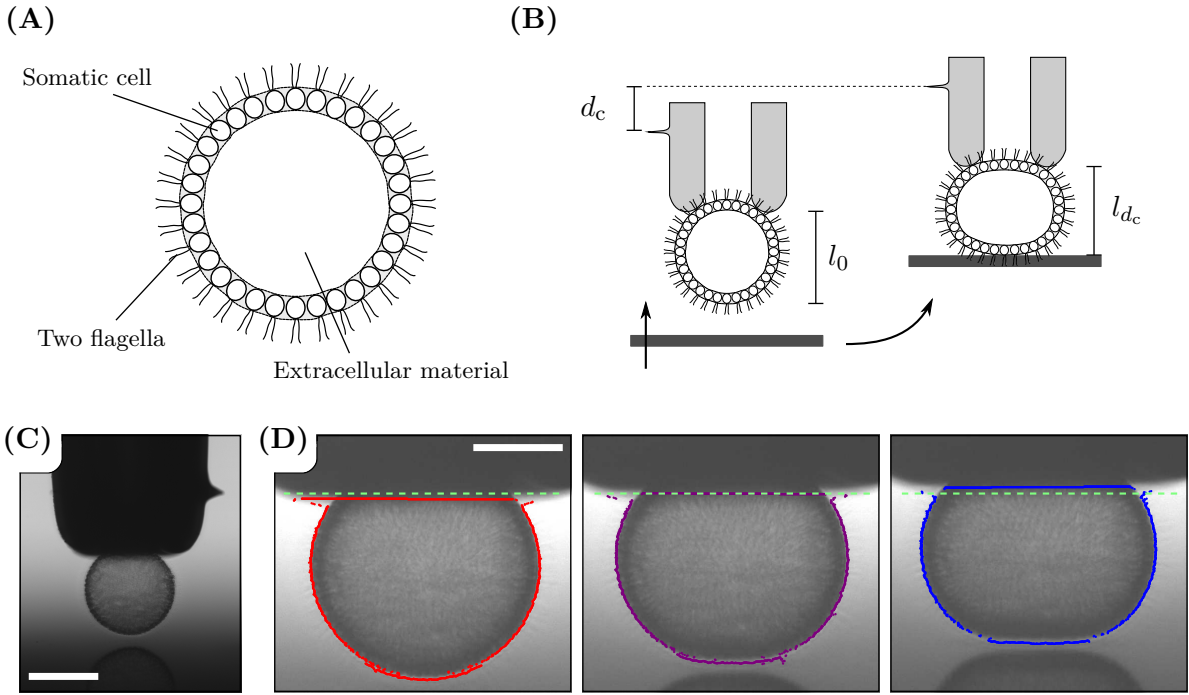


**Figure B.1.: Mechanical properties of *Volvox* colonies.** (A) Sketch of a *Volvox* colony: a cellular sheet consisting of ten thousands of somatic cells surrounding extracellular material. (B) A substrate is pressed against the *Volvox* colony and deflects the cantilever by a distance  $d_c$ . The restoring force of the cantilever deforms the colony from an initial diameter  $l_0$  to a final diameter  $l_{dc}$ . (C) Optical micrograph of the *Volvox* colony held at the nozzle of the cantilever. A spike at the nozzle (right-hand side) is employed to detect the deflection. Scale bar: 100  $\mu\text{m}$ . (D) Optical micrographs of a *Volvox* colony during the deformation experiment at different times. The dashed green line indicates the initial micropipette position. The solid line indicates the outline of the colony as detected by a custom MATLAB edge-detection code. Scale bar: 50  $\mu\text{m}$ .

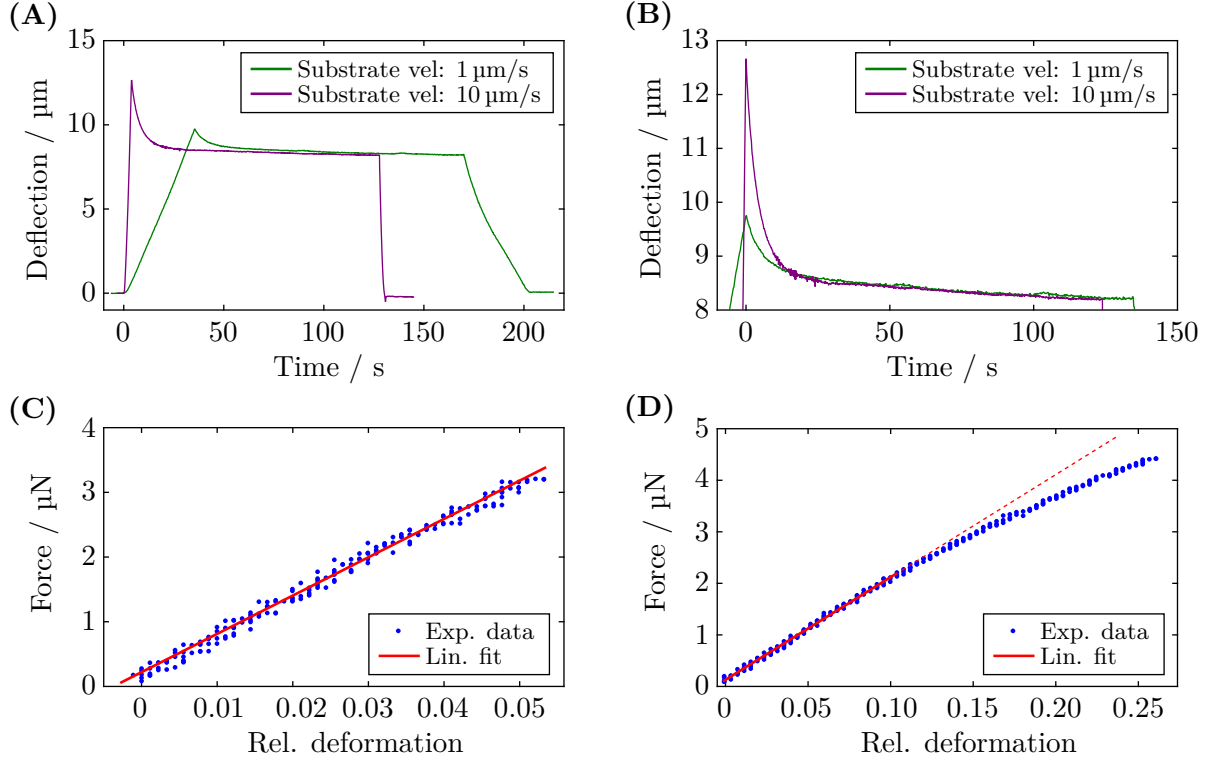


**Figure B.2.: Mechanical properties of *Volvox* colonies.** (A) Raw deflection data for a representative *Volvox* deformation experiment. The initial colony's diameter  $l_0$  was 109  $\mu\text{m}$ . At a high substrate velocity of 10  $\mu\text{m/s}$  the colony exhibits a diameter  $l_{dc}$  of 90  $\mu\text{m}$  after the substrate approach. Subsequently, the colony relaxes to a final diameter of 84  $\mu\text{m}$ . At a substrate velocity of 1  $\mu\text{m/s}$  the diameter before relaxation was  $l_{dc} = 87 \mu\text{m}$ , while the colony relaxed to the same final diameter of 84  $\mu\text{m}$ . The discrepancy to the raw deflection data (suggests relaxation by 4  $\mu\text{m}$  in case of the high substrate velocity) is due to the uncertainty in the edge detection code. The colony-substrate contact is established at  $t = 0$  s. (B) Relaxation of the same colony after two compression rates (section of the data in (A)). The substrate motion is stopped at  $t = 0$  s. The colonies relax to the same final shape. (C) Force-deformation relation of a colony with initial diameter of  $l_0$  of 251  $\mu\text{m}$ . The best fit to a linear slope yields  $k_{\text{Volvox}} = 59.3 \mu\text{N}/\mu\text{m}$ . (D) Force-deformation relation of a colony with initial diameter of  $l_0$  of 131  $\mu\text{m}$ . The colony shows a linear force-deformation relation with slope  $k_{\text{Volvox}} = 19.9 \mu\text{N}/\mu\text{m}$  up to approximately 10 % deformation. The dashed line indicates linear deformation.

ramp rates (higher substrate speed during the substrate approach cycle), which resulted in a larger deflection of the cantilever. Over the course of tens of seconds, the colony relaxed to the same final deformation independent of the deformation after the substrate approach. The rate-dependent deformation and subsequent relaxation process suggest that *Volvox* colonies are viscoelastic. Additionally, the raw deflection files indicate a rate-dependent adhesion, as an adhesion peak was exclusively observed at higher ramp rates (see Figure B.2A).

A correlation of the cantilever's restoring force with the deformation of the colony yielded a linear relation (see Figure B.2C). The proportionality constant of the correlation describes the spring constant of the organism, which was in the order of tens of micronewtons per micrometer. At large deformations, the colonies did not exhibit a linear force-deformation relation (see Figure B.2D).

In summary, micropipettes allows for probing objects and forces in systems of various size from individual *Chlamydomonas* cells up to *Volvox* colonies that are hundred times larger. This versatility can be used to study the visco-elastic behavior of *Volvox* colonies<sup>64</sup>. This work can be expanded to other organisms, cellular aggregates, or organs, as demonstrated earlier by [Backholm et al., 2013].

Future work should include a description of the organism by viscoelastic models (Maxwell model, Kelvin-Voigt model, etc.). Subsequently, *Volvox* species with structural differences in the interior of the colony, which is filled with extracellular material (for example, filaments) could be studied.

## B.2. Spectral Analysis of Micropipette Fluctuations: *Chlamydomonas* Propulsion

Many microorganisms inherit an active locomotion to explore their habitats and to locate areas of optimal growth conditions (see Figure 2.3). Their propulsion is often powered by flagella, which beat, in the case of *Chlamydomonas*, in a regular breaststroke waveform and propel the cell with 100 to 200  $\mu\text{m/s}$  forward. To understand the propulsion mechanism and the interactions of planktonic cells with surfaces, studying the forces generated by flagella is important.

The propulsion forces of *Chlamydomonas* were estimated from their swimming velocity and directly measured in optical tweezers experiments [Minoura and Kamiya, 1995; McCord et al., 2005]. The force generation of the flagella was estimated by resistive-force theory [Bayly et al., 2011]. Whereas these studies characterize the magnitude of the propulsion forces, they cannot quantify the interactions of swimming cells with surfaces. Micropipette cantilevers allow for

---

<sup>64</sup>The visco-elastic behaviour of *Volvox* was found and initially studied by Christian Titus Kreis. Further work on the viscoelastic properties of *Volvox* was performed by Marcin Michal Makowski (unpublished results).



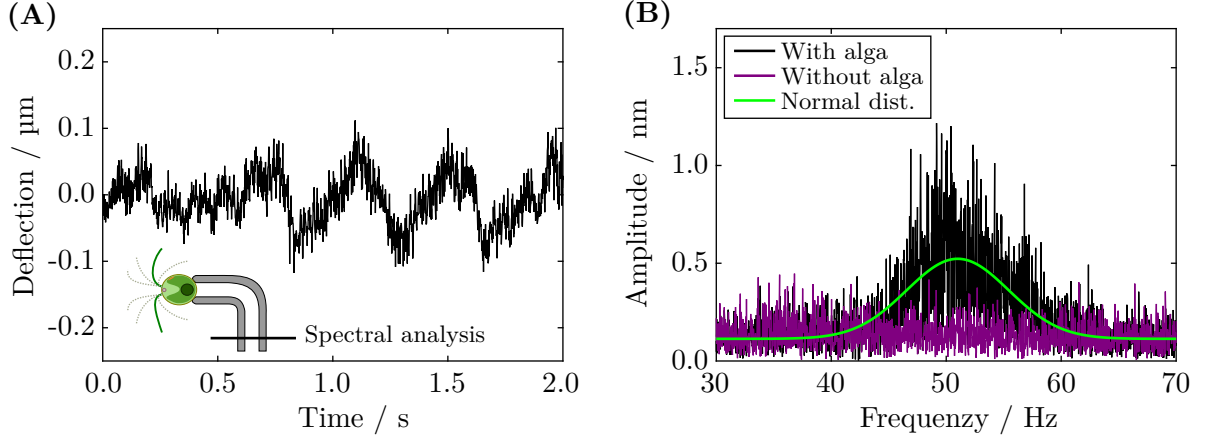


**Figure B.3.: *Chlamydomonas* propulsion force measurement.** (A) Raw deflection data of a micropipette cantilever with a *Chlamydomonas* cell attached to it (recorded at 800 frames per second). (B) Spectral analysis of the cantilever. Section of the spectrum of the same cantilever with a *Chlamydomonas* cell (black) and without a cell (purple) attached to the nozzle. The signature of the cell's propulsion force can be identified as a peak around 50 Hz. The solid green line represents a best fit of the cantilever's spectrum to a normal distribution.

dynamic force measurements that can be employed to tackle these open questions<sup>65</sup>.

To measure the propulsion forces of *Chlamydomonas*, I held a cell with a micropipette cantilever and analyzed the dynamic force response of the cantilever. The raw deflection signal of the cantilever did not show a signature of the force generation of a swimming *Chlamydomonas* cell (see Figure B.3A). In contrast, the spectrum of the cantilever's oscillation, as extracted by a fourier analysis, exhibited a distinct signature at the putative flagellar beating frequency of the cell (see Figure B.3B). This signature can be attributed to the swimming of the cell, as the same cantilever did not exhibit a signature at 50 Hz without a cell attached to it. Future work could quantify the influence of steric and hydrodynamic interactions on the spectrum by precisely varying the cell-substrate distance.

The propulsion force of the cell can be presumably extracted from the spectrum of the cantilever deflection. Therefore, the dynamic response of the cantilever to a periodic externally applied force needs to be calibrated (i.e. the linear response function of the driven harmonic oscillator), in addition to the cantilever's spring constant. In first tests, the linear response function of the cantilever was extracted from its step response in buffer solution, yet the error in consecutive measurements with this method (with the same cantilever) appeared to be huge. Moreover, it is not clear whether the linear response function of the cantilever follows the linear response function predicted by the damping constant and eigenfrequency determined with this

<sup>65</sup>The first steps in this project were performed by Quentin Magdelaine (ESPCI, Paris, France), a summer student tutored by Christian Titus Kreis [Magdelaine, 2015]

method. A more promising approach in further studies could be to measure the linear response function at the relevant frequencies directly, for example, by attaching a magnetic microbead to the cantilever, which oscillates in an external magnetic field.

### B.3. Drying Droplets of Microalgal Suspensions

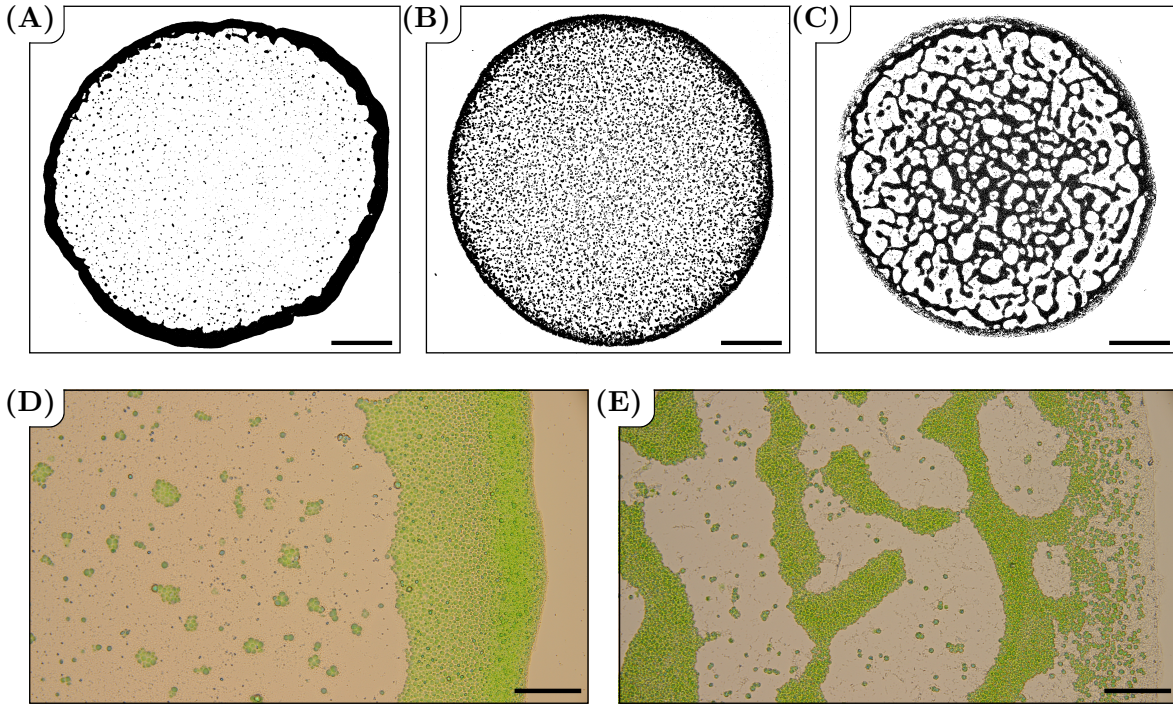


**Figure B.4.: Influence of microalgal activity on pattern formed by dried droplets.** Droplets of microalgal suspensions ( $c \approx 2 \cdot 10^7$  cells/ $\mu\text{l}$ ,  $V_{\text{droplet}} = 7$  ml) were kept in a closed container at high humidity ( $> 90\%$ ). The evaporation process took several hours. **(A)** Population of cells with a high motility: day cycle. The cells are deposited at the edge of the droplet in a distinct algae-ring. Scale bar: 1 mm. **(B)** Population of motile and non-motile cells: night cycle. A fraction of the cells are deposited at the edge of the droplet, while other cells are deposited uniformly in the droplet. Scale bar: 1 mm. **(C)** Population of non-motile cells: dead cells. The deposition pattern shows a web-like structure in the whole droplet. Scale bar: 1 mm. **(D)** Section of the ring-structure in (A). Scale bar: 100  $\mu\text{m}$ . **(E)** Section of the ring-structure in (C). Scale bar: 100  $\mu\text{m}$ .

Micro- or nano-particles suspended in a liquid droplet form microstructures when the droplet of the suspension is drying. This phenomenon can be seen in the everyday life, for example, in coffee, where the particles are deposited in a distinct coffee-ring at the edge of the droplet. The pattern formation in a droplet of coffee originates in an internal flow inside the droplet. This

flow transports the particles to the edge of the droplet where the particles are deposited. Many studies have focused on the pattern formation, the patterns left by dried droplets, and possibilities to manipulate the resultant particle deposition [Deegan et al., 1997; Hu and Larson, 2006]. Depending on the application (for example, electronics and surface coatings), a distinct pattern or a uniform deposition of particles is desired.

The patterns of drying droplets of suspensions were mostly studied for non-motile nanoparticles that are smaller than a single micrometer. In contrast to these studies, *Chlamydomonas* cells are motile and several times larger with a diameter of approximately 10  $\mu\text{m}$ . As the motility of *Chlamydomonas* might affect the flow field inside the droplet, it is not clear whether the patterns left by a suspension of *Chlamydomonas* are similar to the patterns from a coffee droplet, for example.

To study the pattern formation of drying droplets of *Chlamydomonas* suspensions, I placed droplets containing the algal solutions on glass slides. The glass slides were cleaned with ethanol and dried with a nitrogen gas stream. The droplets were kept in darkness during the whole experiment to avoid any light-directed motility of the cells. To identify whether the activity of the cells influences the resultant drying pattern, I performed experiments with populations of *Chlamydomonas* cells that featured a different fraction of motile cells. A sample of motile cells can be directly taken from the *Chlamydomonas* culture during the day cycle when all cells are motile. In a reference experiments, I killed cells of the exact same population with formaldehyde (CAS 50-00-0; Sigma-Aldrich, Germany) to generate a sample of non-motile cells. An experiment performed with the same population of cells during the night cycle represents an intermediate state: a part of the cells were still motile, whereas other cells were dividing and non-motile.

Optical micrographs of the dried droplets indicate that the activity of the cells influences the resultant patterns (see Figure B.4). In a dried droplet with predominantly active cells, I found most cells deposited at the edge of the droplet in a distinct algae ring (see Figure B.4A+D). In contrast, the non-motile cells appeared to be deposited in the whole droplet, where they accumulated to web-like structures (see Figure B.4C+E). The pattern from the experiment during the night cycle exhibited small agglomerations of cells in the whole droplet in addition to a subtle algae-ring (see Figure B.4B).

The algae-ring pattern that resembles the coffee-ring strongly suggests that there is an internal flow inside the droplet that transports the algae towards the edge of the droplet. Optical microscopy during the evaporation process supports an internal flow towards the edge of the droplet. As this internal flow is also found in case of the population of non-motile cells (as verified by optical microscopy), the difference in the patterns must have another origin.

In contrast to previous studies, sedimentation plays a major role in the algal suspensions, as the cells are at least one order of magnitude larger than commonly used particles. In fact, it can be derived from the alga's size and density that the sedimentation of the algae happens much faster than the droplet evaporates. Hence, the different patterns might be related to differences in the sedimentation in the different samples. In case of the motile *Chlamydomonas* cells, the active swimming motility prevents the sedimentation and the cells can be transported by the flow towards the edge of the droplet. The dead *Chlamydomonas* cells are non-active, thus the cells sink to the bottom of the droplet, where they remain fixed and unaffected by the flow. In the experiment during the night cycle, a part of the cells is swimming and transported by the flow towards the edge of the droplet, while the dividing cells are non-motile, and thus sink to the bottom of the droplet. The fraction of cells in the center region seems to affect the resultant pattern, in the sense that the web-like structures can only form if a sufficient amount of cells is deposited in the center.

The findings are substantiated by results from experiments with polystyrene microbeads of approximately 10  $\mu\text{m}$  size in pure water. The patterns of the microbeads resembled the patterns of the cells during the night cycle, while at higher volume fractions the agglomerations appeared to grow in size and became more elongated and connected. In experiments with density matched microbeads (by using heavy water,  $\text{D}_2\text{O}$ ), the resultant pattern looked similar to the algae-ring found for active cells.

In summary, the patterns left by dried droplets containing a *Chlamydomonas* suspension are influenced by the algae's activity. The motility of the cells appear to prevent sedimentation such that the internal flow inside the droplet may transport the cells towards the edge. For a suspension containing motile cells, the resultant pattern resembles the ring-like deposition pattern seen for micro- and nanoparticles.

# Bibliography

[Citing pages are listed after each reference.]

Abraham, S. N., Sun, D., Dale, J. B., and Beachey, E. H. (1988). Conservation of the D-mannose-adhesion protein among type 1 fimbriated members of the family Enterobacteriaceae. *Nature* **336**, 682–684 [Cited on pages 7 and 136.]

Adair, W., Hwang, C., and Goodenough, U. W. (1983). Identification and visualization of the sexual agglutinin from the mating-type plus flagellar membrane of *Chlamydomonas*. *Cell* **33**, 183–193 [Cited on pages 13, 14, and 79.]

Alberts, B., Johnson A., Lewis, J., Raff, M., Roberts, K., Walter, P., (2002). *Molecular Biology of the Cell*. Garland Science, New York [Cited on pages 12 and 13.]

Ochoa de Alda, J. A. G., Esteban, R., Diago, M. L., and Houmard, J. (2014). The plastid ancestor originated among one of the major cyanobacterial lineages. *Nat. Commun.* **5**, 4937 [Cited on page 5.]

Alsteens, D., Dupres, V., Evoy, K. M., Wildling, L., Gruber, H. J., and Dufrêne, Y. F. (2008). Structure, cell wall elasticity and polysaccharide properties of living yeast cells, as probed by AFM. *Nanotechnology* **19**, 384005 [Cited on page 137.]

Apetrei, A. and Sirghi, L. (2013). Stochastic adhesion of hydroxylated atomic force microscopy tips to supported lipid bilayers. *Langmuir* **29**, 16098–16104 [Cited on pages 69, 71, and 72.]

Arrigo, K. R. (2005). Marine microorganisms and global nutrient cycles. *Nature* **437**, 349–355 [Cited on pages 1 and 5.]

Autumn, K., Liang, Y. A., Hsieh, S. T., Zesch, W., Chan, W. P., Kenny, T. W., Fearing, R., and Full, R. J. (2000). Adhesive force of a single gecko foot-hair. *Nature* **205**, 681–685 [Cited on page 125.]

Autumn, K., Sitti, M., Liang, Y. A., Peattie, A. M., Hansen, W. R., Sponberg, S., Kenny, T. W., Fearing, R., Israelachvili, J. N., and Full, R. J. (2002). Evidence for van der Waals adhesion in gecko setae. *PNAS* **99**, 12252–12256 [Cited on page 125.]

- Backholm, M., Ryu, W. S., and Dalnoki-Veress, K. (2013). Viscoelastic properties of the nematode *Caenorhabditis elegans*, a self-similar, shear-thinning worm. *PNAS* **110**, 4528–4533 [Cited on pages 24 and 174.]
- Barthlott, W. and Neinhuis, C. (1997). Purity of the sacred lotus, or escape from contamination in biological surfaces. *Planta* **202**, 1–8 [Cited on page 125.]
- Bayly, P., Lewis, B., Ranz, E., Okamoto, R., Pless, R., and Dutcher, S. (2011). Propulsive forces on the flagellum during locomotion of *Chlamydomonas reinhardtii*. *Biophys. J.* **100**, 2716–2725 [Cited on page 174.]
- Beaussart, A., El-Kirat-Chatel, S., Sullan, R. M. A., Alsteens, D., Herman, P., Derclaye, S., and Dufrêne, Y. F. (2014). Quantifying the forces guiding microbial cell adhesion using single-cell force spectroscopy. *Nat. Protocols* **9**, 1049–1055 [Cited on page 136.]
- Beloin, C., Roux, A., and Ghigo, J. M., (2008). *Escherichia coli* Biofilms. *Curr. Top. Microbiol. Immunol.* **322**, 249–289 [Cited on pages 7 and 136.]
- Bergman, K., Goodenough, U. W., Goodenough, D. A., Jawitz, J., and Martin, H. (1975). Gametic differentiation in *Chlamydomonas reinhardtii*. II. flagellar membranes and the agglutination reaction. *J. Cell Biol.* **67**, 606–622 [Cited on page 14.]
- Bernstein, M. and Rosenbaum, J. L., (1993). Transport to the cell surface of *Chlamydomonas*: mastigonemes as a marker for the flagellar membrane. In: *Molecular Mechanisms of Membrane Traffic*, (Morré, D. J., Howell, K. E., Bergeron, J. J. M., Eds.), pp. 179–180. Springer, Berlin [Cited on page 14.]
- Berthold, P., Tsunoda, S. P., Ernst, O. P., Mages, W., Gradmann, D., and Hegemann, P. (2008). Channelrhodopsin-1 initiates phototaxis and photophobic responses in *Chlamydomonas* by immediate light-induced depolarization. *Plant Cell* **20**, 1665–1677 [Cited on pages 17, 25, 42, 100, 120, and 133.]
- Bidle, K. D. and Falkowski, P. G. (2004). Cell death in planktonic, photosynthetic microorganisms. *Nat. Rev. Micro.* **2**, 643–655 [Cited on pages 1 and 5.]
- Bloodgood, R. A. (1977). Motility occurring in association with the surface of the *Chlamydomonas* flagellum. *J. Cell Biol.* **75**, 983–989 [Cited on pages 14, 19, and 137.]
- Bloodgood, R. A. (1981). Flagella-dependent gliding motility in *Chlamydomonas*. *Protoplasma* **106**, 183–192 [Cited on pages 20, 67, and 112.]
- Bloodgood, R. A., (1987). Glycoprotein dynamics in the *Chlamydomonas* flagellar membrane. In: *Advances in Molecular and Cell Biology*, (Miller, K. R., Ed.), pp. 97–130. Elsevier, Amsterdam [Cited on page 137.]

- Bloodgood, R. A. (1988). Gliding motility and the dynamics of flagellar membrane glycoproteins in *Chlamydomonas reinhardtii*. *J. Protozool.* **35**, 552–558 [Cited on page 11.]
- Bloodgood, R. A., (1990a). *Ciliary and Flagellar Membranes*. (Bloodgood, R. A., Ed.), Springer US, Boston [Cited on pages 10 and 11.]
- Bloodgood, R. A., (1990b). Gliding Motility and Flagellar Glycoprotein Dynamics in *Chlamydomonas*. In: *Ciliary and Flagellar Membranes*, (Bloodgood, R. A., Ed.), pp. 91–128. Springer US, Boston [Cited on pages 12, 13, 18, 20, 67, 86, 91, 92, 114, 137, 139, 150, and 159.]
- Bloodgood, R. A., (2009). The *Chlamydomonas* flagellar membrane and its dynamic properties. In: *The Chlamydomonas Sourcebook (Second Edition)*, (Harris, E. H., Stern, D. B., and Witman, G. B., Eds.), pp. 309–368. Academic Press, London [Cited on pages 12, 14, 18, 20, 64, 65, 68, 71, 105, 107, 123, 147, 150, and 151.]
- Bloodgood, R. A. and May, G. S. (1982). Functional modification of the *Chlamydomonas* flagellar surface. *J. Cell Biol.* **93**, 88–96 [Cited on pages 12, 21, 115, and 116.]
- Bloodgood, R. A. and Salomonsky, N. L. (1994). The transmembrane signaling pathway involved in directed movements of *Chlamydomonas* flagellar membrane glycoproteins involves the dephosphorylation of a 60-kD phosphoprotein that binds to the major flagellar membrane glycoprotein. *J. Cell Biol.* **127**, 803–811 [Cited on page 20.]
- Bloodgood, R. A. and Salomonsky, N. L. (1998). Microsphere attachment induces glycoprotein redistribution and transmembrane signaling in the *Chlamydomonas* flagellum. *Protoplasma* **202**, 76–83 [Cited on page 20.]
- Bloodgood, R. A., Woodward, M. P., and Salomonsky, N. L. (1986). Redistribution and shedding of flagellar membrane glycoproteins visualized using an anti-carbohydrate monoclonal antibody and concanavalin A. *J. Cell Biol.* **102**, 1797–1812 [Cited on pages 12, 13, 18, 20, 21, 69, 92, and 137.]
- Bloodgood, R. A. and Workman, L. J. (1984). A flagellar surface glycoprotein mediating cell-substrate interaction in *Chlamydomonas*. *Cell Motil.* **4**, 77–87 [Cited on pages 14, 18, 79, and 137.]
- Bos, R., van der Mei, H. C., and Busscher, H. J. (1999). Physico-chemistry of initial microbial adhesive interactions – its mechanisms and methods for study. *FEMS Microbiol. Rev.* **23**, 179 [Cited on page 7.]
- Bouck, G. B. (1971). The structure, origin, isolation, and composition of the tubular mastigonemes of the *Ochromonas* flagellum. *J. Cell Biol.* **50**, 362–384 [Cited on page 14.]
- Bousse, L., Mostarshed, S., Shoot, B. V. D., de Rooij, N., Gimmel, P., and Göpel, W. (1991). Zeta potential measurements of Ta<sub>2</sub>O<sub>5</sub> and SiO<sub>2</sub> thin films. *J. Colloid Interface Sci.* **147**, 22–32 [Cited on pages 44 and 133.]

- Brokaw, C. J., Luck, D. J., and Huang, B. (1982). Analysis of the movement of *Chlamydomonas* flagella: the function of the radial-spoke system is revealed by comparison of wild-type and mutant flagella. *J. Cell Biol.* **92**, 722–732 [Cited on page 105.]
- Bruce, V. G. (1970). The biological clock in *Chlamydomonas reinhardi*. *J. Protozool.* **17**, 328–334 [Cited on page 18.]
- Busscher, H. J., Norde, W., and van der Mei, H. C. (2008). Specific molecular recognition and nonspecific contributions to bacterial interaction forces. *Appl. Environ. Microbiol.* **74**, 2559–2564 [Cited on page 7.]
- Callow, J. A. and Callow, M. E. (2011). Trends in the development of environmentally friendly fouling-resistant marine coatings. *Nat. Commun.* **2**, 244 [Cited on pages 2, 7, 8, and 125.]
- Callow, J. A., Crawford, S. A., Higgins, M. J., Mulvaney, P., and Wetherbee, R. (2000). The application of atomic force microscopy to topographical studies and force measurements on the secreted adhesive of the green alga *Enteromorpha*. *Planta* **211**, 641–647 [Cited on pages 8, 82, and 92.]
- Cavalier-Smith, T. (2000). Membrane heredity and early chloroplast evolution. *Trends Plant Sci.* **5**, 174–182 [Cited on page 5.]
- Cayley, D. S., Guttman, H. J., and Jr., M. T. R. (2000). Biophysical characterization of changes in amounts and activity of *Escherichia coli* cell and compartment water and turgor pressure in response to osmotic stress. *Biophys. J.* **78**, 1748–1764 [Cited on page 64.]
- Chacón-Lee, T. and González-Mariño, G. (2010). Microalgae for “healthy” foods – possibilities and challenges. *Compr. Rev. Food Sci. Food Saf.* **9**, 655–675 [Cited on pages 1 and 7.]
- Chambers, L., Stokes, K., Walsh, F., and Wood, R. (2006). Modern approaches to marine antifouling coatings. *Surf. Coat. Technol.* **201**, 3642–3652 [Cited on pages 2, 7, 8, and 125.]
- Chapman, D. L. (1913). Li. a contribution to the theory of electrocapillarity. *Philos. Mag.* **25**, 475–481 [Cited on page 26.]
- Colbert, M. J., Raegen, A. N., Fradin, C., and Dalnoki-Veress, K. (2009). Adhesion and membrane tension of single vesicles and living cells using a micropipette-based technique. *Eur. Phys. J. E* **30**, 117–121 [Cited on pages 24, 63, 69, and 73.]
- Deegan, R. D., Bakajin, O., Dupont, T. F., Huber, G., Nagel, S. R., and Witten, T. A. (2011). Capillary flow as the cause of ring stains from dried liquid drops. *Nature* **389**, 827–829 [Cited on page 177.]
- Deng, Y., Sun, M., and Shaevitz, J. W. (2011). Direct measurement of cell wall stress stiffening and turgor pressure in live bacterial cells. *Phys. Rev. Lett.* **107**, 158101 [Cited on page 64.]



- Deusch, O., Landan, G., Roettger, M., Gruenheit, N., Kowallik, K. V., Allen, J. F., Martin, W., and Dagan, T. (2008). Genes of cyanobacterial origin in plant nuclear genomes point to a heterocyst-forming plastid ancestor. *Mol. Biol. Evol.* **25**, 748–761 [Cited on page 5.]
- Donlan, R. M. (2001). Biofilm formation: A clinically relevant microbiological process. *Clin. Infect. Dis.* **33**, 1387–1392 [Cited on pages 1 and 7.]
- Drescher, K., Goldstein, R. E., Michel, N., Polin, M., and Tuval, I. (2010). Direct measurement of the flow field around swimming microorganisms. *Phys. Rev. Lett.* **105**, 168101 [Cited on pages 23 and 63.]
- Dufrêne, Y. F. (2015). Sticky microbes: forces in microbial cell adhesion. *Trends Microbiol.* **23**, 376–382 [Cited on page 7.]
- Dugdale, T. M., Dagastine, R., Chiovitti, A., Mulvaney, P., and Wetherbee, R. (2005). Single adhesive nanofibers from a live diatom have the signature fingerprint of modular proteins. *Biophys. J.* **89**, 4252–4260 [Cited on pages 8, 82, and 92.]
- Elowitz, M. B., Levine, A. J., Siggia, E. D., and Swain, P. S. (2002). Stochastic gene expression in a single cell. *Science* **297**, 1183–1186 [Cited on page 79.]
- Ettl, H., (1976). Die Gattung Chlamydomonas Ehrenberg. *Nova. Hedwig. Beih.* **47** [Cited on pages 9 and 20.]
- Ettl, H. and Gärtner, G., (2014). *Syllabus der Boden-, Luft- und Flechtenalgen*. Springer, Berlin [Cited on pages 143 and 144.]
- Evans, E. A. (1980). Analysis of adhesion of large vesicles to surfaces. *Biophys. J.* **31**, 425–432 [Cited on pages 22 and 24.]
- Evans, S., Leksono, T., and McKinnell, P. (1995). Tributyltin pollution: A diminishing problem following legislation limiting the use of tbt-based anti-fouling paints. *Mar. Pollut. Bull.* **30**, 14–21 [Cited on page 125.]
- Ferris, P. J., Waffenschmidt, S., Umen, J. G., Lin, H., Lee, J.-H., Ishida, K., Kubo, T., Lau, J., and Goodenough, U. W. (2005). Plus and minus sexual agglutinins from Chlamydomonas reinhardtii. *Plant Cell* **17**, 597–615 [Cited on page 14.]
- Field, C. B., Behrenfeld, M. J., Randerson, J. T., and Falkowski, P. (1998). Primary production of the biosphere: Integrating terrestrial and oceanic components. *Science* **281**, 237–240 [Cited on pages 1 and 5.]
- Finlay, B. and Esteban, G. (1998). Freshwater protozoa: biodiversity and ecological function. *Biodivers. Conserv.* **7**, 1163–1186 [Cited on pages 1 and 5.]

- Firestone, A. J., Weinger, J. S., Maldonado, M., Barlan, K., Langston, L. D., O'Donnell, M., Gelfand, V. I., Kapoor, T. M., and Chen, J. K. (2012). Small-molecule inhibitors of the AAA+ ATPase motor cytoplasmic dynein. *Nature* **484**, 125–129 [Cited on pages 72 and 113.]
- Flemming, H.-C. and Wingender, J. (2010). The biofilm matrix. *Nat. Rev. Micro.* **8**, 623–633 [Cited on pages 1, 7, and 8.]
- Flemming, H.-C., Wingender, J., Szewzyk, U., Steinberg, P., Rice, S. A., and Kjelleberg, S. (2016). Biofilms: an emergent form of bacterial life. *Nat. Rev. Micro.* **14**, 563–575. [Cited on pages 1 and 7.]
- Foster, K. W., Saranak, J., Patel, N., Zarilli, G., Okabe, M., Kline, T., and Nakanishi, K. (1984). A rhodopsin is the functional photoreceptor for phototaxis in the unicellular eukaryote *Chlamydomonas*. *Nature* **311**, 756–759 [Cited on pages 17 and 100.]
- Foster, K. W. and Smyth, R. D. (1980). Light antennas in phototactic algae. *Microbiol. Rev.* **44**, 572–630 [Cited on page 17.]
- Gates, R. S., Reitsma, M. G., Kramar, J. A., and Pratt, J. R. (2011). Atomic force microscope cantilever flexural stiffness calibration: Toward a standard traceable method. *J. Res. Natl. Inst. Stand. Technol.* **116**, 703–727 [Cited on page 35.]
- Gibson, C. T., Watson, G. S., and Myhra, S. (1996). Determination of the spring constants of probes for force microscopy/spectroscopy. *Nanotechnology* **7**, 259 [Cited on page 35.]
- Gittes, F., Mickey, B., Nettleton, J., and Howard, J. (1993). Flexural rigidity of microtubules and actin filaments measured from thermal fluctuations in shape. *J. Cell Biol.* **120**, 923–934 [Cited on page 90.]
- Goldstein, R. E. (2015). Green algae as model organisms for biological fluid dynamics. *Annu. Rev. Fluid Mech.* **47**, 343–375 [Cited on page 9.]
- Goodenough, U. W., Adair, W. S., Collin-Osdoby, P., and Heuser, J. E. (1985). Structure of the *Chlamydomonas* agglutinin and related flagellar surface proteins in vitro and in situ. *J. Cell Biol.* **101**, 924–941 [Cited on page 14.]
- Gouy, M. (1910). Sur la constitution de la charge électrique à la surface d'un électrolyte. *J. Phys. Theor. Appl.* **9**, 457–468 [Cited on page 26.]
- Grangier, A. (2017). Light-switchable adhesiveness as a generic trait for soil-dwelling microalgae. FOKOS e.V. Internship Report, Max Planck Institute for Dynamics and Self-Organization, Göttingen [Cited on pages 135, 143, and 146.]
- Guedes, A. C., Amaro, H. M., and Malcata, F. X. (2011). Microalgae as sources of carotenoids. *Mar. Drugs* **9**, 625–644 [Cited on pages 1 and 7.]

- Gurtovenko, A. A. and Anwar, J. (2007). Modulating the structure and properties of cell membranes: The molecular mechanism of action of dimethyl sulfoxide. *J. Phys. Chem. B* **111**, 10453–10460 [Cited on page 113.]
- Haas, P. A. and Goldstein, R. E. (2015). Elasticity and glocality: initiation of embryonic inversion in *Volvox*. *J. Royal Soc. Interface* **12**, 20150671 [Cited on page 171.]
- Hähl, H., Evers, F., Grandthyll, S., Paulus, M., Sternemann, C., Loskill, P., Lessel, M., Hüsecken, A. K., Brenner, T., Tolan, M., and Jacobs, K. (2012). Subsurface influence on the structure of protein adsorbates as revealed by in situ X-ray reflectivity. *Langmuir* **28**, 7747–7756 [Cited on page 131.]
- Hall-Stoodley, L., Costerton, J. W., and Stoodley, P. (2004). Bacterial biofilms: from the natural environment to infectious diseases. *Nat. Rev. Microbiol.* **2**, 95–108 [Cited on pages 1 and 7.]
- Hamed, I. (2016). The evolution and versatility of microalgal biotechnology: A review. *Compr. Rev. Food Sci. Food Saf.* **15**, 1104–1123 [Cited on pages 1 and 7.]
- Harris, E. H. (2001). *Chlamydomonas* as a model organism. *Annu. Rev. Plant Biol.* **52**, 363–406 [Cited on page 9.]
- Harris, E. H., (2009a). Cell architecture. In: *The Chlamydomonas Sourcebook (Second Edition)*, (Harris, E. H., Stern, D. B., and Witman, G. B., Eds.), pp. 25–64. Academic Press, London [Cited on page 9.]
- Harris, E. H., Stern, D. B., and Witman, G. B., (2009). *The Chlamydomonas Sourcebook (Second Edition)*. (Harris, E. H., Stern, D. B., and Witman, G. B., Eds.), Academic Press, London [Cited on pages 9, 10, 16, 41, 42, 65, and 100.]
- Harz, H. and Hegemann, P. (1991). Rhodopsin-regulated calcium currents in *Chlamydomonas*. *Nature* **351**, 489–491 [Cited on pages 17, 22, 23, 63, 101, and 102.]
- He, X., Wang, J., Abdoli, L., and Li, H. (2016).  $Mg^{2+}/Ca^{2+}$  promotes the adhesion of marine bacteria and algae and enhances following biofilm formation in artificial seawater. *Colloids Surf., B* **146**, 289–295 [Cited on page 8.]
- Hegemann, P. and Berthold, P., (2009). Sensory photoreceptors and light control of flagellar activity. In: *The Chlamydomonas Sourcebook (Second Edition)*, (Harris, E. H., Stern, D. B., and Witman, G. B., Eds.), pp. 395–429. Academic Press, London [Cited on pages 18 and 146.]
- Helenius, A. and Aebi, M. (2004). Roles of N-linked glycans in the endoplasmic reticulum. *Annu. Rev. Biochem.* **73**, 1019–1049 [Cited on pages 137, 138, and 139.]
- Helmholtz, H. (1853). Ueber einige Gesetze der Vertheilung elektrischer Ströme in körperlichen Leitern mit Anwendung auf die thierisch-electrischen Versuche. *Ann. Phys.* **165**, 211–233 [Cited on page 26.]

- Henzler-Wildman, K. and Kern, D. (2007). Dynamic personalities of proteins. *Nature* **450**, 964–972 [Cited on page 139.]
- Hermentin, P., Witzel, R., E.-J., K., Diderrich, G., Hoffmann, D., Metzner, H., Vorlop, J., and Haupt, H. (1996). The hypothetical N-glycan charge: a number that characterizes protein glycosylation. *Glycobiology* **6**, 217–230 [Cited on page 137.]
- Hirn, K. E. (1900). Monographie und Iconographie der Oedogoniaceen. *Acta Societatis Scientiarum Fennicae* **27**, 1–394 [Cited on page 141.]
- Hochmuth, R. M. (2000). Micropipette aspiration of living cells. *J. Biomech.* **33**, 15–22 [Cited on page 24.]
- Hsu, L. C., Fang, J., Borca-Tasciuc, D. A., Worobo, R. W., and Moraru, C. I. (2013). Effect of micro- and nanoscale topography on the adhesion of bacterial cells to solid surfaces. *Appl. Environ. Microbiol.* **79**, 2703–2712 [Cited on page 7.]
- Huang, K. and Beck, C. F. (2003). Phototropin is the blue-light receptor that controls multiple steps in the sexual life cycle of the green alga *Chlamydomonas reinhardtii*. *PNAS* **100**, 6269–6274 [Cited on page 100.]
- Hughes, T. P., Baird, A. H., Bellwood, D. R., Card, M., Connolly, S. R., Folke, C., Grosberg, R., Hoegh-Guldberg, O., Jackson, J. B. C., Kleypas, J., Lough, J. M., Marshall, P., Nyström, M., Palumbi, S. R., Pandolfi, J. M., Rosen, B., and Roughgarden, J. (2003). Climate change, human impacts, and the resilience of coral reefs. *Science* **301**, 929–933 [Cited on page 5.]
- Hultgren, S. J., Abraham, S., Caparon, M., Falk, P., Geme, J. W., and Normark, S. (1993). Pilus and nonpilus bacterial adhesins: Assembly and function in cell recognition. *Cell* **73**, 887–901 [Cited on pages 7 and 136.]
- Hunnicut, G. R., Kosfisz, M. G., and Snell, W. J. (1990). Cell body and flagellar agglutinins in *chlamydomonas reinhardtii*: the cell body plasma membrane is a reservoir for agglutinins whose migration to the flagella is regulated by a functional barrier. *J. Cell Biol.* **111**, 1605–1616 [Cited on page 11.]
- Hu, H., and Larson, R. G. (2006). Marangoni effect reverses coffee-ring depositions. *J. Phys. Chem. B* **110**, 7090–7094 [Cited on page 177.]
- IMO (2017). International Maritime Organization. London, UK. Retrieved: 08.08.2017 [Cited on page 125.]
- Israelachvili, J. N., (1991) *Intermolecular and Surface Forces*, Academic Press, London [Cited on pages 24 and 26.]
- Jefferson, K. K. (2004). What drives bacteria to produce a biofilm? *FEMS Microbiol. Lett.* **236**, 163–173 [Cited on page 1.]

- Kamimura, S. and Takahashi, K. (1981). Direct measurement of the force of microtubule sliding in flagella. *Nature* **293**, 566–568 [Cited on pages 23 and 63.]
- Kenrick, P. and Crane, P. R. (1997). The origin and early evolution of plants on land. *Nature* **389**, 33–39 [Cited on page 5.]
- Kesaano, M. and Sims, R. C. (2014). Algal biofilm based technology for wastewater treatment. *Algal Res.* **5**, 231–240 [Cited on page 7.]
- Kirk, D., Bircham, R., and King, N. (1986). The extracellular matrix of Volvox: a comparative study and proposed system of nomenclature. *J. Cell Sci.* **80**, 207–231 [Cited on page 171.]
- Kis, A., Kasas, S., Babić, B., Kulik, A. J., Benoît, W., Briggs, G. A. D., Schönenberger, C., Catsicas, S., and Forró, L. (2002). Nanomechanics of microtubules. *Phys. Rev. Lett.* **89**, 248101 [Cited on page 90.]
- Kishino, A. and Yanagida, T. (1988). Force measurements by micromanipulation of a single actin filament by glass needles. *Nature* **334**, 74–76 [Cited on pages 22, 23, 24, and 63.]
- Klumpp, S. and Lipowsky, R. (2005). Cooperative cargo transport by several molecular motors. *PNAS* **102**, 17284–17289 [Cited on page 114.]
- Kolewe, K. W., Peyton, S. R., and Schiffman, J. D. (2015). Fewer bacteria adhere to softer hydrogels. *ACS Appl. Mater. Interfaces* **7**, 19562–19569 [Cited on page 7.]
- Komsic-Buchmann, K., Wöstehoff, L., and Becker, B. (2014). The contractile vacuole as a key regulator of cellular water flow in *Chlamydomonas reinhardtii*. *Eukaryot. Cell* **13**, 1421–1430 [Cited on page 10.]
- Kozminski, K. G. (2012). Intraflagellar transport – the “new motility” 20 years later. *Mol. Biol. Cell* **23**, 751–753 [Cited on page 20.]
- Kozminski, K. G., Johnson, K. A., Forscher, P., and Rosenbaum, J. L. (1993). A motility in the eukaryotic flagellum unrelated to flagellar beating. *PNAS* **90**, 5519–5523 [Cited on page 20.]
- Kreis, C. T., Le Blay, M., Linne, C., Makowski, M. M., and Bäumchen, O. (2017). Adhesion of *Chlamydomonas* microalgae to surfaces is switchable by light. *Nat. Phys.* Published online 25.09.2017 [Cited on pages 38, 63, 64, 95, 96, 97, 99, 101, 104, 106, and 107.]
- Laib, J. A., Marin, J. A., Bloodgood, R. A., and Guilford, W. H. (2009). The reciprocal coordination and mechanics of molecular motors in living cells. *PNAS* **106**, 3190–3195 [Cited on pages 9, 20, 71, 82, 89, and 114.]
- Landoulsi, J., Cooksey, K., and Dupres, V. (2011). Review – interactions between diatoms and stainless steel: focus on biofouling and biocorrosion. *Biofouling* **27**, 1105–1124 [Cited on pages 2, 7, 8, and 125.]

- Le Blay, M. (2016). Adhesion of Chlamydomonas. FOKOS e.V. Internship Report, Max Planck Institute for Dynamics and Self-Organization, Göttingen [Cited on pages 97 and 115.]
- Leckband, D. and Israelachvili, J. (2001). Intermolecular forces in biology. *Q. Rev. Biophys.* **34**, 105–267 [Cited on page 24.]
- Lee, H., Scherer, N. F., and Messersmith, P. B. (2006). Single-molecule mechanics of mussel adhesion. *PNAS* **103**, 12999–13003 [Cited on page 125.]
- Lefebvre, P. A. and Rosenbaum, J. L. (1986). Regulation of the synthesis and assembly of ciliary and flagellar proteins during regeneration. *Annu. Rev. Cell Biol.* **2**, 517–546 [Cited on pages 21 and 79.]
- Lessel, M., Bäumchen, O., Klos, M., Hähl, H., Fetzner, R., Paulus, M., Seemann, R., and Jacobs, K. (2015). Self-assembled silane monolayers: an efficient step-by-step recipe for high-quality, low energy surfaces. *Surf. Interface Anal.* **47**, 557–564 [Cited on pages 43 and 129.]
- Lewin, R. A. (1982). A new kind of motility mutant (non-gliding) in chlamydomonas. *Experientia* **38**, 348–349 [Cited on page 20.]
- Linne, C. (2017). Light-switchable adhesion of microalgae to surfaces. Master’s thesis, Georg-August-Universität Göttingen, Germany [Cited on pages 67, 83, 108, 111, 114, 123, 144, and 146.]
- Lista, L., (2016). *Statistical Methods for Data Analysis in Particle Physics*. Springer, Cham [Cited on page 55.]
- Lodish, H., Berk, A., Matsudaira, P., Kaiser, C. A., Krieger, M., Scott, M. P., Zipursky, S. L., and Darnell, J., (2004) *Molecular Cell Biology*. W. H. Freeman and Company, New York [Cited on pages 10, 11, 12, 13, 16, and 137.]
- Loskill, P. (2012). Unraveling the impact of subsurface and surface properties of a material on biological adhesion - a multi-scale approach. Ph.D. thesis, Universität des Saarlandes, Saarbrücken, Germany [Cited on pages 69 and 71.]
- Loskill, P., Hähl, H., Faidt, T., Grandthyll, S., Müller, F., and Jacobs, K. (2012a). Is adhesion superficial? silicon wafers as a model system to study van der waals interactions. *Adv. Colloid Interface Sci.* **179**, 107–113 [Cited on pages 27, 43, and 131.]
- Loskill, P., Hähl, H., Thewes, N., Kreis, C. T., Bischoff, M., Herrmann, M., and Jacobs, K. (2012b). Influence of the subsurface composition of a material on the adhesion of staphylococci. *Langmuir* **28**, 7242–7248 [Cited on pages 7, 44, 131, and 136.]
- Loskill, P., Pereira, P., Jung, P., Bischoff, M., Herrmann, M., Pinho, M., and Jacobs, K. (2014). Reduction of the peptidoglycan crosslinking causes a decrease in stiffness of the staphylococcus aureus cell envelope. *Biophys. J.* **107**, 1082–1089 [Cited on page 64.]

- Loskill, P., Puthoff, J., Wilkinson, M., Mecke, K., Jacobs, K., and Autumn, K. (2012c). Macroscale adhesion of gecko setae reflects nanoscale differences in subsurface composition. *J. Royal Soc. Interface* **10**, 20120587 [Cited on pages 125 and 131.]
- Luykx, P., Hoppenrath, M., and Robinson, D. G. (1997). Structure and behavior of contractile vacuoles in *Chlamydomonas reinhardtii*. *Protoplasma* **198**, 73–84 [Cited on page 10.]
- Ma, M. and Hill, R. M. (2006). Superhydrophobic surfaces. *Curr. Opin. Colloid Interface Sci* **11**, 193–202 [Cited on page 125.]
- Magdelaine, Q. (2015). *Chlamydomonas reinhardtii* propulsion force measured with micropipettes. FOKOS e.V. Internship Report, Max Planck Institute for Dynamics and Self-Organization, Göttingen [Cited on pages 155, 156, and 175.]
- Maier, G. P., Rapp, M. V., Waite, J. H., Israelachvili, J. N., and Butler, A. (2015). Adaptive synergy between catechol and lysine promotes wet adhesion by surface salt displacement. *Science* **349**, 628–632 [Cited on page 125.]
- Martin, W., Baross, J., Kelley, D., and Russell, M. J. (2008). Hydrothermal vents and the origin of life. *Nat. Rev. Micro.* **6**, 805–814 [Cited on page 1.]
- Mayer, A. M. (1968). *Chlamydomonas*: Adaptation phenomena in phototaxis. *Nature* **217**, 875–876 [Cited on page 18.]
- McAdams, H. and Arkin, A. (1997). Stochastic mechanisms in gene expression. *PNAS* **94**, 814–819 [Cited on page 79.]
- McCord, R. P., Yukich, J. N., and Bernd, K. K. (2005). Analysis of force generation during flagellar assembly through optical trapping of free-swimming *Chlamydomonas reinhardtii*. *Cell Motil. Cytoskeleton* **61**, 137–144 [Cited on page 174.]
- McGuirk, R. (2017). Great barrier reef being killed by coral bleaching, unesco warns. The Independent. Retrieved: 17.07.2017 [Cited on page 5.]
- McLean, R. J., Katz, K. R., Sedita, N. J., Menoff, A. L., Laurendi, C. J., and Brown, R. M. (1981). Dynamics of concanavalin A binding sites on *Chlamydomonas moewusii* flagellar membranes. *Ber. Dtsch. Bot. Ges.* **94**, 387–400 [Cited on page 13.]
- McLean, R. J., Laurendi, C. J., and Brown, R. M. (1974). The relationship of gamone to the mating reaction in *Chlamydomonas moewusii*. *PNAS* **71**, 2610–2613 [Cited on page 14.]
- Minoura, I. and Kamiya, R. (1995). Strikingly different propulsive forces generated by different dynein-deficient mutants in viscous media. *Cell Motil. Cytoskeleton* **31**, 130–139 [Cited on page 174.]

- Mitchell, B. F., Grulich, L. E., and Mader, M. M. (2004). Flagellar quiescence in *Chlamydomonas*: Characterization and defective quiescence in cells carrying sup-pf-1 and sup-pf-2 outer dynein arm mutations. *Cell Motil. Cytoskeleton* **57**, 186–196 [Cited on pages 68, 71, 105, and 107.]
- Mittag, M., Kiaulehn, S., and Johnson, C. H. (2005). The circadian clock in *Chlamydomonas reinhardtii*. what is it for?: What is it similar to? *Plant Physiol.* **137**, 399–409 [Cited on page 18.]
- Miyamoto, Y., Muto, E., Mashimo, T., Iwane, A. H., Yoshiya, I., and Yanagida, T. (2000). Direct inhibition of microtubule-based kinesin motility by local anesthetics. *Biophys. J.* **78**, 940–949 [Cited on pages 72 and 118.]
- Mykhaylyk, T., Evans, S., Fernyhough, C., Hamley, I., and Henderson, J. (2003). Surface energy of ethylene-co-1-butene copolymers determined by contact angle methods. *J. Colloid Interface Sci.* **260**, 234–239 [Cited on page 44.]
- Nakamura, S., Tanaka, G., Maeda, T., Kamiya, R., Matsunaga, T., and Nikaido, O. (1996). Assembly and function of *chlamydomonas* flagellar mastigonemes as probed with a monoclonal antibody. *J. Cell Sci.* **109**, 57–62 [Cited on pages 14 and 137.]
- Neher, E. and Bert, S. (1976). Single-channel currents recorded from membrane of denervated frog muscle fibres. *Nature* **260**, 799–902 [Cited on page 23.]
- Newman, J. R. S., Ghaemmaghami, S., Ihmels, J., Breslow, D. K., Noble, M., DeRisi, J. L., and Weissman, J. S. (2006). Single-cell proteomic analysis of *s. cerevisiae* reveals the architecture of biological noise. *Nature* **441**, 840–846 [Cited on page 79.]
- Oro, J., Miller, S. L., , and Lazcano, A. (1990). The origin and early evolution of life on earth. *Annu. Rev. Earth Planet. Sci.* **18**, 317–356 [Cited on page 1.]
- van Oss, C. (1993). Acid – base interfacial interactions in aqueous media. *Colloids Surf., A* **78**, 1–49 [Cited on pages 28 and 44.]
- Ostapenko, T., Schwarzendahl, F. J., Böddeker, T., Kreis, C. T., Cammann, J., Mazza, M. G., and Bäumchen, O. (2016). Curvature-guided motility of microalgae in geometric confinement. *arXiv:1608.00363* [Cited on page 120.]
- O’Toole, G., Kaplan, H. B., and Kolter, R. (2000). Biofilm formation as microbial development. *Annu. Rev. Microbiol.* **54**, 49–79 [Cited on pages 1, 7, and 71.]
- Pazour, G. J., Agrin, N., Leszyk, J., and Witman, G. B. (2005). Proteomic analysis of a eukaryotic cilium. *J. Cell Biol.* **170**, 103–113 [Cited on pages 79 and 83.]
- Perera-Costa, D., Bruque, J. M., González-Martín, M. L., Gómez-García, A. C., and Vadillo-Rodríguez, V. (2014). Studying the influence of surface topography on bacterial adhesion



- using spatially organized microtopographic surface patterns. *Langmuir* **30**, 4633–4641 [Cited on page 7.]
- Petit, J., Thomi, L., Schultze, J., Makowski, M., Negwer, I., Koynov, K., Herminghaus, S., Wurm, F., Bäumchen, O., and Landfester, K. (2017). A modular approach for multifunctional polymersomes with tunable adhesive properties. *In preparation* [Cited on page 120.]
- Pizarro-Cerdá, J. and Cossart, P. (2006). Bacterial adhesion and entry into host cells. *Cell* **124**, 715–727 [Cited on page 7.]
- Poppele, E. H. and Hozalski, R. M. (2003). Micro-cantilever method for measuring the tensile strength of biofilms and microbial flocs. *J. Microbiol. Methods* **55**, 607–615 [Cited on page 24.]
- Porter, K. G. (1977). The plant-animal interface in freshwater ecosystems: Microscopic grazers feed differentially on planktonic algae and can influence their community structure and succession in ways that are analogous to the effects of herbivores on terrestrial plant communities. *Amer. Sci.* **65**, 159–170 [Cited on pages 1 and 5.]
- Prechtel, K., Bausch, A. R., Marchi-Artzner, V., Kantlehner, M., Kessler, H., and Merkel, R. (2002). Dynamic force spectroscopy to probe adhesion strength of living cells. *Phys. Rev. Lett.* **89**, 028101 [Cited on page 24.]
- Proft, T. and Baker, E. N. (2008). Pili in gram-negative and gram-positive bacteria — structure, assembly and their role in disease. *Cell. Mol. Life Sci.* **66**, 613 [Cited on pages 7 and 136.]
- Pröschold, T., Marin, B., Schlösser, U. G., and Melkonian, M. (2001). Molecular phylogeny and taxonomic revision of *Chlamydomonas* (Chlorophyta). I. emendation of *Chlamydomonas* Ehrenberg and *Chloromonas* Gobi, and description of *Oogamochlamys* gen. nov. and *Lobochlamys* gen. nov. *Protist* **152**, 265–300 [Cited on pages 9 and 144.]
- Purcell, E. M. (1977). Life at low reynolds number. *Am. J. Phys.* **45**, 3–11 [Cited on page 9.]
- Quarmby, L. M., (2009). Deflagellation. In: *The Chlamydomonas Sourcebook (Second Edition)*, (Harris, E. H., Stern, D. B., and Witman, G. B., Eds.), pp. 43–69. Academic Press, London [Cited on page 40.]
- Ramamonjy, A. (2017). Interplay between intraflagellar transport and light-switchable adhesiveness of *Chlamydomonas reinhardtii*. FOKOS e.V. Internship Report, Max Planck Institute for Dynamics and Self-Organization, Göttingen [Cited on pages 109, 113, 114, and 118.]
- Ramaswamy, S., Suresh, D., Bathula, H., Mahapatra, O., Arunachalam, K., and Gopalakrishnan, C. (2013). Nanoscale analysis of surface topography and adhesion force measurements of flagella isolated from *Chlamydomonas reinhardtii*. *J. Adv. Microsc. Res.* **8**, 163–170 [Cited on pages 8, 81, and 92.]

- Rampelotto, P. H. (2013). Extremophiles and extreme environments. *Life* **3**, 482–485 [Cited on page 1.]
- Reinhart, F. D. and Bloodgood, R. A. (1988). Gliding defective mutant cell lines of *Chlamydomonas moewusii* exhibit alterations in a 240 kDa surface-exposed flagellar glycoprotein. *Protoplasma* **144**, 110–118 [Cited on page 20.]
- Ringo, D. L. (1967). Flagellar motion and fine structure of the flagellar apparatus in *Chlamydomonas*. *J. Cell Biol.* **33**, 543–571 [Cited on pages 14 and 17.]
- Roberts, K., Gurney-Smith, M., and Hills, G. (1972). Structure, composition and morphogenesis of the cell wall of *Chlamydomonas reinhardi*. *J. Ultrastruct. Res.* **40**, 599–613 [Cited on page 10.]
- Robinson, M., Pask, J. A., and Fuerstenau, D. W. (1964). Surface charge of alumina and magnesia in aqueous media. *J. Am. Ceram. Soc.* **47**, 516–520 [Cited on pages 44 and 133.]
- Rosenbaum, J. L., Moulder, J. E., and Ringo, D. L. (1969). Flagellar elongation and shortening in *Chlamydomonas*. *J. Cell Biol.* **41**, 600–619 [Cited on pages 21, 73, and 79.]
- Rosenbaum, J. L. and Witman, G. B. (2002). Intraflagellar transport. *Nat. Rev. Mol. Cell Biol.* **3**, 813–825 [Cited on page 20.]
- Rothschild, L. J. and Mancinelli, R. L. (2001). Life in extreme environments. *Nature* **409**, 1092–1101 [Cited on page 1.]
- Rudd, P. M., Wormald, M. R., Stanfield, R. L., Huang, M., Mattsson, N., Speir, J. A., DiGenaro, J. A., Fetrow, J. S., Dwek, R. A., and Wilson, I. A. (1999). Roles for glycosylation of cell surface receptors involved in cellular immune recognition. *J. Mol. Biol.* **293**, 351–366 [Cited on page 138.]
- Rüffer, U. and Nultsch, W. (1985). High-speed cinematographic analysis of the movement of *Chlamydomonas*. *Cell Motil.* **5**, 251–263 [Cited on page 17.]
- Rüffer, U. and Nultsch, W. (1987). Comparison of the beating of cis- and trans-flagella of *Chlamydomonas* cells held on micropipettes. *Cell Motil. Cytoskeleton* **7**, 87–93 [Cited on pages 17 and 23.]
- Rüffer, U. and Nultsch, W. (1990). Flagellar photoresponses of *Chlamydomonas* cells held on micropipettes: I. Change in flagellar beat frequency. *Cell Motil. Cytoskeleton* **15**, 162–167 [Cited on page 63.]
- Rüffer, U. and Nultsch, W. (1991). Flagellar photoresponses of *Chlamydomonas* cells held on micropipettes: II. Change in flagellar beat pattern. *Cell Motil. Cytoskeleton* **18**, 269–278 [Cited on pages 17, 23, and 63.]

- Rüffer, U. and Nultsch, W. (1995). Flagellar photoresponses of chlamydomonas cells held on micropipettes: III. shock response. *Botanica Acta* **108**, 255–265 [Cited on page 105.]
- Sachs, L. and Hedderich, J., (2006). *Angewandte Statistik - Methodensammlung mit R*. Springer, Berlin [Cited on page 55.]
- SAG (2017a). Dun Medium. Culture Collection of Algae, Göttingen, Germany, Medium Recipe. Retrieved: 27.07.2017 [Cited on page 42.]
- SAG (2017b). +V Medium. Culture Collection of Algae, Göttingen, Germany, Medium Recipe. Retrieved: 27.07.2017 [Cited on page 42.]
- Saito, A., Suetomo, Y., Arikawa, M., Omura, G., Mostafa Kamal Khan, S., Kakuta, S., Suzaki, E., Kataoka, K., and Suzaki, T. (2003). Gliding movement in *Peranema trichophorum* is powered by flagellar surface motility. *Cell Motil. Cytoskeleton* **55**, 244–253 [Cited on pages 20 and 150.]
- Sakmann, B. and Neher, E. (1984). Patch clamp techniques for studying ionic channels in excitable membranes. *Annu. Rev. Physiol.* **46**, 455–472 [Cited on page 23.]
- Schmidt, J. A. and Eckert, R. (1976). Calcium couples flagellar reversal to photostimulation in *Chlamydomonas reinhardtii*. *Nature* **262**, 713–715 [Cited on page 105.]
- Schötz, F., Bathelt, H., Arnold, C. G., and Schimmer, O. (1972). Die Architektur und Organisation der *Chlamydomonas*-Zelle. *Protoplasma* **75**, 229–254 [Cited on page 10.]
- Schulman, R. D., Backholm, M., Ryu, W. S., and Dalnoki-Veress, K. (2014). Dynamic force patterns of an undulatory microswimmer. *Phys. Rev. E* **89**, 050701 [Cited on page 24.]
- Sekar, R., Venugopalan, V., Satpathy, K., Nair, K., and Rao, V. (2004). Laboratory studies on adhesion of microalgae to hard substrates. *Hydrobiologia* **512**, 109–116 [Cited on page 8.]
- Sheng, G.-P., Yu, H.-Q., and Li, X.-Y. (2010). Extracellular polymeric substances (EPS) of microbial aggregates in biological wastewater treatment systems: A review. *Biotechnol. Adv.* **28**, 882 – 894 [Cited on page 7.]
- Shih, S. M., Engel, B. D., Kocabas, F., Bilyard, T., Gennerich, A., Marshall, W. F., and Yildiz, A. (2013). Intraflagellar transport drives flagellar surface motility. *eLife* **2**, e00744 [Cited on pages 9, 20, 72, 82, 112, 113, and 114.]
- Shingyoji, C., Higuchi, H., Yoshimura, M., Katayama, E., and Yanagida, T. (1998). Dynein arms are oscillating force generators. *Nature* **393**, 711–714 [Cited on page 20.]
- Siaut, M., Cuiné, S., Cagnon, C., Fessler, B., Nguyen, M., Carrier, P., Beyly, A., Beisson, F., Triantaphylidès, C., Li-Beisson, Y., and Peltier, G. (2011). Oil accumulation in the model green alga *Chlamydomonas reinhardtii*: characterization, variability between common

- laboratory strains and relationship with starch reserves. *BMC Biotechnol.* **11**, 7 [Cited on pages 1 and 7.]
- Sigal, A., Milo, R., Cohen, A., Geva-Zatorsky, N., Klein, Y., Liron, Y., Rosenfeld, N., Danon, T., Perzov, N., and Alon, U. (2006). Variability and memory of protein levels in human cells. *Nature* **444**, 643–646 [Cited on page 79.]
- Singh, R. and Sharma, S. (2012). Development of suitable photobioreactor for algae production – a review. *Renewable Sustainable Energy Rev.* **16**, 2347–2353 [Cited on pages 1 and 7.]
- Sizova, I., Greiner, A., Awasthi, M., Kateriya, S., and Hegemann, P. (2013). Nuclear gene targeting in *Chlamydomonas* using engineered zinc-finger nucleases. *Plant J.* **73**, 873–882 [Cited on page 120.]
- Slezak, M. (2016). The great barrier reef: a catastrophe laid bare. The Guardian. Retrieved 17.07.2017 [Cited on page 5.]
- Smith, V. H. (2003). Eutrophication of freshwater and coastal marine ecosystems a global problem. *Environ. Sci. Pollut. Res.* **10**, 126–139 [Cited on page 5.]
- Snell, W. J. (1976). Mating in *Chlamydomonas*: a system for the study of specific cell adhesion. I. ultrastructural and electrophoretic analyses of flagellar surface components involved in adhesion. *J. Cell Biol.* **68**, 48–69 [Cited on page 14.]
- Snell, W. J., Buchanan, M., and Clausell, A. (1982). Lidocaine reversibly inhibits fertilization in *Chlamydomonas*: a possible role for calcium in sexual signalling. *J. Cell Biol.* **94**, 607–612 [Cited on pages 72 and 118.]
- Snell, W. and Goodenough, U., (2009). Flagellar Adhesion, Flagellar-Generated Signaling, and Gamete Fusion during Mating. In: *The Chlamydomonas Sourcebook (Second Edition)*, (Harris, E. H., Stern, D. B., and Witman, G. B., Eds.), pp. 369–394. Academic Press, London [Cited on pages 16 and 139.]
- Song, F. and Ren, D. (2014). Stiffness of cross-linked poly(dimethylsiloxane) affects bacterial adhesion and antibiotic susceptibility of attached cells. *Langmuir* **30**, 10354–10362 [Cited on page 7.]
- Starckx, S. (2012). A place in the sun. Flanders Today. Retrieved 19.09.2017 [Cited on page 141.]
- Stepanek, L. and Pigino, G. (2016). Microtubule doublets are double-track railways for intraflagellar transport trains. *Science* **352**, 721–724 [Cited on page 81.]
- Stern, O. (1924). Zur Theorie der elektrolytischen Doppelschicht. *Zeitschrift für Elektrochemie und angewandte physikalische Chemie* **30**, 508–516 [Cited on page 26.]

- Sullan, R. M. A., Beaussart, A., Tripathi, P., Derclaye, S., El-Kirat-Chatel, S., Li, J. K., Schneider, Y.-J., Vanderleyden, J., Lebeer, S., and Dufrene, Y. F. (2014). Single-cell force spectroscopy of pili-mediated adhesion. *Nanoscale* **6**, 1134–1143 [Cited on pages 82, 92, and 136.]
- Sullan, R. M. A., Li, J. K., Crowley, P. J., Brady, L. J., and Dufrêne, Y. F. (2015). Binding forces of streptococcus mutans p1 adhesin. *ACS Nano* **9**, 1448–1460 [Cited on pages 7 and 86.]
- Svoboda, K., Schmidt, C. F., Schnapp, B. J., and Block, S. M. (1993). Direct observation of kinesin stepping by optical trapping interferometry. *Nature* **365**, 721–727 [Cited on page 20.]
- Sze, S. and Ng, K. K., (2006). *Physics of Semiconductor Devices*. John Wiley & Sons, Inc., Hoboken [Cited on page 27.]
- TAP (2017). TAP Medium. Thermo Fisher Scientific, Waltham, USA, Technical Resources – Media Formulations. Retrieved: 27.07.2017 [Cited on page 41.]
- Thewes, N., Loskill, P., Jung, P., Peisker, H., Bischoff, M., Herrmann, M., and Jacobs, K. (2014). Hydrophobic interaction governs unspecific adhesion of staphylococci: a single cell force spectroscopy study. *Beilste.* **5**, 1501–1512 [Cited on pages 7, 83, 125, and 136.]
- Thewes, N., Loskill, P., Spengler, C., Hümbert, S., Bischoff, M., and Jacobs, K. (2015a). A detailed guideline for the fabrication of single bacterial probes used for atomic force spectroscopy. *Eur. Phys. J. E* **38**, 140 [Cited on pages 35 and 73.]
- Thewes, N., Thewes, A., Loskill, P., Peisker, H., Bischoff, M., Herrmann, M., Santen, L., and Jacobs, K. (2015b). Stochastic binding of staphylococcus aureus to hydrophobic surfaces. *Soft Matter* **11**, 8913–8919 [Cited on pages 7, 73, 82, 83, 92, 116, and 125.]
- Thomas, W. (2008). Catch bonds in adhesion. *Annu. Rev. Biomed. Eng.* **10**, 39–57 [Cited on pages 69 and 72.]
- Toba, S., Watanabe, T. M., Yamaguchi-Okimoto, L., Toyoshima, Y. Y., and Higuchi, H. (2006). Overlapping hand-over-hand mechanism of single molecular motility of cytoplasmic dynein. *PNAS* **103**, 5741–5745 [Cited on page 20.]
- Tomson, A. M., Demets, R., van Spronsen, E. A., Brakenhoff, G. J., Stegwee, D., and van den Ende, H. (1990). Turnover and transport of agglutinins in conjugating Chlamydomonas gametes. *Protoplasma* **155**, 200–209 [Cited on page 14.]
- Tsang, P. H., Li, G., Brun, Y. V., Freund, L. B., and Tang, J. X. (2006). Adhesion of single bacterial cells in the micronewton range. *PNAS* **103**, 5764–5768 [Cited on pages 24 and 63.]
- Umen, J. G. and Goodenough, U. W. (2001). Control of cell division by a retinoblastoma protein homolog in Chlamydomonas. *Genes Dev.* **15**, 1652–1661 [Cited on page 16.]
- Waite, J. H. (2017). Mussel adhesion – essential footwork. *J. Exp. Biol.* **220**, 517–530 [Cited on pages 125 and 138.]

- Wan, K. Y. and Goldstein, R. E. (2016). Coordinated beating of algal flagella is mediated by basal coupling. *PNAS* **113**, E2784–E2793 [Cited on page 23.]
- Wan, K. Y., Leptos, K. C., and Goldstein, R. E. (2014). Lag, lock, sync, slip: the many ‘phases’ of coupled flagella. *J. Royal Soc. Interface* **11** [Cited on page 23.]
- Watnick, P. and Kolter, R. (2000). Biofilm, city of microbes. *J. Bacteriol.* **182**, 2675–2679 [Cited on pages 1 and 7.]
- Weiss, R. L., Goodenough, D. A., and Goodenough, U. W. (1977). Membrane particle arrays associated with the basal body and with contractile vacuole secretion in *Chlamydomonas*. *J. Cell Biol* **72**, 133–143 [Cited on pages 11 and 19.]
- Wellman, C. H., Osterloff, P. L., and Mohiuddin, U. (2003). Fragments of the earliest land plants. *Nature* **425**, 282–285 [Cited on page 5.]
- Wells, M. L., Potin, P., Craigie, J. S., Raven, J. A., Merchant, S. S., Helliwell, K. E., Smith, A. G., Camire, M. E., and Brawley, S. H. (2017). Algae as nutritional and functional food sources: revisiting our understanding. *J. Appl. Phycol.* **29**, 949–982 [Cited on pages 1 and 7.]
- Witman, G. B. (1993). *Chlamydomonas* phototaxis. *Trends Cell Biol.* **3**, 403 – 408 [Cited on page 18.]
- Witman, G. B., Carlson, K., Berliner, J., and Rosenbaum, J. L. (1972). *Chlamydomonas* flagella. *J. Cell Biol.* **54**, 507–539 [Cited on page 14.]
- Yakovenko, O., Sharma, S., Forero, M., Tchesnokova, V., Aprikian, P., Kidd, B., Mach, A., Vogel, V., Sokurenko, E., and Thomas, W. E. (2008). FimH forms catch bonds that are enhanced by mechanical force due to allosteric regulation. *J. Biol. Chem.* **283**, 11596–11605 [Cited on pages 69 and 72.]
- Yeung, A. K. and Pelton, R. (1996). Micromechanics: a new approach to studying the strength and breakup of flocs. *J. Colloid Interface Sci.* **184**, 579–585 [Cited on page 24.]
- Yoneda, M. (1960). Force exerted by a single cilium of *Mytilus edulis*. I. *J. Exp. Biol.* **37**, 461–468 [Cited on page 23.]
- Yongsunthon, R. and Lower, S. K. (2006). Force spectroscopy of bonds that form between a staphylococcus bacterium and silica or polystyrene substrates. *J. Electron Spectrosc. Relat. Phenom.* **150**, 228–234 [Cited on page 136.]
- Yoshimura, K. and Kamiya, R. (2001). The sensitivity of *chlamydomonas* photoreceptor is optimized for the frequency of cell body rotation. *Plant Cell Physiol.* **42**, 665–672 [Cited on page 18.]
- Zeng, G., Müller, T., and Meyer, R. L. (2014). Single-cell force spectroscopy of bacteria enabled by naturally derived proteins. *Langmuir* **30**, 4019–4025 [Cited on page 136.]







## C. The Story of my PhD Research and the Discovery of Light-Switchable Adhesion

In October 2014, I started my PhD research on the patterns left-behind by dried liquid drops containing an algal suspension (see section B.3). At the beginning of 2015, I performed first attempts with the micropipette setup; and after my first thesis committee meeting, I started to work exclusively with micropipettes to help Marcin to get the micropipette setups fully operational. During this time, Tanya and I were still working on optimizing the cultivation of our *Chlamydomonas* cells to establish the organism in the laboratory.

Grabbing and holding a *Chlamydomonas* with the micropipette force sensors worked pretty quickly, but adhesion force experiments did not work reliably for almost one year. Although I picked the cell from the substrate where they were sticking, the experiments did not work properly. Sometimes I saw adhesion events in force-distance curves, sometimes I did not see adhesion. As the cells seemed to stick beforehand, these results were confusing and quite frustrating, and we had no idea what the problem in the experimental routine was at that time. *Reflection: The problem was due to light-switchable adhesion, which was unknown at this time. I harvested the cells from the substrate in white light, whereas consecutive experiment were mostly done in red light.*

In summer 2015, I tutored Quentin during his three-month lab rotation, who worked on the propulsion of *Chlamydomonas* and the optimization of some MATLAB-codes for the micropipette setup (see section A.1). After a detour on the propulsion project (see section B.2), it was time to look back at the adhesion project. I had the idea to test the adhesion of *Volvox* colonies. I thought that the colonies should exhibit higher adhesion forces, as the colonies have many more flagella that would interact with the substrate. Whereas this hypothesis was not true, the experiments yielded another interesting outcome: the *Volvox* colonies deformed when I pushed the substrate against them. The restoring force of the micropipette and the deformation, which I detected with a self-written MATLAB code, could be used to measure mechanical properties of the colonies (see section B.1). After I completed the first steps in this project, Marcin took over the *Volvox* project at the beginning of 2016 and continued with it.

At the beginning of 2016, the force spectroscopy with *Chlamydomonas* did not work reliably and I had no idea of the origin of the problems. To address this issue systematically, I wanted to verify that the flagella are not damaged during the force spectroscopy experiments. My idea was to observe the flagella dynamics close to the substrate and to check whether the cells deflagellated in the force spectroscopy experiments. Therefore, I used high-speed imaging in white-light conditions, as this enabled a shorter camera exposure time and higher frame rates.

## 28.01.2016 – The Experiments Started to Work

On this Thursday, I was using the same experimental routine as always, which yielded the same result as always: the cells were sticking to the substrate, but were not sticking in the succeeding experiment. As planned, I verified that the cell did not deflagellate and afterwards I tried to visualize the flagella in close proximity to the substrate with a high-speed camera. Therefore, I brought the cell into contact with the substrate, but I could not see the flagella in close proximity to the substrate (see section 3.3). This first test was not successful, I could not identify the problem in the experimental routine. Afterwards, I took a break while the high-speed camera was saving the images from the first test, which always took a while until the computer got upgraded with a solid-state-drive. Surprisingly, when I came back from the break, the cell was in contact with the substrate. When I retracted the micropipette, I confirmed that the cell was indeed adhered to the substrate, which left me totally astonished, as the exact same cell did not adhere before. *Reflection: Luckily, the cell-substrate distance was small enough when I left for the break. As I used white light for the high-speed imaging, the cell pulled itself to the substrate in a process I later termed auto-adhesion. I cannot imagine what next steps I would have taken without this coincidence ...*

This surprising incidence aroused my interest and curiosity. I placed the cell close to the substrate, watched what happened, and recorded the process. Again, the cell pulled itself to the substrate and exhibited significant adhesion when I retracted the substrate. This experiment got the ball rolling that the light conditions were maybe the key parameter in the experiment that always caused the problems. Consequently, I performed some force-distance experiments in white and red light conditions on the same day. These force-distance experiments showed the light-switchable adhesion and I was optimistic that I found the problem in the experimental routine, which I told Oliver euphorically. The plan for the next day was clear: perform force-distance curves in white and red light and confirm the findings. The experiments on the next day confirmed the previous results. I finally solved the mystery why the experiments were not working properly beforehand.

In the next weeks, I collected more data on this newly discovered phenomenon. In May 2016, I started to tutor two students, Marine (three-month lab rotation) and Christine (Mas-

ter's thesis), who supported me in the data collection. At the same time, I started to work on my first lead-author publication, which was on light-switchable adhesion of *Chlamydomonas* (first version submitted 29.09.2016 to *Nature*, accepted 15.08.2017 *Nature Physics*). During the review process, I did the experiments on different substrates (see chapter 7), the consistency checks, the tests with different organisms, as well as many additional experiments for the revised version of the manuscript. In March 2017, Thomas and Anni (Master's thesis) joined the lab and started to work together with me on the *Chlamydomonas* adhesion to substrates (Anni) and *Chlamydomonas* propulsion (Thomas). In summer 2017, I had the opportunity to tutor Alice and Aina (three-month lab rotation), who worked on the adhesion of gametic cells (Alice) and the connection between auto-adhesion, light-switchable adhesion, and intraflagellar transport (Aina). Around that time, I started to focus completely on writing the dissertation and a second manuscript about the universal adhesion mechanism of *Chlamydomonas*.

In conclusion, although I had a hard time with force spectroscopy experiments with *Chlamydomonas* on model substrates at the beginning, after my discovery of light-switchable adhesion the experiments worked very well in the second half of my PhD. All the results of *Chlamydomonas* adhesion (besides the force-distance curves shown in Figure 7.5C+D) were obtained after the discovery of light-switchable adhesion on 28.01.2016. After that day, I performed single-cell experiments with 380 *Chlamydomonas* cells: 332 force spectroscopy experiments (1131 sets including five force-distance curves), 20 auto-adhesion experiments, and 28 supporting experiments.

## The End.

The end of my PhD story is a great opportunity to acknowledge all the colleagues and students that contributed data and material to my work:

- Marcin, for constructing the micropipette setups, his support and good discussions related to micropipettes and force spectroscopy,
- Tanya, for her support during the first steps with *Chlamydomonas*, the cultivation and maintenance of *Chlamydomonas* in the lab, and other technical support,
- Quentin, for his work on the auto-correlation analysis and the first steps towards measuring the propulsion forces of *Chlamydomonas*,
- Marine, for her significant contribution to the data sets published in my first lead-author paper,
- Christine, for her significant contribution to the light-switchable adhesion, the work on *Chlamydomonas noctigama*, the in-depth investigation of the auto-adhesion, and some other experiments,

- Thomas, for continuing the propulsion project,
- Anni, for her work on the force spectroscopy with *Chlamydomonas*,
- Alice, for her work with gametes and *Oogamochlamys gigantea*,
- Aina, for his studies on the influence of intraflagellar transport on auto-adhesion.

The specific contributions are marked throughout the thesis. Thank you, for the support, all your work, and the experiences I gained while work with you.

# Acknowledgement

Thank you to everyone who supported my work during my PhD research. First, I want to thank Oliver Bäumchen for the opportunity to conduct my PhD research. It was great to pioneer force spectroscopy on *Chlamydomonas* and to help establish the micropipette setup in your lab. I am particularly thankful for the freedom to give my own ideas a try, and for the opportunity to tutor in total seven students: four students from the ESPCI, Paris for short-term projects and three long-term projects for Master's theses. Without this independence and help, the work would have been less complete. The work on biological systems started with my first research project in the lab of Karin Jacobs, who ultimately raised my interest in this research direction, this should not go unmentioned. Moreover, I want to thank the members of the Thesis Advisory Committee, Christoph Schmidt and Marcus Müller, and Examination Board, Stefan Klumpp, Karen Alim, and Jörg Enderlein.

Thank you, "Team Chlamy", for your support and the fun times in the lab (Tanya, Christine, Marine, Anni, Alice, Quentin, Aina, Thomas, and Alex). In particular, Tanya for her support throughout my entire studies, the time together in the lab, many running trips, and the discussions about all kind of stuff. In the same breath, Christine for bringing a good mood in the lab and initiating social activities. The other members of the lab, Julien, Oliver, Marcin and Marco, the running team, the department, and the institute for such a great time. Many thanks to Maike from the Culture Collection of Algae for a lot of discussions about the fascinating world of algae, help on some practical things, and for the support whenever I wanted to try a new organism. A special thanks to Albert B. for his great tip on "how to get water through the micropipettes". Thank you, Kris for all the technical support with the experimental setup and being spontaneous when I wanted to modify something on the micropipette setups. Thank you, Monika and Guido for all the administrative work and Thomas and Kris for the IT service.

Thank you, to everyone who helped to reduce the amount of typos and polish the language in the thesis: Sarah, Tanya, and Christine.

Finally, I want to thank my friends for the great times in Göttingen, and Sarah for the nice time in the last years. Zu guter Letzt, ein großes Dank an meine Familie für den Ansporn, die Unterstützung, und die Besuche fern der Heimat.



# Eidesstattliche Erklärung

Hiermit versichere ich an Eides statt, dass ich die vorliegende Dissertation selbständig verfasst habe und lediglich die angegebenen Hilfsmittel verwendet wurden. Die aus anderen Quellen oder indirekt übernommenen Daten und Konzepte sind unter Angabe der Quelle gekennzeichnet.

Die Arbeit wurde an keiner Hochschule im In- oder Ausland in gleicher oder ähnlicher Form in einem Promotionsverfahren vorgelegt.

Christian Titus Kreis

Göttingen, den 29. September 2017





# Curriculum Vitae

## Christian Titus Kreis

Date of birth: 10.06.1989

Cite of birth: Trier, Germany

### ACADEMIC QUALIFICATION

<b>Doctoral candidate, Physics</b>	2014 – present
International Max Planck Research School – Physics of Biological and Complex Systems, Georg-August University, Göttingen, Germany	
<b>Master of Sciences (Physics)</b>	04/2014
Saarland University, Saarbrücken, Germany	
<b>Bachelor of Sciences (Physics)</b>	08/2011
Saarland University, Saarbrücken, Germany	

### SCIENTIFIC CONTRIBUTIONS

#### Oral Conference Contributions

Multiscale Mechanochemistry & Mechanobiology; Berlin, Germany	2017
DPG Spring Meeting; Dresden, Germany	2017
DPG Spring Meeting; Regensburg, Germany	2016
DPG Spring Meeting; Dresden, Germany	2014
9. ThGOT Thementage Grenz- und Oberflächentechnik; Zeulenroda, Germany	2013
DPG Spring Meeting; Regensburg, Germany	2013

#### Poster Presentations

DPG Spring Meeting; Regensburg, Germany	2016
DPG Spring Meeting; Berlin, Germany	2015

#### Publications

- C.T. Kreis**, M. Le Blay, C. Linne, M. M. Makowski, O. Bäümchen. “Adhesion of *Chlamydomonas microalgae* is switchable by light” *Nature Physics* in press
- T. Ostapenko, F.J. Schwarzendahl, T. Boddiker, **C.T. Kreis**, J. Cammann, M.G. Mazza, O. Bäümchen. “Curvature-guided motility of microalgae in geometric confinement.” arXiv:1608.00363 (under review, Jan. 2017)
- P. Loskill, H. Hähl, N. Thewes, **C. T. Kreis**, M. Bischoff, M. Herrmann and K. Jacobs, “Influence of the subsurface composition of a material on the adhesion of staphylococci” *Langmuir* **28** (2012) 7242



